CALIFORNIA PATH PROGRAM
INSTITUTE OF TRANSPORTATION STUDIES
UNIVERSITY OF CALIFORNIA, BERKELEY

Development of the Advanced Rotary Plow (ARP) for Snow Removal Operations

Han-Shue Tan, Fanping Bu, Bénédicte Bougler, Shiang-Lung Koo, David Nelson, Joanne Chang, Thang Lian

California PATH Research Report
UCB-ITS-PRR-2006-17

This work was performed as part of the California PATH Program of the University of California, in cooperation with the State of California Business, Transportation, and Housing Agency, Department of Transportation, and the United States Department of Transportation, Federal Highway Administration.

Final Report for RTA 65A0068

August 2006

ISSN 1055-1425

CALIFORNIA PARTNERS FOR ADVANCED TRANSIT AND HIGHWAYS

Development of the Advanced Rotary Plow (ARP) for Snow Removal Operations

Final Report

Han-Shue Tan, Fanping Bu, Bénédicte Bougler, Shiang-Lung Koo,
David Nelson, Joanne Chang & Thang Lian

Abstract

This final report describes the development and the initial field test of an automated snowblower, focusing on one of the more difficult snow removal operations: blowing snow off the freeway along side a guardrail without touching the guardrail. The objective is to minimize damage to the snowblower, guardrail, and other elements of the infrastructure by deploying highly accurate and robust automated steering. The automatic steering is accomplished by following magnets embedded under the roadway. The development process includes transforming this real-world automated highway winter maintenance operation into a control problem, modeling snowblower, designing control algorithms, devising human machine interface, instrumenting a 20-ton snowblower, and conducting demonstration and field tests. The modified snowblower was equipped with add-on sensors, actuator, computer and driver interfaces; the test site includes eight guardrail sections between Kingvale and Soda Springs on the shoulders of Interstate-80 in the Sierra Mountain region near Donner Summit in California, USA. The ride-along and test data demonstrated that the prototype system achieved all initial performance goals, and very positive feedback was received from various stakeholders as well as the operators who tried it.

Keywords: Snowblower, automation, magnets, sensors

Executive Summary

This project demonstrated an Advanced Rotary Plow (ARP) with automatic steering that allows the ARP to follow magnets embedded in the pavement. This project is one of the first real-world applications derived from PATH/Caltrans research in the area of automated vehicle control. A modified snowblower with add-on sensors, actuator, computer and driver interfaces was developed, and initial field tests were conducted along the 8 guardrail sections between Kingvale and Soda Springs on the shoulders of Interstate-80 near Donner Summit. The results from the field tests and ride-along demonstrated that the prototype system achieved all critical performance goals and received very positive feedback from various stakeholders as well as the operators. Although a full winter field operational tests were not completed due to the end of the winter season, the successful development as well as the initial field tests suggests feasibility toward deployment.

Objective

A snowblower is a key component of the snow removal strategy. To achieve effective removal of the snow built up along the roadside, created by either a single snowplow or a fleet of snowplows, an operator needs to drive the snowblower at the edge of the road in order to eliminate the leftover snow "bleeding" back into the highway. However, such operations often cause severe damage to the guardrail. An operator generally uses the rear steering joystick to position the snowblower to an appropriate "crab" angle and "tries" to maintain constant contact between the blower head and the guardrail using his hands (feeling the pressure), his ears (hearing the contact sounds), and his eyes (looking for the snow poles and obstacles) as he plows forward. "Riding on the guardrail," as the operators commonly put it, creates damage to the rail such as tilting, ripping and tearing of the guardrail (Figure 2). This damage leads to frequent repairs and replacements of the guardrails often in treacherous mountain regions. While guardrails require rehabilitation throughout all the areas maintained by Caltrans, the frequency of rehabilitation due to snowblower damage represents a significant cost, thus becoming an opportunity for excellent return through application of advanced technologies such as precision steering control. Application of precision steering control has the following potential advantages:

1) Increased operational safety
   - The driver knows where the guardrail is without having to "drive by feel".
   - It reduces driver fatigue by allowing him to concentrate on the plow and not where the guardrail is.
   - It increases safety in areas that have steep ravines or canyons.
2) Reduced maintenance costs
   - It reduces wear and tear on guardrails since the blower no longer needs to touch the guardrail.
   - It reduces wear and tear on the plow by reducing guardrail contact.

Development

In 2000, Caltrans, the Advanced Highway Maintenance and Construction Technology Center (AHMCT) at U. C. Davis, and the Partners for Advanced Transit and Highways

(PATH) at U. C. Berkeley started a pooled fund study, "Development of the Advanced Rotary Plow (ARP) for Snow Removal Operations," with Nevada and Alaska's DOT as partners. Caltrans manages the overall project and coordinates resources for field tests and evaluation. AHMCT conducts feasibility studies on the radar warning system, GPS application and rotary protection device. PATH is responsible for the design and development of the ARP automated control system. The ultimate goal of the ARP project is to develop a prototype automated snowblower that will be used by the Caltrans' operators and to perform real snow removal operations under harsh winter environments. In 2002, the project responsibilities were divided more clearly between PATH and AHMCT for efficiency. PATH is responsible for developing a turn-key lateral control system that includes the design of HMI for lateral display functions. This report focuses on the development of the ARP lateral control system.

Various lateral sensing and referencing technologies were investigated for this application; what was found was that machine vision does not penetrate snow, and that the GPS system does not provide sufficient reliability under possible multipath and blockage scenarios. A magnetic-marker-based sensing system was chosen for the initial implementation primarily because of its high reliability and accuracy (better than 1 cm) under all weather conditions. The mountainous highway I-80 near Donner Summit (close to Lake Tahoe) was chosen to be the first field test site. In 2001, magnets were installed along the eastbound and westbound guardrails of I-80, at 4 feet apart and 4 feet away from the guardrail. Binary coding of the magnetic markers was designed (north pole up vs. south pole up) to provide information about guardrail characteristics, such as the shoulder side (right or left of the blower) and the end of guardrail. Eight sections of the guardrail were equipped with magnets for the initial feasibility operations with a total length of 1.46 km (0.9 mile) between Soda Springs and Kingvale.

The basic performance requirements for the automated snowblower system requested by the Caltrans' Maintenance and formulated by the researchers are as follows:

- "Tracks" accurately along guardrail (i.e., lateral error: 2 to 4 inches)
- Supports various snow removal operations
- Survives harsh winter environments (snow, ice, salt, water, dirt, wind)
- Employ simple operation procedure, tolerating operator mistakes, easy to train
- Create low distraction to operator
- Provide reliable and safe automated operation

The first prototype automated control was a truly "add-on" system with the following components added to a conventional Kodiak Northwest single-engine rotary snowplow with full hydrostatics:

- A computer, together with a data acquisition unit, which processes information and determines control and guidance actions
- Magnetometers underneath the blower body for measuring the field strength of magnetic markers installed under the roadway
- A DC motor attached to the steering column with angular sensors as the steering actuator
- A yaw gyro and speed sensor for measuring vehicle yaw rate and speed

- Human Machine Interface (HMI) or Driver Vehicle Interface (DVI) consisting of the local electronic circuit, a toggle switch, LED displays and an audible unit

The key software components that collectively constitute the necessary intelligence of the automated system are:

- Reliable signal processing algorithm that provides consistent location estimates despite large vehicle movement and environmental irregularities
- Smart steering servo that carries out the steering command under highly nonlinear mechanical characteristics and unpredictable disturbances
- Robust high-gain "lane-keeping" controller that accurately follows the "magnets" under all operational conditions without slope and curvature information
- Adaptive exception controls that cope with any imaginable "abnormal" scenarios such as sudden potholes, guardrail touching, actuator saturation, unknown oscillations, operator mistakes or interventions
- A dependable "transition" controller that executes "on-demand" transitions between automated and manual control under all operational conditions
- A simple and transparent DVI that facilitates clear operator state awareness and prompts timely and correct responses under both normal and emergency scenarios
- A fault detection and management system that detects system irregularities and provides a warning while at the same time conducting preventive actions

The effectiveness of the design is evident, for example, in the simple DVI system. It consists of the following four elements (see Section 11):

- A transition toggle switch, located under the radio, allowing the operator to switch the system on and off
- The status LED's, located underneath the air filter indicator, displaying the system's current status
- The guidance LED's, located underneath the voltmeter, displaying the position of the tip of the blower head with respect to the guardrail
- An audible unit that produces the following three different sounds: acknowledgment (transition to auto steering), end of magnets (end of guardrail), and emergency (take over control now)

The automated operation is simple and straightforward. An operator simply approaches the guardrail the same way as he always does. The operator can use the guidance LED's displays to observe the "tip location" of the blower head. Once the blower is within its appropriate crab angle range, the system is ready to transition to automation, and the GREEN LED will be lit. Once the GREEN status LED is on, the operator can switch to automated control any time he wishes by pushing down the AUTO switch. With a soft acknowledgement sound, the BLUE status LED will then be lit, indicating the blower is now under automated steering control. The operator can resume manual control by pushing the MANUAL switch or by overriding the steering wheel at any time. The flashing RED LED, with an emergency sound beeping simultaneously, signals the driver to take over control immediately.

Result

On October 15, 2003, Caltrans conducted an ARP ride-along demonstration to more than 30 stakeholders from 3 states at Kingvale. The demonstration used a simulated guardrail and the ARP was tested under various operational scenarios for over 3 hours. All comments received were positive about the system and performance, especially those from people who had previous experience working with snow removal equipment.

During March 2005, three sets of initial field tests were successfully conducted along the guardrails of the Interstate-80 under real winter operational conditions. The last set of the tests, on March 22, 2005, was conducted under a heavy winter storm, and the ARP was blowing accumulated wet snow. Five operators test operated the automated snowblower.

The initial operator trial and survey, operational test data, as well as the stakeholders' feedbacks strongly indicated the following:

- The concept of applying automated steering control to snowblower operation is feasible; the application will improve safety and efficiency of the snow removal operations.
- The implementation of the current automation technology to the snowblower is likely to succeed.
- The operators liked the system performance and would accept and use the system.

Recommendation

It is therefore appropriate to start moving toward the deployment of such technology. Additional R&D effort should address various deployment issues such as reliability, cost, maintenance, and commercialization. With respect to the continuation of the ARP technology development, improving safety and flexibility of automation technologies, investigating operator interface with guidance and control system in real world, as well as incorporating DGPS to extend the automated operation beyond guardrail sections are all important possibilities.

Table of Contents

Abstract i
Executive Summary ii
Objective ii
Development ii
Result v
Recommendation v
Table of Contents vi
List of Figures viii
Acknowledgements xii
1. Introduction 1
1.1 Background 1
1.2 Tasks and Responsibilities 6
1.3 Accomplishments and Milestones 12
2. Requirements and Solutions 14
2.1 Requirement Formulation 14
2.2 Solution Description 16
3. Software Architecture and Description 20
3.1 Software Architecture 20
3.2 Software Description 22
4. Magnetic Lateral Sensing 32
4.1 Magnetic Noise Effects 33
4.2 Tire-induced Magnetic Noise 34
4.2 Magnetic Sensing Algorithm 36
4.3 Signal Processing 38
5. Magnet Installation 40
5.1 Test Site 40
5.2 Magnet Code Description 41
6. Hardware Modifications 44
6.1 Hardware Components 44
6.2 Wiring and Circuit Diagram 49
6.3 Rear Magnetometer Bar Installation 52
7. Steering Actuator 56
7.1 Actuator System Configuration 56
7.2 Position Servo Design 59
8. Actuator Fault Detection 65
8.1 Fault Detection Method 65
8.2 Experimental Validation 70
9. Snowblower Tire Model 73
9.1 Impact of Snow Chains to Vehicle Lateral Dynamics 73
9.2 Impact of Low-Speed Tire Characteristics to Vehicle Steering Dynamics 85
9.3 Improve Bicycle Model Validation 99
10. Control Design 104
10.1 Snowblower lateral dynamics modeling for control 104

10.2 Lateral control design 107
10.3 Integrated Control 111
11. Human Machine Interface/Driver Vehicle Interface 113
11.1 Design Concept 113
11.2 HMI Components and Location 114
12. Procedure, Training, and Operator Survey 121
12.1 Operation Procedure 121
12.2 Test Procedure and Training 122
12.3 Operator Interview and Human Factor Study Preparation 124
12.4 Operator Feedback Questionnaire and Preliminary Results 127
13. Tests and Results 134
13.1 Initial Algorithm Test at RFS 134
13.2 Initial Prototype System Test at RFS 136
13.3 Initial Kingvale Maintenance Yard Tests 138
13.4 Problem-Solving Test at Kingvale Maintenance Yard Tests 140
13.5 Simulated Guardrail and Operator Feedback at Kingvale 140
13.6 Stakeholder Demonstration 141
13.7 Final RFS System Calibration 143
13.8 Initial I-80 Guardrail Tests: 149
13.9 Winter Operational Field Tests 151
14. Conclusion and Recommendation 158
References 161

List of Figures

Figure 1. 1 Two sections of guardrail damaged by snowblower 2
Figure 1. 2 Example of a blower head with scratch mark 2
Figure 1. 3 Example of guardrail rehabilitation 3
Figure 1. 4 Rotary Snowblower in Operation near Donner Summit. 3
Figure 2. 1 Illustration of snowblower crab angle and sensor range 15
Figure 2. 2 ARP Tasks 16
Figure 2. 3 Automated Snowblower: prototype system components 18
Figure 2. 4 HMI display: Status lights and operations 19
Figure 3. 1 Software architecture relationship 20
Figure 3. 2 Software architecture with respect to database 21
Figure 3. 3 Lateral control software 23
Figure 3. 4 Status DVI/HMI 23
Figure 3. 5 Guidance DVI/HMI 24
Figure 3. 6 Lateral source code 25
Figure 3. 7 Front magnetometer bar configuration 26
Figure 3. 8 Rear magnetometer bar configuration 26
Figure 3. 9 Calibration table for snowblower rear center @ 2 cm division calibration 27
Figure 3. 10 Calibration table for snowblower (vertical strength vs lateral position) 27
Figure 3. 11 Calibration table for snowblower (horizontal strength vs lateral position) 28
Figure 3. 12 Transition state machine 29
Figure 3. 13 Control state machine 29
Figure 4. 1 Examples of Snowblower magnetic field noise interference from tire 35
Figure 4. 2 Snowblower tire magnetic noise vs. magnetometer sensor bar locations 35
Figure 4. 3 Snowblower Front Magnetometer Calibration Tables 37
Figure 4. 4 Snowblower Rear Magnetometer Calibration Table 37
Figure 4. 5 Rear sensor new calibration & signal processing comparison. 38
Figure 4. 6 “Peak-Mapping” Magnetometer Signal Processing Block Diagram 38
Figure 4. 7 Peak detection block diagram 39
Figure 5. 1 Map of the test area 40
Figure 5. 2 Magnet Installation 40
Figure 5. 3 Magnets along guardrail 41
Figure 5. 4 Illustration of guardrail installed with magnets in I-80 41
Figure 5. 5 Illustration of beginning and ending of a magnet section 42
Figure 6. 1 Enclosure and components 45
Figure 6. 2 Steering actuator (not assembled) 46
Figure 6. 3 Yaw rate sensor and enclosure 47
Figure 6. 4 Existing dented front magnetometer bar and a spare 47
Figure 6. 5 Speed sensor (left: old; right: improved) 47
Figure 6. 6 Interface between snowblower sensors and computer (1) 48
Figure 6. 7 Interface between snowblower sensors, commands and computer (2) 48
Figure 6. 8 HMI and heart beat timing 49
Figure 6. 9 Snowblower wiring and circuit diagram (overall) 50

Figure 6. 10 Snowblower wiring and circuit diagram (steering actuator & transition switches) 50
Figure 6. 11 Snowblower wiring and circuit diagram (AT-MIO-64E-3 & magnetometers) 51
Figure 6. 12 Snowblower wiring and circuit diagram (I/O boards)..... 51
Figure 6. 13 Snowblower wiring and circuit diagram (HMI circuit)..... 52
Figure 6. 14 Snowblower wiring and circuit diagram (heart beat detection) 52
Figure 6. 15 Possible rear magnetometer bar location..... 53
Figure 6. 16 Rear sensor bar housing and the magnetometers before final assembly 55
Figure 6. 17 Rear sensor bar after assembly 55
Figure 7. 1 Block diagram of steering actuator..... 57
Figure 7. 2 Steering actuator installation 57
Figure 7. 3 Schematic of steering actuator motor assembly 58
Figure 7. 4 Current drive loop in ECU 58
Figure 7. 5 Snowblower steering actuator open loop frequency response 60
Figure 7. 6 Friction effect 60
Figure 7. 7 Closed loop diagram of steering actuator position servo 61
Figure 7. 8 Step input of a PD controller..... 61
Figure 7. 9 Friction effect for small amplitude command 62
Figure 7. 10 Step input with friction compensation..... 62
Figure 7. 11 Overshoot when command input is large 63
Figure 7. 12 Step input with anti-windup 63
Figure 7. 13 Closed loop response..... 64
Figure 8. 1 Block diagram of motor dynamics 65
Figure 8. 2 Drive current in PWM motors: DC plus small ripples..... 66
Figure 8. 3 Schematic of fault detection 66
Figure 8. 4 Large signals: the desired (solid line) and actual (dash line) voltages 67
Figure 8. 5 Small signals: the desired (solid line) and measured (dash line) voltages 67
Figure 8. 6 Probability distribution of system parameters under fault or no fault..... 69
Figure 8. 7 Components in the steering workbench 70
Figure 8. 8 Motor/ECU in normal condition 71
Figure 8. 9 Motor/ECU under fault..... 71
Figure 9. 1Typical lateral force versus slip angle [2] 75
Figure 9. 2 Lateral force versus slip angle (RAW data) 76
Figure 9. 3 Typical linear system identification 77
Figure 9. 4 Proposed identification procedure..... 77
Figure 9. 5 Non-parametric approach using look-up tables..... 78
Figure 9. 6 Estimated force at each slip angle of the nonlinear relation..... 80
Figure 9. 7 Flow diagram of the identification procedure 80
Figure 9. 8 Experimental results on sand-covered road (continued) 83
Figure 9. 9 # of points at each slip angle in configuration 1..... 83
Figure 9. 10 Experimental results on dry pavement 84
Figure 9. 11 General system diagram for a typical vehicle 87
Figure 9. 12 Top view of (a) lateral deflection and associated force (b) yaw deflection and associated moment 89
Figure 9. 13 Freq. response: steering angle to yaw rate at (a)V = 0.5m/s (b)V = 20m/s.. 97

Figure 9. 14 Freq. response: steering angle to lateral acceleration at (a)0.5 m/s; (b)20 m/s 98
Figure 9. 15 Freq. response: steering angle to yawrate at (a)0 m/s (b)0.45 and 1.6 m/s 102
Figure 10. 1 Frequency response from front steering angle to yaw rate..... 106
Figure 10. 2 Block diagram of control loop..... 107
Figure 10. 3 Synthesized and matched 6th order controller frequency responses from lateral deviation at blower head to steering angle for $v_r = 1m/s$ 110
Figure 10. 4 Synthesized and matched 5th order controller frequency responses from vehicle yaw angle to steering angle for $v_r = 1m/s$ 111
Figure 10. 5 Control algorithm structure 112
Figure 11. 1 HMI system and components 114
Figure 11. 2 Location of the transition switch 115
Figure 11. 3 Transition switch actions 115
Figure 11. 4 Emergency button and Auto system switch on the center console 116
Figure 11. 5 Locations of the status display and guidance display..... 117
Figure 11. 6 General meanings of the status display 117
Figure 11. 7 General meaning of the guidance display 119
Figure 11. 8 Audible unit 120
Figure 12. 1 Automated Rotary Snow Plow Use Instruction (1)..... 123
Figure 12. 2 Automated Rotary Snow Plow Use Instruction (2)..... 124
Figure 12. 3 Camera views of snowblower operator testing 128
Figure 13. 1 Initial test result at RFS test track (1st north bound run) 135
Figure 13. 2 Initial test result at RFS test track (2nd south bound run) 135
Figure 13. 3 Servo performances for the steering actuator..... 136
Figure 13. 4 Lateral and transition control..... 137
Figure 13. 5 HMI control and display results 138
Figure 13. 6 Snowblower arrived at Kingvale Maintenance yard 139
Figure 13. 7 Data collected during stakeholder demonstration 143
Figure 13. 8 Simulated guardrail testing at Richmond Field Station..... 145
Figure 13. 9 Curve section on the simulated guardrail testing at RFS 146
Figure 13. 10 ARP Simulated Guardrail Tests at RFS (Left Guardrail, 11-01-04): Constant Rear Steering 147
Figure 13. 11 ARP Simulated Guardrail Tests at RFS (Left Guardrail, 11-01-04): Changing Rear Steering 148
Figure 13. 12 ARP Simulated Guardrail Tests at RFS (Right Guardrail, 11-01-04): Rear Steering Change, Wrong Crab Angle, Auto-Ejection, Sharp Speed Changes, Switch on/off..... 148
Figure 13. 13 Automatic steering along guardrail on I-80 on Dec. 2004 149
Figure 13. 14 Test run on a fair weather condition (2/3/2005)..... 150
Figure 13. 15 Snowblower Tests along Guardrail on I-80 (Right Guardrail #1, 02-03-05): No Snow on the Ground 151
Figure 13. 16 Test run on a light snowy day (3/4/2005)..... 152
Figure 13. 17 Field test (blowing wet snow during a winter storm 3/22/2005)..... 153
Figure 13. 18 Operator using automated steering control along I-80 guardrail..... 153
Figure 13. 19 Snowblower Tests along Guardrail on I-80 (Right Guardrail #2, 03-04-05): Light Snow on the Ground..... 154

Figure 13. 20 Snowblower Tests along Guardrail on I-80 (Right Guardrail #1, 03-22-05): Heavy Wet Snow on the Ground 155
Figure 13. 21 ARP Tests along Guardrail on I-80 (Right Guardrail #2, 03-22-05): Heavy Wet Snow on the Ground..... 155
Figure 13. 22 Post-processed lowest snowblower operational speeds 157

Acknowledgements

This work was sponsored by the California AHMCT Program, in cooperation with the State of California Business, Transportation and Housing Agency, Department of Transportation. The contents of this report reflect the views of the authors, who are responsible for the facts and accuracy of the data presented herein. The contents do not necessarily reflect the official views or policies of the State of California. This report does not constitute a standard, specification, or regulation.

The authors thank the California State Department of Transportation for their support. In addition, the researchers would like to thank the Caltrans Equipment Service Center and Caltrans Maintenance for their invaluable contributions, particular in the instrumentation and maintenance of the Advanced Rotary Plow. Finally, the authors would like to thank the Sierra Snowfighters at the Kingvale Maintenance Center, without their participation and feedback the project would not have been accomplished.

1. Introduction

1.1 Background

A snowblower, a.k.a. a rotary snowplow, is a massive snow removal apparatus that blows snow high into the air and off the roadway. It is a key component of the snow removal strategy employed by snow fighters, especially on highways that travel across mountains. To effectively remove the snow built up along the roadside created by either a single snowplow or a fleet of snowplows, an operator needs to drive the snowblower on the edge of the road and often with a very tight tolerance range in order to prevent the left-over snow from "bleeding" back into the highway. This method of driving becomes even more difficult when the snowblower is operated along a guardrail.

In current operation, an operator generally uses the rear steering joystick to position the large snowblower in the appropriate "crab" angle (Figure 14) before he reaches a section of guardrail. Typically, the rear edge of the vehicle is about 0.1-0.6 of a meter further away from the edge of the road or guardrail than that of the front end of the blower. The operator then drives the huge vehicle body toward the guardrail until the front side of the blower's head touches it. He then "tries" to maintain a somewhat continuous contact between the blower's head and the guardrail using his hands (to feel the pressure), his ears (to hear the contact sounds), and his eyes (to look for snow poles and obstacles) as he plows forward. Since the blower's head can weigh up to 6 tons, it creates a natural oscillation when it hangs in front of the snowplow body. Consequently, the snowblower continuously "bounces" into and off the guardrail. "Riding on the guardrail," as the operators commonly term it, creates damage such as tilting, ripping and tearing of the guardrail that is serious enough to be easily identified by travelers passing through (see Figure 1.1 for an example of a section of damaged guardrail).

Such damage leads to frequent repairs and replacements of guardrails in treacherous mountain regions. At an average cost of approximately $100/meter of guardrail, including material, equipment and labor, rehabilitation of guardrails is very costly. While guardrails require rehabilitation throughout all the areas maintained by the Department of Transportation, the frequency of rehabilitation due to snowblower damage, typically once every couple of years, represents a significant cost, and thus becomes an opportunity for a cost effective application of advanced lane-guidance technologies such as precision steering control. In addition, the practice of guiding by guardrails often causes serious damage to the approximately $300,000 snowblower, increasing the frequency of repair and replacement. Please refer to Figure 1.2 for an example of a snowblower exhibiting scratches on the head resulting from the above-mentioned operation; and to Figure 1.3 for an example of guardrail rehabilitation. A successful application of precision steering control can reduce; even eliminate contact between the snowblower and guardrail, while improving the consistency and accuracy of the work performed. Furthermore, this application will increase operational safety by allowing the operator to concentrate on "plowing", remove the exhausting necessity of "drive by feeling", as well as reduce the operator's visual fatigue, a major complaint during long-hour winter operations. In addition, limiting the damage to the guardrail also improve the safety of the traveling

vehicles in the event of an emergency situation. The current work, targets at application in mountainous areas with guardrails, rather than areas without guardrails. However, the researchers recognize that there could also be significant safety enhancements in areas with steep ravines or canyons.

Figure 1. 1 Two sections of guardrail damaged by snowblower

Figure 1. 2 Example of a blower head with scratch mark

Figure 1. 3 Example of guardrail rehabilitation

Figure 1. 4 Rotary Snowblower in Operation near Donner Summit.

In addition, due to a great number of stalled or abandoned vehicles in mountainous areas, combined with the buildup of snow to be removed by the blower, there is an

increased risk that the blower might collide with these vehicles. Natural objects, such as large rocks and debris, also present collision hazards. Due to the large mass of the blower vehicle and the action of the rotary mechanism, such collisions have a high potential for damage to vehicles, even at the low operating speed (approximately 1 - 5 MPH, 0.45 – 2.2 m/s). Impact with foreign objects can also damage or destroy the expensive rotary mechanism. Thus, inclusion of Collision Warning Systems technology will provide added safety, as well as reduced liability and repair costs. Figure 1.4 shows a front-discharge Kodiak rotary snowblower in operation near Donner Summit in California.

The Advanced Highway Maintenance and Construction Technology (AHMCT) Research Center at the University of California - Davis (UCD), in partnership with the California Partners for Advanced Transit and Highways (PATH) of the University of California at Berkeley (UCB), proposed, in 2000, automation of the driving functions for a rotary snowblower, including fully automated steering, and possibly automated throttle and brake. Along with automation of the driving function, the research included investigation of obstacle detection and collision warning in the context of the snowblower operation. The proposed combination of automatic vehicle control and obstacle detection is referred to as the Advanced Rotary Plow, or ARP.

Researchers at the AHMCT Research Center, as well as our research partners at the California State Department of Transportation (Caltrans) and PATH, have long considered the benefits of providing guidance information and vehicle control to enhance winter maintenance activities. AHMCT and PATH, along with the Western Transportation Institute (WTI) of Montana State University, have completed Phase I and II of their Advanced Snowplow Project (ASP-I & ASP-II), which provides lateral guidance and collision warning information to significantly enhance the safety and efficiency of the snow plowing operation. Based on the success of these projects, there is an increased interest in applying similar technologies to related winter maintenance activities, particularly on the rotary snowblower. Since the blower operation requires the vehicle to operate very close to the guardrail without actually contacting it, tight tolerances must be achieved. Attempting to drive within these tolerances, even with an advanced display of all available roadway information similar to that in the Advanced Snowplow, is not an easy task; therefore driver assistance in this form was not considered in this project. Full automation can eliminate the high level of operator stress as they attempt to operate very near the guardrail without impacting it. This endeavor provides a unique opportunity to clearly demonstrate the near-term benefits of AVCSS and IVI technologies, including vehicle automation and obstacle detection in a semi-controlled and geographically limited operating environment. Caltrans has installed infrastructure elements to support the development and testing of an automated snowblower at Donner Summit on Interstate 80 during this project period.

This project started with developing a prototype automated snowblower to be used by the California Department of Transportation operators and to perform real snow removal operations under harsh winter environments [1]. Various lateral sensing and referencing technologies were available to provide lateral position for the precision steering control. For example, in [2][3], video cameras are used to determine the vehicle position for

guidance or for control. However, the vision based systems are generally more sensitive to the environmental factors such as lighting, weather or pavement conditions; and the machine vision does not penetrate snow and ice that cover the lane markings. GPS is another way to determine vehicle position for the purposes of guidance or control with a lower infrastructure cost [4][5][6]. However, current GPS system does not provide sufficient reliability under possible multipath and blockage scenarios in the mountainous areas. In order to quickly demonstrate the feasibility of the automatic lane guidance concept, a magnetic marker-based sensing system [7][8] was chosen for the initial implementation primarily because of its high reliability and accuracy (better than 1 cm) under all weather conditions [9]. The mountainous highway I-80 near Donner Summit, 30 km from Lake Tahoe, was chosen to be the first field test site.

The overall goal of this project is to relieve the operator of the stressful task of driving the vehicle in close proximity to the guardrail without physical contact. The proposed system would also provide obstacle detection and warning to prevent injury or property damage, thus allowing the operator to perform his duties safely and efficiently. The application of AVCSS technologies can assist the blower operator in performing snow removal, while preserving the integrity of the highway guardrail infrastructure, and avoiding any objects or vehicles located in the path of the snowblower. A subsidiary goal is the demonstration of the beneficial near-term application of AVCSS and IVI technologies in the maintenance environment. The project culminates in demonstrations in the Advanced Winter Maintenance test corridor on California's Interstate 80.

As proposed, the blower automation functions include automated steering, possibly automated throttle and brake, short-range forward collision warning, and the required Human-Machine Interface (HMI) technology. The proposed project included the following developments:

a. Vehicle lateral control: The lateral control system includes a sensing system and control algorithms. The main approach for lane position sensing was developed by PATH using the embedded magnetic reference marker system for lateral position indication within the lane. Feasibility of this technology was shown at the 1997 NAHSC and other automated vehicle demonstrations, and its current application for ASP-I and ASP-II also suggests the technology is robust and well-suited for this application. Alternative approaches, including magnetic tape, side-fire radar, etc, were investigated early in the project. The research team has also implemented multiple technologies on the rotary plow to achieve higher reliability and robustness, as well as to comparatively evaluate them on a single field-deployed platform.

   As it turned out, the actuation mechanism and vehicle dynamics are significantly different from any of the vehicle systems concerned in the previous work in the area of vehicle automation. The blower operating conditions are safety and operational critical (i.e., large resistance forces and low tire/road friction and cornering forces), and the system is complicated with additional vehicle dynamics such as tire and snow chain effects. PATH analyzed the control problems and

investigated approaches for providing robust and safe control for blower operation.

b. Collision warning systems would be developed by AHMCT. Due to the short operating range, low speed, and need to image obstacles through dense layers of ice and snow, the requirements for the current application differ significantly from those for ASP-I and ASP-II, For example, imaging through snowbanks with varying height, density, debris, salt content, and conductivity, is expected to present significant sensing and algorithmic challenges. AHMCT would investigate various technologies to determine the best match for the current application.

c. AHMCT and PATH would jointly develop the required Human-Machine Interface (HMI), which includes a display system, as well as necessary interfaces to allow transition to and from automated control.

In 2002, the project responsibilities were divided more clearly between PATH and AHMCT for efficiency. PATH is responsible for developing a turn-key lateral control system that includes design of HMI for lateral display functions, while AHMCT takes charge in developing an obstacle detection system, the HMI for obstacle display and other functions, and optionally an alternative lateral controller. This report therefore focuses on the development of the ARP lateral control system at PATH.

1.2 Tasks and Responsibilities

The tasks in the overall ARP project consist of the following components: infrastructure and equipment, hardware and software, design and analysis, as well as report and testing. All components are needed to support the automated functions.

Caltrains leads the efforts in overall project management and coordination, infrastructure installation and snowblower acquisition, as well as field test support and performance evaluation. PATH is responsible for automated steering system design and development. It includes system architecture design, hardware installation, sensor signal processing, control algorithms, HMI development, operator training and feedback evaluation, performance review and improvements, as well as support field tests. AHMCT is responsible for various feasibility studies that include radar based collision warning system, GPS system, and rotary protection.

In order to provide the automated steering control functions, the first prototype automated steering system was developed and tested on a conventional Kodiak Northwest single engine rotary snowplow with full hydrostatics. The system consists of the following system elements:

- Magnetic markers installed along the highway shoulder, 4 feet from the guardrail at a 4-foot spacing. Tolerances and binary coding were specified by PATH.
- Arrays of magnetometers installed on appropriate locations of the snowblower.
- Motion sensors, including accelerometers, a yaw gyro, and speed sensors.

- Steering actuators.
- Control computer

Detailed discussions of the tasks to develop the system capabilities are provided below.

Task 1 – Review Organization and Operator Needs

The project began with a thorough study of the needs of the DOT and its snowblower operators. Interviews were conducted with operators, engineers, site managers, equipment shop personnel, and others within Caltrans. This step ensures that the system development targets the true needs of the customer, and provides the right capabilities to enhance the safety, efficiency, and cost-effectiveness of the operation.

Task 2 – Develop System Specifications

Based on the results of Task 1, detailed system requirement specifications were developed by the research partners, in conjunction with the appropriate parties within Caltrans and subject to Caltrans review. The development turned out to be an iterative process since the specifications were often modified based on the trial and field test feedbacks. The resulting specifications were used to direct the development for the project.

Task 3 – System Design

Subsystem and overall system design were conducted based on the specifications obtained from Task 2. The design involved detailed design of each subsystem (sensing, actuation, power, HMI hardware, computer, electronics and software), as well as the architecture of the overall integrated system. A design review process was employed to ensure the incorporation of lessons learned from prior projects as well as feedbacks from the field tests.

Task 4 – Vehicle Automation

The development of vehicle automation consists of three basic sub-tasks: sensor development, actuator integration and controller design.

- Sensors

A number of sensing devices are installed on the snowblower in order to facilitate automated control operation. These sensors include:

- Magnetic sensors: In this project, magnetic sensors are used as the primary location sensors for snowblower steering control based on its proven accuracy and reliability under the winter operation environment. Two arrays of magnetometers are installed under the snowblower, which detects the magnetic field from the magnetic markers embedded in the roadway. Through a signal processing algorithm, the lateral position of the vehicle and information encoded in the magnetic markers are obtained from the magnetic field. The number and the locations of magnetometers to install is determined based on the requirement specifications as well as on the limitations that imposed by the configuration of the equipment (snowblower) used.

- Motion sensors: Motion sensors are installed on the snowblower for measuring vehicle accelerations and rate. Two accelerometers (for both lateral and longitudinal accelerations) and an angular yaw rate sensor are installed. However, the yaw rate sensor turns out to be the only motion sensor that is used for the lateral control.

- Steering angle sensor: In the prototype system, the steering angle measurements are obtained through measuring the position of the steering actuator. A position sensor, consisting of an encoder and a potentiometer, is installed as part of the steering actuator design in order to provide accurate measurements of the steering angle.

- Vehicle speed: Accurate vehicle speed measurements are crucial for the control of low-speed operation. Electronic circuitry that can be installed to interface the existing speed measurement mechanism was attempted; however, the results did not achieved required resolution and accuracy for the speed measurements. Investigation was conducted and new speed sensor was installed in the drive shaft to provide speed sensing on the plow. Field tests have also indicated that a speed sensor that can operate at speed at least as low as 0.3 m/s will be required.

- Brake pressure: A brake pressure sensor could be installed if it is required. However, It has been determined not to pursuit longitudinal control in this phase the project.

- GPS: GPS can be used in conjunction with the motion sensors to provide position measurements to supplement the magnetic–marker-based sensing system. AHMCT explored the feasibility of using such sensor. An automated snowblower control based on sensor fusion of position measurements of magnetic sensing and integrated GPS/INS is left for future study.

- Steering actuator

The experience and knowledge of developing automated steering vehicles has shown that the steering actuator design is an integral part of the development of any automated steering system. Moreover, the system analysis suggests that the practical limitations of the steering actuator have an adverse effect on the lane-keeping performance, especially when a look-down lateral sensing system, such as the magnetic-marker-based reference system, is employed. The bandwidth and phase characteristics of the actuator have a significant impact on the steering control design.

The configuration of the front steering actuator consists of the following components:
(1) An add-on DC motor with gear interface on the steering column that drives the existing hydraulic system;
(2) Encoders and a potentiometer installed on the motor shaft and coupled with the steering shaft, which measure the steering positions for the steering servo loop;
(3) A computer that determines the steering command to the steering motor.

A torque sensor could be installed on the steering shaft for additional flexibility in the HMI design. Due to the complexity, the sensor was not included during the design phase. Should it be needed, the function of the torque sensor can also be approximated by the

current command of the steering actuator, since the motor is a current-mode commend DC-motor.

Furthermore, although an array of LVDT could be installed on the rear steering mechanism to measure or detect the rear wheel steering position or state for the rear steering servo loop. The associated closed-loop rear steering control could be achieved using additional servo valves. However, they are not installed in the development phase of this project due to the reasons described below.

The possible steering servo loop designs are: (1) front wheel closed-loop control without the direct measured knowledge of the rear wheel location, (2) front wheel closed-loop control with knowledge of the locked rear wheel location, (3) front wheel closed-loop control with limited rear wheel movement control, i.e. use of set-point positions for left, right, and center steer of rear wheels, and (4) front and rear wheel complete closed-loop controls. Option (1) involves the most challenging controller design, and it is also the most preferred method, if it is achievable. Options (2), (3), and (4) require certain forms of rear steering position measurements; Options (3) and (4) each requires a different level of rear steering control capability.

Several design constraints favor not to install unnecessary new sensors or rear-steering actuators in the snowblower. Since the current manual rear steering is an “open-loop” steer-by-wire hydraulic system, the survivability of the exposed rear steering sensors or actuator is low. In addition, the ability of an operator to frequently adjust the rear-steering angle for different speeds and load conditions turns out to be a very crucial factor for operation. Therefore, the design focuses on Option (1).

To satisfy the performance requirements, iterations of the hardware and algorithm design are performed in the development of the steering actuator. The design procedure includes: model development and validation, control configuration design, data analysis, linear compensator design, small signal and friction analysis, hydraulic evaluation, nonlinear compensator design, benchmark and vehicle performance validation, user interface development, software interface development, and fault management development.

- Controller Design

The controller design involves the following processes: system requirement definition, control configuration determination, snowblower model development and validation, control algorithm design, control software development, fault management development and vehicle testing. The control configuration are determined by the system requirement, steering actuator configuration, snowblower dynamics, and HMI method.

The controller needs to satisfy all the system requirements under various uncertainties. The system requirements include tracking accuracy, ride comfort, and easy driver interaction; while the uncertainties include road adhesion variations, preview errors, marker installation misalignments, actuator limitations, blower load changes, speed

variations, vehicle dynamic changes, suspension modes, and all reasonable sensor and vehicle noise.

The control algorithm consists of the following elements:
(1) A steering servo adapter algorithm that coordinates controls between front and rear wheels;
(2) A high-gain robust lane-keeping algorithm that guarantees small tracking error along the magnet line;
(3) A transitional algorithm that switches between manual and automated steering.
(4) An adaptive lane-catching algorithm that provides smooth trajectories from manual steering to automated steering;
(5) A state machine that coordinates the above schemes based on the sensor signals, available road information, and maneuver demands.

Task 5 – Collision Warning
The task involving collision warning will not be discussed in this report; however a brief description is included here for completeness. The ARP proposal includes a forward Collision Warning System (CWS), which detects vehicles and other obstacles buried under the large snow build-up to be removed by the blower. While AHMCT and PATH have significant combined experiences in the application of CWS in a variety of situations, e.g., the snow environment for the ASP, the unique operating conditions of the rotary blower require innovative developments. Specific issues include low rotary blower forward speed, reduced sensor range, increased sensor accuracy and resolution, large snow build-up, and close proximity to fixed infrastructure, i.e. the guardrail. Furthermore, Imaging through snow banks with varying height, density, debris, salt content, and conductivity, also presents significant sensing and algorithmic challenges. These issues place restrictions on the CWS hardware and algorithms. AHMCT is responsible for the investigation of various sensing technologies, such as FMCW Doppler radar and surface penetrating radar, to determine the best match for the current application. Additional effort needs to be dedicated to developing the signal processing algorithms appropriate for the identified conditions and the selected sensing technology.

In addition to the sensing aspect of the CWS, the nature of the warning to the operator also needs consideration. Possible approaches are visual, audible, and tactile indication. Audible indication is expected to be difficult, given the noisy operating environment in the snowblower cab. In principle visual and/or tactile warning is preferred.

Task 6 – Human Machine Interface
Although the snowblower is automated, it is necessary to provide information to the operators so that they can supervise, make transition into or take over the automated system. Lateral position, speed, curve information, and system status are the candidate information available to the operator for the purpose of monitoring system performance and integrity. Without a proper HMI, the efficiency and safety of the system are at risk. This is especially true during whiteout and deep snow conditions when the operator has difficulty observing a system fault.

The ultimate design criterion is “simple and clear”. Of particular concern are workload and driver/machine control. Operator overload will result in high stress, while underload may lead to driver inattention. The process for an operator to override or adjust automatic control must be safe and intuitive. In addition, the frequency of transitions between automated and manual control also influences the design requirements. The HMI design started with conducting interviews with operators and other DOT personnel, as well as analyzing the test site configuration and operations.

The HMI development began with an integrated approach that considers an “operator” as a part of the system, especially during transitions. Upon each modification, the snowblower operators were invited to evaluate the modified HMI. Their comments, as well as the observations of the research staff, were used to produce a HMI specific to snowblower operation.

Following implementation, data are collected to examine the operator-display-activation interaction. This data assists additional improvements and overall system validation.

Task 7 – Vehicle Integration

A snowblower provided by Caltrans was instrumented with a power system, sensors, the steering actuator, and computers. Work of integration typically occurred during the summer, so that the blower would be ready for the winter testing when the infrastructure is available. However, due to various unplanned blower hardware maintenance issues during the project period, the snowblower lost several opportunities for testing on I-80 under snow removal operations.

The control computer, including sensor and actuator I/O, software modules, and system communications, was developed using standard industrial PC hardware and the QNX Real-Time Operating System (RTOS). This system architecture and software structure has been used as the basis of the AVCSS research and development at PATH for many years. Hardware and software improvements specific to this project, such as deduced sensor spacing, low-speed sensing and control, and HMI control circuit, are the results of the design and implementation iterations.

Task 8 – Infrastructure Installation

Caltrans installed magnetic markers in the highway shoulder at 4 feet away from the guardrail (half of the vehicle width). The distance between markers is also 4 feet (1.2m). PATH designed, provided and double-checked tolerance specifications for both the lateral and longitudinal placement of the magnets. The position of markers was carefully established though survey to ensure smoothness, and binary coding was encoded in the magnetic markers to provide information needed for control. Magnets were extended beyond the length of the guardrail (15m) for an appropriate distance in each direction, in order to provide transitions between automated and manual operation. Eight sections of the guardrail were equipped with magnets for the initial feasibility operations with a total length of 1.46 km (0.9 mile) between Soda Springs and Kingvale.

Task 9 – Testing and Demonstration

Various open-loop experiments have been conducted to verify the dynamic behavior of the snowblower. These tests were designed to determine the steering responses, tire-road interaction (particularly the corning stiffness, the effects of tire chains), speed control, and braking responses. Test data collected using on-board sensors was used to verify the dynamic model, which in turn is used for the design of the controller.

The ARP system was finally tested in the Advanced Winter Maintenance Testbed around the Donner area. The testbed was originally developed by Caltrans for the ASP project.

The various subsystems developed for the ARP were tested individually and as a system. Subsystem tests began in laboratory development, continued at the test track in Richmond Field Station (FRS), and ended with tests in the snow environment at the Kingvale test track. The overall system was tested in the deployment environment along I-80. Quantitative and qualitative measures are used. Quantitative measures include control accuracy, and transition speed. Qualitative measures are obtained by interviews with operators that include impressions of ease-of-use, HMI design, operator comfort in automated operation and during transitions to and from automated mode.

Task 10 – Data Analysis and Reporting
The members of the research team provided quarterly reports at the end of each fiscal quarter. These reports describe tasks initiated and/or completed, percentage progress to date, funds and percentage expended for current fiscal year as well as the overall project, detailed description of tasks for the quarter, and anticipated work for the following quarter. In addition, any problem areas related to the previous or subsequent quarter are included as part of the quarterly reports. This final report presents details of the system development process, background technical discussion, details of the system design hardware and software, and results of quantitative and qualitative tests.

1.3 Accomplishments and Milestones

The major tasks related to the Automated Snowblower that have been accomplished are listed as follows:

1. Completed system design (2002)
2. Installed, tested and refined sensors and signal processing algorithms (2002-2004)
3. Installed, developed and tested the steering actuator, including its hardware, software and servo algorithm (2002-2003)
4. Developed, tested and refined automated control algorithms (2002-2004)
5. Developed, installed, tested, and refined operator interface components including sounds, display and switches (2003-2004)
6. Successfully conducted operator training and interviews (2003-2004)
7. Successfully demonstrated the first prototype system to stakeholders (California, Nevada and Alaska) at Kingvale yard with simulated guardrails (10/17/2003)
8. Tested and refined the second prototype “turn-key” system along guardrails on I-80 under no-snow conditions (12/2004-3/2005)
9. Successfully conducted the first operational trial along guardrails on I-80 under heavy snow condition (3/22/2005)

The major milestones that have been reached are:

6/25/02: Snowblower reached Richmond Field Station ready for system installation

10/30/02: First prototype hardware and software drivers installed

12/17/02: First prototype control and operator interface system installation ready; snowblower left Richmond Field Station

3/6/03: Snowblower arrived at Kingvale; initial system calibration started at Kingvale yard

4/3/03: First prototype system ready; performance requirements are achieved at Kingvale yard

4/29/03: Successfully conducted first operator trials at Kingvale yard with simulated guardrail; survey results showed very positive responses from the operators

10/17/03: Successfully conducted automated snowblower demonstration at Kingvale yard for various stakeholders (California, Nevada and Alaska)

3/22/05: Successfully conducted initial field tests along I-80 guardrails under winter operational conditions.

Various unplanned blower hardware maintenance issues affected opportunities for winter field tests on I-80. The following is a time line of these issues:

- Head gasket repair: 2001-2002
- Blower head removal and modification: from after winter 2001/2002 to 11/02
- Hydraulic circuit breakdown: 9/02 – 10/02
- Warranty repairs: 12/02 – 2/03, 11/03 – 12/03

2. Requirements and Solutions

This section provides formulation of the snowblower steering control problem, as well as a brief description of the solution.

2.1 Requirement Formulation

The initial "performance requirement" from the Maintenance department seemed to suggest that it is a difficult but straightforward project: controlling a snowblower at a distance between 2 and 4 inches from the guardrail. An examination of the project objectives revealed that the success of the project would stem on the positive responses of the following questions: (1) Does the system reduce or eliminate guardrail damage caused by the blower? (2) Does the system effectively support snow removal operations? And (3) does the operator like the system and would the operator use the system? As a result, the initial requirements for the automated snowblower system were defined as follows:

- "Track" accurately along guardrail (2 to 4 inches)
- Support various snow removal operations
- Survive harsh winter environments (snow, ice, salt, water, dirt, wind)
- Simple operation procedure, tolerate operator mistake, easy to train
- Low operator distraction
- Reliable and safe automated operation

During the first winter's ride-along observation in a snowblower, the researchers soon realized that accurately controlling a 6-ton oscillatory blower head on a 20-ton vehicle along the highway shoulder dotted with potholes while pushing and blowing snow and ice was not easy! Let alone that the driver, from time to time, has to adjust the rear steering angle to compensate for various cutting load and road curvature, move the head (so-call "box") position and tilt angle to account for different road slope, inclination and resistant force, as well as change the speed from stop to go to react for various road and snow conditions. The control system must allow the operator to engage automation at ease and to switch off any time he wants. The system also needs to survive both the operator's intervention, either intentionally or unintentionally; and the environmental disturbances such as hitting a guardrail and running into an ice patch. Furthermore, during the early literature survey stage, we also found out that little research work exists in the area of snow chain effects as well as the under-damped low-speed heavy vehicle model. Nevertheless, the project goals dictated that all obstacles needed to be overcome. The system requirements were then modified to include the following additional specific items:

- Automatically compensate operator's rear steering action
- Robust against various blower head positions and the resultant front tire loading conditions
- Robust against rough and uneven road surface conditions including potholes
- Provide sufficient control at any operational speeds including stop and go
- Allow on-demand operator transitions and interventions

- Not touching the guardrail and survive the consequence should it occur

In addition, there are several specific requirements that are the results from the specific implementation with respect to either the magnetic sensing system or from the existing steering hydraulic assist and DC-motor actuator:

- Less than 2 ft of effective operation sensor range (the effective range starts from magnetic sensor first "sees" the magnets till when the blower head "touches" the guardrail – Fig. 2.1 for illustration)
- Nonlinear and under-powered steering hydraulic assist (main nonlinearities: under-power assist at very low speeds, insufficient assist when stop, large variation in hydraulic assist power when other hydraulic components requires power (*full hydrostatics*)

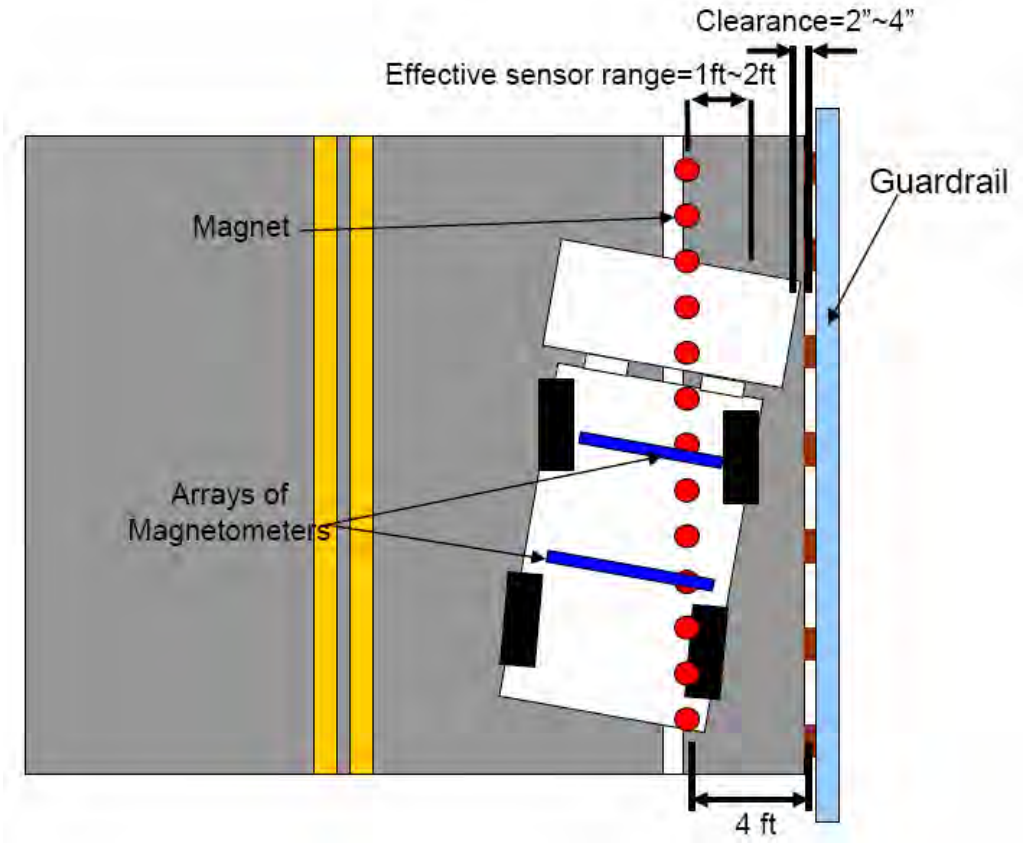

Figure 2. 1 Illustration of snowblower crab angle and sensor range

Since the snowblower used for this study still performs normal winter snow removal operations, several design constraints were imposed based on the considerations in safety, operation and maintenance. First of all, the installation and application of any components to the snowblower, especially the steering actuator, should not affect normal driver manual operations, nor should it imperil or degrade performance of any existing vehicle components. Second, unless a rear steering sensor can survive the harsh winter exposure, it is not recommended. The rear wheel is actuated by open-loop hydraulic valves. Driver controls the rear steering using a "joy-stick" type controller with 7 LED's, each connecting to a contact switch, indicating the location of the rear wheel angle. Since

getting precise position reading by measuring flow rates of transmission fluid and installing sensors on the linkages next to rear wheel are both difficult. High-precision position sensors, such as rotary position encoder and linear transducer, are not encouraged to mount on the rear steering mechanism that can be potentially encapsulated in an ice ball. Finally, since the operator cuts in and out of the guardrail operation, the only reliable information that is available through the magnetic pattern is the indicators for left/right shoulder, and for the approaching of the "end of magnets." Typical preview road information such as curvature, super-elevation will not be available to the controller.

Many critical tasks were performed during the development of the automated snowblower under the above limitations and requirements (see Fig. 2.2 for a list of ARP development tasks). It started with the above problem and requirement formulation; followed by modeling and basic controller design. A system configuration were then designed and rehashed based on the analysis results and the operational observations. Hardware and software were developed that included sensor installation and signal processing coding, actuator installation and servo controller design, computer setup and circuit implementation. Human machine interface (HMI) was then developed and instrumented based on operational analysis, operator feedback, and field tests. Safety-critical issues were designed and reviewed that included robust control, fault detection, failure mode analysis, warning system and redundancy. Finally, various tests were conducted to evaluate and refine the system design.

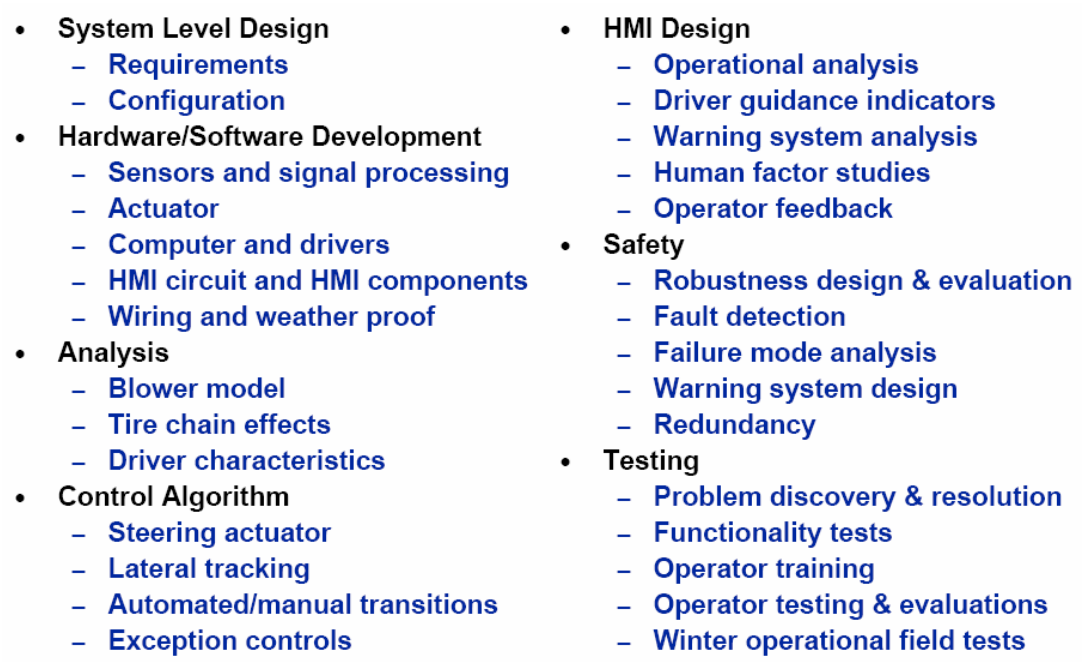

Figure 2. 2 ARP Tasks

2.2 Solution Description

To date, no automated precision steering control system has been designed to operate under such harsh winter conditions subject to extreme external disturbances. And not

only that, but designed also with extensive un-modeled dynamics, under severely "non-ideal" actuating limitations, and requiring transparent "interfacing" with an average operator performing multiple tasks. As the project proceeded, especially under the short time period the snowblower was available to the design team, the researchers soon realized that mathematic models often do not portray certain important real characteristics accurately. The design of this automated system is a combination as well as iterations of "design methodology" and "design synthesis". It requires continuously evolving "solutions" to all of the following elements: problem definition, requirement specification, system configuration, hardware installation, software architecture, control algorithms, human machine interface, fault detection and management, and testing and evaluation.

The first prototype automated control was a truly "add-on" system with the following components, as shown in Figure 2.3, added to a conventional Kodiak Northwest single engine rotary snowplow with full hydrostatics. A computer with a data acquisition unit that processes information and determines control and guidance actions is the "brain" of the system. The lateral positioning system consists of two sets of magnetometers, one underneath the front axle, and the other one mounted in between the front and rear wheels, measuring the field strength of magnetic markers installed under the roadway. A DC motor attached to the steering column with angular sensors is the steering actuator. A yaw gyro and an axle speed sensor measuring vehicle yaw rate and speed are used as the supplementary sensors during extremely low speed operations. Finally, a Human Machine Interface (HMI) unit (or Driver Vehicle Interface (DVI) unit), consisting of the local electronic circuit, a toggle switch, LED displays and an audible device, interfaces with the operator with essential information and commands for automation.

The key software components that collectively constitute the necessary intelligence of the automated system are:

- Reliable signal processing algorithm that provides consistent location estimates despite large vehicle movements and enormous environmental irregularities
- Smart steering servo that firmly carries out the steering command under highly nonlinear mechanical characteristics and unpredictable disturbances
- Robust high-gain "lane-keeping" controller that accurately follows the "magnets" under all operational conditions even without slope and curvature information
- Adaptive exception controls that cope with any imaginable "abnormal" scenarios such as sudden potholes, guardrail touching, actuator saturation, unknown limit cycle oscillations, operator mistakes or interventions
- A dependable "transition" controller that executes "on-demand" transitions between automated and manual control under all operational conditions
- A simple and transparent HMI (DVI) that facilitates clear operator state awareness and prompts timely and correct responses under both normal and emergency scenarios
- A fault detection and management system that detects system irregularities and provides a warning while at the same time conducting preventive actions

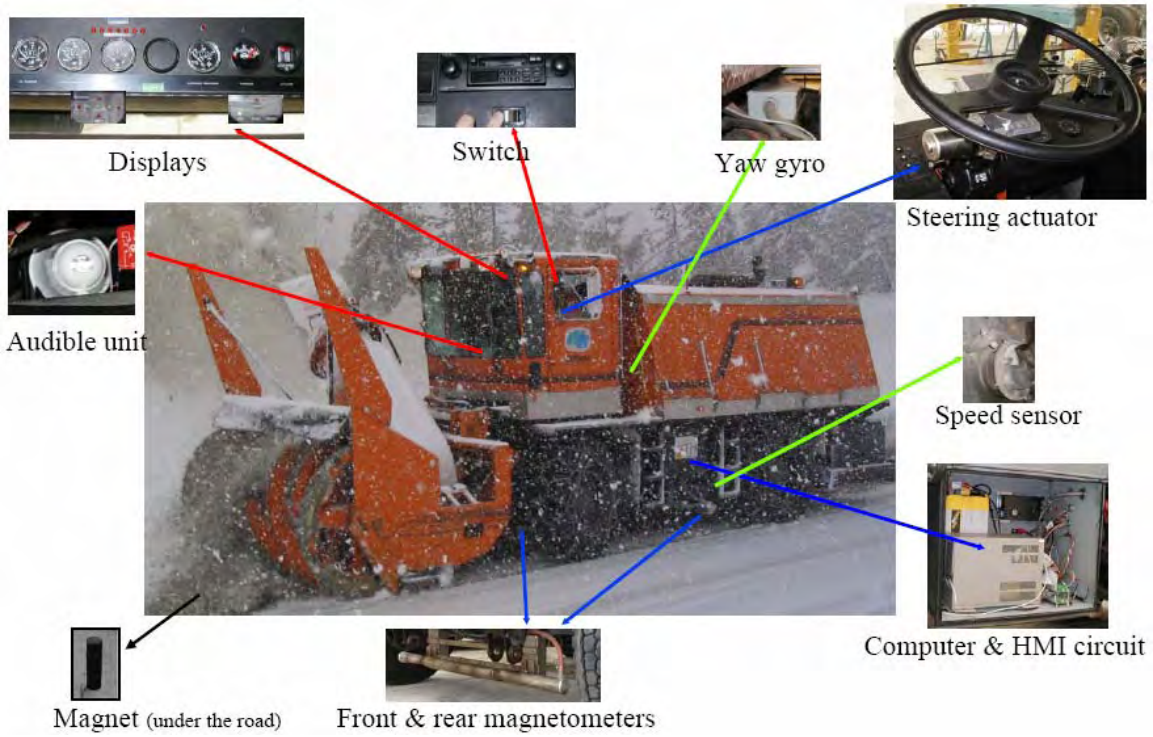

Figure 2. 3 Automated Snowblower: prototype system components

The effectiveness of the design is evident, for example, in the HMI (DVI) system. It consists of the following four elements:

- A transition toggle switch, located under the radio, allowing the operator to switch the system on and off
- The status LED's, located underneath the air filter indicator, displaying the system's current status (Figure 2.4)
- The guidance LED's, located underneath the voltmeter, displaying the position of the tip of the blower head with respect to the guardrail
- An audible unit that produces the following three different sounds: acknowledgment (transition to auto steering), end of magnets (approaching end of guardrail), and emergency (take over control now)
- An emergency button, located on the console just right to the operator right hand, allowing the driver to "kill" the steering actuator at any time.

The core of this HMI (DVI) is four status LED's: GREEN when the system is ready for transition; WHITE when it is under driver's control; BLUE when it is automated; and RED when there's a problem. It identifies the four key pieces of information for automation: system on or off, ready for transition or not, current state of automation, and fault or not. The operator simply approaches the guardrail the same way as he always does. A separate supportive guidance LED's displays the current "tip location" of the blower head. Once the blower is within its appropriate crab angle range, the system is ready to transition to automation, and the GREEN LED will be lit. Once the GREEN status LED is on, the driver can switch to automated control any time he wishes by pushing down the AUTO switch. With a soft acknowledgement sound, the BLUE status

LED will then be lit, indicating the blower is now under automated steering control. The operator can resume manual control by pushing the MANUAL switch or by overriding the steering wheel at any time. The flashing RED LED, with an emergency sound beeping simultaneously, signals the driver to take over control immediately.

Figure 2. 4 HMI display: Status lights and operations

3. Software Architecture and Description

3.1 Software Architecture

The software architecture consists of a set of processes running on the control computer (a six slot industrial computer) and communicating through the Publish/Subscribe database. All of the software is written in C and runs on the QNX real-time operating system. The functions of the real-time software are to process the signals obtained from the various sensors, give control commands to the steering actuator and send display parameters to the Driver Vehicle Interface. To achieve those functions, the real-time software is structured as (as shown in Figure 3.1):

- device drivers
- database manager
- steering controller

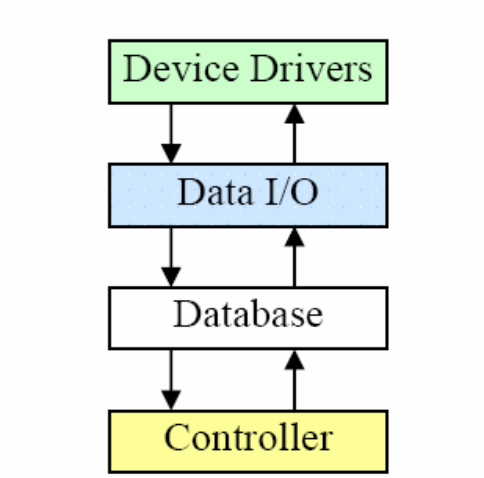

Figure 3. 1 Software architecture relationship

The computer is decked with four cards:

- PC-TIO-10: for timers inputs and digital I/O
- AT-AO-6: for analog outputs and digital I/O
- AT-MIO-64E-3: for timer inputs, analog inputs and outputs, and digital I/O
- EIC-325: encoder interface card from Industrial Microcomputers Systems

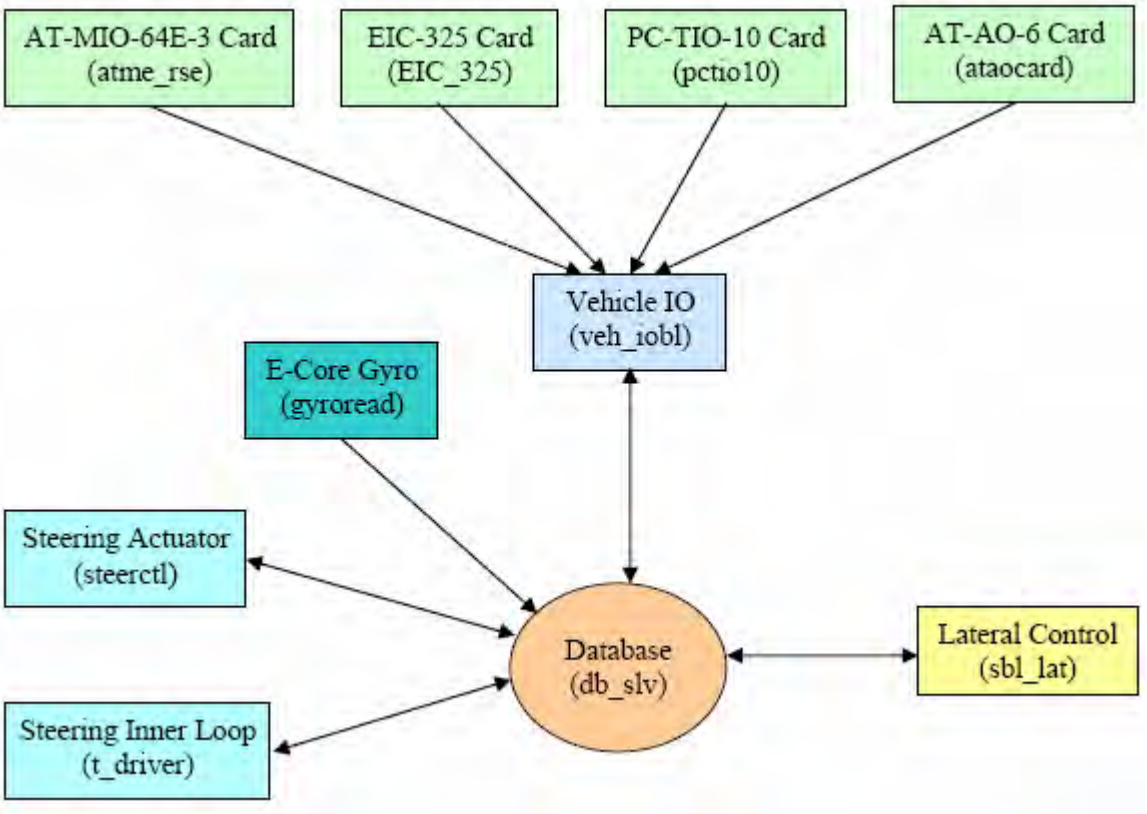

Figure 3. 2 Software architecture with respect to database

Ten processes are running together on the control computer. The database runs at priority 25, the highest among all the processes. Device drivers run at priority 19; since hardware interrupt handlers are part of the device drivers, they inherit their priority. The lateral control process runs at priority 18 because it needs to read the magnetometer channels every 2 msec. The steering actuator inner loop is running at priority 17 simply because the processing speed of computer processor used is too slow (otherwise the steering controller becomes unstable because of the time delay). The vehicle input/output process runs at priority 15. All other processes run at priority 10, which is the default. Regarding scheduling, the static-priority scheduling policy of QNX is used. Each process is assigned a priority, from 0 (lowest) to 31 (highest). At any time, a highest-priority process is chosen to run among the ready (i.e. non blocked) processes

Below is a table of the processes as well as their output variables written to the database and the process priorities.

Table 3.1 Processes, output variables and priorities

Process name	Process description	Output variables	Process priority
db_slv	Database manager	-	25
atme_rse	Interface to AT-MIO-64E-3 card	-	19

Process name	Process description	Output variables	Process priority
EIC_325	Interface to EIC-325 encoder interface card	-	19
pctio10	Interface to PC-TIO-10 card	-	19
ataocard	Interface to AT-AO-6 card	-	19
veh_iobl	Vehicle Input Output	long_input lat_input_front_mag lat_input_rear_mag lat_input_sensors	15
gyroread	Interface to E-Core gyro	gyro	10
steerctl	Steering actuator	lat_output lat_steer_input	10
t_driver	Steering actuator inner loop	lat_steer_output lat_control_input	17
sbl_lat	Lateral control	lat_control_output lat_dvi_output lat_heartbeat_output	18

The database variables exchanged by data I/O and control processes are created and stored in the database. There is a single producer for each variable, that is, each variable is updated by only one process, though it can be read by many processes.

3.2 Software Description

Lateral Control Software

The lateral control software gets a trigger from the front magnetometers, i.e. every 2 msec, and reads the following six structures from the database:

- front magnetometers (DB_LAT_INPUT_FRONT_MAG)
- rear magnetometers (DB_LAT_INPUT_REAR_MAG)
- steering actuator inputs (DB_LAT_CONTROL_INPUT)
- other lateral sensors (DB_LAT_INPUT_SENSORS)
- vehicle speed (DB_LONG_INPUT)
- yaw rate from the gyro (DB_GYRO)

For debugging purpose, it also reads:

- output from the steering actuator inner loop (DB_LAT_STEER_OUTPUT)
- output from the steering actuator driver (DB_LAT_OUTPUT)

The lateral control software (see Figure 3.3) writes the three following structures to the database:

- lateral outputs for the steering actuator (DB_LAT_CONTROL_OUTPUT) every 2 msec
    - steering actuator mode (0=manual, 1=auto high, 2=auto low)
    - steering command in deg
    - steering actuator control mode
- computer heartbeat (DB_LAT_HEARTBEAT_OUTPUT) every 50 msec
- DVI (HMI) outputs to the LEDs and speaker (DB_LAT_DVI_OUTPUT) every 50 msec

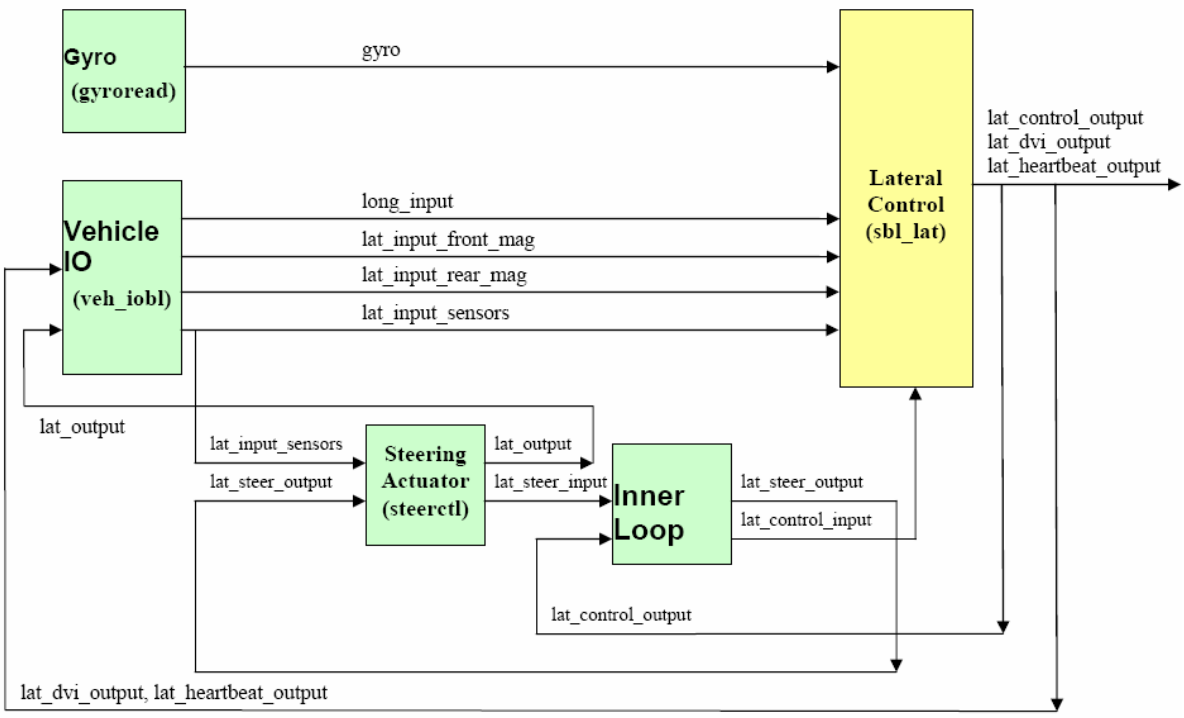

Figure 3. 3 Lateral control software

The DVI/HMI outputs are of 3 kinds:

- lights to the control DVI/HMI
- lights to the guidance DVI/HMI
- sound to the speakers

Figure 3. 4 Status DVI/HMI

The control DVI/HMI (see Figure 3.4) has 4 lights:

- control manual (white LED on)
- control auto (blue LED on)
- control warning (red LED on)
- control ready (green LED on)

The guidance DVI/HMI (Figure 3.5) has 7 lights:

- guidance left (if the snowblower is on the far left side of the magnets)
- guidance center left (if the snowblower is on the left side of the magnets)
- guidance center (if the snowblower is on top of the magnets)
- guidance center right (if the snowblower is on the right side of the magnets)
- guidance right (if the snowblower is on the far right side of the magnets)
- guidance up (LED on if speed is too low)
- guidance down (LED on if speed is too high)

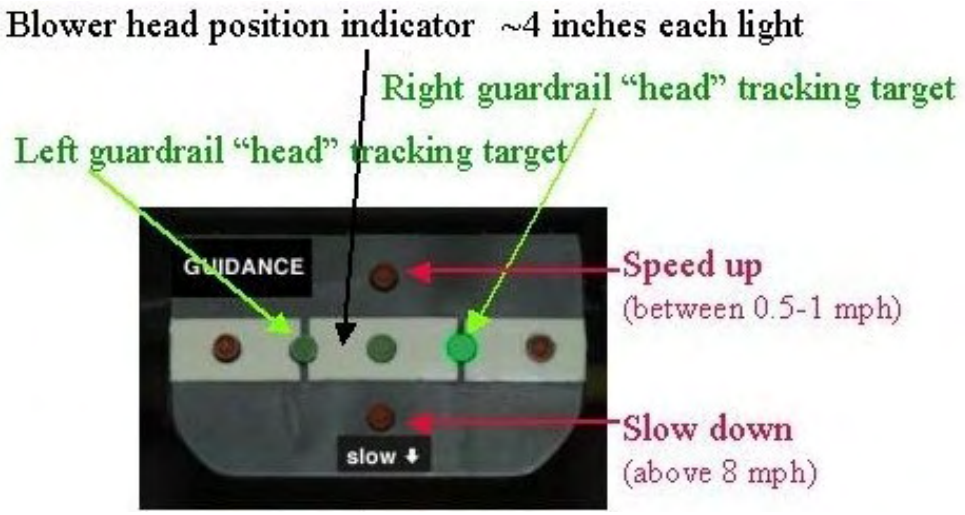

Figure 3. 5 Guidance DVI/HMI

Three different sounds are sent to the speakers:

- audible emergency (when there is a fault)
- audible takeover (when end of magnets, i.e. end of guardrail)
- audible acknowledge (transition to auto steering)

7 kinds of fault are detected:

- yaw rate sensor fault
- steering actuator sensor (potentiometer) failure
- HMI/DVI fault (not used)
- magnetometer (rear magnetomer health signal) or speed sensor fault
- steering actuator fault (motor failure, power off, command failure, driver failure, encoder failure or startup failure)
- system fault (if we have a continuous spike under automated control)
- multiple faults (if we have 2 faults of more)

Only the 4 last faults require emergency control.

Lateral Source Code

The main file for lateral control is sbl_main.c. The compilation command is "make exec/sbl_lat", to be executed from the "lat" directory. Below is the list of the main files and they associated functions (see also Figure 3.6):

- hst_cont.c: steering controller
- sbl_code.c: decoder calls for all sites
- sbl_db.c: database communication
- sbl_dvi.c: DVI/HMI controller
- sbl_func.c: basic functions
- sbl_i80.c: decoder for I-80 (shoulder side and end of magnets)
- sbl_mark.c: magnetometer signal processing
- sbl_obs.c: observer and fault detection
- sbl_stat.c: state machines
- sbl_trajc.: trajectory planning

and the associated header files are:

- nat.h: definition of the structures (front and rear magnetometers, and DVI)
- constant.h: definition of constants used in different files
- sites.h: definition for the different sites (RFS, Crows Landing and I-80)

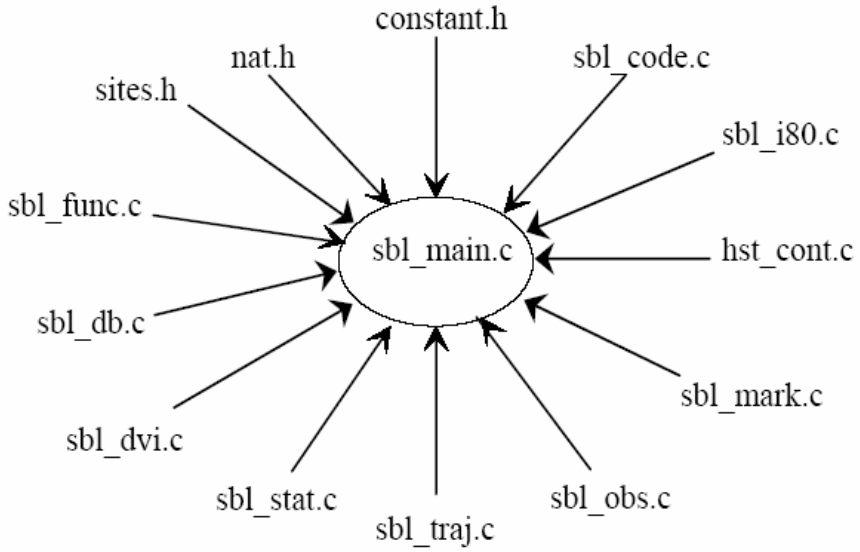

Figure 3. 6 Lateral source code

The magnetometer calibration tables are in the "mag_tab" directory. The calibration was performed for a ceramic type magnet, for the 6 sensors at the front of the snowblower and the 7 sensors at the rear of the snowblower. The low and high heights for calibration chosen were 7 and 11 inches (0.18 and 0.28 m) for the front magnetometer bar, and 7.5 and 11.5 inches (0.19 and 0.29 m) for the rear one. The magnetometers are

installed as follows, with a total sensor range of [-0.84 cm, 0.84 cm] on the front and [-1.1 m, 1.1 m] on the rear.

See Figure 3.7 for the front magnetometer bar configuration; and Figure 3.8 for the rear magnetometer bar.

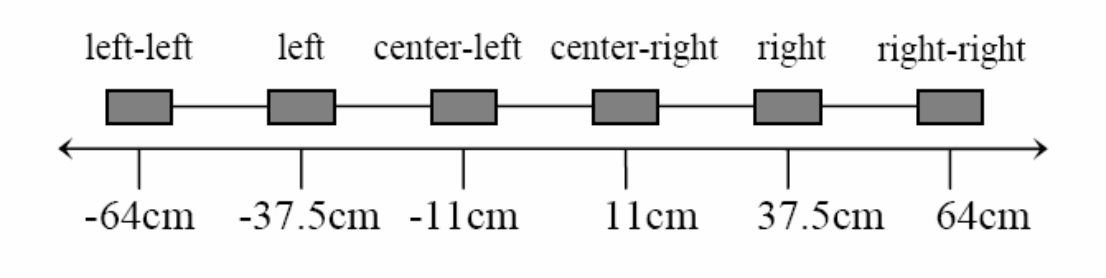

Figure 3. 7 Front magnetometer bar configuration

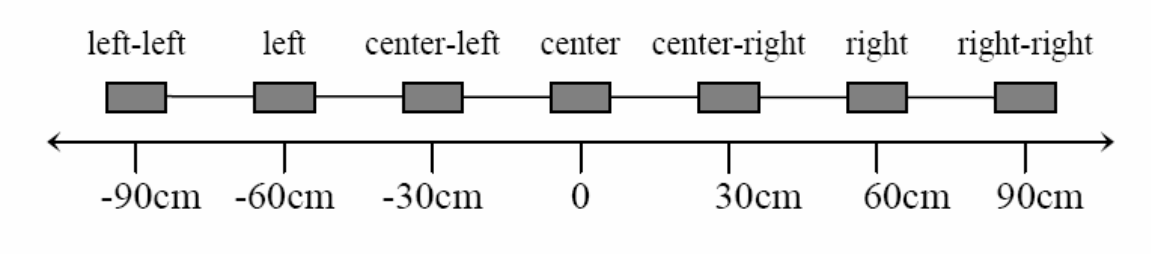

Figure 3. 8 Rear magnetometer bar configuration

The magnetometer calibration files are generated automatically using the calibration software. The magnetic calibration tables consist of vertical and horizontal magnetic strength data that were stored during calibration process. Such table can be plotted as magnetic strength data at the low and at the high calibration heights as discussed above. See Figure 3.9, 3.10 and 3.11 for plots of one such table. The snowblower magnetometer calibration files consist of the following ".h" files:

- t_cer_fll.h: table for the front most left magnetometer
- t_cer_fl.h: table for the front left magnetometer
- t_cer_fcl.h: table for the front center left magnetometer
- t_cer_fcr.h: table for the front center right magnetometer
- t_cer_fr.h: table for the front right magnetometer
- t_cer_frr.h: table for the front most right magnetometer
- t_cer_bll.h: table for the rear most left magnetometer
- t_cer_bl.h: table for the rear left magnetometer
- t_cer_bcl.h: table for the rear center left magnetometer
- t_cer_bc.h: table for the rear center magnetometer
- t_cer_bcr.h: table for the rear center right magnetometer
- t_cer_br.h: table for the rear right magnetometer
- t_cer_brr.h: table for the rear most right magnetometer

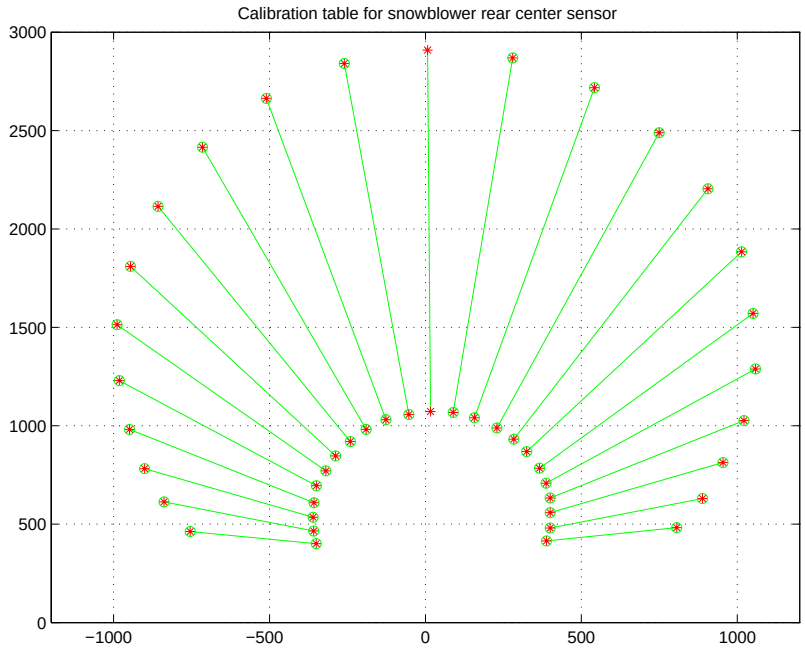

Figure 3. 9 Calibration table for snowblower rear center @ 2 cm division calibration

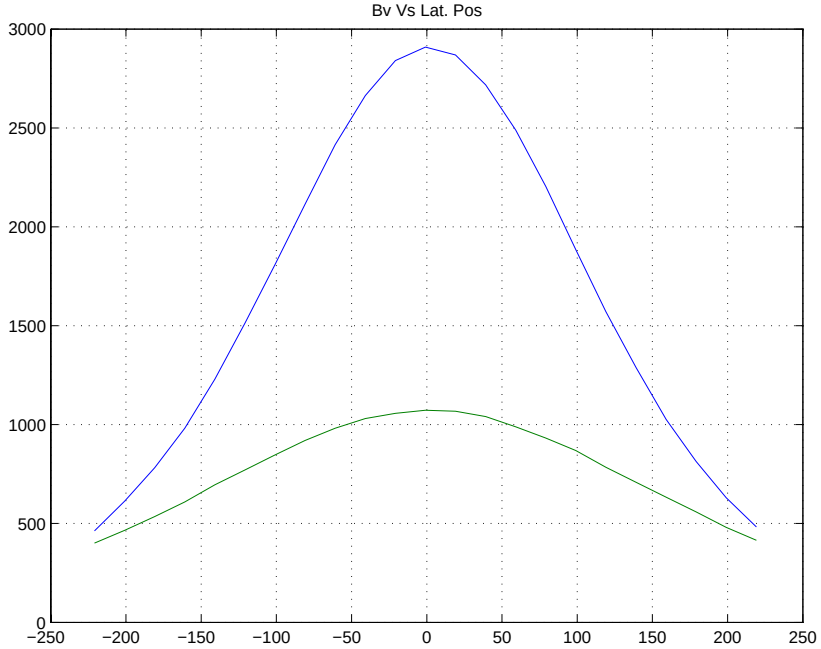

Figure 3. 10 Calibration table for snowblower (vertical strength vs lateral position)

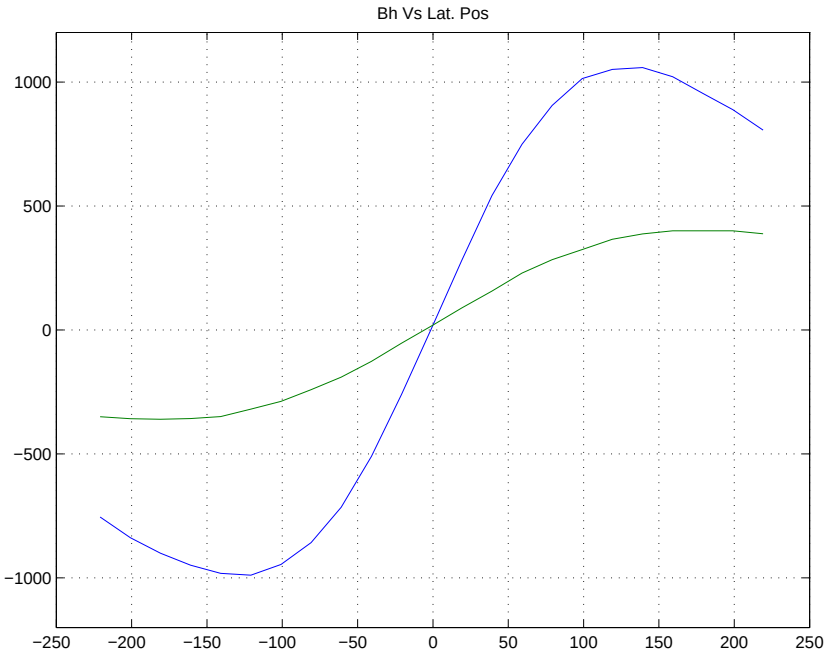

Figure 3. 11 Calibration table for snowblower (horizontal strength vs lateral position)

Lateral Control Algorithm

The detailed operational procedure of the algorithm of the lateral control module is described as follows:

1. Get command option and set internal flag accordingly.
2. Call all initialization routines, which include:
   - initialization of testing site and decoder
   - initialization of observer, state machine, controller
   - initialization of magnetometer signal processing
   - initialization of database
3. Set priority of the program to 18
4. Set exit point
5. Wait from trigger from database
6. Read database to retrieve sensor measurements
7. Process front and rear magnetometer signals
8. Decode the markers for shoulder side and end of magnets code
9. Call observer for vehicle angle and road curvature
10. Determine which side the blower is tracking on
11. Do fault detection
12. Call finite state machine to transition between different operational states
13. Call finite state machine to switch between different controller states
14. Determine DVI (HMI) states
15. Call steering controller and switch controller mode through finite state machine
16. Write steering command, DVI (HMI) outputs and heartbeat to database
17. Save lateral data to file
18. Goto step 5

The transition state machine in Step 12 above has 8 states as shown in Figure 3.12.

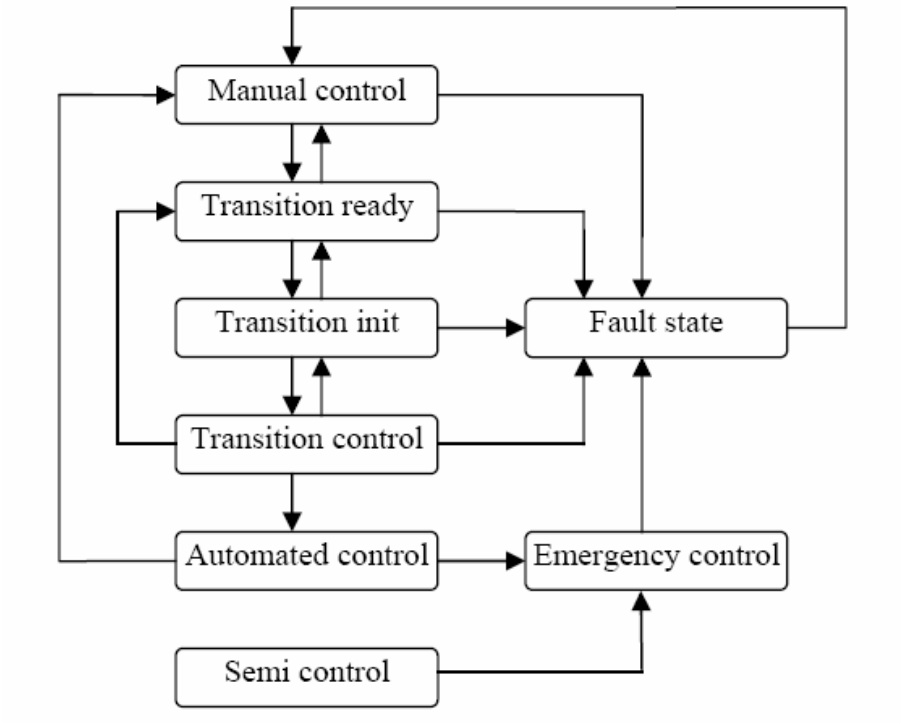

Figure 3. 12 Transition state machine

Furthermore, the control state machine in Step 13 above has 4 states as shown in Figure 3.13.

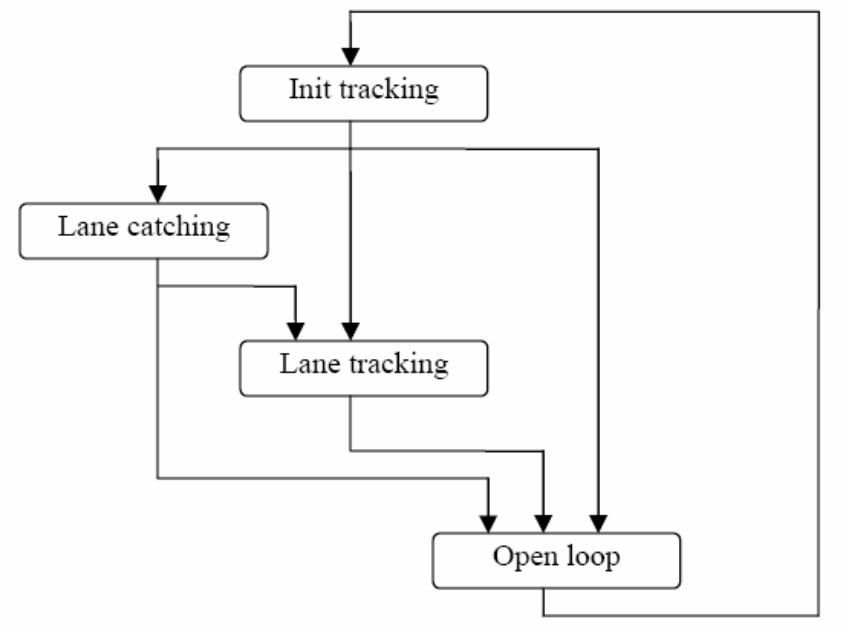

Figure 3. 13 Control state machine

Software operation procedure

When the snowblower is turned on (ignition on), all the processes are automatically started using the script file “phstart” in /home/blower/test. On the other hand, to start the lateral control manually, the operating procedure is the following:

1. Turn on the ignition switch of the snowblower and the on switch for the PC in the rear of the cabin.
2. Start the control menu by logging in on the laptop as "blower" with the password “avcs”. Go to QNX Photon and get three windows: use one to run the startup menu, and two to do any debugging.
3. Change to the test directory by typing "cd test".
4. Run the menu by typing "avcs". The menu looks like this:
    1. Show configurations
    2. Run device drivers
    3. Vehicle → MENU
    4. Controller & Site → MENU
    5. Run lateral control
    6. Plot lateral data
    7. Plot DVI data
    8. Stop device drivers
5. In general, the control menu works by:
    - using numerical options to run items.
    - the letter ‘q’ to quit.
    - pressing the return key to return to a menu after the menu task is complete.
    - text entry to change parameters.
6. **Menu item #4**: check the controller and the site.
    1. Set lateral controller
    2. Show lateral controller configuration
    3. Change lateral controller configuration
    4. Show site location
    5. Change site location

    The site should be set to 2 for I-80 at Donner Summit.
7. **Menu item #5**: run the lateral control. The device drivers have already been automatically started. The lateral control can be terminated by pressing the return key.
8. **Menu item #6**: plot lateral data. It contains 4 windows with 4 graphs each:
    - window 1:
        - measured front lateral measurement before and after trajectory planning (m)
        - measured rear lateral measurement before and after trajectory planning (m)
        - measured and desired steering wheel angle (deg)
        - computed head position of the blower (m)
    - window 2:
        - vehicle velocity (m/s)
        - magnet spacing (m)
        - estimated vehicle angle (rad)
        - estimated road curvature (1/m)

- window 3:
  - transition state
  - steering actuator status and mode
  - controller state
  - gyro rate (deg/sec)
- window 4:
  - computed vehicle travel angle (rad)
  - desired and sent steering torque
  - mode
  - clutch state and fault mode

4. Magnetic Lateral Sensing

The development of a reliable and accurate lateral referencing system is crucial to the success of the lateral guidance system for any steering guidance and control systems of heavy vehicles, let alone when such vehicle is under severe weather, as well as large road and load variations. Since the snowblower steering control system operating along guardrail has very strong accuracy requirements as described in Section 2, the accuracy when snowblower is operating at a very close distance to the guardrail was used to set the benchmark accuracy for the magnetometer sensor design for the snowblower. For any precision steering/lateral control system, the accuracy requirement for the lateral sensing system is directly proportional to the required lane tracking accuracy. The desired tracking accuracy tolerance is set to be no more than 10 cm; such tracking tolerance under large disturbances and uncertainties implies the need for a high gain control system. The lateral sensing accuracy requirement was set to be at about 1 centimeter based on (a) it is 1/10 of the maximum tracking tolerance; and (2) it is half of the smallest operational distance (2cm) to the guardrail. The assumption also include that the installation and measurement accuracy are randomly and evenly distributed along the correct position.

PATH has proposed and developed a lateral referencing and sensing system that is based on the magnetic markers embedded under the road to provide the lateral position and road geometric information. The automatic steering guidance system based on such technology provides the control system with the following two fundamental pieces of information: the vehicle position with respect to the roadway, and the current and future road geometry. Two arrays of magnetometers, one located just under the front axle and the other at about mid-point behind the front and rear axle.

Extensive development and experiments have been performed on magnetic marker-based lateral sensing systems for many PATH vehicles equipped with automated steering control. The vast knowledge available about this lateral sensing technique as well as its high reliability under winter operational conditions was two of the primary reasons that this technology was first chosen to support the snowblower automation. Other positive characteristics of this lateral sensing technique include good accuracy (better than one centimeter), insensitivity to weather conditions, and support for binary coding. The requirement of modifying the infrastructure (installing magnets) and the inherent “look-down” nature (the sensor measures the lateral displacement at locations within the vehicle physical boundaries, versus look-ahead ability) of the sensing system are two known limitations of this technology. The principle idea for this sensing system is straightforward. Magnetic markers are installed under the roadway delineating the center of each lane or any other appropriate lines for the specific applications. Magnetometers mounted under the vehicle sense the strength of the magnetic field as the vehicle passes over each magnet. Onboard signal processing software calculates the relative displacement from the vehicle to the magnet based on the magnetic strength and the knowledge of the magnetic characteristics of the marker. This computation is designed to

be insensitive to the vehicle bouncing (e.g., heave and pitch) and the ever-present natural and man-made magnetic noises.

Furthermore, the road geometric information, such as road curvatures and super-elevation can be encoded as a sequence of bits, with each bit corresponding to a magnet. The polarity of each magnet represents either 1 (one) or 0 (zero) in the code. In the snowblower operations, only four kinds of information are coded: right-side or left-side guardrail, end-of-magnets, begin-of-bridge. No curvature information is coded. The basic reason is to ensure a short enough magnetic code length that the snowblower can start tracking the guardrail as soon as it "sees" the magnets. In our case, the snowblower knows the direction of the guardrail within three magnets. In addition to the lateral displacement measurement and road preview information, other vehicle measurements such as yaw rate, lateral acceleration, and steering wheel angle may also be used to improve the performance of such a lateral guidance system.

4.1 Magnetic Noise Effects

Four major noise sources are usually present in the magnetic signal measurements in a typical vehicle operational environment: earth field, local magnetic field distortion, vehicle internal electromagnetic field, and electrical noise.

The most frequent external disturbance is the ever-present earth's permanent magnetic field, which is usually on the order of 0.5 Gauss. The value of the earth field measured by the magnetometers on the vehicle depends on the location of the vehicle on earth as well as the altitude and orientation of the vehicle. Although the earth magnetic field usually changes slowly, sharp turns and severe braking can quickly change the field measurements along the vehicle axes.

The most serious noise problems are caused by local anomalies due to the presence of roadway structural supports, reinforcing rebar, and the ferrous components in the vehicle or under the roadway. Underground power lines are another source of such local field distortion. Rebar or structural support usually creates a sharp change in the background magnetic field and sometimes is difficult to identify. Most signal processing algorithms will have some difficulty recovering from such sharp distortions. The ferrous components in the vehicle, on the other hand, can be isolated as long as their locations are fixed with respect to the magnetometers, or are located at a significant distance from the sensors.

A third source of noise comes from the alternating electric fields generated by various motors or rotating permanent magnets or magnetized materials operating in the vehicle. These rotating "magnets" may include alternator, fan, electric pump, steal belts inside tires, compressor and other actuators. However, their effects vary according to the rotational speed and distance from the magnetometers. The higher the rotating speed, or the farther it is placed away from the magnetometers, the less the resultant noise becomes. Sometimes modest changes in sensor placement can alter the size of such disturbances.

The last common noise source arises from the electronic noise in the measurement signal itself. Such noise can be created by the voltage fluctuations in the electrical grounding or from the power source. It can also be a result of poor wiring insulation against electromagnetic disturbances. Usually, the longer the wire, the higher such noise. Although low-pass filtering can reduce the magnitude of such disturbances, noticeable degradation of the magnetic sensor signal process algorithm occurs when such noise level exceeds 0.04 Gauss. Digital transmission of magnetic field measurements or local embedded processor is two possible approaches that can significantly reduce such noise.

4.2 Tire-induced Magnetic Noise

One less-common magnetic noise observed in the snowblower is the tire-induced magnetic noise. Such noise typically appears as alternating magnetic fields from the magnetized steel-belted tires. Magnetic field strengths have been measured as a function of frequency directly at the tire rotation. Measurements at the tire showed field strength up to 1 Gauss (100 microTesla).

To ensure such magnetic noise does not affect the accuracy of the lateral measurements. Before a new magnetometer sensor bar can be installed on the snowblower, PATH has constructed a temporary wooden magnetometer bar that can be "strapped" to the snowblower to investigate the magnetic noise effect resulted from the magnetized rear tires. For example, before mounting the rear magnetometer bar, four different sensor bar locations were tested: at locations 13, 19, 25, and 31 inches to the rear tires; and all at 10 inches above the ground. Figure 4.1 shows two examples of the magnetic field interference characteristics from the magnetized rear tires. The left-most and right-most sensors were chosen as examples because they are the closest to the rear tires and hence have the most noise impact. As can be observed in Figure 4.1, the right-most sensor exhibits the strongest interference from the tire magnetic field; and the further away the sensor, the less the interference. Moreover, the magnetic field measurement resulted from the "noise" of the rear tire can be as high as 200 mV (1V=0.67G) peak to peak at a distance of 13 inches to the tire rim; a 10 folds noise increase to the nominal 20 mV static noise of the magnetometers. Figure 4.2 shows the tire magnetic noise effect (peak-to-peak value) to the 3 right magnetometers with respect to various magnetometer sensor bar locations. It concludes that the sensor bar would requires at least 19 inches distance from the tire rim in order to has a noticeable reduction of the tire magnetic interference.

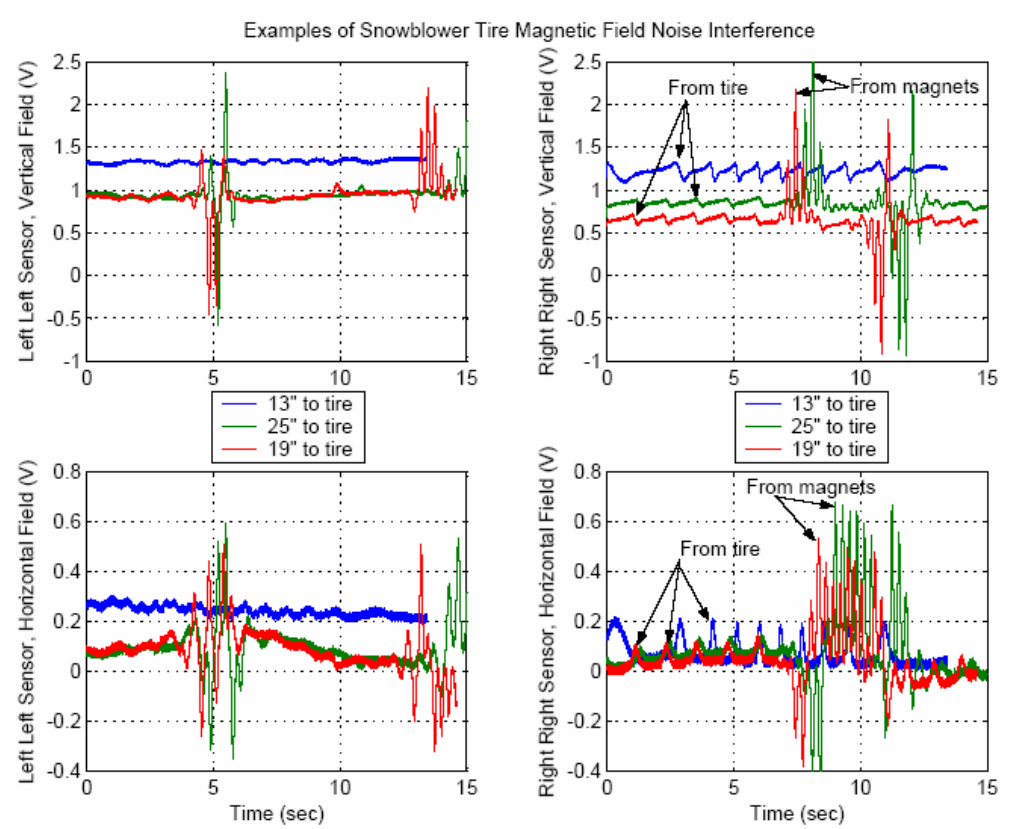

Figure 4. 1 Examples of Snowblower magnetic field noise interference from tire

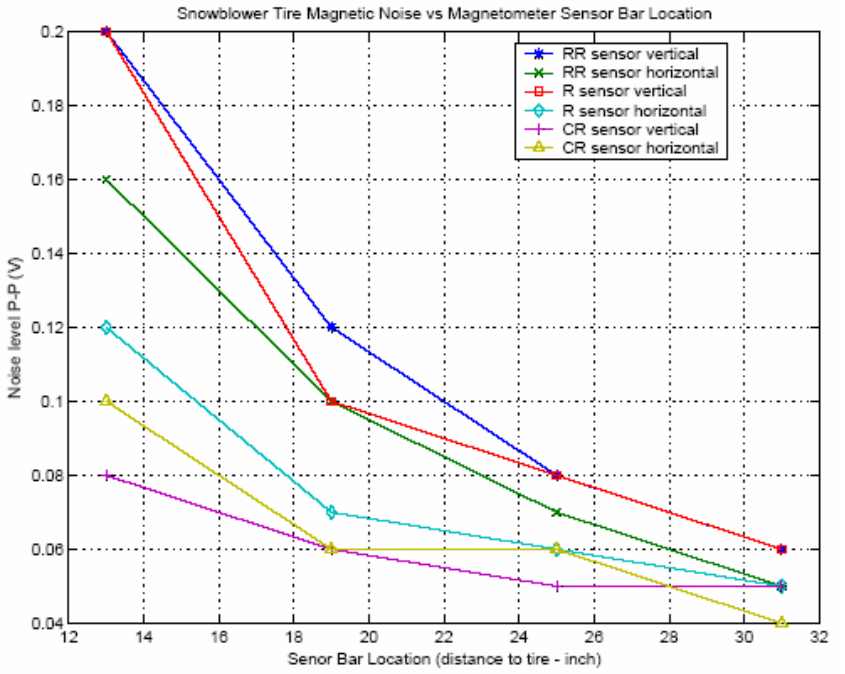

Figure 4. 2 Snowblower tire magnetic noise vs. magnetometer sensor bar locations

4.2 Magnetic Sensing Algorithm

One of the important attributes of the lateral sensing system is its reliability. Currently, there exist several algorithms designed to detect the relative position between the marker and sensor (magnetometer), as well as to read the code embedded within a sequence of these markers. Three magnetic marker detection and mapping algorithms have been experimented with by PATH. The first is called the “peak-mapping” method that utilizes a single magnetometer to estimate the marker’s relative lateral position when the sensor is passing over the magnet. The second algorithm is the “vector ratio” method that requires a pair of magnetometers to sample the field at two locations. It returns a sequence of lateral estimates in a neighborhood surrounding, but not including the peak. The third is the “differential peak-mapping” algorithm that compares the magnetic field measurements at two observation points to eliminate the common-mode contributions and reconstructs a functional relationship between the differential sensor readings and the lateral position using the knowledge of the sensor geometry. The “peak-mapping” algorithm was selected for the snowblower project because it has been proven effective over a wide range of speeds and has been widely applied in many experimental applications conducted by PATH.

In the heavy vehicle operational environment, the magnetic field maps can deviate quite significantly from the theoretical dipole equation prediction because of the massive amount of ferrous material from the body structure located just above the magnetometers. Numerical mapping created by empirical data gathering (calibration) is used to create the associated inverse maps. Figures 4.3 and 4.4 show the front and rear magnetic tables for the snowblower, respectively. The figures consist of tables of the seven magnetometers starting from the right side of the bus to the left, designated as follows: right-right, right, center-right, center, center-left, left and left-left. Each table is obtained with two sets of calibration data, one at a lower sensor height (at around 7 inches from the magnetometer to the magnet) and the other at a higher sensor height (at 11 inches from the magnetometer to the magnet). Each half-circle in the table consists of vertical and horizontal fields of the marker that are collected at 2-cm interval of lateral displacement. The magnetic tables clearly depict the nonsymmetrical natural for the magnetic field due the adjacent ferrous material. The calibration process was repeated for every magnetometer to ensure that the static local magnetic effects for each magnetometer were accounted for.

When a magnetometer bar is not properly calibrated, the lateral position measured can exhibit significant error. Figure 4.5 shows the both the problem areas before the proper calibration (using the rear center table for all rear magnetometers) and the smooth rear measurements (using appropriate calibration tables) when the snow blower is driven across the magnet track from right side of the road toward the left.

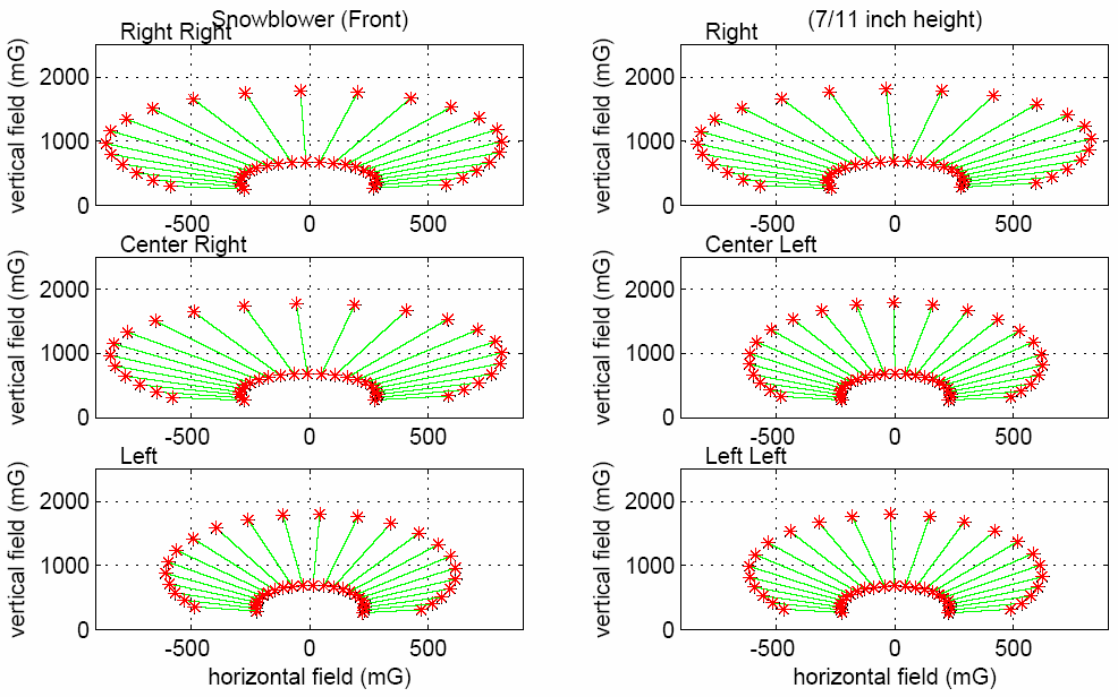

Figure 4. 3 Snowblower Front Magnetometer Calibration Tables

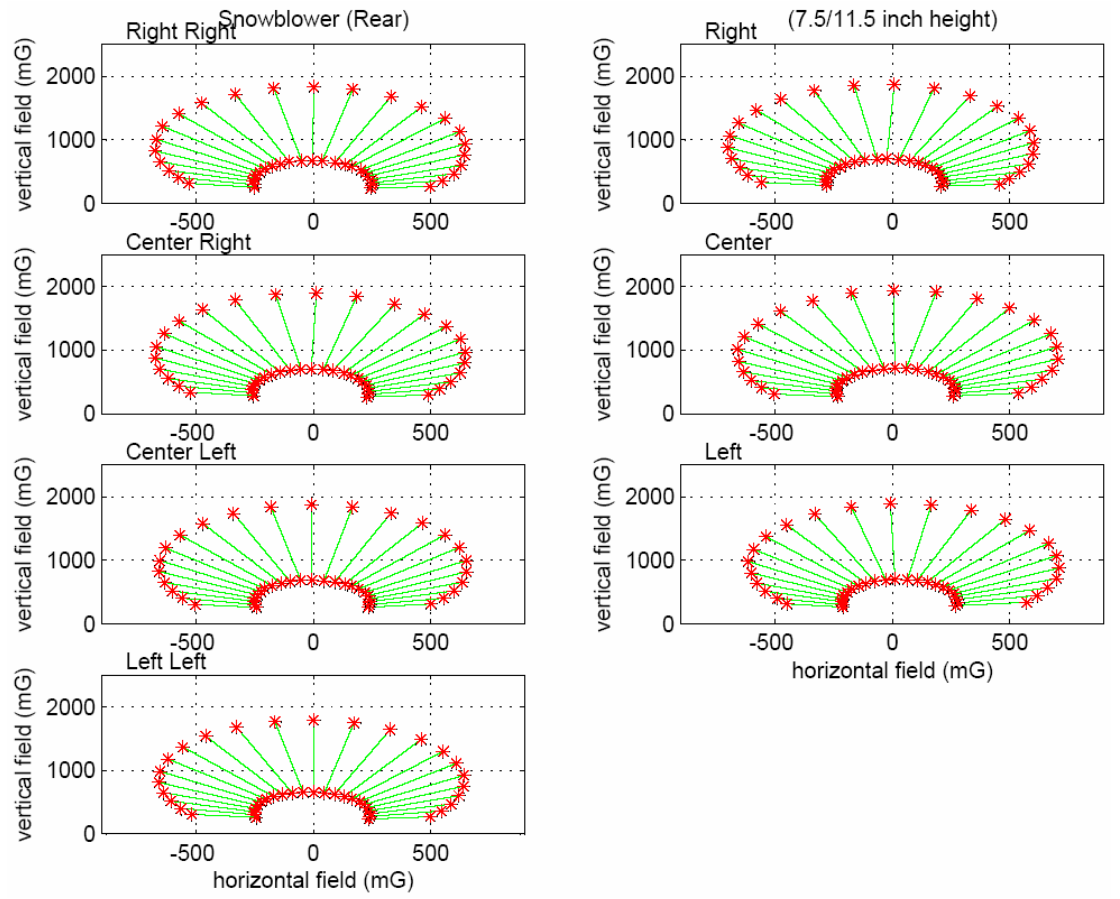

Figure 4. 4 Snowblower Rear Magnetometer Calibration Table

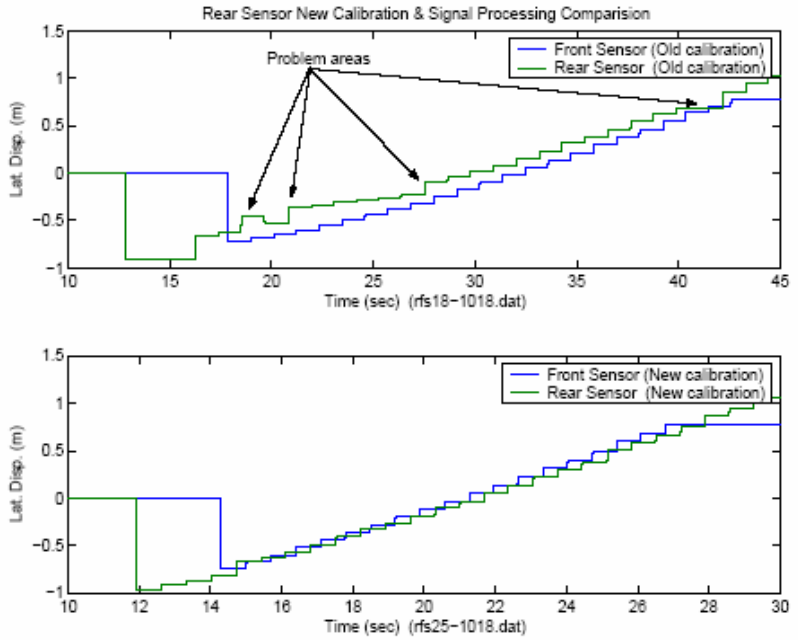

Figure 4. 5 Rear sensor new calibration & signal processing comparison.

4.3 Signal Processing

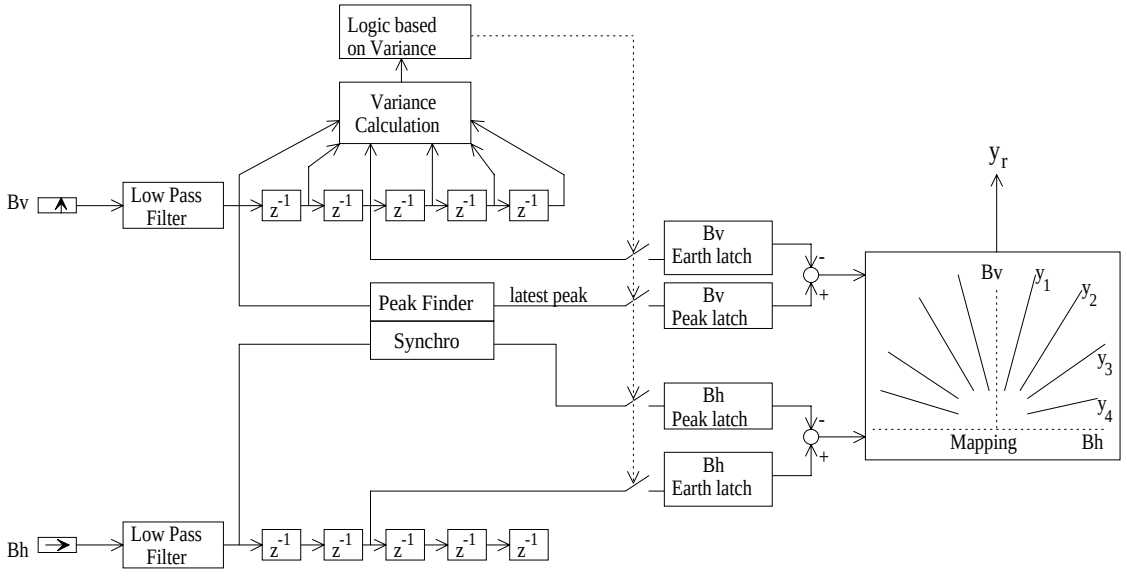

Figure 4. 6 “Peak-Mapping” Magnetometer Signal Processing Block Diagram

The magnetometers signal processing for the “peak-mapping” method involves three procedures: peak detection, earth field removal and lateral displacement table look-up (see Figure 4.6 for block diagram of signal processing algorithm, and Figure 4.7 for one of the peak detection algorithm). Although it is straightforward in principle, it becomes complicated when the reliability of the process is the major concern. Many parameters in

the lateral sensing signal processing software need to be tuned in order to provide consistent lateral displacement information regardless of vehicle speeds, orientations, operating lateral offsets and vehicle body motions. Debugging can become very time consuming when failure conditions cannot be recreated. To improve the reliability of the lateral sensing system with the magnetic road markers, PATH has developed a "reconstructive" software system for the lateral sensing signal processing that supports the tuning of the parameters using stored real-time data. In such a setup, any erroneous situation can be recreated in a lab environment and debugged with ease.

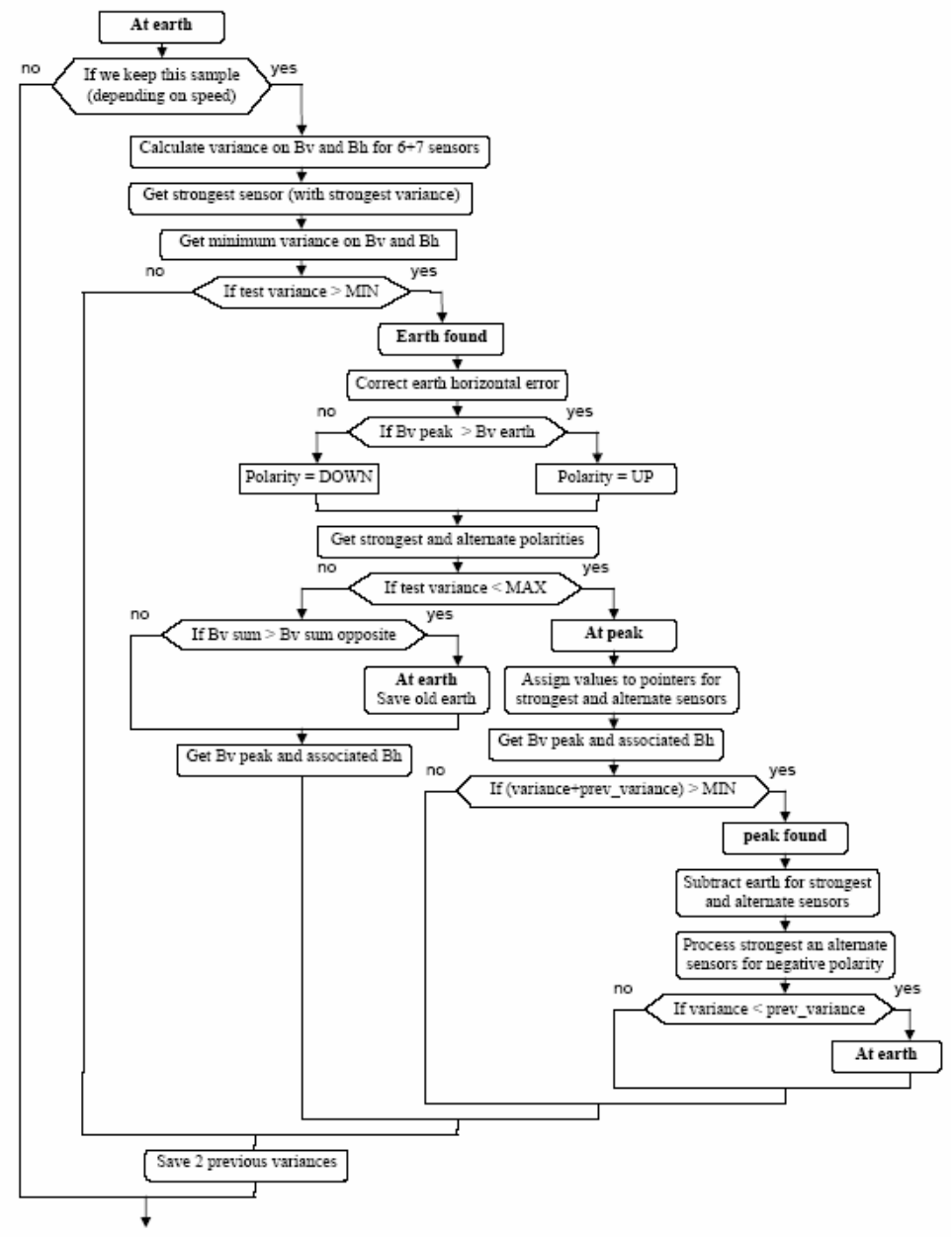

Figure 4. 7 Peak detection block diagram

5. Magnet Installation

5.1 Test Site

Magnets were installed along the eastbound and westbound guard rails of Interstate 80 at Lake Tahoe around Donner Summit (see a map in Figure 5.1) in 2001, at 1.2 meter spacing and 4 feet away from the guardrail. See Figure 5.2 for a photo of the installation process; and also Figure 5.3 for a photo of the magnets installed along the guardrail. There are 5 sections on the westbound shoulder and 3 sections on the eastbound shoulder, between Soda Springs and Kingvale. The total number of magnets installed is 1222, i.e. a total length of about 1 mile.

Figure 5. 1 Map of the test area


Figure 5. 2 Magnet Installation

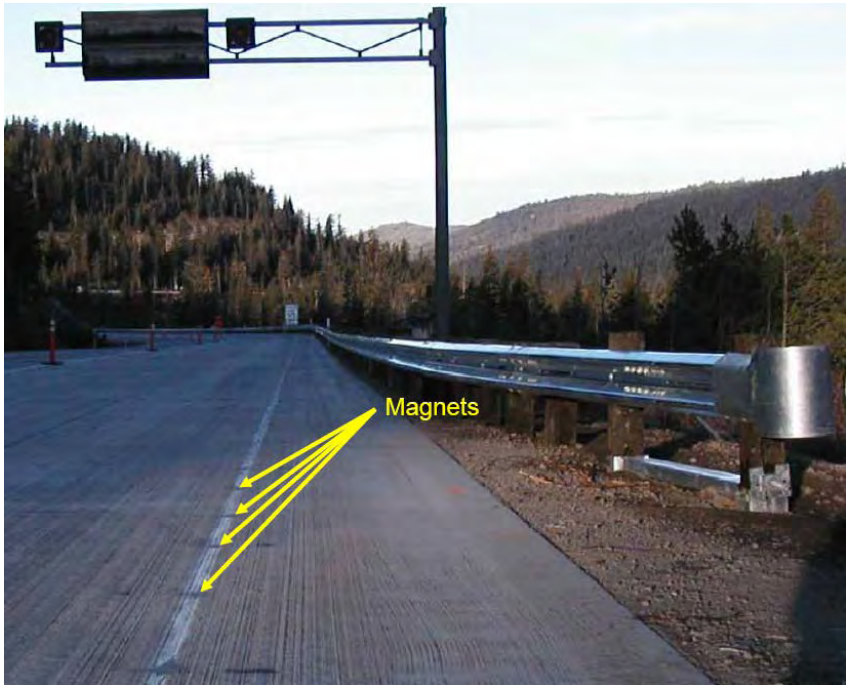

Figure 5. 3 Magnets along guardrail

There are 8 sections of guardrail with magnets installed, including:

- 5 sections on the WB lane (4 on the right shoulder, 1 on the left shoulder)
- 3 sections on the EB lane (2 on the right shoulder, 1 on the left shoulder)

The longest section is 477 magnets long, the shortest one 55 magnets. Figure 5.4 illustrates these guardrails with magnets. The sharpest curve is 457 m radius to the left. Magnets were also installed on both shoulders of the Kingvale overpass, in each direction. All the magnets are ceramic type, except for the Kingvale overpass where they are rare earth.

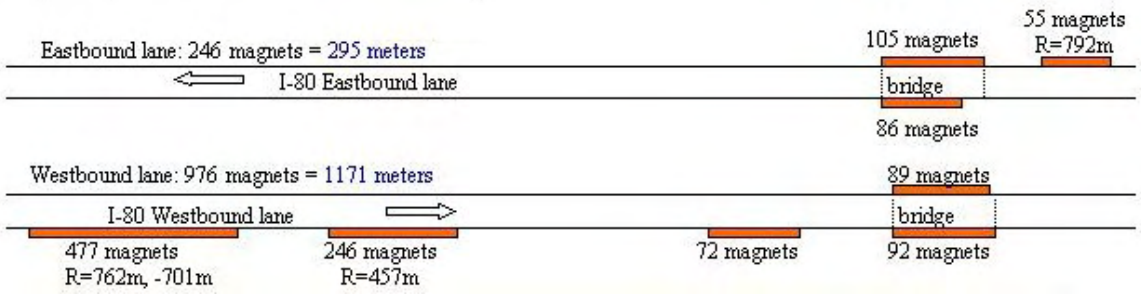

Figure 5. 4 Illustration of guardrail installed with magnets in I-80

5.2 Magnet Code Description

For each section of guardrail, 25 magnets were installed before the guardrail (to turn the auto-steering on) and 10 magnets after (to turn the auto-steering off). The magnet polarity is 0 (south pole up) on the right-side shoulder and 1 (north pole up) on the left-side shoulder. The code for the “end of magnets” is to the interchange the polarity for the

last 12 magnets, for example [101010101010]. Note that there is no curvature information coded due to the required fast "control initialization" as well as the long code length to encode different curvature and curvature changes.

Figure 5. 5 Illustration of beginning and ending of a magnet section

The westbound shoulder magnets are as follows:

- Section 1:
  station 3395.6 -> 2824.4
  477 magnets on the right shoulder
  25 magnets before the guard rail, 10 magnets after
  code on last 12 magnets
  curvatures in the section: 762 m (to the left) , straight , -701.04 m (to the right)
- Section 2:
  station 2280.0 ->1986.0
  246 magnets on the right shoulder
  25 magnets before the guard rail, 11 magnets after
  code on last 12 magnets
  curvatures in the section: straight, 457.2 m (to the left)
- Section 3:
  station 13536.3 ->13451.1
  72 magnets on the right shoulder
  25 magnets before the guard rail, 10 magnets after
  code on last 12 magnets
  curvature in the section: straight
- Section 4:
  station 13000.6 -> 12891.4
  92 magnets on the right shoulder of the bridge
  25 magnets before the guard rail, 10 magnets after
  magnets 49 & 50: [11] for beginning of bridge
  magnets 78 & 79: [11] for end of bridge
  code on last 13 magnets
  curvature in the section: straight
- Section 5:
  station 12997.0 -> 12891.4
  89 magnets on the left shoulder of the bridge
  25 magnets before the guard rail, 10 magnets after
  magnets 49 & 50: [00] for beginning of bridge
  magnets 78 & 79: [00] for end of bridge
  code on last 13 magnets
  curvature in the section: straight

The eastbound shoulder magnets are as follows:

- Section 1:
  station 12521.5 -> 12586.3
  55 magnets on the right shoulder
  25 magnets before the guard rail, 10 magnets after
  code on last 12 magnets
  curvatures in the section: 792.48 m (to the left)
- Section 2:
  station 12832.1 -> 12956.9
  105 magnets on the right shoulder of the bridge
  25 magnets before the guard rail, 10 magnets after
  magnets 59 & 60: [11] for beginning of bridge
  magnets 94 & 95: [11] for end of bridge
  code on last 10 magnets
  curvature in the section: straight
- Section 3:
  station 12854.9 -> 12956.9
  86 magnets on the left shoulder
  25 magnets before the guard rail, 10 magnets after
  magnets 59 & 60: [00] for beginning of bridge
  magnets 94 & 95: [00] for end of bridge
  code on last 10 magnets
  curvature in the section: straight

6. Hardware Modifications

6.1 Hardware Components

As illustrated in Figure 2.3, the automated steering control is implemented to a conventional Kodiak Northwest single engine rotary snowplow with full hydrostatics. The concept of implementation is to maintain all "manual" operational functionalities the same as those of the original snowblower. All automated steering components are "add-on" devices or systems. The main add-on components are described below. A computer with a data acquisition unit processes information and determines control and guidance actions. The lateral positioning system, consisting of two arrays of magnetometers, measures the field strength of magnetic markers installed under the roadway. The steering actuator, using a custom-made DC motor attached to the steering column with angular sensors, steers the front wheels. A yaw gyro and an axle speed sensor provide supplementary motion data under extremely low speeds. A Human Machine Interface (HMI) or Driver Vehicle Interface (DVI) unit, consisting of electronic circuit, a toggle switch, LED displays and an audible device, interfaces with the operator with information and commands for automation. Table 6.1 details these add-on components.

Table 6.1 Automated snowblower add-on components

Component	Description	Functions
Computer	10 slot industrial computer	Control/actuation/signal processing/HMI/fault detection
Power supply & inverter	EGS (GLQ-04-200) power supply & Statpower PROSine 1000 inverter	Provide power to computer & circuits
Front magnetometer bar	6 Applied Physics ASPS535 magnetometers with custom-made enclosure	Measure magnetic strengths from buried magnets
Rear magnetometer bar	7 Applied Physics ASPS535 magnetometers with custom-made enclosure	Measure magnetic strengths from buried magnets
I/O board (inside computer)	National Instrument AT-MIO-64E-3	Use for timer inputs, analog inputs and outputs, and digital I/O including data from magnetometers
I/O board (inside computer)	National Instrument AT-AO-6	Use for analog outputs and digital I/O
I/O board (inside computer)	PC-TIO-10	Use for timer and digital I/O
I/O board (inside computer)	Microcomputer Systems EIC-325	Use for interfacing encoder (steering sensor)
Steering actuator	NSK custom-made	DC-motor actuator with current-mode control and steering angle sensors (see

		Section 7)
Speed sensor and circuit	Magnetic pick-up and custom-made circuit	Measure drive shaft speed
Yaw rate sensor	KVH E-core Fiber optic rate gyro	Measure yaw rate
HMI: control circuit	Custom-made	Provide independent HMI control
HMI: switch & button	Custom-made	Allow driver to input to the automated system
HMI: LED display	Custom-made (LED's)	Provide driver with information about the automated system
HMI: audible unit	Custom-made, speaker & sound board	Provide driver with audible information
Enclosure		Provide weather-proof enclosure for computer, I/O boards, power supplies, and HMI circuit

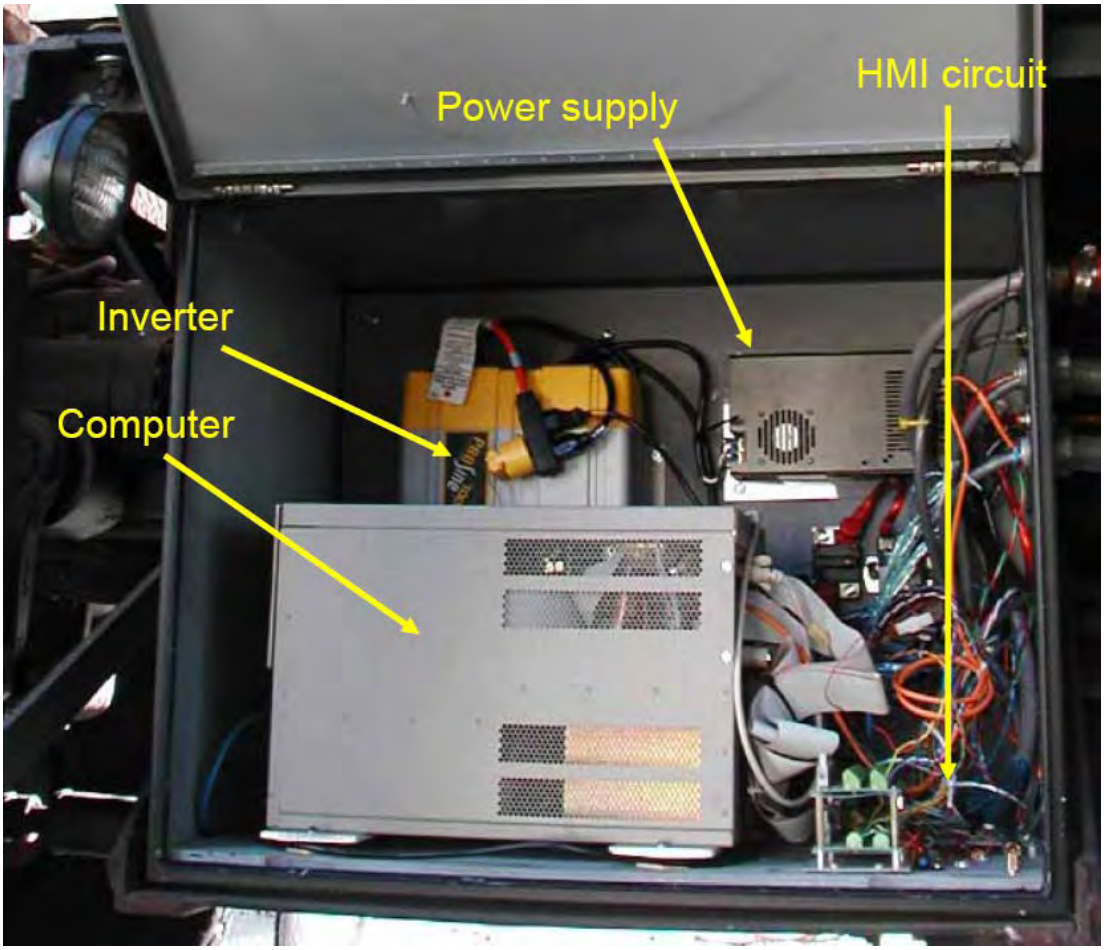

Figure 6. 1 Enclosure and components

Power supplies

The 12V power supply, coming from the snowblower batteries, is used for powering most sensors and electronics on the system. The 12V batteries are also connected to a 120V AC inverter for powering the computer (see Figure 6.1). All the circuit boards and electronics are powered by 12V bus bar supply through 10A circuit breaker. The steering actuator is powered by 12V connected to the battery through 60A circuit breaker. All the sensors power supply is directly from 12V bus bar except for the magnetometers. The magnetometers are powered by +/-15V which is powered from the 12V bus bar. Bypass capacitors are put at the output of the power adapters to reduce the power noise.

Steering actuator

The motor assembly is manufactured by NSK as shown in Figure 6.2. The steering actuator motor assembly consists of a steering column, DC motor actuating steering column, an electromagnetic clutch, angle sensors (incremental encoder and potentiometer), and ECU. See Section 7 for detailed description.

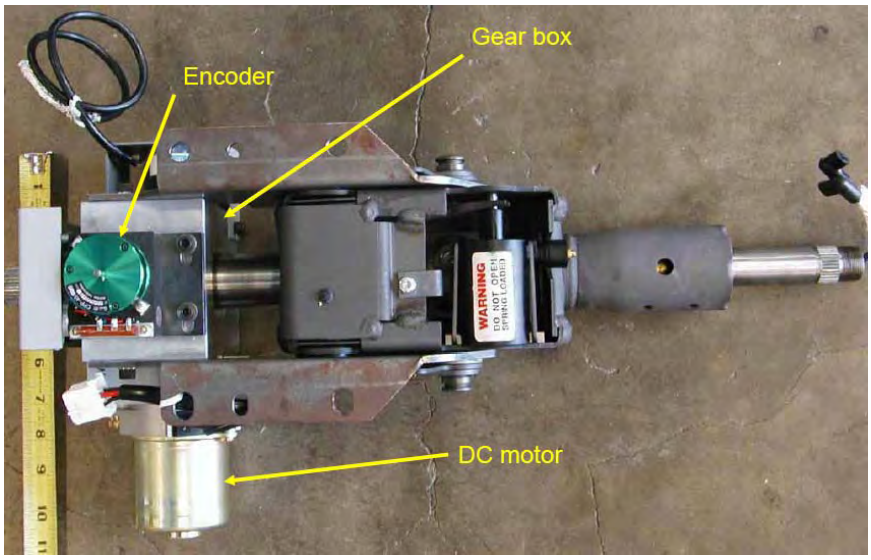

Figure 6. 2 Steering actuator (not assembled)

Sensors

Yaw rate sensor (see Figure 6.3) is behind the cab of the snowblower. Magnetometers are mounted on weather-proof enclosures under the front axle and in between the front and rear axle. The front sensor bar has a dent resulted from a past winters operation. The performance of the front sensor bar has been verified despite the dent. Figure 6.4 shows the dented front sensor bar and a spare in case of a severe damage in the future. On the other hand, several installation issues with respect to the rear magnetometers were encountered during the development and test periods; see Section 6.2 for detailed description on those issues. For steering position, steering pot and encoder (see Figure 6.2) are used and installed as part of the steering actuator (Refer to Section 7 for more detailed descriptions). The speed sensor has been modified several times in the development and test cycles. The original speed sensor (Figure 6.5, left) operated to speed as low as 2 mph (~1m/s) based on the initial speed requirement of minimum 3mph. The current speed sensor, as shown in Figure 6.5-right, was reinstalled and the associated

speed-signal processing algorithm was tested to extend to the low speed range from 2 mph to 0.25 mph (~0.5m/s).

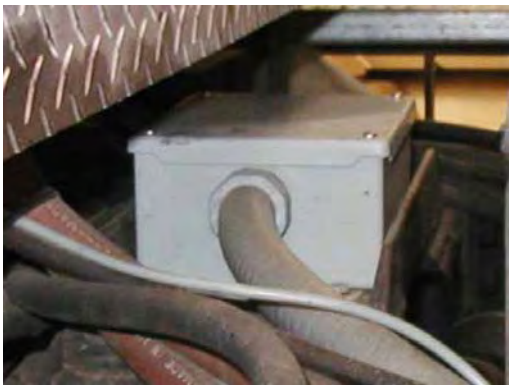

Figure 6. 3 Yaw rate sensor and enclosure

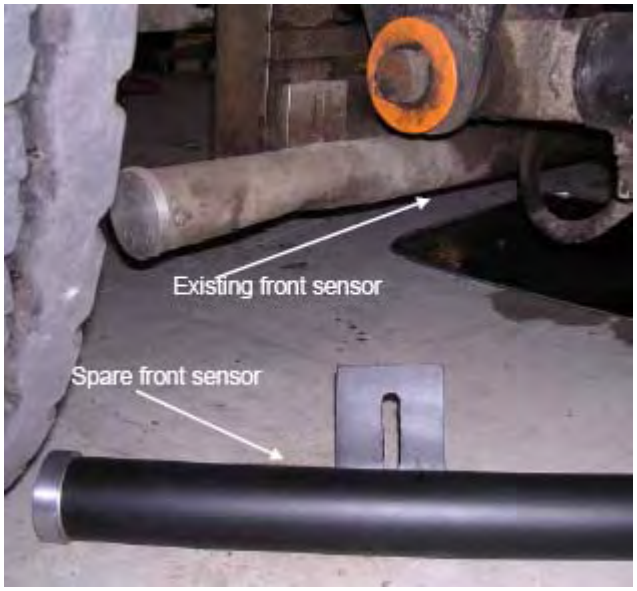

Figure 6. 4 Existing dented front magnetometer bar and a spare

Figure 6. 5 Speed sensor (left: old; right: improved)

Sensor interface

Sensors are connected with computer through I/O boards as illustrated in Figure 6.6 and 6.7. Thirty-nine input channels are used on AT-MIO-64E-3 card. Twenty-six channels are used for thirteen magnetometers (two channels for each magnetometer), and two channels are used for steering potentiometer and steering motor condition. Three digital inputs and two analog outputs are used on AT-A0-6. Thirteen digital input channels are used for magnetometer health signals on PC-TIO-10. In addition, two digital inputs are used for auto/manual transition switches. Sixteen channels outputs are used for outputs to HMI and steering actuator. Three channels for triggering three different sounds recorded in the alert audible system. Eleven channels are for various LED's: seven for guidance display and four for status display. There are two additional channels, one is for steering clutch, and the other for steering torque command.

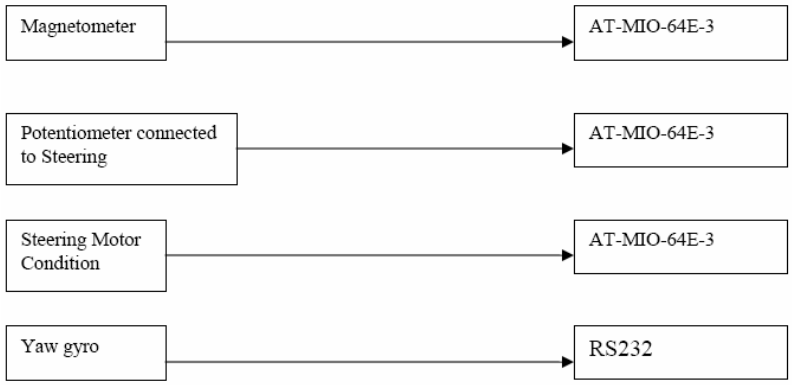

Figure 6. 6 Interface between snowblower sensors and computer (1)

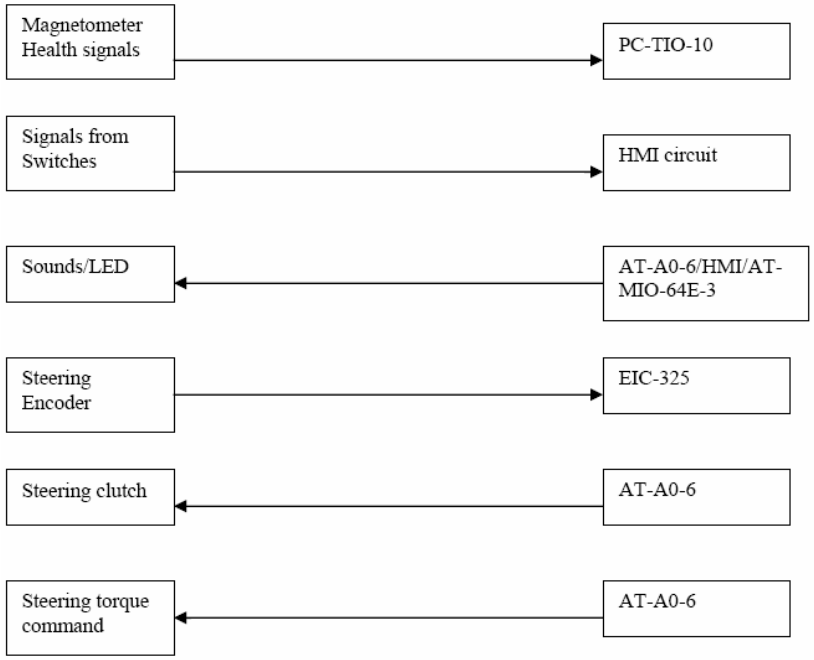

Figure 6. 7 Interface between snowblower sensors, commands and computer (2)

HMI & HMI circuit

The HMI (human machine interface) consists of a transition toggle switch, a set of status LED's, a set of guidance LED's, an audible unit, a system switch, and an emergency button. They are controlled by a HMI circuit which decides whether the control is based on the HMI circuit or through the computer commands. This HMI circuit will warn the driver when the automated control failed to function. This warning system listens to the beat sent from computer. It will do nothing as long as the heart beat is on. This system will trigger the emergency sound when the heart beat dies or the beat misses beating more than twice as shown in the diagram below (Figure 6.8). The timer chip is set to be triggered every 250ms (millisecond). The out put of the chip will be held high as long as the chip is triggered every 250ms, therefore, the collector of transistor is low and the emergency sound will be silenced. The circuit will also provide LED and sound command during computer boot-up period as well as when there is no heart-beat. However, it will also relinquish LED/sound control to the computer command when there is a heart-beat.

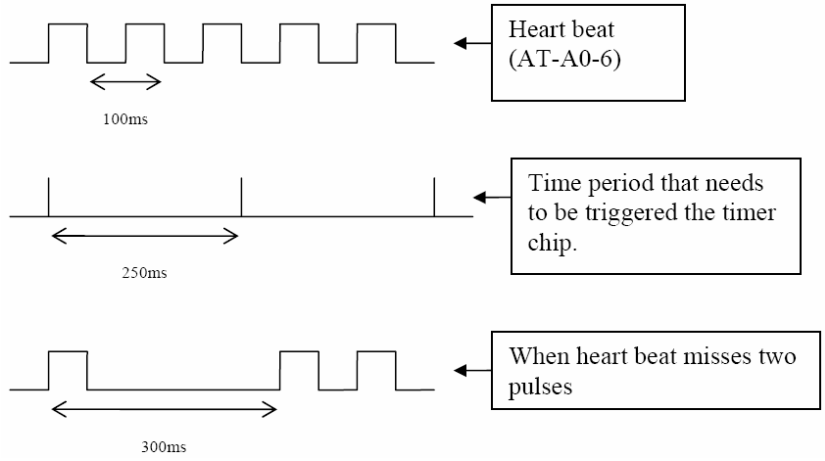

Figure 6. 8 HMI and heart beat timing

6.2 Wiring and Circuit Diagram

This section exhibits various wiring diagrams for the snowblower hardware installation.

Figure 6.9 shows the overall snowblower automated system wiring and circuit diagram. The highlighted areas in Figure 6.9 indicate those diagrams that with a more detailed figure followed. Figure 6.10, 6.11, 6.12, 6.13, 6.14 illustrate these more detailed wiring/circuit diagrams; they are steering actuator & transition switches, AT-MIO-64E-3 & magnetometers, I/O boards, HMI circuit, and heat-beat detection, respectively.

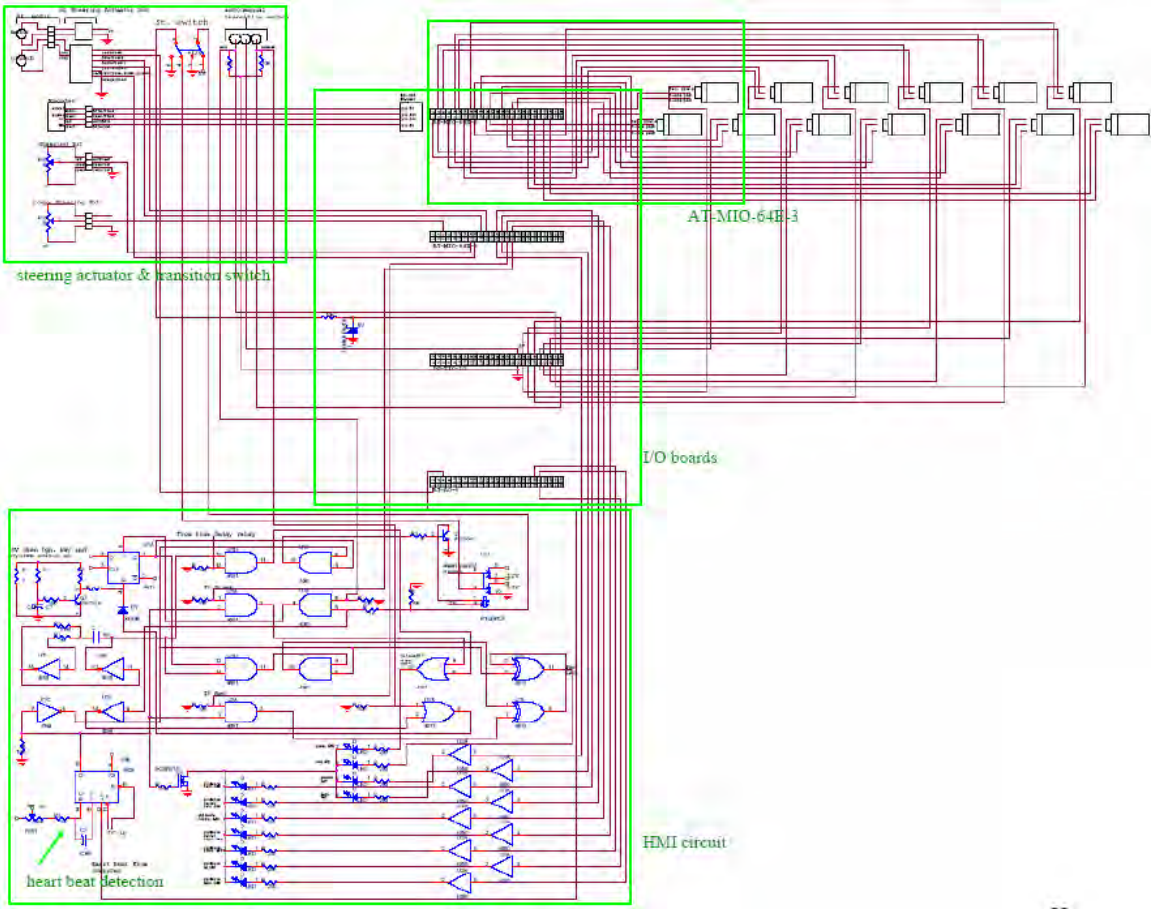

Figure 6. 9 Snowblower wiring and circuit diagram (overall)

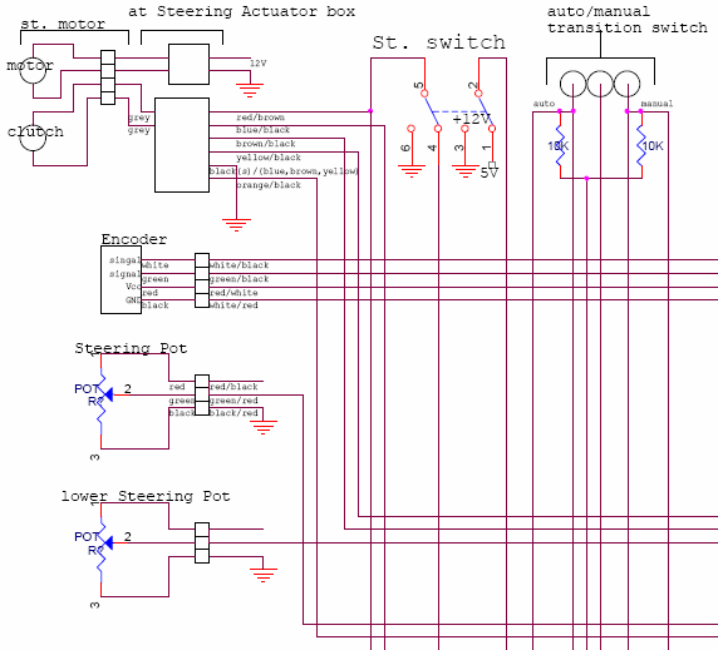

Figure 6. 10 Snowblower wiring and circuit diagram (steering actuator & transition switches)

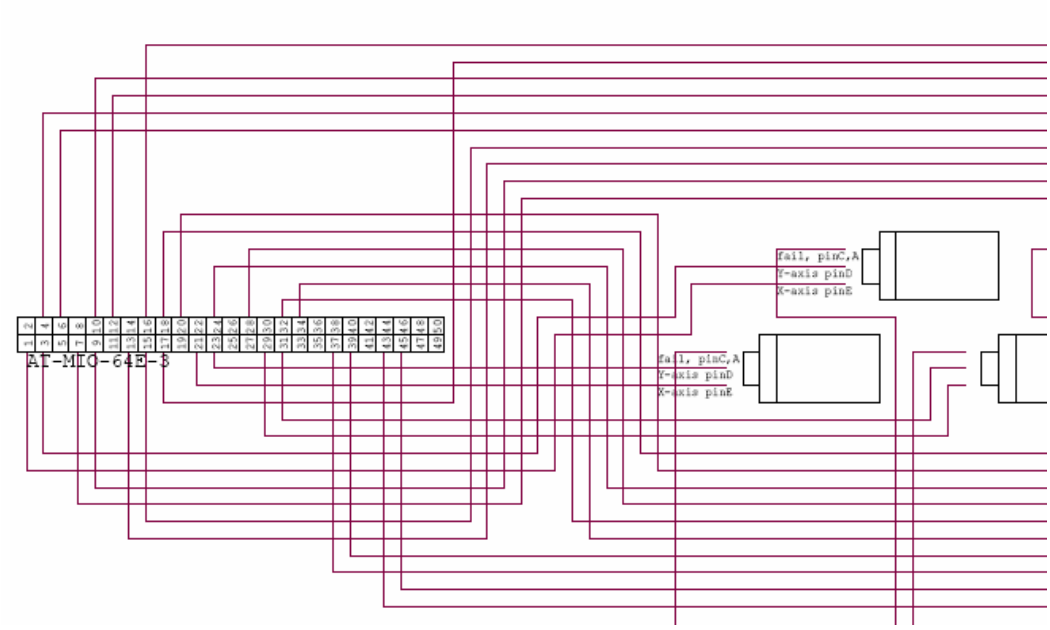

Figure 6. 11 Snowblower wiring and circuit diagram (AT-MIO-64E-3 & magnetometers)

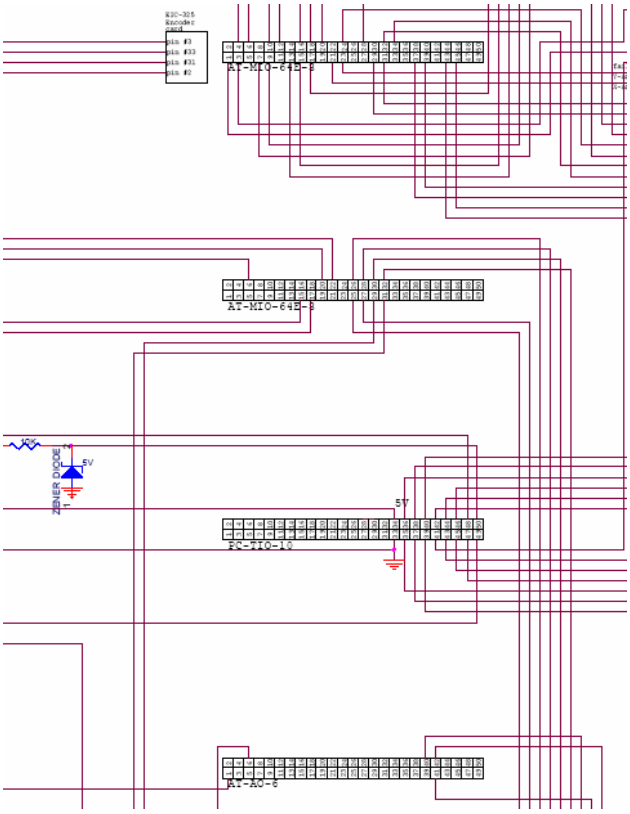

Figure 6. 12 Snowblower wiring and circuit diagram (I/O boards)

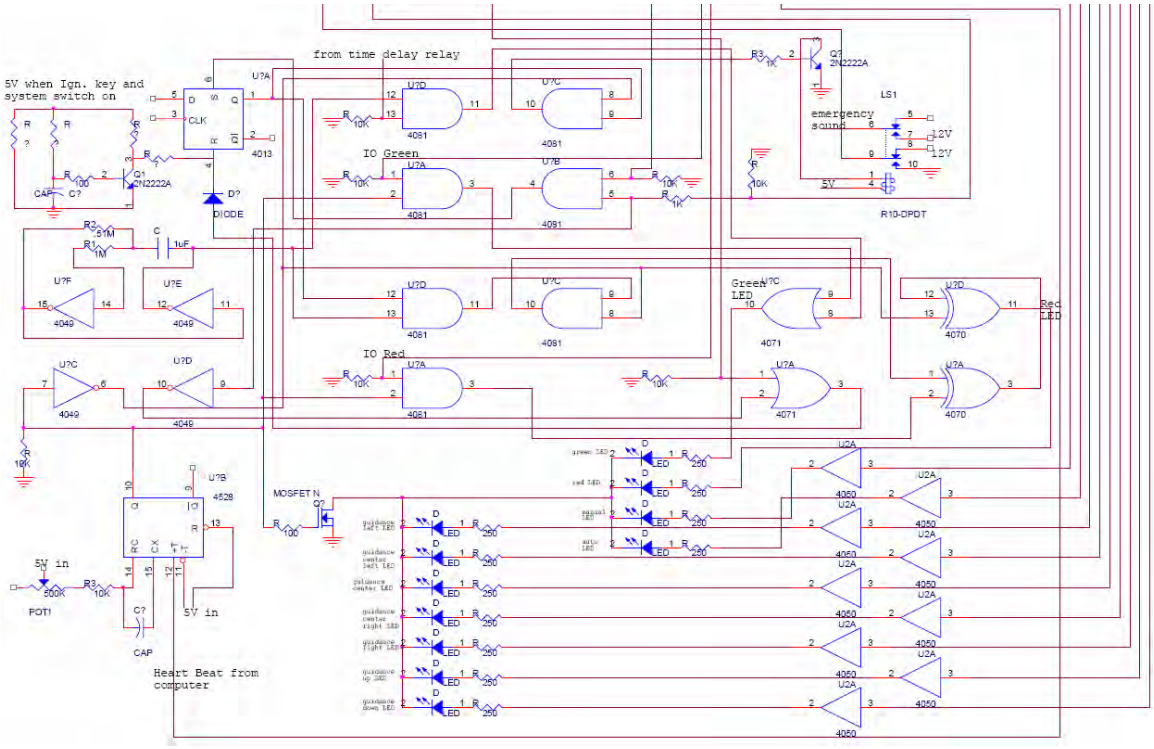

Figure 6. 13 Snowblower wiring and circuit diagram (HMI circuit)

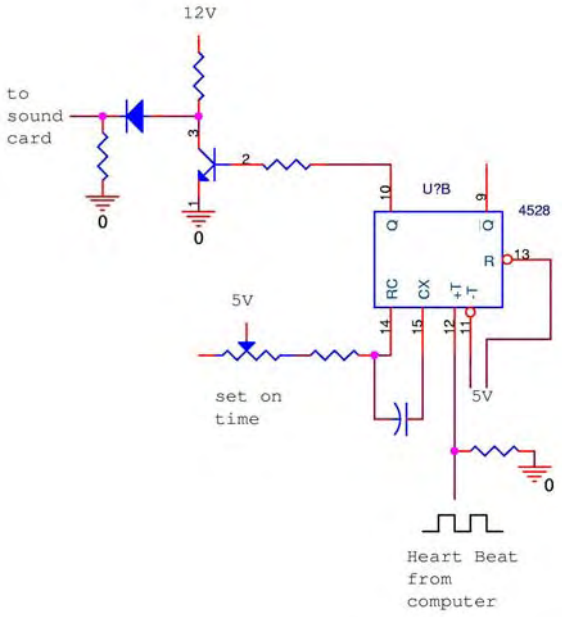

Figure 6. 14 Snowblower wiring and circuit diagram (heart beat detection)

6.3 Rear Magnetometer Bar Installation

One problem encountered during hardware installation worthwhile noted relates to the rear magnetometer bar installation. The rear magnetometer bar was first installed under the rear bumper of the snowblower to minimize the noise amplification during vehicle angle computation by maximizing the distance between the front and rear bars.

Through the discussions with the Kingvale maintenance yard lead mechanics, this original rear magnetometer bar was not installed at an appropriate location. The tail end of the snowblower may not be compatible with one of the snow removal operations that performed by the snowblower: cutting down drainage path along highway. The original rear magnetometer bar would likely be damaged by one of such maneuvers when the snowblower went down deep and back up from the steep drainage pathway. Once understood the cause of this potential problem, the rear bar was immediately removed and the re-design process started. The decision of a better location would need to trade off the following design constraints: minimum downward movement during the above-mentioned maneuver, far enough distance from the front magnetometer bar to provide sufficient signal to noise ratio for "blower" angle estimation, as well as existing screw holes in the blower body to allow senor installation without compromising blower structure integrity. The final decision was made by (1) additional examination of the relative height "invariance" of the sensor location with respect to the blower head's configuration; and (2) the interference effect from the magnetic field noise of the rear tires.

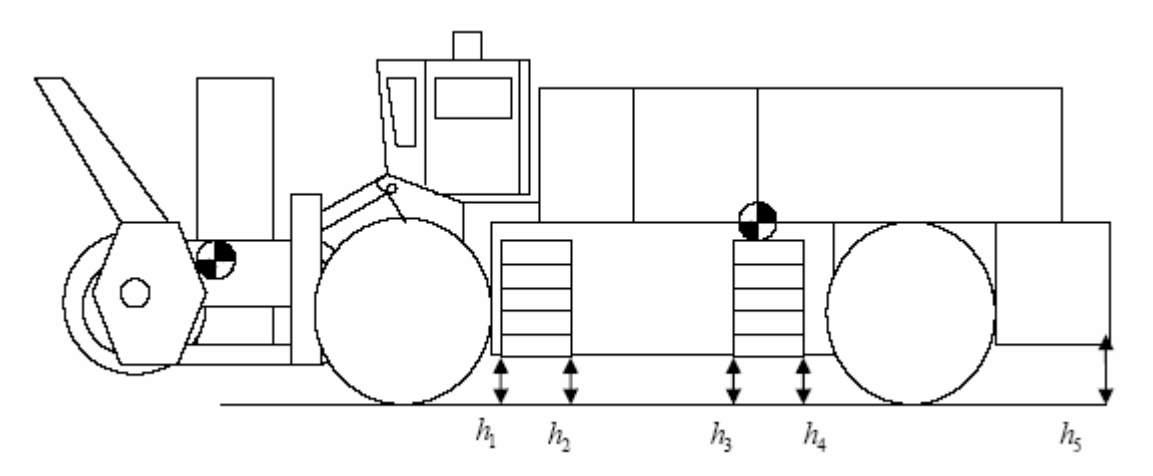

Figure 6. 15 Possible rear magnetometer bar location

Base on the initial observations and analysis, the candidate locations of rear magnetometer sensor bar should be around Location h_3 and h_4 as shown in Figure 6.15. Table 6.2 lists the relative height measurements at various locations under the following blower head configurations: the blower head is lifted to its highest point, the blower head is lifted to about 1 inch above the ground, the blower head is pushed all the way down on the ground, as well as the blower head is pushed with half the maximum pressure to the ground. The result shows that the Location h_4 is the least sensitive to height invariant with maximum 1/8 inches variation among all possible tested head configurations. It follows by Location h_3 with maximum 1/4 inches height variation. Remember that Figure 4.2 in Section 4.1 shows the tire magnetic noise effect (peak-to-peak value) to the 3 right magnetometers with respect to various magnetometer sensor bar locations. Figure 4.2 concludes that the sensor bar would requires at least 19 inches distance from the tire rim in order to has a noticeable reduction of the tire magnetic interference. However, the only available existing screw holes in the blower body to allow senor installation that are also near Locations h_3 and h_4 are 9, 14 and 19 inches to the rear tire rim. Therefore the final

rear sensor bar location is decided at 2 inches ahead of h_3, at 19 inches in front of the rear tire rim.

Table 6.2. Height variations based on blower head movement

Original heights when parked in the tent			Head lifted up to the upper dead point		
	Left	Right		Left	Right
h_1	N/A	N/A	h_1	17 9/16	17 3/4
h_2	N/A	N/A	h_2	17 11/16	17 5/8
h_3	18 1/8	18	h_3	18	18
h_4	18 1/16	17 7/8	h_4	18 1/16	17 15/16
h_5	N/A	N/A	h_5	16 1/2	15 11/16
Head lifted up 1~2 cm above ground			Head pushed down with full pressure		
h_1	17 9/16	17 3/4	h_1	18 15/16	N/A
h_2	17 11/16	17 5/8	h_2	18 3/4	N/A
h_3	18	18	h_3	18 3/16	N/A
h_4	18 1/16	17 15/16	h_4	18 1/16	N/A
h_5	16 1/2	15 11/16	h_5	14 5/16	N/A
Head pushed down with half the pressure					
h_1	N/A	N/A			
h_2	N/A	N/A			
h_3	17 15/16	N/A			
h_4	17 15/16	N/A			
h_5	N/A	N/A			

Figure 6.16 shows both the sensor bar housing as well as the magnetometers and the associated internal structure that will be slide into the bar housing. Figure 6.17 shows the finished rear magnetometer sensor bar.

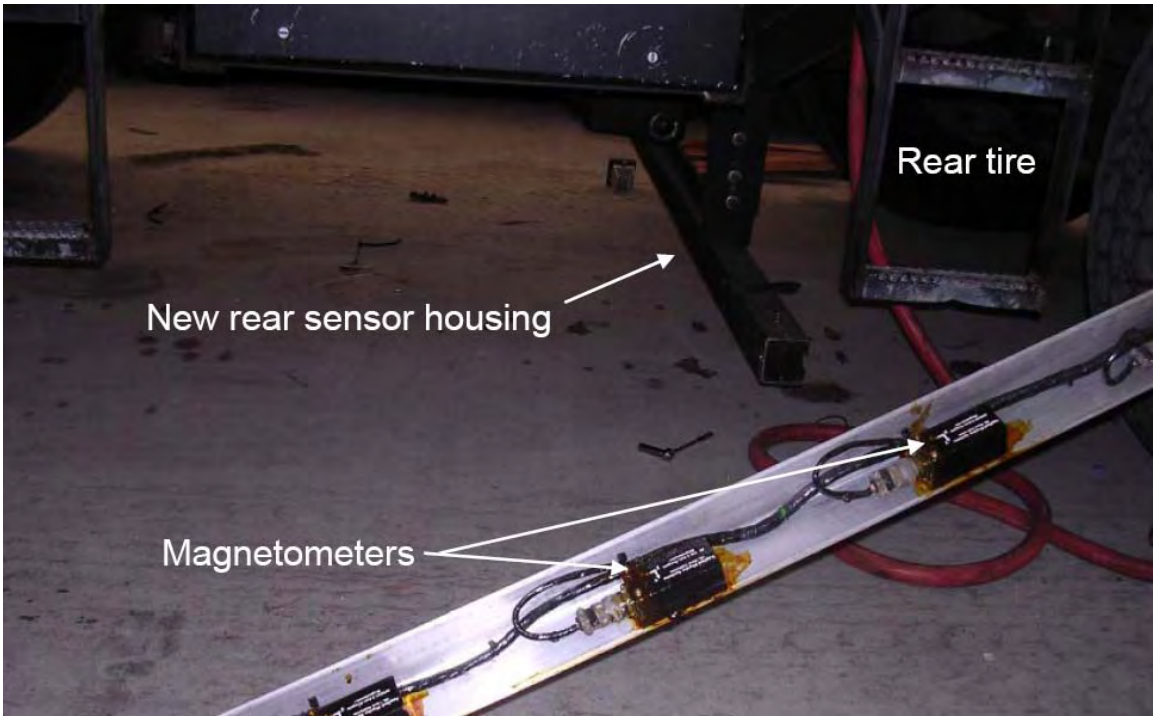

Figure 6. 16 Rear sensor bar housing and the magnetometers before final assembly

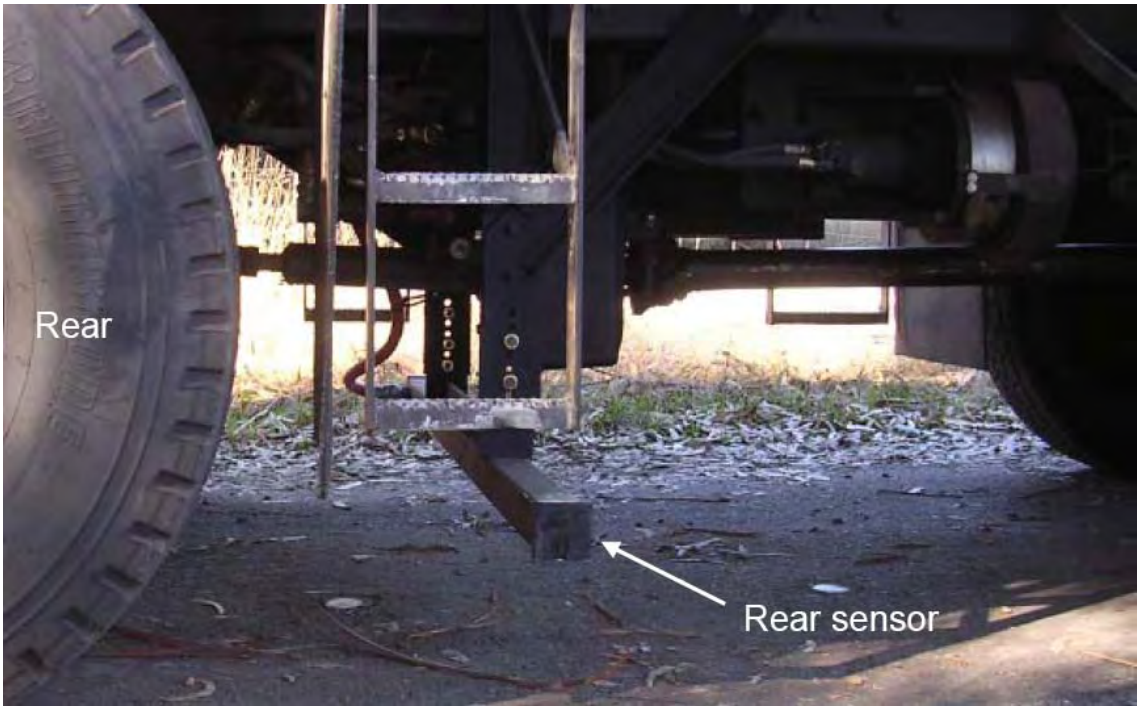

Figure 6. 17 Rear sensor bar after assembly

7. Steering Actuator

The fundamental difficulty of the servo design is the extreme nonlinearities of the front steering mechanism. The torque required to steer the front tire varies significantly with respect to the front-loading conditions. For example, the steering hydraulic assist system cannot move the front tires by more than 50 degrees when the blower head is raised and the vehicle is stopped. In fact, the steering actuator motor often does not have enough torque capacity when the vehicle is at lower speeds or when the commanded rate of change is high. However, these limitations have to be considered under “normal” operating conditions and are required to be overcome by the servo controller. Steering actuator receives steering angle command from upper level later controller and turns steering wheel to the desired steering angle according to the received steering angle command. An add-on steering actuator is designed and installed on the snow blower’s steering column. A local position servo loop is designed for the steering actuator.

7.1 Actuator System Configuration

Figure 7.1 shows the block diagram of the steering actuator. The motor assembly is manufactured by NSK. As shown in Figure 7.2 and Figure7.3, steering actuator motor assembly consists of a steering column, DC motor actuating steering column, an electromagnetic clutch and angle sensors measuring steering wheel position. The DC motor connects to the steering column through clutch and reduction gear. An incremental encoder is mounted on the motor shaft to measure the relative position of steering wheel. A multi-turn potentiometer is connected with column shaft via pulley gear and belt to measure the absolute position of steering wheel. Motor current and clutch ON/OFF is controlled by ECU. The clutch can also be controlled by upper level computer by issuing clutch command to ECU. A current loop control is built in ECU as shown in Figure 7.4. ECU receives torque command from upper level computer and issues corresponding current command so that DC motor will generate required torque. Strict start and shut down sequences are defined to prevent erroneous operation. ECU has some built-in self-diagnostic features. Failure will be declared when torque command is over allowed limit, power supply to the motor is out of range and motor is overheated. The health condition of motor is feedback to upper level computer through motor condition signal.

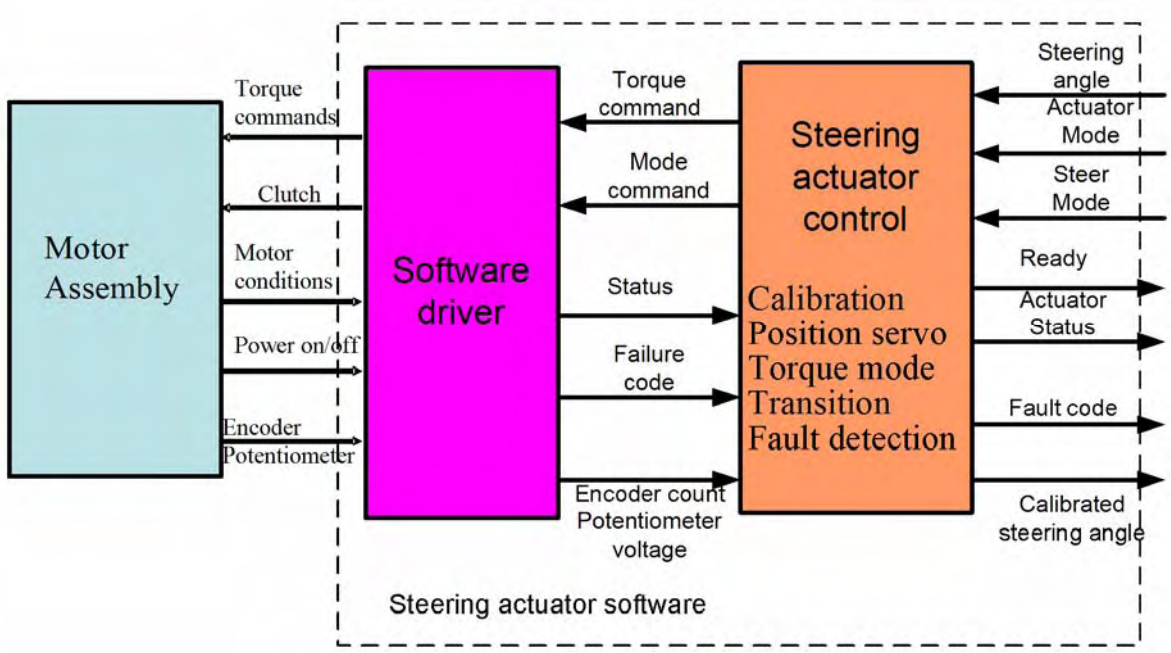

Figure 7. 1 Block diagram of steering actuator

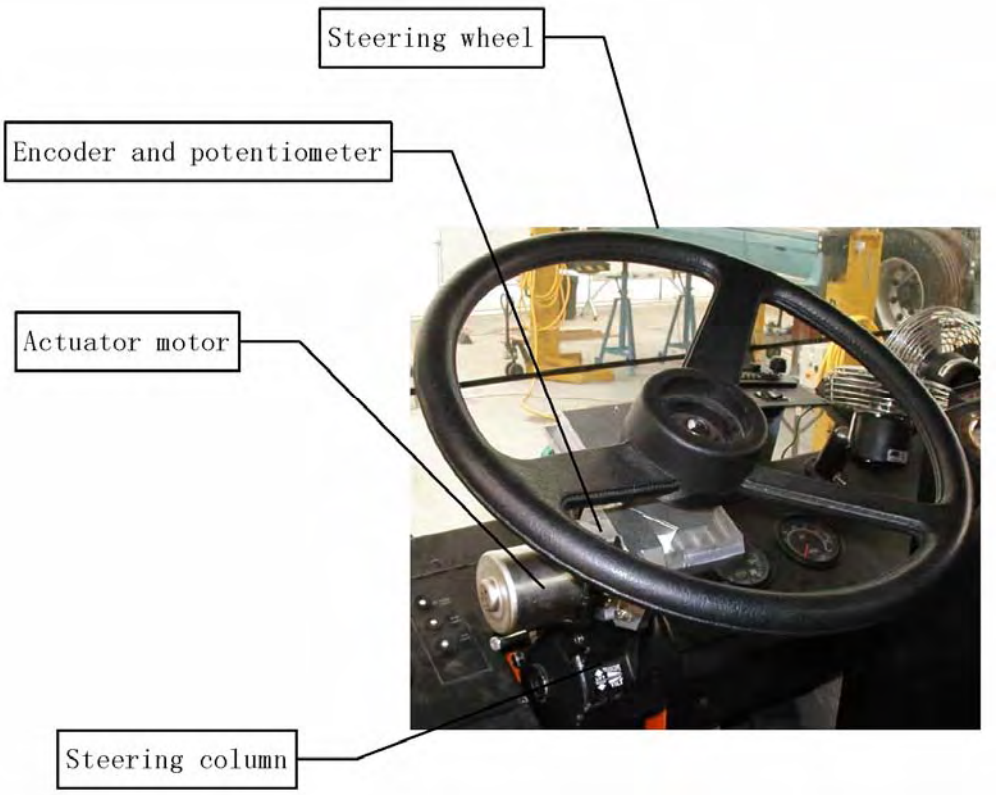

Figure 7. 2 Steering actuator installation

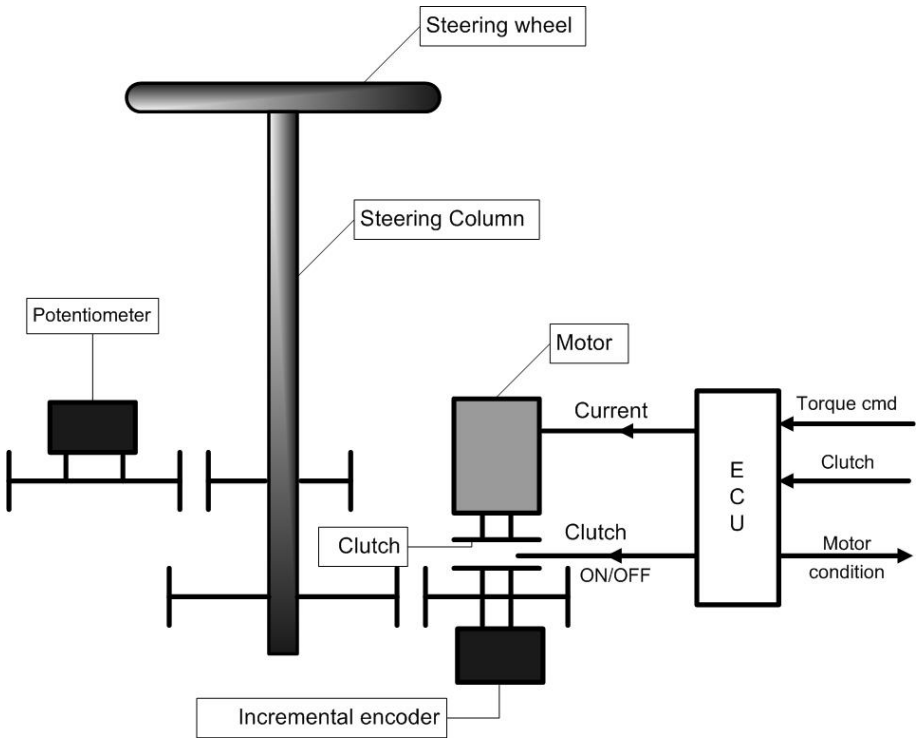

Figure 7. 3 Schematic of steering actuator motor assembly

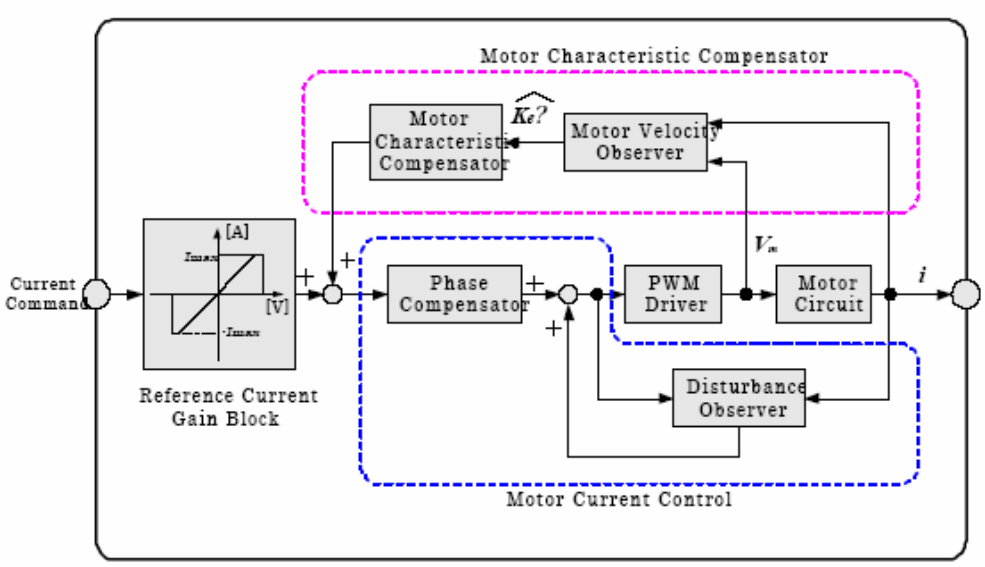

Figure 7. 4 Current drive loop in ECU

Steering actuator software is a software package designed by PATH researcher. Steering actuator software has two modules: software driver and steering actuator control as shown in Figure 7.1. Software driver interfaces with control computer's A/D and D/A board, digital I/O board and encoder interface board which connect directly with the motor assembly. Software driver reads information such as encoder count, potentiometer voltage and motor condition from the motor assembly and sends out commands such as

torque and clutch to the motor assembly through hardware interface. The major functions of software driver are:

a. Interface with motor assembly hardware
b. Perform “start up” and “shut down” procedure
c. Fault detection

Steering actuator control receive steering angle command, steer mode command (torque control, hard position servo and soft position servo) and actuator mode (auto/manual) from upper level lateral controller. It also sends information such as actuator status (torque control or position servo), ready/not ready, fault code and calibrated steering angle to upper level lateral controller. The major functions of steering actuator controller are:

a. Calibration. The function of calibration is to find zero steering angle of snowblower.
b. Position servo. Position servo is a closed loop control. It receives steering angle command and issues torque command to steering actuator hardware so that the steering wheel will turn to the desired steering wheel angle position.
c. Smooth transition between manual and automatic control.
d. Fault detection for sensors and motor.

7.2 Position Servo Design

Position servo is the key function of steering actuator. Successful lateral controller design requires at least 4-5 Hz closed servo loop bandwidth with 1 degree accuracy on steering wheel. Before the servo design can be carried out, extensive experiments are conducted to study open loop characteristics of steering actuator. The experimental results reveal a quite challenging servo design problem.

Open loop model identification

First, sweep sine technique is used to identify open loop frequency response from torque command (V) to steering wheel angle (degree) with different input amplitudes. As shown in Figure 7.5, the open loop bandwidth of snowblower steering actuator is less than 1 Hz. Second, a slow ramp input is sent to study the effect of friction on the road. As shown in Figure 7.6, the friction effect is so dominant that the steering wheel starts moving only when torque command almost reaches its half of full capacity (2V). This means the actuating motor is “under powered” especially when the heavy snowblower head is mounted. Although this may facilitate driver taking over under emergency situation, the “under powered” motor will pose significant difficulty for servo loop design. This is especially true for low speed application such as snowblowing.

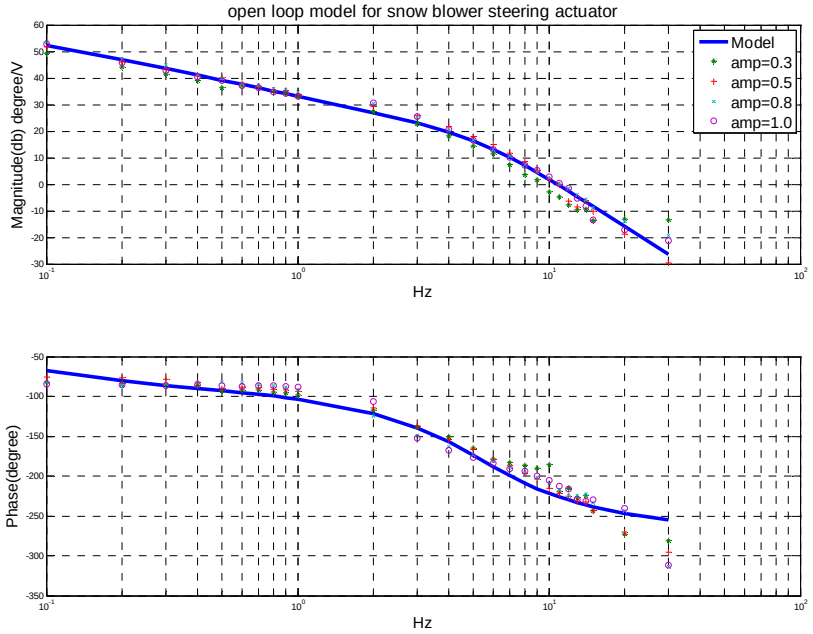

Figure 7. 5 Snowblower steering actuator open loop frequency response

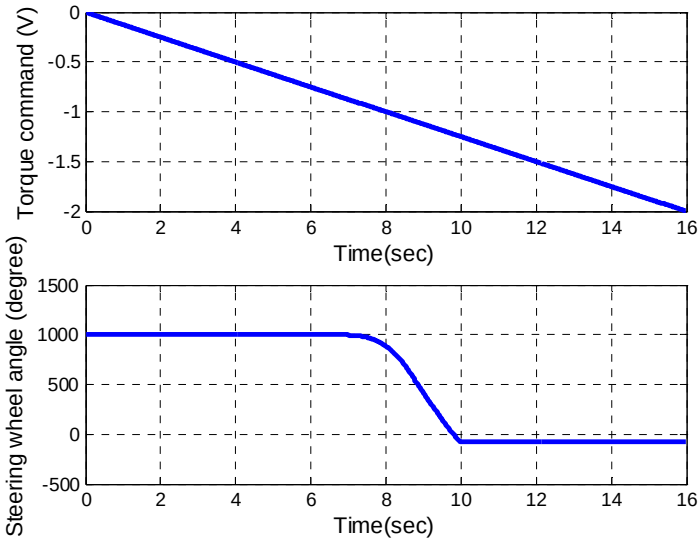

Figure 7. 6 Friction effect

Closed loop servo design

Figure 7.7 shows the closed loop diagram of steering actuator position servo. To address design difficulties mentioned above, different strategies are adopted. First, loop shaping is used to increase closed loop bandwidth as much as possible. In order to overcome friction effect and achieve about 1 degree tracking accuracy up to 4 or 5 Hz, the gain of servo controller has to be sufficient high. However, high gain across all frequency may excite high frequency uncertain dynamics. As shown in Figure 7.8, a PD controller is tested first. Although the gain is not high enough to meet 1 degree accuracy requirement, the response already shows a high frequency chattering. Therefore, the

frequency response of servo controller needs to be carefully shaped to meet stringent performance requirement and avoid exciting high frequency uncertain dynamics simultaneously.

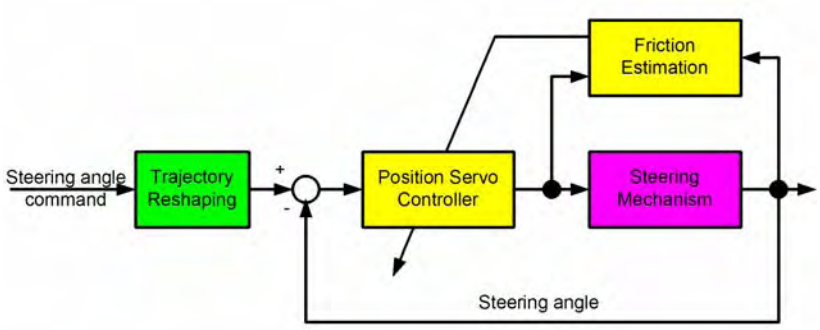

Figure 7. 7 Closed loop diagram of steering actuator position servo

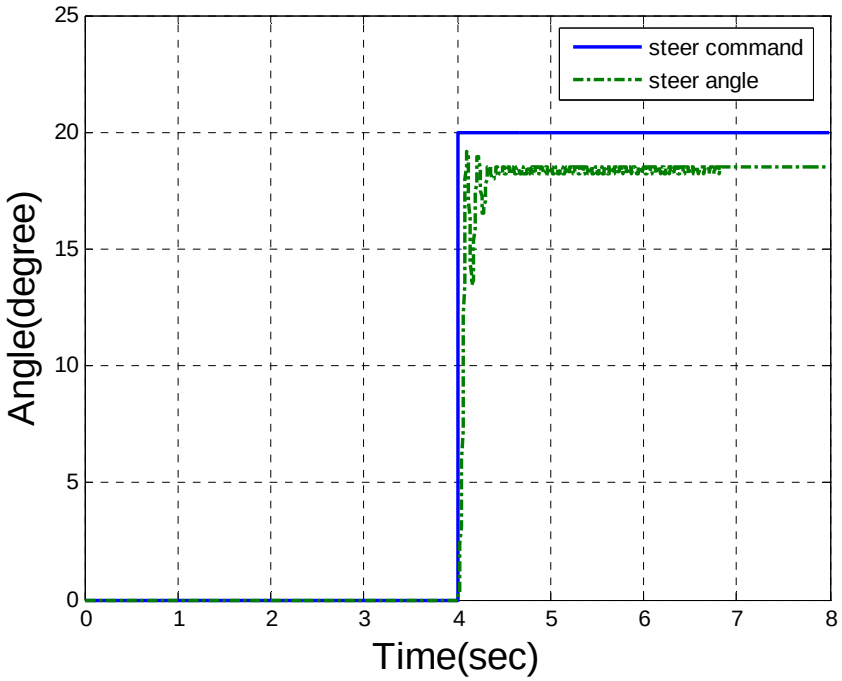

Figure 7. 8 Step input of a PD controller

After loop shaping design, a baseline high gain linear servo controller which will satisfy different performance requirement under most scenarios is obtained. The next step is to take care of different nonlinear phenomena which may have some impacts on system performance under certain conditions. The friction effect will be studied first. Although the gain is high enough to overcome friction and bring tracking error within required 1 degree range as shown in Figure 7.9, the friction can still slow system response when command input amplitude is small. Friction compensation is added to speed response as shown in Figure 7.10. An adaptive feature is also used to accommodate friction changes due to different road conditions.

In our actuator design, the motor torque command is always saturated due to its "under powered" nature. Such saturation may cause large overshoot as shown in Figure 7.11 when command is large. A trajectory reshaping technique and low-and-high gain design are used to address such windup problem. Figure 7.12 shows the step input result with anti-windup design, the overshoot is disappear. The final closed loop frequency response is shown in Figure 7.13 with 6-7 Hz bandwidth.

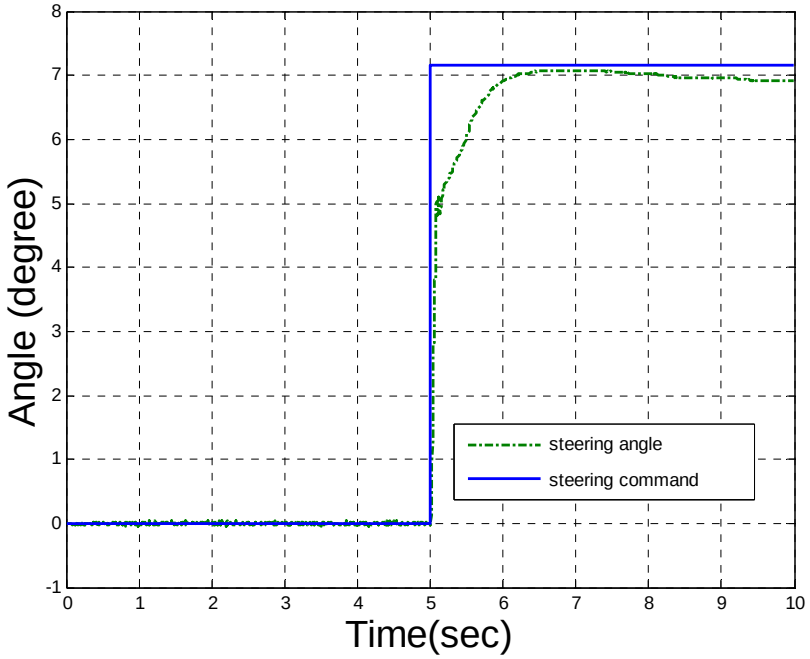

Figure 7. 9 Friction effect for small amplitude command

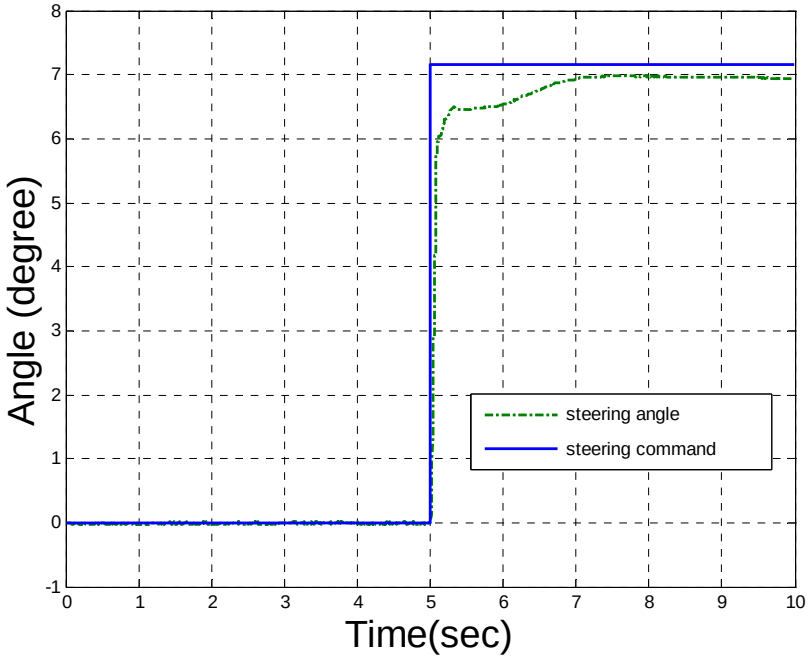

Figure 7. 10 Step input with friction compensation

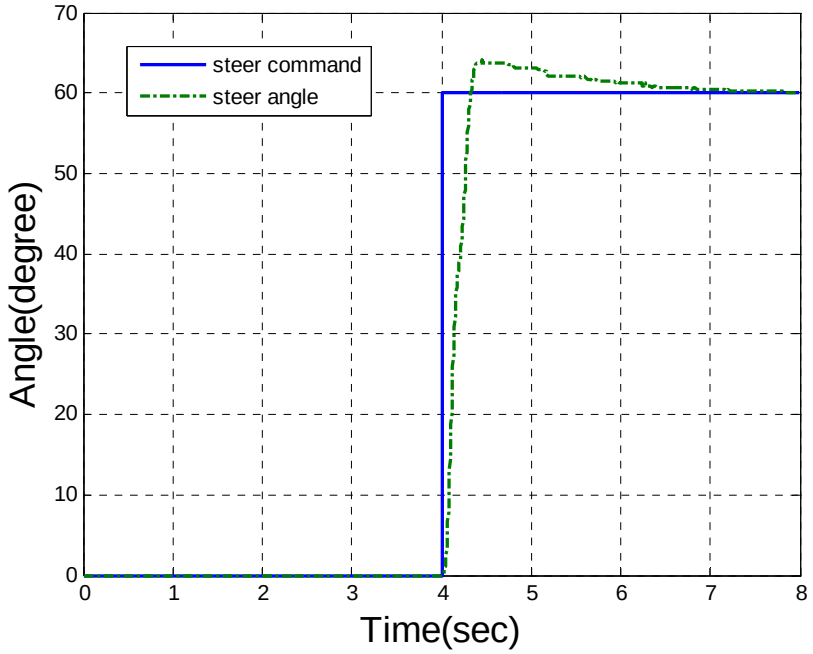

Figure 7. 11 Overshoot when command input is large

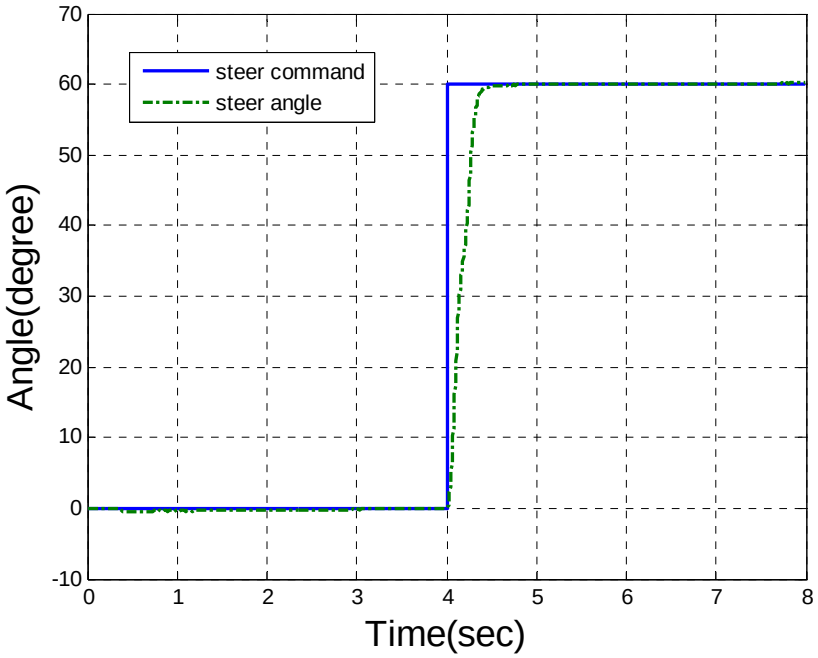

Figure 7. 12 Step input with anti-windup

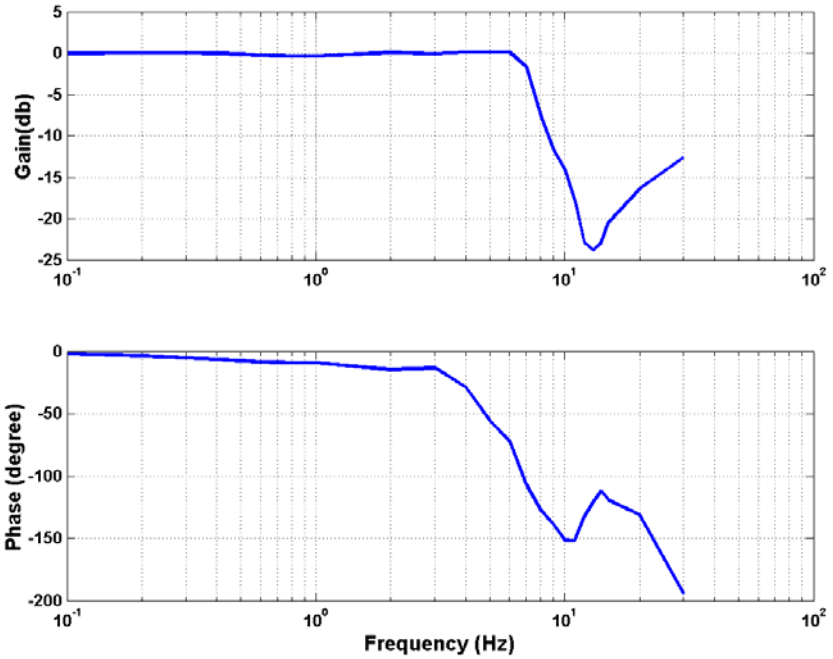

Figure 7. 13 Closed loop response

8. Actuator Fault Detection

During the initial test operations at the Kingvale yard, we came to an understanding that one of the critical system fault is more difficult to detect than the others: the steering actuator motor failures. Motor fault detection is important in acquiring safe and reliable motor operation for crucial applications. This is especially true in snowblower automation since fault of actuators/motors can cause performance degradation or even system failure. The design process started with finding an appropriate diagnosis method for identifying motor failures. The method was first developed and demonstrated in a hardware-in-the-loop (HIL) simulation of steering systems before implementing to the snowblower. This section mainly describes the dynamics of the steering actuator, the resulting model-based fault detection, and the experimental validation by using the Hardware-in-the-Loop simulation.

8.1 Fault Detection Method

Motor Model

The steering actuator includes two major components: DC motor and electronic control unit (ECU). Figure 8.1 shows the dynamics of the DC motor. The rotor windings in the motor generally act as an RL circuit. This imposes first-order dynamics between the voltage and the current. The generated motor torque is proportional to the current times the torque constant, K_t. From Faraday's law, the back electromotive force (back emf) v_b is induced against the armature voltage when the rotor windings spinning in the magnetic field, which reduces the voltage across the RL circuit. An ECU is used to supply electric power to drive the motor. Two different types of ECU are commonly used: current control and voltage control. The ECU used in the snowblower actuator is of the current control type. The study of the fault detection focuses on this type.

The pulse width modulation (PWM) is the prevailing technology in the products of ECU due to its high efficiency and capability to supply large power. This PWM signal generally reaches up to 50 kHz. When the PWM signal is fed into the motor circuit, the coil presents an inductive load and its inductance filters much of the high-frequency energy. The current rises and falls when PWM signal is on and off, respectively. As a result, the current in the motor circuit looks like a DC signal plus small ripples, as shown in Figure 8.2.

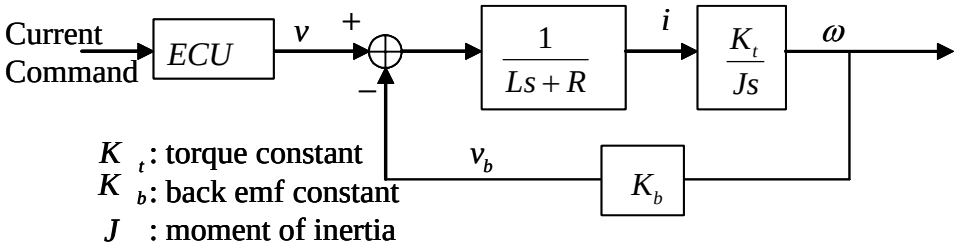

Figure 8. 1 Block diagram of motor dynamics

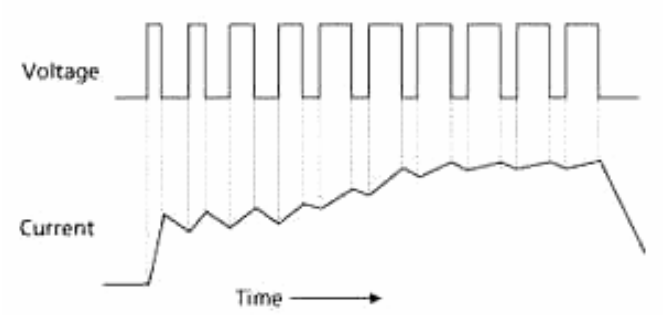

Figure 8. 2 Drive current in PWM motors: DC plus small ripples

Model-Based Fault Detection

The proposed methodology of the motor fault detection relies on the understanding of the motor dynamics. This approach is conducted by identifying the important system parameter: back emf constant K_b, which is estimated using the system states. These states include motor speeds, current, and voltage. Since the input command of the ECU defines the drive current and the motor speed can be calculated from steering encoder information, the detection hinges on the voltage measurements. To extract the low-frequency contents of the PWM voltage signal, simple low pass circuitry is incorporated. Ideally, the measured voltage should be exactly the same as that predicted from the identified model of the actuator under normal conditions and faults are detected as soon as the measured voltage is different from the predicted voltage. Figure 8.3 presents the diagram of this fault detection methodology. The advantage of this method is that a fault can be detected before automation if the motor clutch is engaged. For instance, when a driver turns the steering wheel, a back emf is induced. To keep zero current in the armature windings, the ECU has to respond to the induced voltage. Failed or incorrect response implies the malfunctioned motor/ECU. This argument was verified by using the following test. Figure 8.4 shows the comparison between the measured response from the ECU and from the model. This was performed under large steering motions. The voltage from the ECU follows the desired signal well. It also indicates that the estimated back emf constant $\hat{K}_b$ is the same as the identified value $\bar{K}_b$.

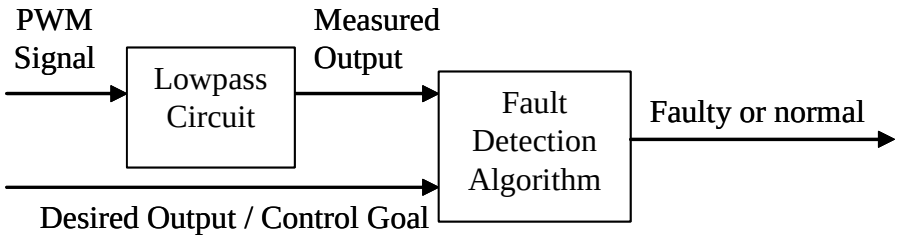

Figure 8. 3 Schematic of fault detection

Under realistic situation, the speed of the steering wheel can be very small. Noise, disturbance, and unmodeled dynamics may cause very low signal-to-noise ratio (S/N

ratio). Figure 8.5 shows the measured and desired signals with very small steering input. It is clear that to estimate the back emf constant $\hat{K}_b$ turns out to be a difficult task.

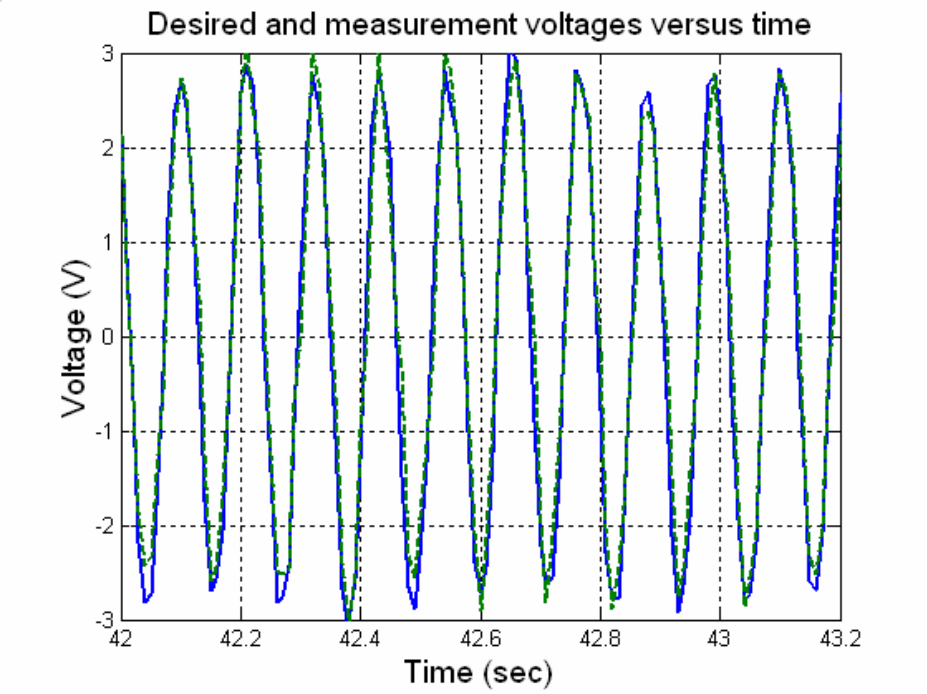

Figure 8. 4 Large signals: the desired (solid line) and actual (dash line) voltages

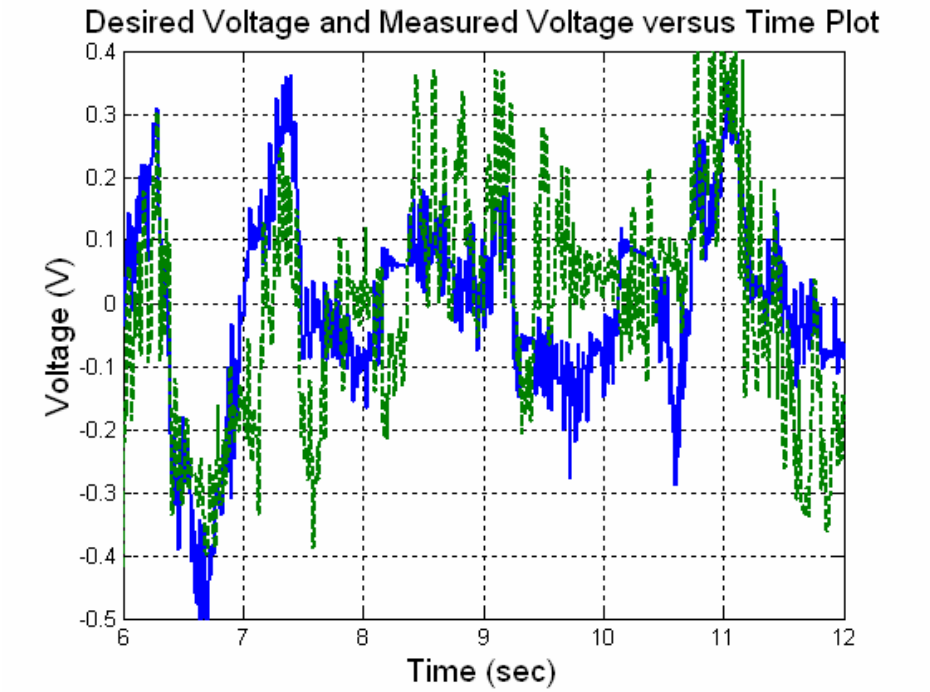

Figure 8. 5 Small signals: the desired (solid line) and measured (dash line) voltages

A least square algorithm is employed to perform the fault identification study. This estimation theory provides a simple and robust approach and is widely used due to the following two reasons: (1) the ease of computation and (2) the best linear unbiased estimation.

Consider the following statistical model:

$$v_i^m = \theta v_i^d + e_i \tag{8.1}$$

where v_i^d and v_i^m are the desired and measured voltages, respectively, e_i is the noise, and θ is defined to be unity if the system is normal. By minimizing the cost function, $J(\theta) = \left\| v^m - \theta v^d \right\|^2$, the estimation of θ is shown in the following manner:

$$\hat{\theta}_{LS} = (v^{d*} v^d)^{-1} v^{d*} v^m = \frac{\sum_i v_i^d v_i^m}{\sum_i (v_i^d)^2} \equiv \frac{\hat{K}_b}{K_b^{true}} \tag{8.2}$$

The estimated back emf constant, $\hat{K}_b$, is determined given the data in the past. It can be shown that the larger the input signal is, the fewer the data points are needed to achieve the desired accuracy.

Eq. (8.3) can be rewritten in a matrix representation:

$$\underset{\sim}{v}_m = \underset{\sim}{v}_d \theta^{true} + \underset{\sim}{e}, \text{ where } \underset{\sim}{e} \sim N(0, I). \tag{8.3}$$

It is easy to observe that:

$$E[\hat{\theta}_{LS} - \theta^{true}] = E[\frac{\underset{\sim}{v}_d{}^T (\underset{\sim}{v}_d \theta^{true} + \underset{\sim}{e})}{\underset{\sim}{v}_d{}^T \underset{\sim}{v}_d} - \theta^{true}] = 0, \tag{8.4}$$

$$E[(\hat{\theta}_{LS} - \theta^{true})^2] = E[(\frac{\underset{\sim}{v}_d{}^T (\underset{\sim}{v}_d \theta^{true} + \underset{\sim}{e})}{\underset{\sim}{v}_d{}^T \underset{\sim}{v}_d} - \theta^{true})^2] = E[\frac{\underset{\sim}{v}_d{}^T \underset{\sim}{e}\underset{\sim}{e}^T \underset{\sim}{v}_d}{(\underset{\sim}{v}_d{}^T \underset{\sim}{v}_d)^2}] = \frac{1}{\underset{\sim}{v}_d{}^T \underset{\sim}{v}_d}. \tag{8.5}$$

Eq. (8.4) presents that that the least square estimate is unbiased and Eq. (8.5) indicates that the algorithm is consistent. By definition, “consistent” means that the variance approaches zero as the length of the data goes to infinity. This implies that the least square estimate converges to the true value with probability 1 if the length of the sequence is sufficiently large. To reach the same accuracy, small signals need more samples than large signals. In implementation, a variable time window can be utilized to collect different numbers of samples.

In reality, this robust algorithm does not guarantee 100% accuracy in estimation since the noise may have correlation with the input signal. When making decisions, a single

threshold may lead to false alarm or missed detection at high possibility. For example, suppose that Figure 8.6 shows the probability density functions of the estimated system parameters for motors with and without fault. Given the respective mean values of the system parameters: $25\%K_b^{true}$ and $100\%K_b^{true}$, it is easy to distinguish the motor status by using a single threshold. This is mainly because the density functions do not overlap. When the mean value of the system parameter for a motor with fault is beyond $25\%K_b^{true}$, the single threshold can cause false alarm and miss detection. This example shows that the difficulties lie in the following issues: (1) the estimated parameter can be viewed as the "noisy version" of the true value; (2) using a single threshold can cause high rates of false alarm and missed detection.

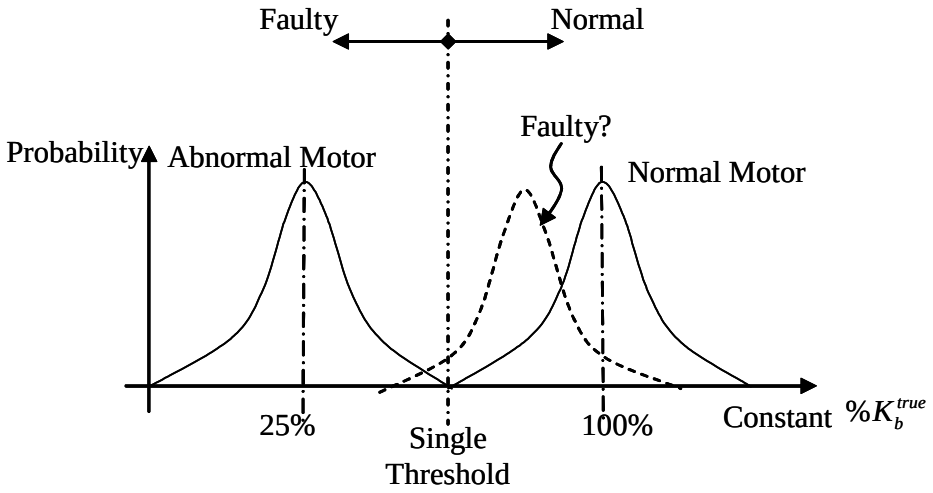

Figure 8. 6 Probability distribution of system parameters under fault or no fault

To solve these problems, two more intermediate states are introduced in this study. As a result, the fault flags contain four states:

$fault\_flag = 0$ (Healthy) if $m_3 > r \geq m_4$

$fault\_flag = 1$ (Not yet determined) if $m_4 > r \geq m_5$ or $m_2 > r \geq m_3$

$fault\_flag = 2$ (Probably Faulty) if $m_5 > r \geq m_6$ or $m_1 > r \geq m_2$

$fault\_flag = 3$ (Faulty) if $r < m_6$ or $r > m_1$

,where $m_1 > m_2 > m_3 > 1 > m_4 > m_5 > m_6 > 0$, $m_1, m_2, m_3, m_4, m_5, m_6 \in \mathrm{R}$, and $r = \frac{\hat{K}_b}{\bar{K}_b}$. A few empirical rules can be integrated into the decision-making procedure. It helps to reduce the probability of false alarm. These rules are listed as follows:

1. Vehicle automation is allowed if the system status remains normal after an amount of time.

2. If the system stays in the “probably-faulty” status for a long time and the power of the desired signal exceeds a threshold, the status turns to “faulty”.
3. If the status is “not-yet-determined” for some time and if the signal power in the time window is larger than a certain quantity, the status turns to “probably faulty”.
4. If the system status falls into “faulty”, the system will be identified as “faulty” and a warning signal must be given to alert the bus driver.

8.2 Experimental Validation

A hardware-in-the-loop (HIL) environment was created to test the proposed fault detection method. This HIL simulation includes most components in an actual steering system: steering wheel, torsion bar, steering column, rack and pinion, and steering actuator, as shown in Fig. 8.7. A reaction motor is also employed to mimic the dynamics of the “unmodeled” system components and the realistic vehicle response. These include the inertia forces from the wheel, the aligning torques from tires, the assist torque from the power steering, as well as the large friction and damping forces from the tire-ground interface.

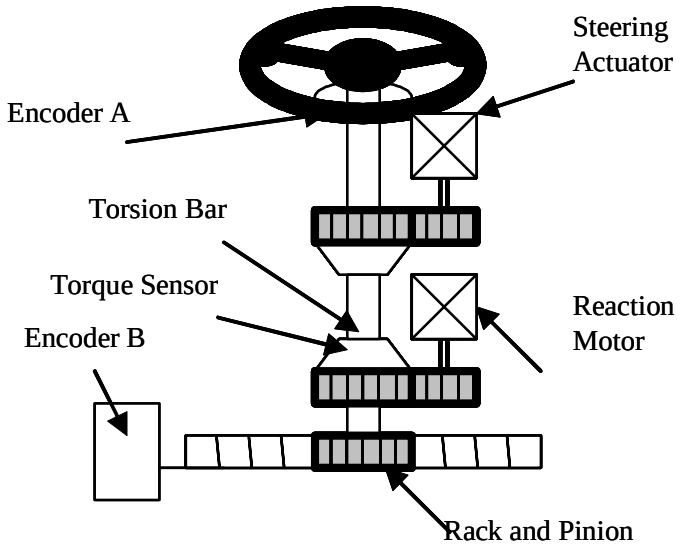

Figure 8. 7 Components in the steering workbench

Figure 8.8 shows the experimental results from a normal motor. The initial system status is set to one. The steering input starts at t = 6 sec and the first identified result shows up at 10.5 sec. The first result is delayed by 5.5 sec due to the small induced voltage. Between 10.5 and 12 sec, the fault flag shows “not-yet-determined” since the magnitude of the measured voltage (dotted line) exceeds the desired voltage (solid line) from 8 to 10.5 sec. After t = 12 sec, the system status remains normal.

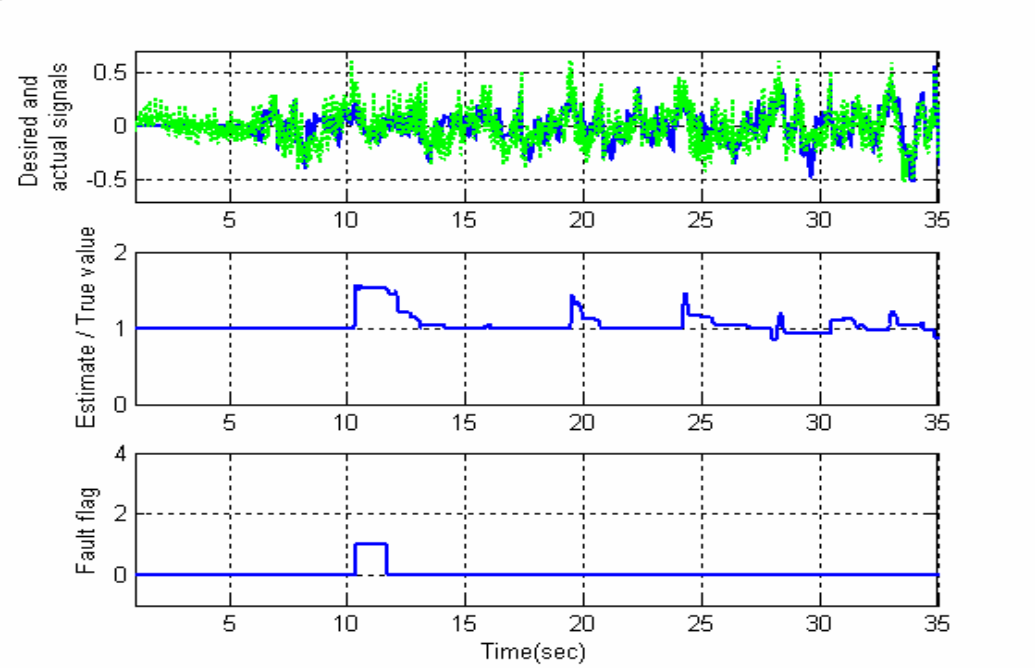

Figure 8. 8 Motor/ECU in normal condition

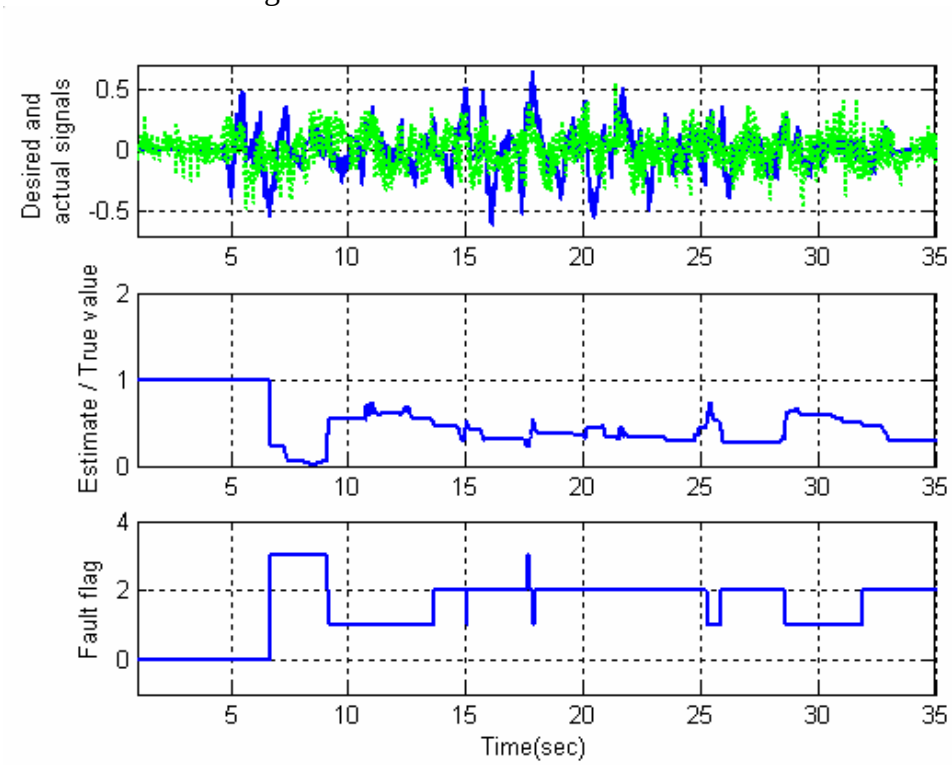

Figure 8. 9 Motor/ECU under fault

Figure 8.9 shows the experimental results under fault. In this example, the true back emf constant was reduced to 40% of the nominal value. The estimated parameter ranges from 0.1 to 0.7. The fault flag shows “faulty” between 7 and 9 seconds. It should be noted that in this experiment the rules in Section 8.2 have not yet been incorporated in the

decision making stage. By using the second or fourth rule, it is easy to see that the motor would be identified as “faulty”.

A model-based fault detection method was developed to monitor the motor fault. This approach employs a minimal set of onboard sensors to collect data. A least square algorithm is used to find the optimal system parameter estimate under measurement noise. The intermediate states and the decision-making rules help to determine the motor fault with low possibility of false alarm. A hardware-in-the-loop simulation, which mimicked the real vehicle environments, validated the effectiveness of the fault detection method. It has been shown that this fault detection approach has the capability to identify motor fault before automation with high confidence.

9. Snowblower Tire Model

A snowblower is a heavy snow removal equipment. It is a two-unit vehicle with four large tires. When modeling the snowblower, it can be treated as a single-unit vehicle due to the rigid linkages between the plow head and the tractor. A bicycle model (with front and rear steering) was analyzed and shown that it could sufficiently describe the dynamics of the snowblower as long as the bicycle model is designed to capture the characteristics of other crucial vehicle components, such as tire, suspension, unsprung inertia, sprung inertia, and actuation devices.

However, there are two major discrepancies between the passenger car and the snowblower during operation: (1) the snowblower tires are typically equipped with snow chains during operation, whose impact to the vehicle steering dynamics is rarely discussed in literature; (2) the snowblower is mostly operated at very low speed (1-5 mph). The low-speed vehicle lateral dynamics are often overlooked in the prior vehicle analysis. There is no guarantee that the conventional vehicle lateral models can accurately predict the dynamics of the snowblower under such conditions. It is desirable to investigate these two issues that in deed play a crucial role in the snowblower dynamics and automation. And it turns out that both issues are strongly related to the tire dynamics that have been over-looked.

Section 9 focuses on two most important modeling issues: the analysis of the snow chain effect and the low-speed steering dynamics. Section 9.1 shows that, with the snow chains installed, the tire force versus slip angle curve is extended to higher slip angles while the cornering stiffness in the *transitional* region is slightly reduced. It concludes that the snow chain effect will not create significant impact on the control design. On the other hand, Section 9.2 shows that, for low-speed operation, the previously unknown low-speed tire characteristics will significantly impact the vehicle lateral dynamics. In Section 9.2, a linearize-able dynamic-deflection tire model is proposed for low-speed vehicle lateral dynamics and control. This tire model describes the empirical tire behaviors as well as captures the often-ignored tire lateral “suspension” modes. When integrated into a vehicle lateral model, the tire model provides sufficient degrees of freedom to match the test data from the snowblower. The low-speed tire model facilitates the automated steering control design for the snowblower in Section 10 and 11.

9.1 Impact of Snow Chains to Vehicle Lateral Dynamics

Since the snow chains impact the tire dynamics directly, it is advantageous to investigate the snow chain effect on tire characteristics. In general, the relationship between the tire lateral force and the slip angle is a crucial element in the analysis and design of vehicle lateral dynamics and controls. This relationship is generally obtained through laboratory tests, but the laboratory test procedures have two major limitations: (I) the simulated road surface may not represent certain real road conditions; (II) the test environment may not sufficiently mimic the tire characteristics under realistic operating conditions, such as large tire-vehicle interactions under emergency conditions or the

changes of suspension and/or steering geometry. As a result, it is very difficult to investigate the tire characteristics with snow chains under a snowy road by using the laboratory tests. It is advantageous to develop an identification approach for tire lateral characteristics using a minimum set of on-board vehicle sensors when the tires are operated in a real configuration and environment. An ideal identification procedure should be insensitive to noise and predict the vehicle lateral behavior accurately. In this section, a point-wise updating approach with an extended Kalman filter using a nonlinear vehicle model is designed to address this problem. This approach successfully identified the characteristic curves between tires with and without snow chains.

Background

Tires follow steering commands and generate forces to control and stabilize the vehicle under various external disturbances. Many researchers divide the tire characteristics into two categories, longitudinal and lateral forces, because of the complexity of tackling both aspects as a whole. This study focuses on the issue of the tire lateral force with respect to the side-slip angle. This is the essential characteristic, which determines vehicle handling and lateral stability properties. Under emergency conditions, severe maneuvers, or extreme road conditions, this relationship can be highly nonlinear and the handling properties may be significantly different from those generated by the linear tire model. Advanced control systems proposed for maintaining lateral stability under these conditions often require accurate tire models to estimate the vehicle state for feedback. In practice, the tire model is obtained through laboratory tests using either a drum or a flat steel belt with various surface treatments to simulate road surfaces. These laboratory procedures have two major limitations: (I) the simulated road condition does not truly represent the actual road surface; (II) there is no guarantee that the tires in a real vehicle configuration will behave exactly the same as those in the laboratory, especially since the tire facility usually tests one tire at a time. For example, it is difficult to simulate snow-covered road conditions or tires under large steering/suspension geometry changes. It is highly desirable to have a simple identification approach using only a minimum set of on-board vehicle sensors, such as wheel encoders and inertial sensors, to identify the tire characteristics under realistic vehicle and road conditions.

The difficulties of such an approach lie on two issues: noises and nonlinearities. In this study, an extended Kalman Filter is employed to deal with the noise problem under nonlinearities. An iterative procedure is proposed to search for a nonlinear relation between the slip angles and the tire forces under quasi-steady-state conditions. This study describes the offline identification procedure and compares the experimental results. By incorporating the identification approach, a passenger car with and without snow chains on a sand-covered test track was used to analyze the impact of the snow chains. This is very important to this project because tires with snow chains under extreme road conditions are rarely discussed in literature and the characteristics are difficult to obtain through laboratory test procedure.

Nonlinear Vehicle and Tire Lateral Characteristics

When a vehicle is cornering, tires generate appropriate lateral forces to support the vehicle along a certain path. These forces create the deformation in the tire tread [10]. As

a result of the deformation, the traveling direction of the tire differs from the wheel center plane by the slip angle. The relation between lateral forces and slip angles determines the vehicle lateral dynamics, which can be very different from those generated by the "geometric model". A typical tire lateral characteristic curve is shown in Figure 9.1. This curve is usually divided into three regions: *linear/elastic*, *transitional*, and *frictional* [11]. Many researchers use a linear tire model to perform analysis on vehicle lateral dynamics and controller design. A linear tire model can be used to predict the properties in the *elastic* region but generally cannot be employed in *transitional* and *frictional* regions. For instance, the vehicle dynamics are unstable when the tires are operated in the *frictional/sliding* region. A linear tire model can not predict the instability.

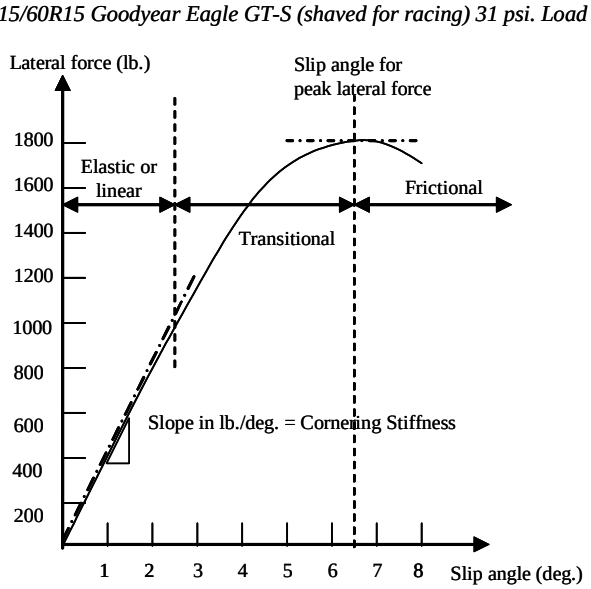

Figure 9. 1Typical lateral force versus slip angle [2]

Since the tread deformation results in side velocity at each tire, the direction of the linear motion of the tire differs from the longitudinal direction of the resulting tire slip angle. The tire slip angle is given by [12]:

$$\alpha_f = \frac{\dot{y}_u + l_1\dot{\varepsilon}}{\dot{x}_u}, \tag{9.1}$$

$$\alpha_r = \frac{\dot{y}_u - l_2\dot{\varepsilon}}{\dot{x}_u}, \tag{9.2}$$

where $\alpha_{f,r}$ is the slip angles of front/rear axles, $l_{1,2}$ is the length between front/rear axles and vehicle C.G., $\dot{x}_u$ is longitudinal velocity in unsprung mass coordinates, $\dot{y}_u$ is the lateral velocity in unsprung mass coordinates, and $\dot{\varepsilon}$ is the yaw rate.

The two equations show that the slip angles can be calculated as long as the vehicle speed, yaw rate and lateral velocity at C.G. can be measured or estimated. When inertia

sensors are used to sense yaw rate, Eq. (9.3) can be employed to estimate lateral velocity at the vehicle C.G.

$$a_x = \ddot{x}_u - \dot{\varepsilon}\dot{y}_u, \tag{9.3}$$

where a_x is the longitudinal acceleration in inertia coordinates and $\ddot{x}_u$ is longitudinal acceleration in unsprung mass coordinates.

The longitudinal acceleration with respect to the inertia frame can be directly measured by a longitudinal accelerometer and the acceleration with respect to the unsprung mass frame can be numerically differentiated from wheel speed sensors. The lateral velocity at C.G. can then be estimated as in Eq. (3). A simple method to predict the lateral force is to use vehicle's onboard sensors and a lateral model given by Eqs. (9.4) and (9.5) below. However, the static nonlinear relationship represented by the resulting force-slip-angle pairs is generally extremely noisy.

$$ma_y = F_f \cos\delta + F_r \tag{9.4}$$

$$I_{zz}\ddot{\varepsilon} = F_f \cos\delta l_1 - F_r l_2 \tag{9.5}$$

where $F_{f,r}$ is the tire lateral forces at front/rear axles, a_y is the lateral acceleration in inertia coordinates, δ is the steering angle, m is the vehicle mass, and I_{zz} is the inertia moment of yaw motion.

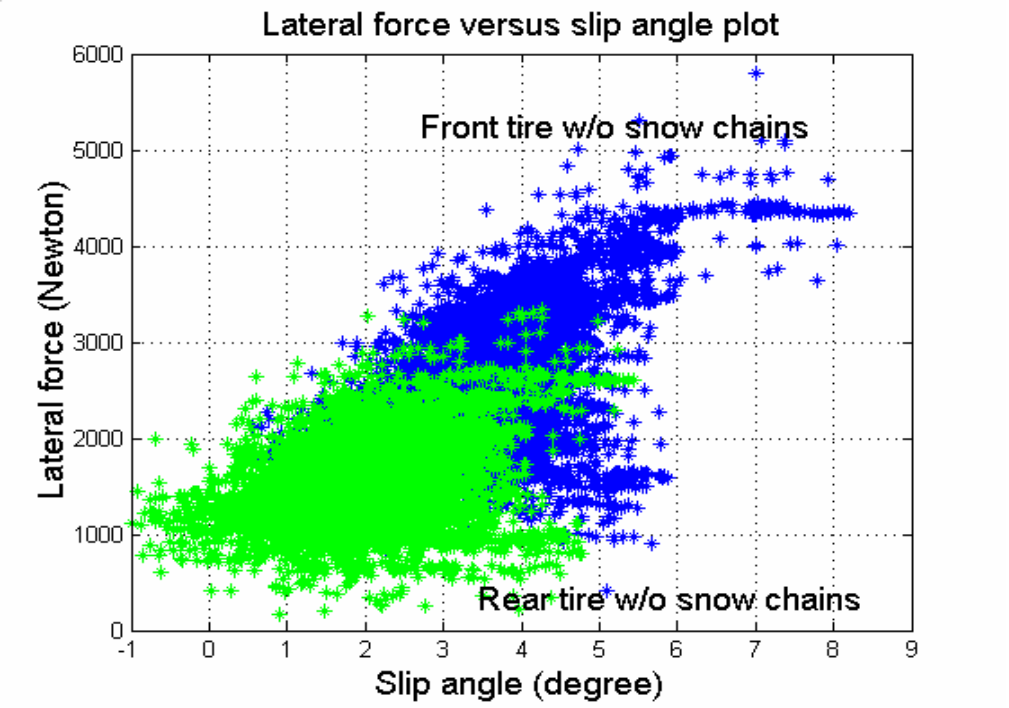

Figure 9. 2 Lateral force versus slip angle (RAW data)

Figure 9.2 is an example of a dispersed plot of such characteristics, which results from feeding the raw test data from a typical vehicle cornering experiment into the equations of force and slip angle estimations. Determining a static nonlinear relationship by using general curve fitting techniques can be difficult. The difficulties lie in: (I) the inherited large noises contained in the vehicle environments and the resulting noise amplification from a nonlinear relationship, (II) a very low signal to noise ratio in the slip angle estimate, (III) the nonlinear relationship between the slip angle and lateral force, and (IV) nonlinearities in the vehicle model under large-angle operating conditions. As a result, the effects of uncertainties and noises are amplified during the calculation of slip angles.

Point-wise Updating Approach with Kalman Filtering

Figure 9.3 shows a typical identification procedure based on a linear model. The adaptation block is designed to minimize the prediction errors by adjusting the system parameters in the linear model [13]. However, this approach cannot be applied to the tire identification due to the nonlinearities and system input noise problems as presented in section II.

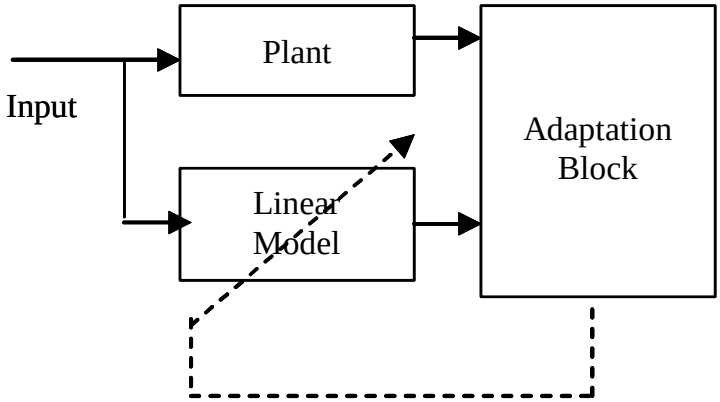

Figure 9. 3 Typical linear system identification

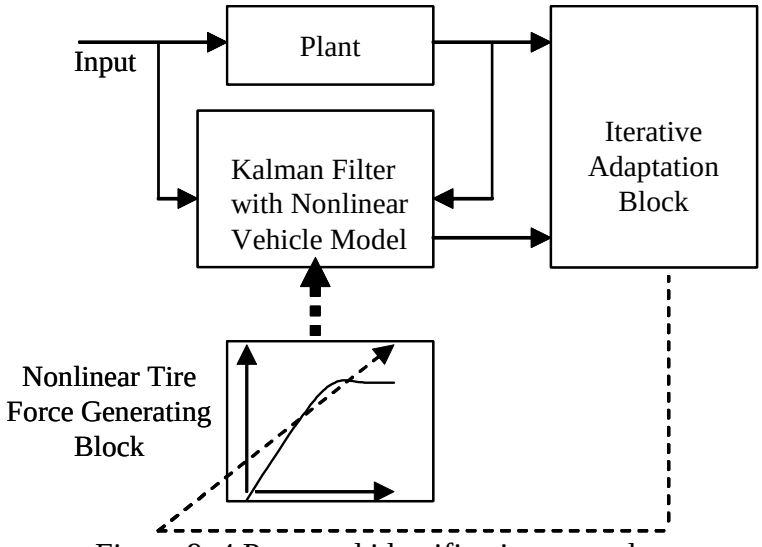

Figure 9. 4 Proposed identification procedure

Frequency-weighted filters can attenuate the measurement noise but fail to account for the nonlinear dynamics. In this study, a Kalman filter is used to reduce the noise effect in the measurements, while a nonlinear vehicle model is incorporated to the filter to account for the nonlinearities. The model-based filtering is found to be effective in addressing both the nonlinearities in the system and the noise in the measurement. The structure of this identification approach is shown in Figure 9.4.

The nonlinear vehicle model [14] used in the modified Kalman filter is expressed as:

$$m(\ddot{y}_u + \dot{x}_u\dot{\varepsilon}) = F_f(\alpha_f)\cos\delta + F_r(\alpha_r) \tag{9.6}$$

$$I_{zz}\ddot{\varepsilon} = F_f(\alpha_f)\cos\delta l_1 - F_r(\alpha_r)l_2 \tag{9.7}$$

Currently, no simple parametric models can effectively describe the tire force generating functions, $F_f(\alpha_f)$ and $F_r(\alpha_r)$, in Eqs. (9.6) and (9.7). "Non-parametric" tire functions are proposed in this study to represent the nonlinear characteristic curves. In practice, the functions $F_f(\alpha_f)$ and $F_r(\alpha_r)$ are parameterized as a set of points (force vs. slip) in a look-up table (see Figure 9.5). Two look-up tables are used to represent the front and rear tire characteristics, respectively. By inserting the two look-up tables into the model in the Kalman Filter, significantly better state estimates can be obtained despite the input/output noise and corresponding nonlinear amplification in the slip angle computation. The errors between the estimates and the measurements will be employed to update the two look-up tables. The "points" on the two "non-parametric" curves will be adjusted iteratively until they converge. The final look-up tables in the iteration are the identified non-parametric curves.

Three key issues in this identification approach will be discussed in detail: (I) modified Kalman filtering, (II) quasi-steady-state operation, and (III) parameter updating algorithm.

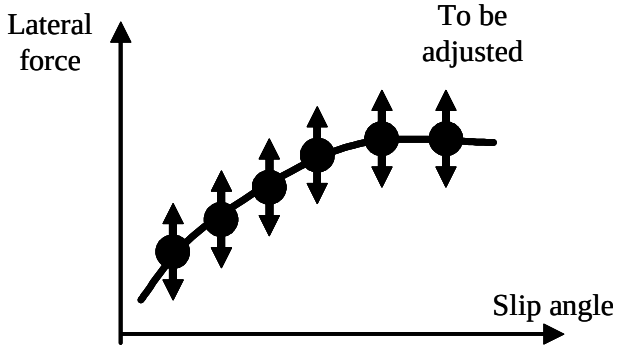

Figure 9. 5 Non-parametric approach using look-up tables

(I) A bicycle vehicle model [15] is used in the modified Kalman filter under the following assumptions:

1. roll and pitch motions are neglected;

2. front/rear two tires are lumped;
3. large steering angle effects are considered;
4. system parameters, such as the inertia and geometric locations are known;
5. time-invariant static nonlinear relations are assumed.

Two system states, yaw rate and lateral velocity at C.G. with respect to the unsprung mass frame, describe the vehicle lateral dynamics. The filter uses yaw rate and the steering angle to generate smooth system states, where the steering angle is the system input and yaw rate is the system output. The filter gain is determined by solving the standard Kalman Filter problem with the linearized mathematical model around each equilibrium point. Gain scheduling is used to ensure the local stability of the filter.

(II) Various types of input can be selected for system identification. One simple choice is to apply step input till the system reaches steady state. The advantages of using step input in the identification of tire lateral properties are: (a) the test can be performed within a small site; (b) noise attenuation can be easily accomplished through "averaging" under steady state conditions. At steady state, a step input usually results in different slip angles on the front and rear tires. If the experiment can be designed to allow both front and rear tires to experience the *elastic*, *transitional*, and *frictional* regions, the parameters on these two characteristic curves can then be fully determined. In the first study, only the characteristic curves in *elastic* and *transitional* regions will be evaluated, since manually steering and stabilizing a vehicle with tires operated in the *frictional* region is difficult. Two basic approaches can be used to create the preferred quasi-steady-state experimental situations:

1. keeping the longitudinal velocity constant and gradually varying the steering angle;
2. keeping steering angle constant and slowly changing the longitudinal velocity.

In this study, the second approach was applied because it allows for a smaller test track using large steering angles.

(III) The two characteristic curves in the look-up tables are the unknowns and need to be initialized before iteration. Iteration can begin with an appropriate guess for each curve. Wrong parameters used in the vehicle model during iteration result in biased estimates. Bias in the estimated states can be computed by averaging the measured and estimated states with a similar estimated slip angle. One widely used approach is to formulate the minimization of the bias as a least-square problem. Consider the following least-square problem. The cost function, $J(\theta) = \|\varepsilon\|^2$ is minimized over θ, where θ represents the unknown system parameters and ε is the vector of the state bias. The gradient descent technique can be employed to search for the minimizer of the cost function. This formulation is similar to the LMS algorithm in the adaptive filtering as can be seen in Eq. (9.8) [16].

$$\hat{\theta}_{k+1} = \hat{\theta}_k - \mu \frac{\partial J}{\partial \theta}\Big|_{\hat{\theta}_k} = \hat{\theta}_k + K\varepsilon \tag{9.8}$$

The gradient of J calculated with the current estimated parameters, $\hat{\theta}_k$, is the steepest descent direction. μ is used for tuning the convergence rate. After some algebra, the term, $-\mu \frac{\partial J}{\partial \theta}\Big|_{\hat{\theta}_k}$, can be expressed as the linear combination of the state bias, $K\varepsilon$, where K is a matrix gain. As a result, the bias is used to update the parameters in the look-up tables. As shown in Figure 9.6, for any given slip angle, $\hat{\alpha}_i$, a corresponding estimated force, $\hat{F}_i(\hat{\alpha}_i)$, will need to be determined, where the subscript i can be f (front) or r (rear). Two consecutive points are connected by splines. The local slope at each point on the characteristic curve can be approximated by differentiating the splines. The local slope is then used for the Kalman filter design. This identification problem can then be regarded as a set of least square problems in solving the forces, F_i's, at the corresponding slip angle, α_i's.

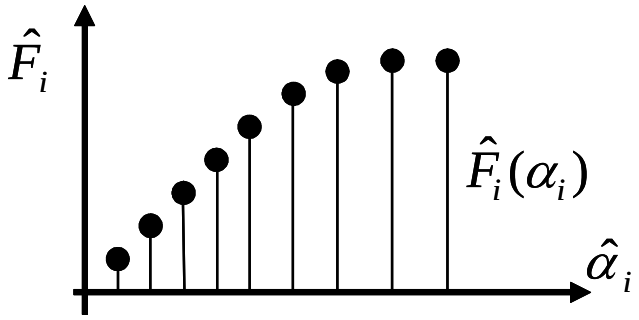

Figure 9. 6 Estimated force at each slip angle of the nonlinear relation

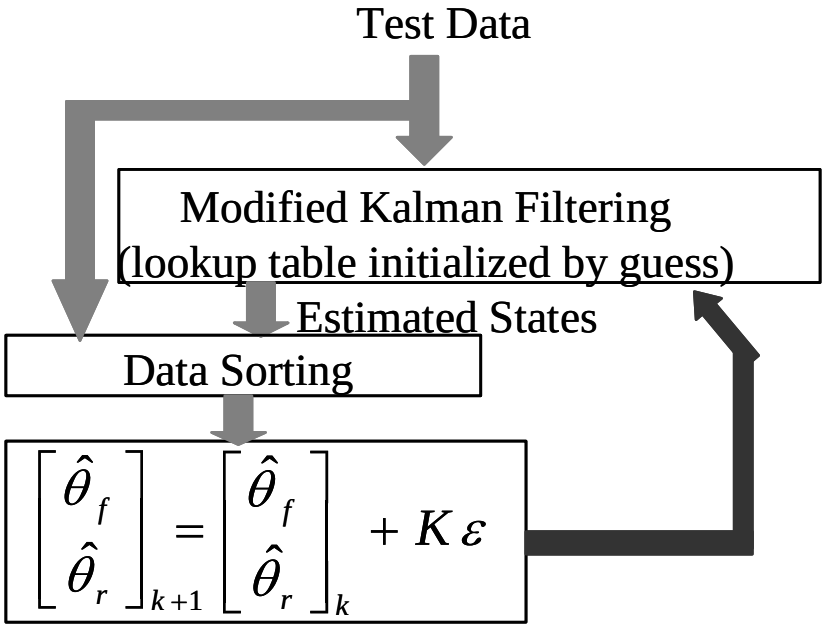

Figure 9. 7 Flow diagram of the identification procedure

The identification procedure is summarized in Figure 9.7. Test data is obtained under the following quasi-steady-state vehicle experiment: slowly changing longitudinal velocities under approximately the same steering input. The data is then fed into the modified Kalman filter. The nonlinear curves of the front and the rear tires in the Kalman filter are initialized by two guessed curves. Estimated and measured states with the similar estimated slip angle are sorted in the same group. The biases are computed by averaging the measured and the estimated states in each group. The curves in the two look-up tables were adjusted by using the linear combination of the state bias. Iteration starts again with newly obtained curves.

Experimental Results

The experiments were conducted on a sand-covered test track. The sand was used to simulate a snow-covered road with reduced road-holding capability. The road was a 2.5-meter-wide circular track with an inner radius of 7.5 meters. The steering angle was fixed at approximately 19 degrees on the front tires and the longitudinal speed was slowly changed from 2 m/sec to 6 m/sec until the wheels began to slide. Three independent configurations were tested in the experiments as shown in Table 9.1.

Table 9.1 Three different configurations using tires with or without snow chains

	Front tire	Rear tire
Configuration 1	w/o snow chains	w/o snow chains
Configuration 2	with snow chains	w/o snow chains
Configuration 3	w/o snow chains	with snow chains

Using the proposed identification approach, Figure 9.8(a), 9.8(b), and 9.8(c) show the final tire lateral force versus slip angle curves of configurations 1, 2, and 3, respectively. Each dot represents the force estimate directly calculated from the measurements and the corresponding slip angle estimate produced from Kalman Filter. The solid line is the non-parametric characteristic curve based on the final iteration. As can be seen in Figures 8.8(d) and 8.8(e), blue lines, green lines, and red lines represent the identified curves for the three configurations, respectively. As expected, the curve of the front tire in configuration 1 is the same as that of the front tire in configuration 3 since neither has snow chains installed. Similarly, the curves for the rear tires in configuration 1 and 2 are the same. The slope of the *elastic* region is almost the same for both tires with and without snow chains. The *elastic* region for tires with snow chains is slightly narrower than that for tires without snow chains. In the *transitional* region, the curves differ much more. With snow chains installed, the *transitional* region of tires with snow chains is able to extend to higher slip angles. On the other hand, the forces in this region will rise up more slowly than those without snow chains. Tires generally slide should they go beyond the *transitional* region. The solid line in the *frictional/sliding* region is not shown in Figure 9.8 because it either violated the assumption of the quasi-steady-state operation or the vehicle was temporarily driven outside the sand-covered test track and onto the pavement. The length of the solid line before the *frictional* region is determined based on the statistics of collected data. Some of the points in the two look-up tables were neglected if the probability was less than a preset threshold. An example is shown in Figure 9.9.

(a)

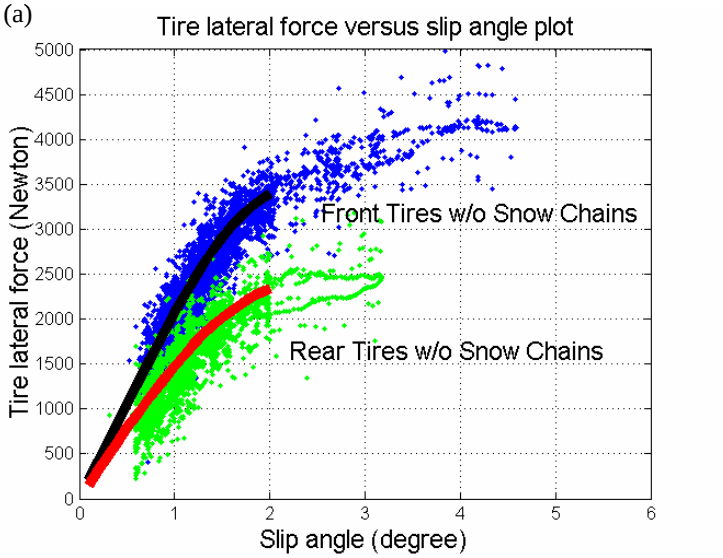
Tire lateral force versus slip angle plot
Tire lateral force (Newton)
Slip angle (degree)
Front Tires w/o Snow Chains
Rear Tires w/o Snow Chains

(b)

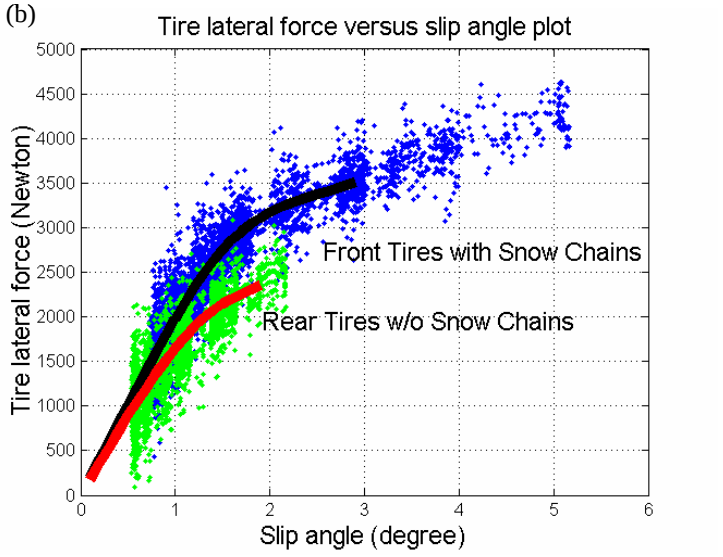
Tire lateral force versus slip angle plot
Tire lateral force (Newton)
Slip angle (degree)
Front Tires with Snow Chains
Rear Tires w/o Snow Chains

(c)

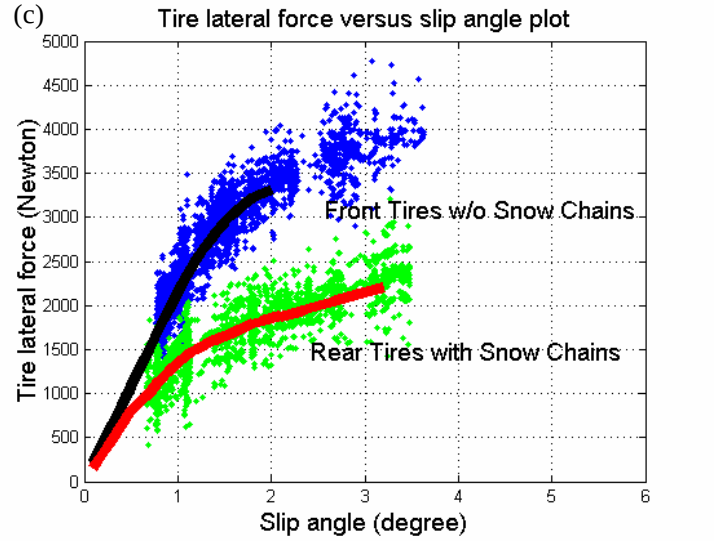
Tire lateral force versus slip angle plot
Tire lateral force (Newton)
Slip angle (degree)
Front Tires w/o Snow Chains
Rear Tires with Snow Chains

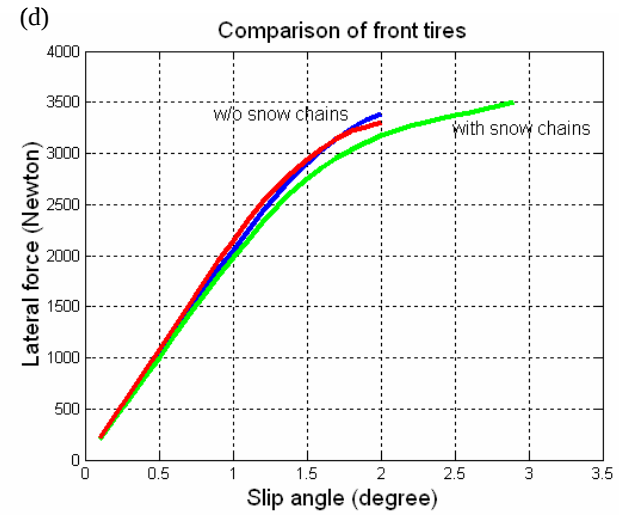

Figure 9. 8 Experimental results on sand-covered road (continued)

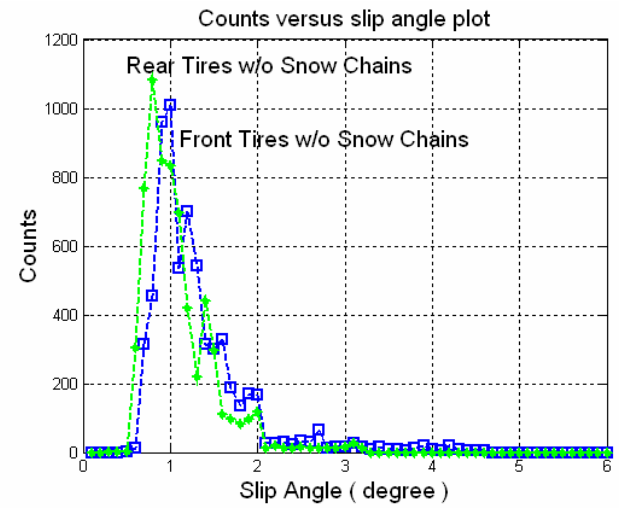

Figure 9. 9 # of points at each slip angle in configuration 1

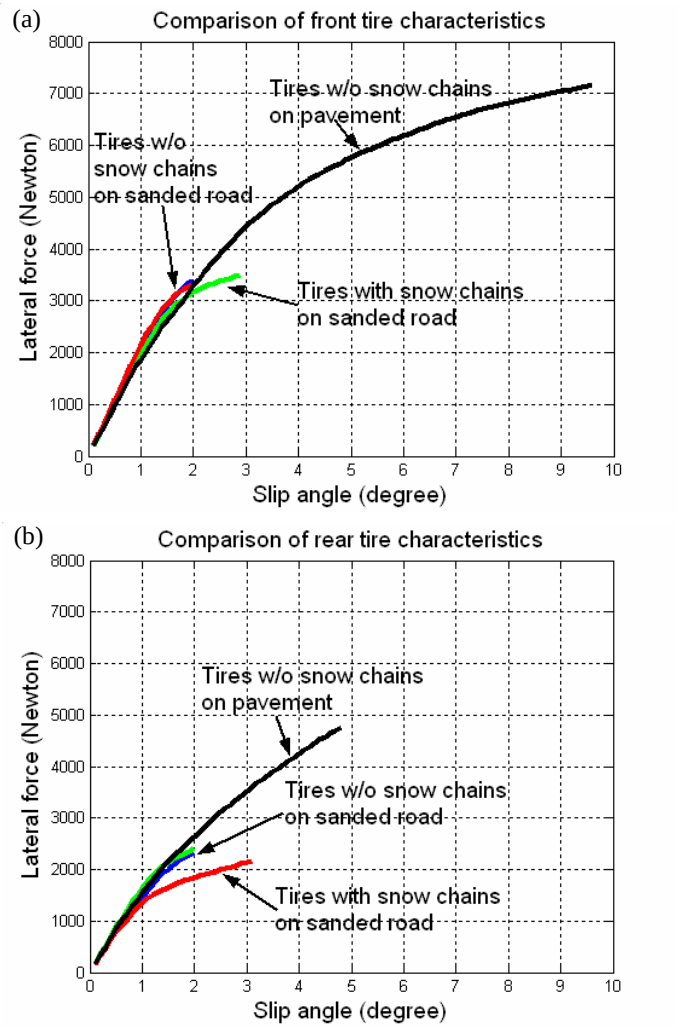

Figure 9. 10 Experimental results on dry pavement

The experiments on dry pavement without snow chains were also performed (configuration 4). The comparison among the identified curves of the four configurations is presented in Figure 9.10(a) and 9.10(b). It can be observed that the curves for either the front or the rear tires in all configurations have approximately the same slope in the *elastic* region. The differences lie in *transitional* regions. The front tire forces saturated at 9.5 degrees for tires without snow chains on pavement, at 2 degrees for tires without snow chains on a sand-covered road, and at 3 degrees for tires with snow chains on a sand-covered road. The rear tire forces can be extended as high as 5 degrees for tires without chains on the pavement, 2 degrees for tires without chains on a sand-covered road, and 3 degrees for tires with snow chains on a sanded road. The results show that this identification approach can be applied to various road conditions.

Conclusion

This study demonstrated that a point-wise updating approach with Kalman filtering using a nonlinear vehicle model can effectively determine the nonlinear tire lateral characteristics by using simple on-vehicle sensors. This offline method successfully

addressed the nonlinearities and the noise problems in a real vehicle environment. The possibility of real-time identification is under investigation. In the example of tires with snow chains, the curve is extended to higher slip angles while the cornering stiffness in the *transitional* region is reduced, which follows our intuition.

9.2 Impact of Low-Speed Tire Characteristics to Vehicle Steering Dynamics

The vehicle lateral dynamics of the snowblower depend heavily on its tire characteristics. A number of tire models were developed to capture the general tire behaviors. Among them, the empirical tire models, generally obtained through lab tests, are commonly used in vehicle dynamics and control analyses. However, the empirical models often do not reflect the actual dynamic interactions between tire and vehicle under real operational environments, especially at low vehicle speeds. This section proposes a dynamic-deflection tire model, which can be incorporated with any conventional vehicle model to accurately predict the resonant mode in the vehicle yaw motion as well as steering lag behavior at low speeds. The snowblower was tested and the data gathered verified the predictions from the improved vehicle lateral model.

Literature Review

Vehicle lateral characteristics are crucial in steering control functions of the advanced vehicle control systems (e.g. automated highway systems (AHS) [17] and advanced chassis control system [18]). In particular, the low-speed characteristics are often overlooked and are very important to vehicle control applications, such as automatic steering systems for bus precision docking [19], the automated rotary plow [20], and the automated rubber tire gantry (RTG) [21]. An accurate tire model is often required to facilitate the design or implementation of these advanced control systems.

Literature review shows that a number of tire models were developed for various purposes. These models generally described the relations between tire deflections and tire forces. However, they all have certain limitations at low vehicle speeds. Tire models can be divided into three categories: physical models, analytical models, and empirical models. (I) The physical models are constructed to underscore several specific tire characteristics such as reinforcement, inflation pressure, rubber elastic behavior, rim contacts, and inertia forces. This model has the ability to describe detailed tire behavior [22]. It is usually employed in a science study to perform simulations to predict tire elastic deformation and tire force. Complex numerical approaches (e.g., the finite element method) are commonly used to solve the equations in these models but are often too cumbersome for vehicle dynamics analysis and control. (II) The analytical model calculates the tire forces and predicts the essential tire elastic characteristics by simplifying the physical equations of a tire. Well-known models include the beam-on-elastic-foundation model and the stretched-string model [23]. They provide a basic understanding of tire lateral behavior. However, the solutions at a non-steady-state involve solving partial differential equations. Therefore, it is not easy to incorporate the PDE models into vehicle control formulation. (III) The empirical model is based on approximations of the relationship between the tire lateral forces and the slip angles. These relationships can be obtained through steady-state lab tests [24] or dynamic lab

tests [25][26]. The linear tire model and the magic formula tire model are two well-known examples that describe steady-state tire behaviors. The relaxation length tire model, essentially a tire model with an additional first-order lag filter, was proposed to describe the dynamical relation between the slip angle and the lateral force for small slip angles based on the dynamic lab test results [27]. For large slip angles, an ad-hoc method that combines the magic formula tire model with the first-order lag was employed [28]. Many studies on the tire dynamic behavior indicate that this lag property is evident at very low speeds.

The empirical tire models are widely used in vehicle dynamics analysis, control designs, and driving simulators. However, these empirical models have two major limitations. (I) They do not represent comprehensive tire lateral dynamics. For example, it is difficult for them to explain the tire shimmy problem [29], which does impact vehicle lateral dynamics. (II) They do not consider the actual tire-vehicle interactions in a real vehicle configuration. These models are generally too simplified to capture both the important secondary tire behaviors as well as the actual interactions between tire and vehicle in a real vehicle configuration.

The main goals included improving the empirical tire model and preserving the ability of the easy applications to control and dynamics analysis. This study describes the development of a simple dynamic-deflection tire model as well as the resulting improvements on the tire-vehicle interface. Low-speed experiments with a snowblower were used to validate the model improvements. The H-infinity theory and μ-synthesis are used to design different steering controllers that show the impact of these specific low-speed dynamics to the vehicle controls. Low-speed vehicle dynamics turn out to be a key factor in designing high-gain automatic snowblower steering control. This important field of dynamics is rarely discussed in literature on vehicle control.

Problem Description

Figure 9.11 shows the system block diagram of a typical vehicle. The vehicle consists of four subsystems - actuation devices, tires, unsprung inertias, and the vehicle body. The actuation devices execute the driver commands to drive the unsprung inertia. Based on the ground conditions and the states of the unsprung inertias, the tires generate forces through the unsprung inertia to control the vehicle body. The common vehicle lateral models, such as the bicycle model [30], the 3-DOF vehicle lateral model [31], and the 6-DOF vehicle model [32], are all within the framework of this block diagram. Each of these models is composed of subsystems with varying degrees of complexity.

The main interests of this study lie in the areas of tire lateral behavior and tire-vehicle interface. Most tire models employed in predicting vehicle lateral controls describe the linear (or nonlinear) static tire behavior with one exception: the relaxation length tire model inserts a speed-dependent first order lag. A large number of vehicle lateral models neglect the dynamics of unsprung inertia. The vehicle body, the unsprung inertia, and the actuation devices are usually treated as a whole. The tire forces are then directly applied to this lumped-together variation of the vehicle body, and the steering mechanism simply imposes a geometric constraint between the wheels and the vehicle body. However, this

simplification may not be applicable under low-speed conditions, when the wheels and the vehicle body have noticeable relative motions. For example, a vehicle yaw motion can be observed clearly when the driver swivels the steering wheel in a vehicle which is nearly standing still. This observation indicates that the "tire yaw suspension" between the vehicle and the ground, and the steering "dynamics" of the front wheels cannot be neglected at very low speeds.

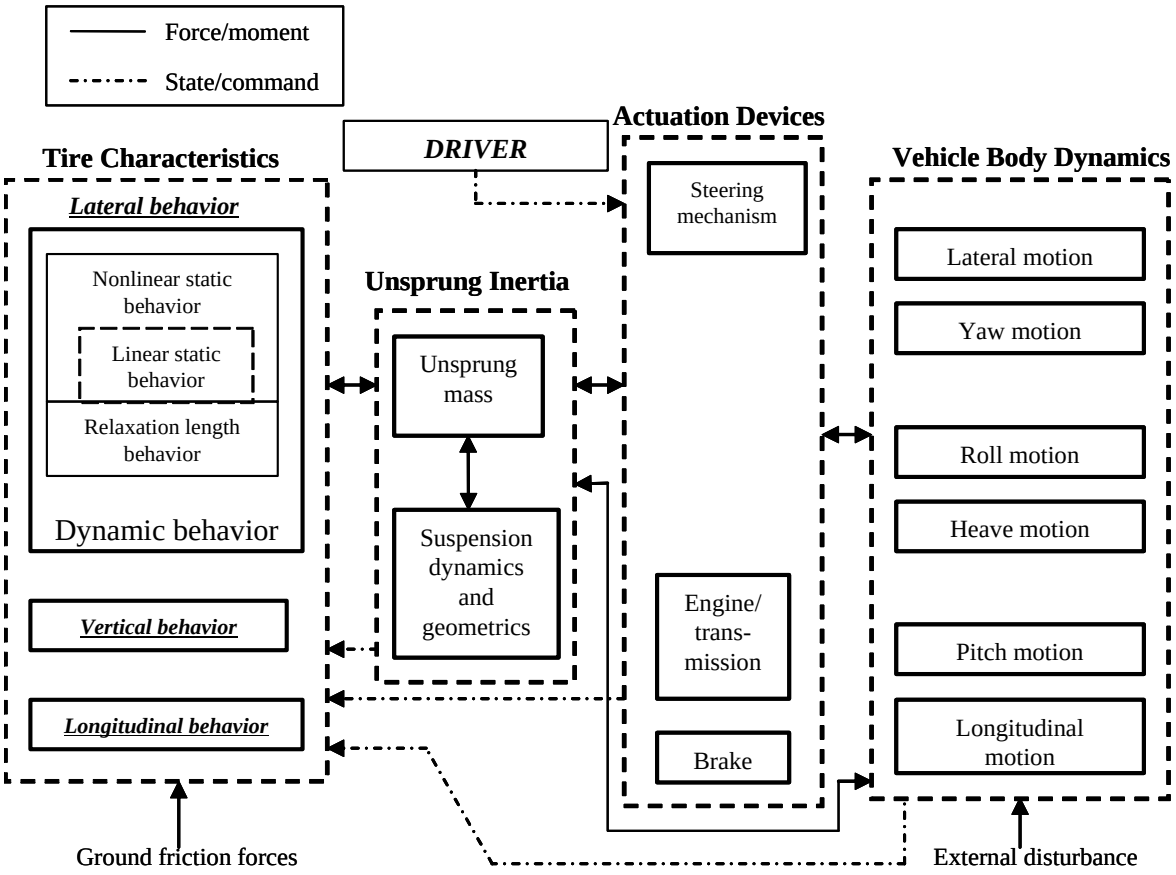

Figure 9. 11 General system diagram for a typical vehicle

To study the impact of the above-mentioned often-ignored tire and interface dynamics, an improved tire model with an augmented tire-vehicle interface is needed. This tire model should have the following properties: (I) it is relatively simple and linearizable for most control system synthesis and analysis; (II) it includes the commonly known tire characteristics, such as the side slip angle and the lag behavior of the tire force; (III) when incorporated into a vehicle lateral model, this model describes the essential modes of the vehicle body; (IV) the resulting tire-vehicle interface captures the internal dynamics between the tires and the vehicle body that cannot be represented by a typical vehicle suspension model.

These following sub-sections describe the improved vehicle lateral model, which includes the proposed dynamic-deflection tire model and the resulting tire-vehicle interface mechanism.

Dynamic-Deflection Tire Model

In principle, vehicle body dynamics have six degrees of freedom (6 DOF). A typical vehicle suspension mechanism allows large relative motions in the roll, pitch, and vertical directions between the vehicle body and the unsprung inertia. The suspension mechanism is generally very stiff in longitudinal, lateral, and yaw directions since it directly transmits the tire forces without internal vibrations. Therefore, the suspension mechanism significantly impacts the vehicle dynamics in the roll, pitch, and vertical axes. As a result, the tire "compliance" characteristics become the most dominant sort of dynamics in the remaining axes: longitudinal, lateral, and yaw. The proposed tire model was developed along these three principal axes.

This 3-DOF tire model should capture the elastic properties of the tires in order to describe tire suspension behaviors that may impact vehicle dynamics. Three independent sets of nonlinear springs and dampers are utilized to represent the tire modes. The springs and dampers are typically characterized by the dynamic relation between tire deflections and forces. The tire deflections $\sigma_x, \sigma_y, \alpha_{yaw}$ are defined as the wheel displacements with respect to the tire contact patch in the three principal axes of the wheel. The tire tread within the contact patch is assumed to be in contact with the ground without sliding. The expressions for these nonlinear springs and dampers are shown in Eq.(9.9), (9.10), and (9.11). These constitute the 3-DOF dynamic-deflection tire model, denoted by 3-DOF DDT model.

$$F_{long} = f_{F_x}(\dot{\sigma}_x, \sigma_x). \tag{9.9}$$

$$F_{lat} = f_{F_y}(\dot{\sigma}_y, \sigma_y). \tag{9.10}$$

$$M_{yaw} = f_{M_z}(\dot{\alpha}_{yaw}, \alpha_{yaw}). \tag{9.11}$$

where σ_x and σ_y represent the longitudinal and lateral tire deflections, respectively, and α_{yaw} is the yaw slip angle of the tire.

Under the small-deflection assumption, Eq. (9.12), (9.13), and (9.14) give the linear representation of the 3-DOT DDT model. The tire lateral force is concentrated behind the center of the contact patch by a distance d_{trail} (pneumatic trail), which helps generate the self-aligning moment.

$$F_{long} \cong D_{long}\dot{\sigma}_x + C_{long}\sigma_x. \tag{9.12}$$

$$F_{lat} \cong D_{lat}\dot{\sigma}_y + C_{lat}\sigma_y. \tag{9.13}$$

$$M_{yaw} \cong D_{yaw}\dot{\alpha}_{yaw} + C_{yaw}\alpha_{yaw}. \tag{9.14}$$

where $D_{long}, D_{lat}, \& D_{yaw}$ are the tire longitudinal, lateral, and yaw damping coefficients, respectively; $C_{longitudinal}, C_{lateral}, \& C_{yaw}$ are the tire longitudinal, lateral, and yaw spring constants, respectively.

Among these tire deflections, the yaw and lateral deflections change the direction the wheel is traveling. This is a result from the facts: (I) the deflection of tire tread is continuous; (II) the tire tread within the contact patch is in contact with the ground without sliding. The kinematics of the wheels and contact patch under the yaw and lateral tire deflections are described as follows.

Define a lateral slip angle α_{lat} and a lateral relaxation length σ_{lat} such that:

$$\alpha_{lat} \cong \sigma_y / \sigma_{lat} = v_s / v_r \tag{9.15}$$

where v_r is the wheel rolling velocity (as shown in Figure 9.12(a)); v_s is contact patch side velocity with respect to the ground. This indicates that the direction the wheel is traveling changes as soon as the tire lateral deflection occurs.

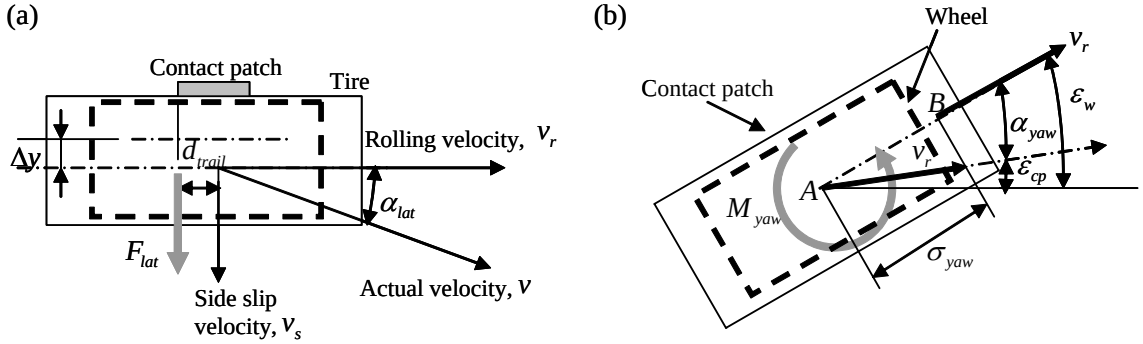

Figure 9. 12 Top view of (a) lateral deflection and associated force (b) yaw deflection and associated moment

In the inertia coordinates, a wheel yaw angle and a contact-patch yaw angle are defined as ε_w and ε_{cp}, respectively. By definition,

$$\alpha_{yaw} = \varepsilon_w - \varepsilon_{cp}. \tag{9.16}$$

As shown in Figure 9.12(b), Point A represents the center of the contact patch and Point B is the location ahead of the contact patch by a distance σ_{yaw} (yaw relaxation length) along the tire equatorial line. Given the wheel speed v_r, the speed of each material point between A and B with respect to the wheel center is also v_r.[1] Without tire lateral forces, the intersection angles between the velocity directions of the points and the wheel center plane vary from $\varepsilon_{cp}(t)$ to $\varepsilon_w(t)$ (from A to B) when the yaw slip angle occurs. The transport of these material points into the contact patch continues to alter $\varepsilon_{cp}(t)$. The small angle between $\varepsilon_{cp}(t)$ and $\varepsilon_w(t)$ determines the rate of $\varepsilon_{cp}(t)$, as shown in Eq.(9.17).

[1] Since the velocity of the material point at A with respect to the ground is zero, $\vec{v}_{wheel\ center} = \vec{v}_A$.

$$\dot{\varepsilon}_{cp}(t) = v_r[\varepsilon_w(t) - \varepsilon_{cp}(t)]/\sigma_{yaw} \tag{9.17}$$

Taking the Laplace transform of Eq.(9.17), the transfer function from ε_w to ε_{cp} is given by:

$$\varepsilon_{cp} = \frac{v_r/\sigma_{yaw}}{s + v_r/\sigma_{yaw}}\varepsilon_w . \tag{9.18}$$

Eq. (9.18) shows that $\varepsilon_{cp}(t)$ follows $\varepsilon_w(t)$ with lag of v_r/σ_{yaw}. By defining actual and effective steering angles as $\delta \equiv \varepsilon_w - \varepsilon_s - \varepsilon_d$ and $\delta_{eff} \equiv \varepsilon_{cp} - \varepsilon_s - \varepsilon_d$, respectively, where ε_s represents the vehicle body yaw angle with respect to the road reference frame and ε_d is the yaw angle of the road reference frame with respect to the inertia frame, the relation between δ and δ_{eff} can then be expressed as:

$$\delta_{eff} = \frac{v_r/\sigma}{s + v_r/\sigma}\delta . \tag{9.19}$$

In the above equation, the vehicle yaw angle $(\varepsilon_s + \varepsilon_d)$ does not appear because changing this angle does not generate tire yaw slip angles directly but slightly alters the rolling speeds of each wheel.

The tire dynamics described by the 3-DOF DDT model should comply with the empirical tire characteristic: the relationship between the lateral force F_y and the slip angle α as found in the lab tests. Since the slip angle α is defined as the angle between the wheel center plane and the traveling direction of the wheel center, it can be rewritten as:

$$\alpha = \alpha_{lat} + \alpha_{yaw} . \tag{9.20}$$

In addition, Eq. (9.20) shows the governing equation of the Relaxation Length Tire model (denoted by the RLT model).

$$F_y = C_\alpha \frac{v_r/\sigma}{s + v_r/\sigma}\alpha , \quad \text{(RLT model)} \tag{9.21}$$

where σ : relaxation length,
C_α : tire cornering stiffness.

By combining Eq. (9.13) and (9.15), lateral force in the 3-DOF DDT model can be rewritten in terms of the lateral slip angle α_{lat}, as shown in Eq. (9.22). By using Eq. (9.20) and (9.18), Eq. (9.23) gives the tire lateral force in terms of the side slip angle α.

$$F_{lat} = (D_{lat}s + C_{lat})\alpha_{lat}\sigma_{lat} \tag{9.22}$$

$$= (D_{lat}\sigma_{lat}s + C_{lat}\sigma_{lat})\frac{v_r / \sigma_{yaw}}{s + v_r / \sigma_{yaw}}\varepsilon_w . \tag{9.23}$$

Note that the wheel yaw angle is the same as the steering angle in the lab test scenario (i.e. $\varepsilon_w = \alpha$).

The cornering frequency of $(D_{lat}\sigma_{lat}s + C_{lat}\sigma_{lat})$ is generally in the order of 5 Hz. To keep the low-frequency characteristic in Eq. (9.23) the same as that in Eq. (9.21), it is easy to see that:

$$C_{lat} = C_\alpha / \sigma_{lat} , \tag{9.24}$$

$$\sigma_{yaw} = \sigma . \tag{9.25}$$

Improved Tire-Vehicle Interface

The most evident relative motions in the tire-vehicle interface are the suspension motions between the vehicle body and the unsprung mass, the deflections between the wheel and the tire contact patch, and the front wheel steering motion. Conventional vehicle lateral models determine the tire forces based upon the vehicle geometry and velocities, but not the tire deflections. The resultant tire forces are usually described along lateral and longitudinal axes and applied directly to the unsprung mass. Because the relative lateral and longitudinal motions between the unsprung inertia and the vehicle body are very small, the tire forces along these two axes essentially determine the yaw moment of the vehicle. Since the moment of inertia of the front wheels is far less than that of the vehicle body, the yaw dynamics of the front wheels are often ignored. As a result, the relative motions that are sometimes included in the vehicle models are simply the roll, pitch, and heave suspension motions.

It is easy to see that the other two relative motions cannot be captured by the conventional suspension models. The 3-DOF DDT model uses the tire deflections to calculate the tire forces and moments and thus, creates a natural tire suspension to describe the relative motions between the wheel and the contact patch. The following two examples demonstrate the “tire suspension behaviors” along vehicle yaw and lateral axes.

Example 1 – tire yaw suspension behavior: At a vehicle speed of 0 mph, turning the front wheel assembly requires moment, generated by the steering mechanism. The reaction moment forces the vehicle body to turn in the opposite direction. Such a vehicle yaw motion can be formulated using the 3-DOF DDT model. The moments of inertia of the steering components that turn with the vehicle body are lumped together into I_1; the moment of inertia of the front wheel assembly is denoted by I_2. The equations of motion for the two moments of inertia are given by:

$$I_1\ddot{\varepsilon}_s = \sum M_i + \tau , \tag{9.26}$$

$$I_2(\ddot{\varepsilon}_s + \ddot{\delta}) = M_f - \tau , \tag{9.27}$$

where τ : internal moment between I_1 and I_2.

In principle, the 3-DOF DDT model requires an independent set of longitudinal, lateral, and yaw displacements for the contact patch of each tire to calculate tire forces and moments in a planar motion. To avoid unnecessary complexity and to focus on vehicle lateral behavior, y_u^f and y_u^r correspond to the lateral positions of the contact patch at front and rear axles in the road reference frame; δ_{eff} represent the yaw angle of the contact patch at the front axle. For convenience, (y_u , ε_u) are defined as:

$$y_u = (l_2 y_u^f + l_1 y_u^r)/(l_1 + l_2)\,, \tag{9.28}$$

$$\varepsilon_u = (y_u^f - y_u^r)/(l_1 + l_2)\,. \tag{9.29}$$

By applying the 3-DOF DDT tire model, the moments exerted on I_1 and I_2 are shown in Eq. (9.30) and (9.31), respectively.

$$\begin{aligned}\sum M_i = &-2(D_{lat}^f l_1 + D_{lat}^r l_2)(\dot{\varepsilon}_s - \dot{\varepsilon}_u) - 2(C_{lat}^f l_1 + C_{lat}^r l_2)(\varepsilon_s - \varepsilon_u) \\ &-(D_{long}^f + D_{long}^r)(\dot{\varepsilon}_s - \dot{\varepsilon}_u)d - (C_{long}^f + C_{long}^r)(\varepsilon_s - \varepsilon_u)d\,,\end{aligned} \tag{9.30}$$

$$M_f = -[2D_{yaw}^f(\dot{\delta} - \dot{\delta}_{eff}) + 2C_{yaw}^f(\delta - \delta_{eff})]\,. \tag{9.31}$$

where l_1 and l_2 are the distances from the front axle to vehicle C.G. and from the rear axle to vehicle C.G., respectively; d is the track width of the vehicle; $\varepsilon_u = 0$ in this example

By combining Eq. (9.26)-(9.31), a second-order dynamic relation between the vehicle yaw angle and the steering angle is shown in Eq. (9.32), describing the vehicle yaw characteristic with respect to the "tire yaw suspension".

$$\begin{aligned}\frac{\varepsilon_s}{\delta} = &-(I_2 s^2 + 2D_{yaw}^f s + 2C_{yaw}^f)/\{(I_1 + I_2)s^2 + [2(D_{lat}^f l_1 + D_{lat}^r l_2) + (D_{long}^f + D_{long}^r)d]s \\ &+[2(C_{lat}^f l_1 + C_{lat}^r l_2) + (C_{long}^f + C_{long}^r)d]\}\,.\end{aligned} \tag{9.32}$$

Example 2 – tire lateral suspension behavior: A vehicle is traveling at a constant speed v_r on a straight road. A lateral force F_{ext} is applied to the vehicle C.G. and the vehicle exhibits mainly a lateral motion. For convenience, the vehicle yaw dynamics can be ignored. The kinematical equation for the contact patch and the equation of motion for the vehicle are shown as:

$$\dot{y}_u = v_r(y_s - y_u)/\sigma_{lat}.^2 \tag{9.33}$$

[2] Without loss of generality, $\sigma_{lat} = \sigma_{lat}^f = \sigma_{lat}^r$ is assumed.

$$M\ddot{y}_s = F_{lat}^f + F_{lat}^r + F_{ext}. \tag{9.34}$$

where M is the vehicle mass; y_s is the lateral displacement of the vehicle C.G in the road reference coordinates.

The tire lateral forces on the front and rear axles are expressed as:

$$F_{lat}^f = -2D_{lat}^f(\dot{y}_s - \dot{y}_u) - 2C_{lat}^f(y_s - y_u), \tag{9.35}$$

$$F_{lat}^r = -2D_{lat}^r(\dot{y}_s - \dot{y}_u) - 2C_{lat}^r(y_s - y_u). \tag{9.36}$$

Combining Eq. (9.33) through Eq. (9.36), Eq. (9.37) shows a third-order relationship between the input force F_{ext} and the lateral displacement y_s.

$$\frac{y_s}{F_{ext}} = \frac{s + v_r/\sigma_{lat}}{[Ms^2 + (2D_{lat}^f + 2D_{lat}^r + Mv_r/\sigma_{lat})s + (2C_{lat}^f + 2C_{lat}^r)]s}. \tag{9.37}$$

Eq. (9.38) shows the governing equation of a typical bicycle model under the same situation.

$$\frac{y_s}{F_{ext}} = \frac{v_r}{[Mv_r s + 2(C_\alpha^f + C_\alpha^r)]s} = \frac{v_r}{[Mv_r s + 2(C_{lat}^f + C_{lat}^r)\sigma_{lat}]s}. \tag{9.38}$$

When v_r is very small or equal to zero, Eq. (9.37) describes the "tire lateral suspension behavior." The typical bicycle model cannot explain this vehicle lateral motion, as shown in Eq. (9.38). When v_r is very large, the two models exhibit similar characteristics, except at high frequency.

Improved Vehicle Lateral Model

The yaw and lateral motions are the two most dominant portions of vehicle dynamics in lateral control. As discussed in Section 9.2, the often-ignored tire dynamics affect both vehicle yaw and lateral characteristics. A simple bicycle model incorporated with the 3-DOF DDT model can be used to investigate the impact of these neglected dynamics to vehicle yaw and lateral behaviors.

For a vehicle traveling at a constant velocity v_r, the translational and angular velocities of the contact patch centers of the four tires are expressed in Eq. (9.39) and (9.40). These equations are derived from the vehicle geometry and the tire deflections.

$$\dot{y}_u = v_r\varepsilon_u + v_r\delta_{eff}l_2/(l_1 + l_2) + v_r(y_s - y_u)/\sigma_{lat}. \tag{9.39}$$

$$\dot{\varepsilon}_u = v_r\delta_{eff}/(l_1 + l_2) + v_r(\varepsilon_s - \varepsilon_u)/\sigma_{lat} - \dot{\varepsilon}_d. \tag{9.40}$$

The dynamic equations of the improved bicycle model are given by:

$$M\ddot{y}_s = F_{lat}^f + F_{lat}^r - Mv_r\dot{\varepsilon}_d\,, \tag{9.41}$$

$$I_1\ddot{\varepsilon}_s = \sum M_i + \tau\,, \tag{9.42}$$

$$I_2(\ddot{\varepsilon}_s + \ddot{\delta}) = M_f - \tau\,. \tag{9.43}$$

Based on the 3-DOF DDT model, the tire forces and moments are expressed in Eq. (9.44) -(9.47).

$$F_{lat}^f = -2D_{lat}^f[\dot{y}_s - \dot{y}_u + l_1(\dot{\varepsilon}_s - \dot{\varepsilon}_u)] - 2C_{lat}^f[y_s - y_u + l_1(\varepsilon_s - \varepsilon_u)]\,, \tag{9.44}$$

$$F_{lat}^r = -2D_{lat}^r[\dot{y}_s - \dot{y}_u - l_2(\dot{\varepsilon}_s - \dot{\varepsilon}_u)] - 2C_{lat}^f[y_s - y_u - l_2(\varepsilon_s - \varepsilon_u)]\,, \tag{9.45}$$

$$\sum M_i = -c_1(\dot{\varepsilon}_s - \dot{\varepsilon}_u) - k_1(\varepsilon_s - \varepsilon_u) + F_{lat}^f l_1 - F_{lat}^r l_2\,, \tag{9.46}$$

$$M_f = -c_2(\dot{\delta} - \dot{\delta}_{eff}) - k_2(\delta - \delta_{eff})\,, \tag{9.47}$$

where $k_1 = (C_{long}^f + C_{long}^r)d$, $k_2 = 2C_{yaw}^f$, $c_1 = (D_{long}^f + D_{long}^r)d$, $c_1 = 2D_{yaw}^f$.

In general, the damping force and the inertia force on I_2 are relatively small compared with its spring force at low frequencies. The two respective terms $I_2\ddot{\delta}$ and $c_2(\dot{\delta} - \dot{\delta}_{eff})$ in Eq. (9.43) and (9.47) can be ignored. This sacrifices the plant response accuracy at high frequencies but facilitates control designs by lowering the plant order. By combining Eq. (9.39)-(9.47), a 7th order state-space representation can be found as the State Space Form of the Improved Bicycle Model in Section 9.3. The state variables are $[y_u \;\; y_s \;\; \dot{y}_s \;\; \varepsilon_u \;\; \varepsilon_s \;\; \dot{\varepsilon}_s \;\; \delta_{eff}]^T$ and the input is the steering angle δ.

Analysis of the Improved Models

The following sub-sections compare the DDT model and the RLT model in a simulated test scenario, as well as the improvements in predictions of vehicle dynamics from the frequency-domain perspective.

Comparison between RLT Model and DDT Model in a Simulated Test Scenario

The RLT and DDT models utilize a similar first-order relationship. Section 9.1 has shown that the two models typically exhibit the same low-frequency characteristics when testing tires. This section compares the two models under a typical simulated test scenario and the results show again that the two models can have very similar behavior at low frequencies.

This simulated test was designed to investigate the response of a single tire in lateral velocities from external lateral forces. In this scenario, the lateral force F_{ext} is applied to the center of the wheel such that the wheel yaw motion can be ignored. The lateral velocity of the wheel is v_s. The governing equations of the two models in this simulated test are shown below.

(I) <u>*RLT Model*</u>: the equation of motion for the RLT model is given by:

$$m_w s v_s = -C_\alpha \frac{v_r/\sigma}{s + v_r/\sigma} \frac{v_s}{v_r} + F_{ext} . \tag{9.48}$$

where m_w is the total mass of the tire, the wheel, and the vertical load.

By rearranging Eq. (9.48), the transfer function from F_{ext} to v_s can be calculated as:.

$$\frac{v_s}{F_{ext}} = \frac{s + (v_r/\sigma)}{m_w s^2 + (m_w v_r/\sigma)s + (C_\alpha/\sigma)} . \tag{9.49}$$

(II) <u>*3-DOF DDT Model*</u>: the governing equations for the 3-DOF DDT model are expressed as:

$$\dot{y}_{cp} = v_r \sigma_y / \sigma_{lat}, \tag{9.50}$$

$$m_w \dot{v}_s = m_w (\ddot{y}_{cp} + \ddot{\sigma}_y) = -D_{lat}\dot{\sigma}_y - C_{lat}\sigma_y + F_{ext}. \tag{9.51}$$

where y_{cp} is lateral displacement of tire contact patch with respect to the test road. By combining Eq. (9.50) and (9.51), Eq. (9.1)(9.52) shows the transfer function from F_{ext} to v_s.

$$\frac{v_s}{F_{ext}} = \frac{\dot{y}_{cp} + \dot{\sigma}_y}{F_{ext}} = \frac{s + (v_r + \sigma_{lat})}{m_w s^2 + (m_w v_r/\sigma_{lat} + D_{lat})s + C_{lat}} . \tag{9.52}$$

It is clear that the differences between Eq. (9.49) and Eq. (9.52) lie on the following two terms: σ_{lat} and D_{lat}. If σ is equal to σ_{lat}, the frequency responses of the two transfer functions are almost the same at high speeds. At low speeds, the damping constant D_{lat} dominates the damping term $(m_w v_r/\sigma_{lat} + D_{lat})$ for the DDT model. This simulated test shows the following facts.

- The two tire models have the similar characteristics at high speeds in this simulated test scenario.
- Raising the vehicle speed increases the dynamic damping term $m_w v_r/\sigma_{lat}$ in Eq. (9.49) and Eq. (9.52).
- The RLT model exhibits the undamped motion at nearly zero speed; the 3-DOF DDT model keeps the damping coefficient, D_{lat}. Therefore, the 3-DOF DDT model matches more closely to true tire behavior at low speeds.

Analysis of Improved Bicycle Model with DDT Model

This sub-section compares four vehicle lateral models, the geometric model, bicycle model, bicycle model with the RLT model, and bicycle model with the DDT model. These comparisons show the model improvements made in the vehicle yaw and lateral characteristics from the DDT model under dynamic steering inputs. The governing equations of the above four models can be found in Appendix B, C, D, and A, respectively. Inserting the identified parameters of the snowblower from Table 1[3] into the four models, Figure 9.13(a) and 9.13(b) show their respective frequency responses from the steering angle to the yawrate at low and high speeds; Figure 9.14(a) and 9.14(b) illustrate the corresponding responses from steering angle to lateral acceleration at the vehicle C.G.

At high speeds, there are only small differences present among the three "bicycle-based" models. The geometric model does not accurately match any of the bicycle-based models due to its neglected tire dynamics. At low speeds and low frequencies, the geometric model and the bicycle model are equivalent. The bicycle model with the RLT model matches the original bicycle model up to 0.5 Hz. Only the bicycle model with the DDT model and the bicycle model with the RLT model exhibit resonant modes. The following list compares the discrepancies of the resulting low-speed vehicle dynamics between the DDT and RLT models.

- Using the DDT model, the vehicle phase starts to drop significantly above 0.1 Hz. This decrease shows that the vehicle exhibits a steering lag behavior at low frequencies. None of the other models predicts this characteristic.
- At very low speeds, the bicycle model with RLT has a nearly undamped system response; the bicycle model with DDT keeps the tire damping force.
- At zero vehicle speed, only the bicycle model has the singularity problem (divided by $v_r = 0$). Both the geometric model and the bicycle model with RLT have null gains for the transfer functions. The bicycle model with DDT is the only model which exhibits the resonant yaw motion.
- The above observations make it clear that the vehicle model with DDT is the only tire model that matches real-world behavior of vehicles & tires at low speeds.

[3] The identification procedure of the snowblower parameters will be discussed in Section 5.

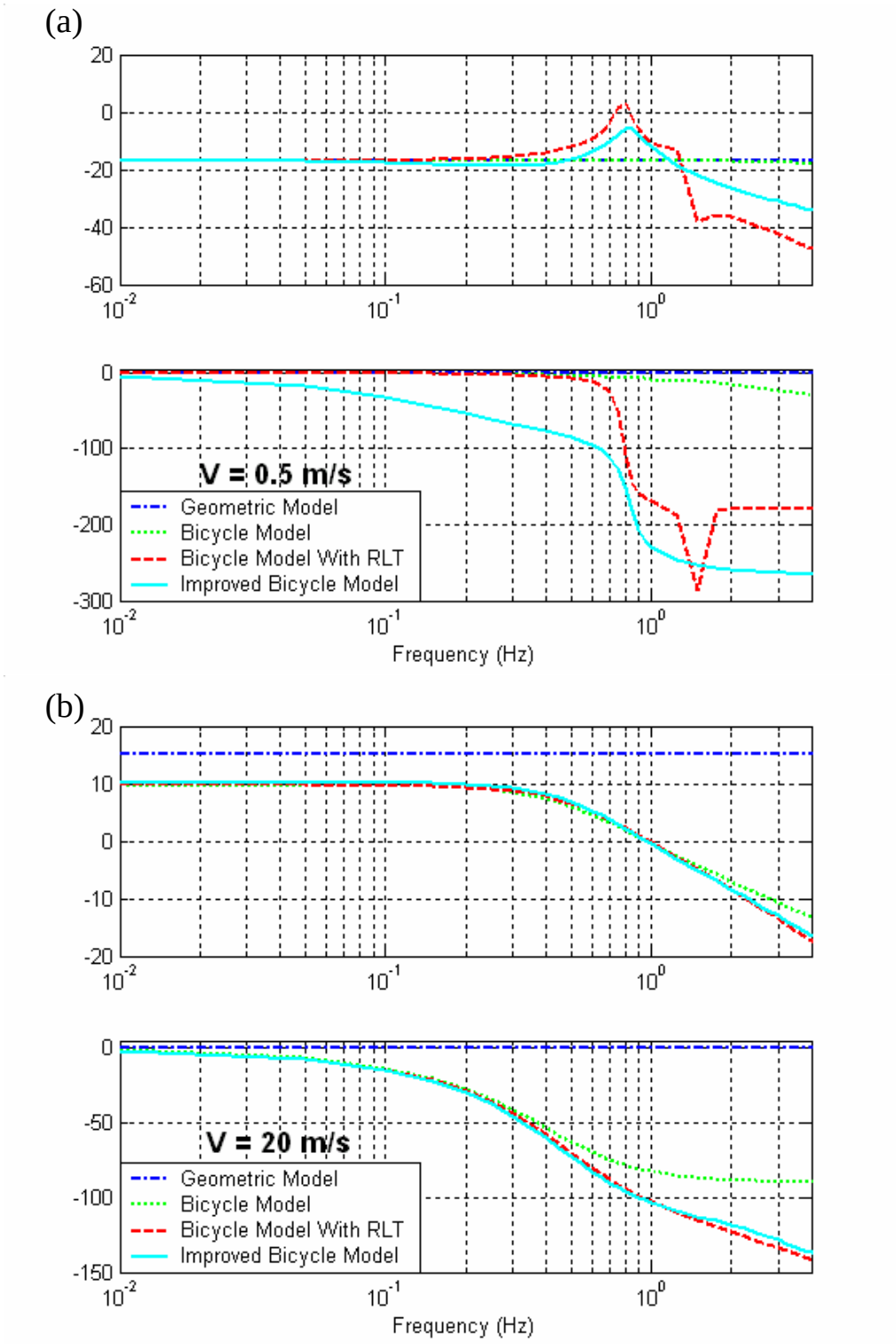

Figure 9. 13 Freq. response: steering angle to yaw rate at (a)V = 0.5m/s (b)V = 20m/s

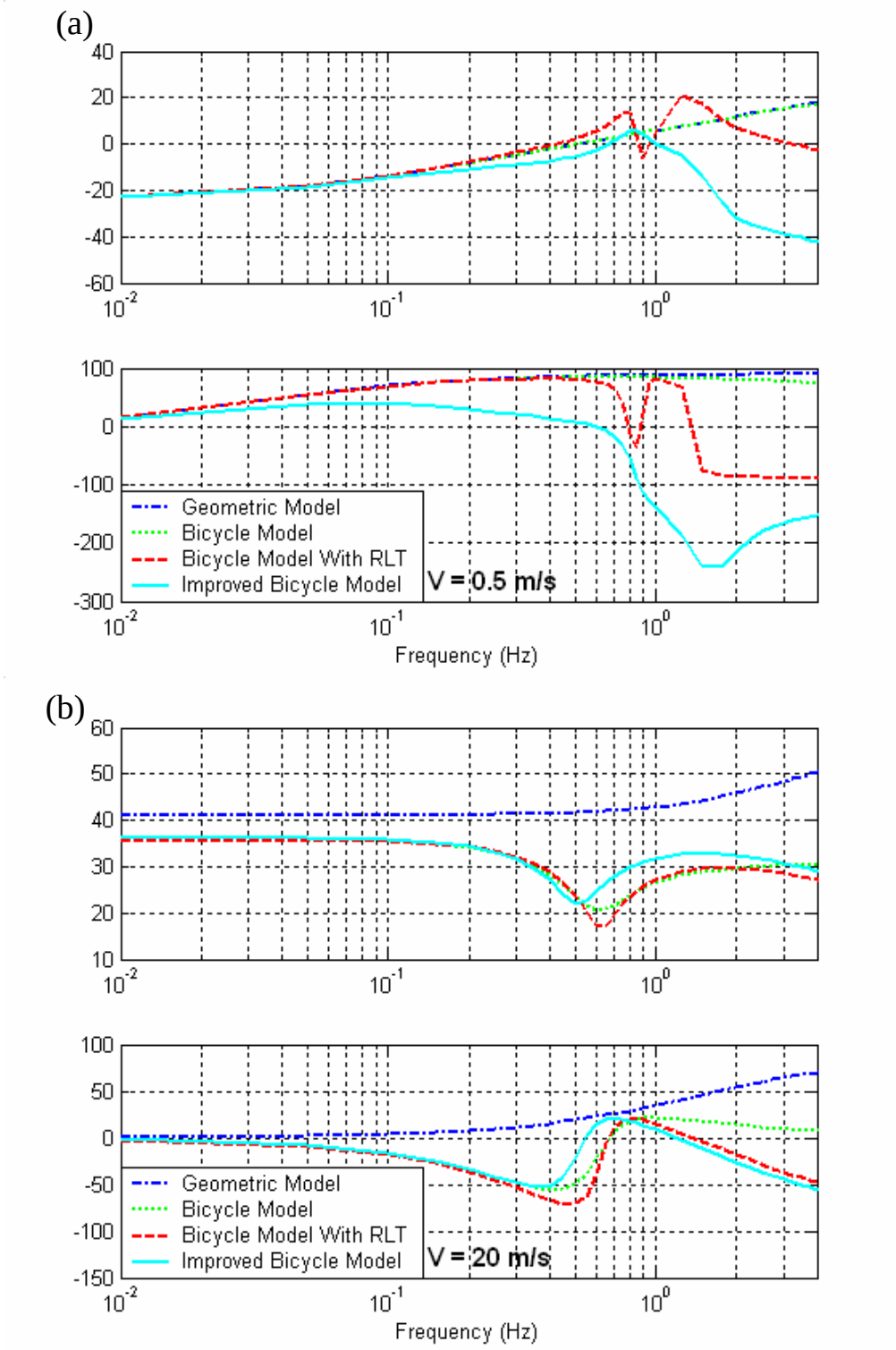

Figure 9. 14 Freq. response: steering angle to lateral acceleration at (a)0.5 m/s; (b)20 m/s

9.3 Improve Bicycle Model Validation

This section experimentally validates the improved bicycle model (with DDT tire model).

State Equations

This section list the state space equations of the following vehicle models: improved bicycle model, geometric model, original bicycle model, and bicycle model with RLT model.

A. State Space Form of the Improved Bicycle Model

$$\begin{bmatrix} 1 & 0 & 0 & 0 & 0 & 0 & 0 \\ 0 & 1 & 0 & 0 & 0 & 0 & 0 \\ -2(D_{lat}^{f}+D_{lat}^{r}) & 0 & M & -2(D_{lat}^{f}l_1-D_{lat}^{r}l_2) & 0 & 0 & 0 \\ 0 & 0 & 0 & 1 & 0 & 0 & 0 \\ 0 & 0 & 0 & 0 & 1 & 0 & 0 \\ -(2D_{lat}^{f}l_1-2D_{lat}^{r}l_2) & 0 & 0 & -(2D_{lat}^{f}l_1^{2}+2D_{lat}^{r}l_2^{2}+c_1) & 0 & (I_1+I_2) & 0 \\ 0 & 0 & 0 & 0 & 0 & 0 & 1 \end{bmatrix} \begin{bmatrix} \dot{y}_u \\ \dot{y}_s \\ \ddot{y}_s \\ \dot{\varepsilon}_u \\ \dot{\varepsilon}_s \\ \ddot{\varepsilon}_s \\ \dot{\delta}_{eff} \end{bmatrix}$$

$$= \begin{bmatrix} A_{11} & A_{12} & 0 & A_{14} & 0 & 0 & A_{17} \\ 0 & 0 & 1 & 0 & 0 & 0 & 0 \\ A_{31} & A_{32} & A_{33} & A_{34} & A_{35} & A_{36} & 0 \\ 0 & 0 & 0 & A_{44} & A_{45} & 0 & A_{47} \\ 0 & 0 & 0 & 0 & 0 & 1 & 0 \\ A_{61} & A_{62} & A_{63} & A_{64} & A_{65} & A_{66} & A_{67} \\ 0 & 0 & 0 & 0 & 0 & 0 & A_{77} \end{bmatrix} \begin{bmatrix} y_u \\ y_s \\ \dot{y}_s \\ \varepsilon_u \\ \varepsilon_s \\ \dot{\varepsilon}_s \\ \delta_{eff} \end{bmatrix} + \begin{bmatrix} 0 \\ 0 \\ 0 \\ 0 \\ 0 \\ -k_2 \\ v_r/\sigma_{yaw} \end{bmatrix} \delta + \begin{bmatrix} 0 \\ 0 \\ -Mv_r\varepsilon_d \\ -\varepsilon_d \\ 0 \\ 0 \\ 0 \end{bmatrix}.$$

where $A_{11}=-v_r/\sigma_{lat}$, $A_{12}=v_r/\sigma_{lat}$, $A_{14}=v_r$,
$A_{17}=l_2v_r/(l_1+l_2)$, $A_{31}=2(C_{lat}^{f}+C_{lat}^{r})$, $A_{32}=-2(C_{lat}^{f}+C_{lat}^{r})$,
$A_{33}=-2(D_{lat}^{f}+D_{lat}^{r})$, $A_{34}=2(C_{lat}^{f}l_1-C_{lat}^{r}l_2)$, $A_{35}=-2(C_{lat}^{f}l_1-C_{lat}^{r}l_2)$,
$A_{36}=-2(D_{lat}^{f}l_1-D_{lat}^{r}l_2)$, $A_{44}=-v_r/\sigma_{lat}$, $A_{45}=v_r/\sigma_{lat}$,
$A_{47}=v_r/(l_1+l_2)$, $A_{61}=2(C_{lat}^{f}l_1-C_{lat}^{r}l_2)$, $A_{62}=-2(C_{lat}^{f}l_1-C_{lat}^{r}l_2)$,
$A_{63}=-2(D_{lat}^{f}l_1-D_{lat}^{r}l_2)$, $A_{64}=2(C_{lat}^{f}l_1^{2}+C_{lat}^{r}l_2^{2})+k_1$, $A_{65}=-2(C_{lat}^{f}l_1^{2}+C_{lat}^{r}l_2^{2})-k_1$,
$A_{66}=-(D_{lat}^{f}l_1^{2}+D_{lat}^{r}l_2^{2})-c_1$, $A_{76}=v_r/\sigma_{yaw}$, $A_{77}=-v_r/\sigma_{yaw}$.

B. State Space Form of the Geometric Model

$$\begin{bmatrix} \dot{y}_s \\ \dot{\varepsilon}_s-\dot{\varepsilon}_d \end{bmatrix} = \begin{bmatrix} 0 & v_r \\ 0 & 0 \end{bmatrix} \begin{bmatrix} y_s \\ \varepsilon_s-\varepsilon_d \end{bmatrix} + \begin{bmatrix} l_2v_r/(l_1+l_2) \\ v_r/(l_1+l_2) \end{bmatrix} \delta .$$

C. State Space Form of the Original Bicycle Model

$$\begin{bmatrix} \dot{y}_s \\ \ddot{y}_s \\ \dot{\varepsilon}_s \\ \ddot{\varepsilon}_s \end{bmatrix} = \begin{bmatrix} 0 & 1 & 0 & 0 \\ 0 & \dfrac{-2(C_\alpha^f + C_\alpha^r)}{Mv_r} & \dfrac{2(C_\alpha^f + C_\alpha^r)}{M} & \dfrac{-2(C_\alpha^f l_1 - C_\alpha^r l_2)}{Mv_r} \\ 0 & 0 & 0 & 1 \\ 0 & \dfrac{-2(C_\alpha^f l_1 - C_\alpha^r l_2)}{I_{zz} v_r} & \dfrac{2(C_\alpha^f l_1 - C_\alpha^r l_2)}{I_{zz}} & \dfrac{-2(C_\alpha^f l_1^2 + C_\alpha^r l_2^2)}{I_{zz} v_r} \end{bmatrix} \begin{bmatrix} y_s \\ \dot{y}_s \\ \varepsilon_s \\ \dot{\varepsilon}_s \end{bmatrix} + \begin{bmatrix} 0 \\ 2C_\alpha^f / M \\ 0 \\ 2C_\alpha^f l_1 / I_{zz} \end{bmatrix} \delta + \begin{bmatrix} 0 \\ 2(l_1 C_\alpha^f - l_2 C_\alpha^r)\dot{\varepsilon}_d / (Mv_r) - v_r \dot{\varepsilon}_d \\ 0 \\ -2(l_1^2 C_\alpha^f + l_2^2 C_\alpha^r)\dot{\varepsilon}_d / (I_{zz} v_r) \end{bmatrix}.$$

where I_{zz}: inertia moment of vehicle.

D. State Space Form of the Bicycle Model with RLT Model

$$\begin{bmatrix} \dot{y}_s \\ \ddot{y}_s \\ \dot{\varepsilon}_s \\ \ddot{\varepsilon}_s \\ \dot{F}_{lat}^f \\ \dot{F}_{lat}^r \end{bmatrix} = \begin{bmatrix} 0 & 1 & 0 & 0 & 0 & 0 \\ 0 & 0 & 0 & 0 & 1/M & 1/M \\ 0 & 0 & 0 & 1 & 0 & 0 \\ 0 & 0 & 0 & 0 & l_1 / I_{zz} & -l_2 / I_{zz} \\ 0 & -2C_\alpha^f / \sigma & 2v_r C_\alpha^f / \sigma & -2C_\alpha^f l_1 / \sigma & -v_r / \sigma & 0 \\ 0 & -2C_\alpha^r / \sigma & 2v_r C_\alpha^r / \sigma & 2C_\alpha^r l_2 / \sigma & 0 & -v_r / \sigma \end{bmatrix} \begin{bmatrix} y_s \\ \dot{y}_s \\ \varepsilon_s \\ \dot{\varepsilon}_s \\ F_{lat}^f \\ F_{lat}^r \end{bmatrix} + \begin{bmatrix} 0 \\ 0 \\ 0 \\ 0 \\ 2C_\alpha^f v_r / \sigma \\ 0 \end{bmatrix} \delta + \begin{bmatrix} 0 \\ -v_r \dot{\varepsilon}_d \\ 0 \\ 0 \\ 2C_\alpha^f l_1 / \sigma \\ -2C_\alpha^r l_1 / \sigma \end{bmatrix}.$$

Experimental Setup

The improved bicycle model was validated using test data from the snowblower. The snowblower is a form of massive snow removal equipment with very stiff suspension, which makes it uniquely convenient in testing the dynamic validity of the 3-DOF DDT model. The sensors installed on the snowblower were the steering encoder, the yawrate sensor, and the lateral position sensors. The frequency sweep technique was used to obtain the frequency responses from steering angles to sensor outputs at different velocities.

The identified parameters of the snowblower are shown in Table 9.2. The inertias and the vehicle dimensions are the known parameters; the other parameters can be estimated by using the following procedure.

1. C_α^f and C_α^r, are estimated by using the yawrate outputs when the vehicle is cornering at steady state.
2. σ_{yaw} can be found by matching the low-frequency phase lag in the frequency response from steering angle to yawrate.
3. k_1, k_2, and σ_{lat} are tuned to match the yaw resonant frequency and low-frequency gain in a standstill vehicle.
4. D_{lat}^f, D_{lat}^f, and c_1, are used to fit the magnitudes of the resonant peaks.

Table 9.2 Identified parameters of the snowblower

M	20,500 kg	C_α^r	350,000 Nt/rad	D_{lat}^f	9,000Nt-s/m
I_1	168,250 kg-m^2	σ_{yaw}	0.45 m	D_{lat}^f	9,000Nt-s/m
l_1	1.3 m	σ_{lat}	1.0 m	k_1	500,000 Nt/m
l_2	2.2 m	C_{lat}^f	350,000 Nt/m	k_2	80,000 Nt/m
C_α^f	350,000 Nt/rad	C_{lat}^r	350,000 Nt/m	c_1	10,000 Nt-s/m

Vehicle Lateral Dynamics Validation

This section validates the DDT model using the experimental data. Figure 9.15(a) uses both the original bicycle model and the improved bicycle model with the DDT model to estimate the "best" matching frequency response from steering input to yawrate at zero vehicle speed. The solid line illustrates data from the improved bicycle model; the asterisks represent the experimental data. The original bicycle model does not appear in this figure due to the singularity problem.[4] This clearly indicates that the improved bicycle model is the only model that has the appropriate degrees of freedom to match the test data between zero to almost zero speed, including the resonant peak at 0.8 Hz.

Figure 9.15(b) plots the responses from steering input to yawrate at 0.4 m/s and 1.5 m/s. The solid lines illustrate the matched results of the improved bicycle model and the dash lines represent the fitted results of the original bicycle model. It is easy to see that the improved bicycle model matches the experimental data very well (especially the phase characteristic at low frequency and the resonant peak at 0.8 Hz). It is impossible to adjust the parameters in the original bicycle model to match these frequency responses at low speeds. The original bicycle model can fit the experimental results up to 0.1 Hz at very low frequency. The discrepancies between the bicycle models with and without DDT in phase and gain plots are up to 200 degrees and 10 dB, respectively. Such discrepancies have the potential to impact any closed-loop controller design.

[4] The bicycle model has almost null gains when the speed is extremely small.

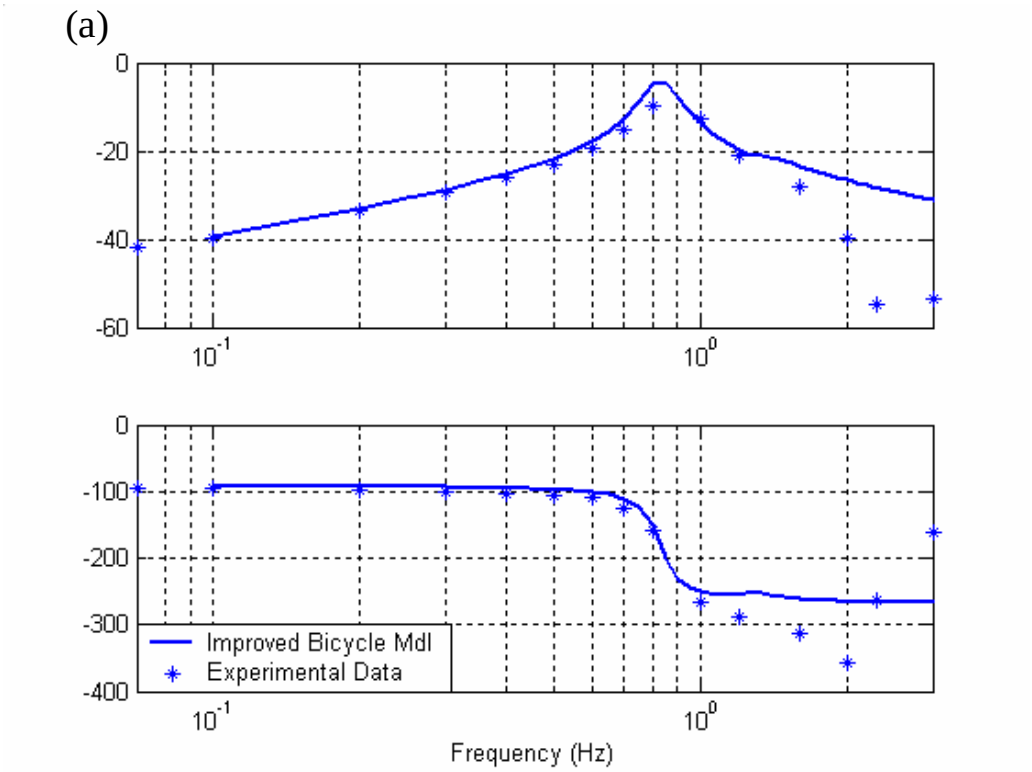

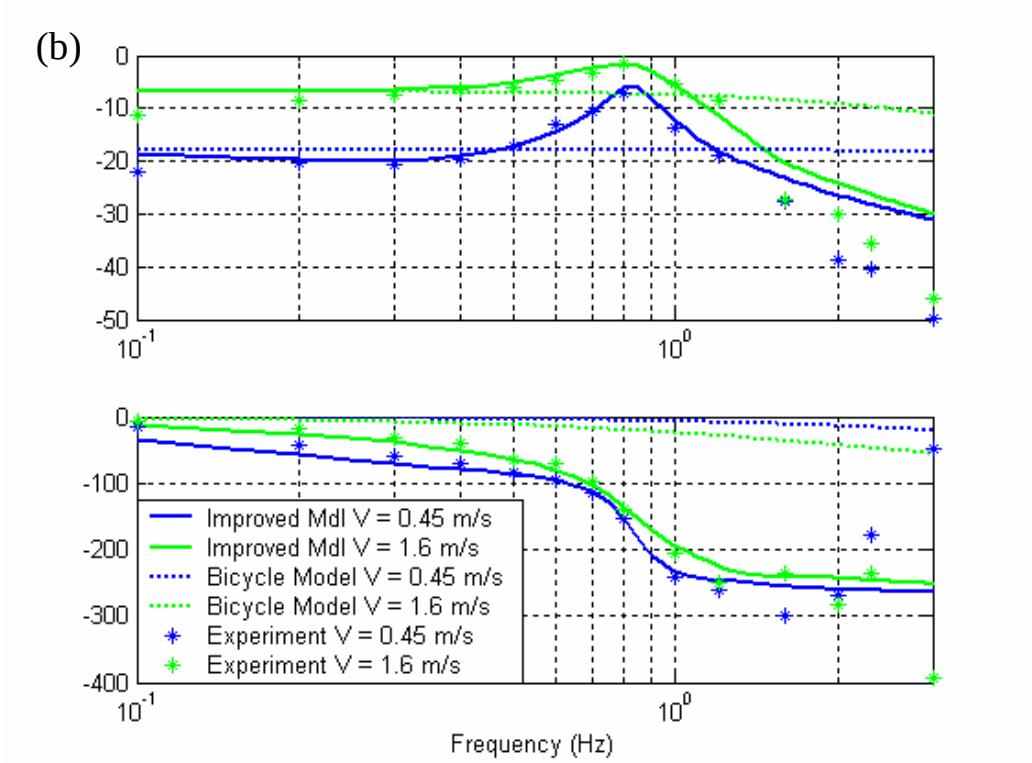

Figure 9. 15 Freq. response: steering angle to yawrate at (a)0 m/s (b)0.45 and 1.6 m/s

Conclusion

A linearizable dynamic-deflection tire model is proposed for low-speed vehicle lateral dynamics and control. This tire model captures the empirical tire characteristics, the often-ignored tire suspension modes, and the steering lag behaviors. This model is easily implemented with the existing vehicle lateral models. When integrated into a vehicle lateral model, the new tire model provides sufficient degrees of freedom to match the snowblower test data.

10. Control Design

10.1 Snowblower lateral dynamics modeling for control

This section describes the snowblower lateral dynamics used for controller design that includes a new dynamic deflection tire model (in Section 9.2) to account for the low-speed induced tire oscillations; it also presents the controller design process that utilizes the linear matrix inequality (LMI) optimization as a tool and results in a simple control law under multiple control constraints. This controller law is the base controller for the snowblower steering control in this report.

Most steering control algorithms are developed based on the bicycle model [7]. According to the bicycle model, controlling vehicles at low speeds is, for the most part, straightforward. However, tests and operator responses show that it is quite difficult to keep the blower in a straight line. The blower head tends to oscillate in response to any steering inputs. Furthermore, in the conventional bicycle model, the rear wheel is assumed to be fixed to the vehicle body. Lateral force is a linear static force which is proportional to the vehicle side slip angle. For the vehicle lateral dynamics, the tires are assumed to have deformations only in the lateral direction due to the vehicle side slip. Such a simplified bicycle model is not adequate in describing lateral dynamic behavior of a snowblower:

- A snowblower is a four-wheel-steering vehicle. Rear wheel steering is independent of front wheel steering and controlled by the operator.

- A snowblower is a heavy-duty vehicle with about 20 tons' worth of weight. A 6-ton snowblower head is installed on the front of the vehicle. Such weight distribution creates large normal force on the front tires and "amplifies" the effects of the front tires' flexible torsion mode. As evident in the experimental data in Fig. 10.1, a resonant mode due to tire's flexibility shows up around 0.8Hz in the frequency response from steering angle to yaw rate, especially under low operating speeds. This phenomenon turns out to be the dominant low-speed dynamics of the snowblower; and it cannot be explained by the simple conventional bicycle model.

- A snowblower during operation is subject to various disturbances. These disturbances come from snow blowing operation, different road surface conditions due to the snow and ice distributions, unevenness of the road surface at the shoulder, and different road curvatures.

In order to capture the fundamental characteristic of snowblower lateral dynamics and provide an accurate design model for the automatic steering controller design, an enhanced bicycle model, which incorporates rear wheel steering, tire flexible mode and different disturbances, is developed and verified with experimental data. Vehicle dynamics equations are derived using Newtonian method and Dynamic Deflection Tire (DDT) model in Section 9.

When assuming small steering angles and constant vehicle speed v_r, the lateral dynamics of the snowblower with respect to the road reference frame can be expressed in the state space representation Eq. (10.1). The state vector $x=[y_u, y_s, \dot{y}_s, \varepsilon_u, \varepsilon_s, \dot{\varepsilon}_s, \delta_{eff}^f]^T$ includes: y_u, ε_u, the tire contact patch position and angle; δ_{eff}^f, the effective front steering angle; y_s, $\dot{y}_s$, the vehicle lateral displacement and its derivative at CG w.r.t. road reference frame; and $\varepsilon_s, \dot{\varepsilon}_s$, the vehicle yaw angle and its derivative w.r.t. road reference frame. The system control input u is the front steering angle δ_f. The disturbances are: ρ, the road curvature; δ_r, rear steering angle; F_d, the disturbance force at CG along the lateral direction; and M_d, the disturbance torque about yaw axis. Disturbances from snow blowing operation, different road surface conditions due to snow and ice distributions and unevenness of road surface at the shoulder are hard to model. Their effects are lumped into disturbance force F_d and disturbance torque M_d. The sensor measurement inputs are vehicle speed v_r; vehicle lateral displacement y_s (measured by front and rear magnetometers); and vehicle yaw angle ε_s (computed by the measurements from the front and rear magnetometers and yaw rate). Table 10.1 lists the variables and parameters that were identified from the test data. Figure 10.1 shows the comparisons among the conventional bicycle model, the enhanced bicycle model and the experimental data. The enhanced bicycle model matches the experimental data especially on the resonant peak around 0.8Hz. It is worthwhile noticing that this particular resonant mode is more prominent at low speeds; it exhibits the same characteristics as those observed and recorded during the snowblower test drives. This additional resonant mode is also the key control obstacle that needs to be overcome [33].

Table 10.1 Identified parameters for snowblower

$M\,(kg)$	20,500	$l_2\,(m)$	2.2	$C_{lat}^f\,(N/m)$	350,000	$D_{lat}^r\,(Ns/m)$	9,000
$I(kgm^2)$	168,250	$\sigma_{yaw}\,(m)$	0.45	$C_{lat}^r\,(N/m)$	350,000	$k_2\,(Nm)$	500,000
$l_1\,(m)$	1.3	$\sigma_{lat}\,(m)$	1.0	$D_{lat}^f\,(Ns/m)$	9,000		

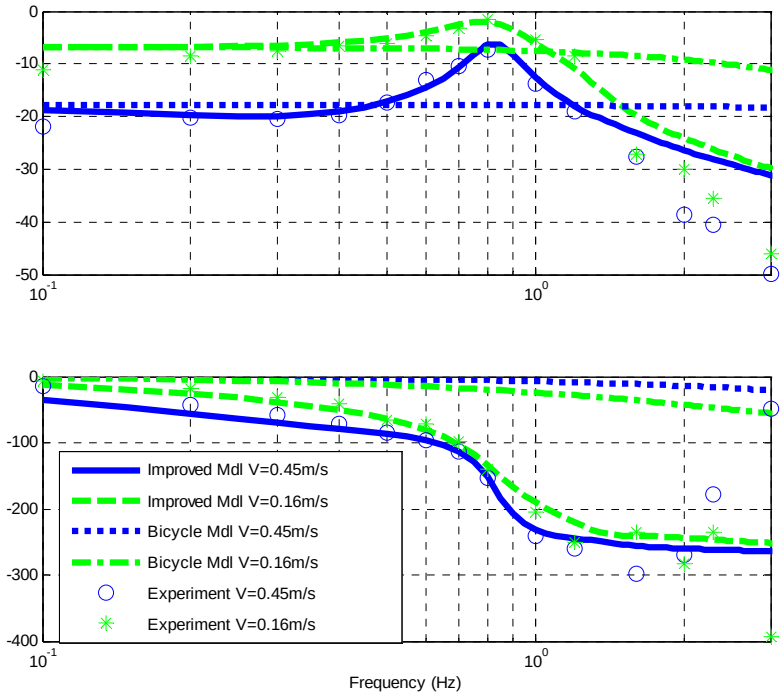

Figure 10. 1 Frequency response from front steering angle to yaw rate

$$
\begin{bmatrix}
1 & 0 & 0 & 0 & 0 & 0 & 0 \\
0 & 1 & 0 & 0 & 0 & 0 & 0 \\
-2(D_{lat}^{f}+D_{lat}^{r}) & 0 & M & -2(D_{lat}^{f}l_1-D_{lat}^{r}l_2) & 0 & 0 & 0 \\
0 & 0 & 0 & 1 & 0 & 0 & 0 \\
0 & 0 & 0 & 0 & 1 & 0 & 0 \\
-(2D_{lat}^{f}l_1-2D_{lat}^{r}l_2) & 0 & 0 & -(2D_{lat}^{f}l_1^{\,2}+2D_{lat}^{r}l_2^{\,2}) & 0 & I & 0 \\
0 & 0 & 0 & 0 & 0 & 0 & 1
\end{bmatrix}
\begin{bmatrix}
\dot{y}_u \\ \dot{y}_s \\ \ddot{y}_s \\ \dot{\varepsilon}_u \\ \dot{\varepsilon}_s \\ \ddot{\varepsilon}_s \\ \dot{\delta}_{eff}^{f}
\end{bmatrix}
$$

$$
=\begin{bmatrix}
A_{11} & A_{12} & 0 & 0 & A_{15} & 0 & A_{17} \\
0 & 0 & 1 & 0 & 0 & 0 & 0 \\
A_{31} & A_{32} & A_{33} & A_{34} & A_{35} & A_{36} & 0 \\
0 & 0 & 0 & A_{44} & A_{45} & 0 & A_{47} \\
0 & 0 & 0 & 0 & 0 & 1 & 0 \\
A_{61} & A_{62} & A_{63} & A_{64} & A_{65} & A_{66} & A_{67} \\
0 & 0 & 0 & 0 & 0 & 0 & A_{77}
\end{bmatrix}
\begin{bmatrix}
y_u \\ y_s \\ \dot{y}_s \\ \varepsilon_u \\ \varepsilon_s \\ \dot{\varepsilon}_s \\ \delta_{eff}
\end{bmatrix}
+\begin{bmatrix}
0 \\ 0 \\ 0 \\ 0 \\ 0 \\ -k_2 \\ v_r/\sigma_{yaw}
\end{bmatrix}
\delta_f+
\begin{bmatrix}
\frac{v_r}{l_1+l_2} & 0 & 0 & 0 \\
0 & 0 & 0 & 0 \\
0 & -Mv_r^2 & 1 & 0 \\
\frac{-v_r}{l_1+l_2} & v_r & 0 & 0 \\
0 & 0 & 0 & 0 \\
0 & 0 & 0 & 1 \\
0 & 0 & 0 & 0 \\
0 & & &
\end{bmatrix}
\begin{bmatrix}
\delta_r \\ \rho \\ F_d \\ M_d
\end{bmatrix}
\tag{10.1}
$$

where $A_{11} = -v_r / \sigma_{lat}$, $A_{12} = v_r / \sigma_{lat}$, $A_{15} = v_r$,

$A_{17} = l_2 v_r /(l_1 + l_2)$, $A_{31} = 2(C_{lat}^f + C_{lat}^r)$, $A_{32} = -2(C_{lat}^f + C_{lat}^r)$,

$A_{33} = -2(D_{lat}^f + D_{lat}^r)$, $A_{34} = 2(C_{lat}^f l_1 - C_{lat}^r l_2)$, $A_{35} = -2(C_{lat}^f l_1 - C_{lat}^r l_2)$,

$A_{36} = -2(D_{lat}^f l_1 - D_{lat}^r l_2)$, $A_{44} = -v_r / \sigma_{lat}$, $A_{45} = v_r / \sigma_{lat}$,

$A_{47} = v_r /(l_1 + l_2)$, $A_{61} = 2(C_{lat}^f l_1 - C_{lat}^r l_2)$, $A_{62} = -2(C_{lat}^f l_1 - C_{lat}^r l_2)$,

$A_{63} = -2(D_{lat}^f l_1 - D_{lat}^r l_2)$, $A_{64} = 2(C_{lat}^f l_1^2 + C_{lat}^r l_2^2)$, $A_{65} = -2(C_{lat}^f l_1^2 + C_{lat}^r l_2^2)$,

$A_{66} = -(D_{lat}^f l_1^2 + D_{lat}^r l_2^2)$, $A_{67} = k_2$, $A_{77} = -v_r / \sigma_{yaw}$

10.2 Lateral control design

Figure 10.2 shows the block diagram of control loop that we adopt in the control design. As shown in Figure 10.2, $G(s)$ represents open-loop snowblower lateral dynamics and $K(s)$ represents the controller that will be synthesized. W_d , W_{δ_r} , W_{δ_f} and W_{y_h} are the control design weighting functions.

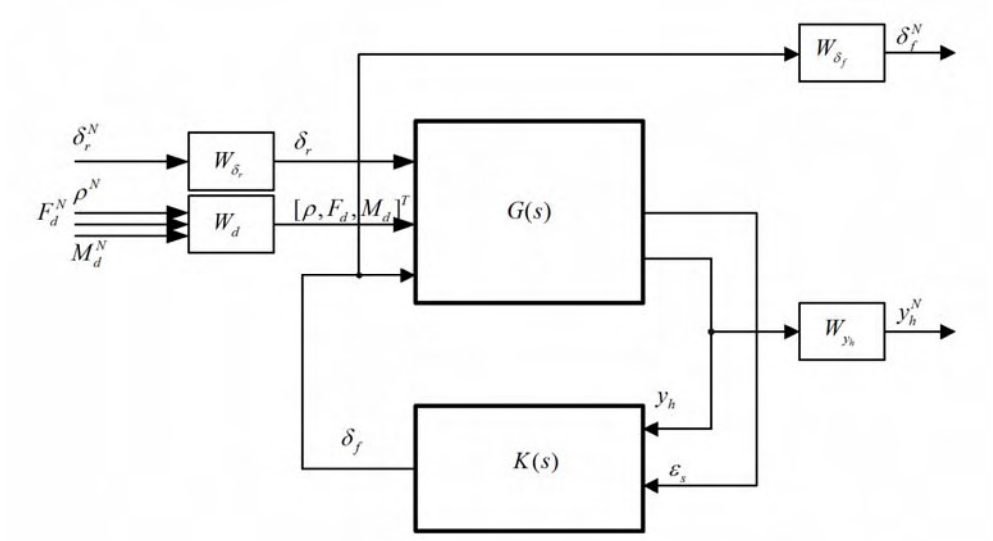

Figure 10. 2 Block diagram of control loop

The objective of the automated snowblower steering controller is to keep the lateral error at the head of the snowblower, $y_h = y_s + l_3 \varepsilon_s$, small by using front steering angle δ_f as the control input, where l_3 is the distance between blower head and CG. During the operation, blower head should not touch guardrail in the worst cases. Therefore, another performance constraint is $y_h < d_g$, where d_g is the distance between magnetic track and guardrail. There are several difficulties inherent in the design of this controller:

- Since installing reliable and accurate sensors that measure the driver's rear steering actuation under the current project phase is not economical and practical; the rear steering is treated as a major source of disturbance.

- The system is subject to uncertainties (such as changes in road surface conditions); and large external disturbances from road curvature (ρ) change and external loads from blowing and pushing snow and ice. These external loads are represented by the lumped disturbance force F_d and disturbance torque M_d.

- The resonant peak around 0.8Hz shown in Figure 10.1 is close to the desired close-loop bandwidth. The effect of this resonant peak is similar to that of a flexible structure mode: it can introduce large close-loop oscillation when proper "damping force" is not provided by the controller.

To address above issues, following design strategies are adopted:

- Direct vehicle angle feedback: First, the vehicle angle feedback is used to attenuate disturbance from rear steering action. Second, direct vehicle angle feedback provides additional damping for the control design as shown in the "look-ahead" control scheme [34].

- Performance and Robustness criterions: How to choose design criterions for performance and robustness is very important for the control design. The generalized H_2 norm is very convenient to express performance requirement such as disturbance rejection specification, especially for the control of snowblower operation. Since the generalized H_2 norm represents the system gain from L_2 to L_∞, its value can be interpreted as the worst time-domain amplification for the disturbance input with finite energy [35]. The H_∞ criterion is a natural expression for the system robustness.

- Mixed H_2 / H_∞ synthesis for both performance and robustness: As shown in Figure 10.2, the closed loop transfer functions are defined as:

$$y_h^N = T_1(s)\begin{bmatrix} \delta_r^N \\ \rho^N \\ F_d^N \\ M_d^N \end{bmatrix} \qquad \delta_f^N = T_2(s)\begin{bmatrix} \delta_r^N \\ \rho^N \\ F_d^N \\ M_d^N \end{bmatrix}. \tag{10.2}$$

T_1 is the transfer function from disturbance to the snowblower head lateral deviation. Minimizing its H_2 norm will impose the performance requirement. T_2 is the transfer function from disturbance to the front steering control. Minimizing its H_∞ norm will increase the system robustness against unstructured additive uncertainties. Since T_1 and T_2 represent two channels with very different roles in the control design, it is desirable to treat these two channels separately. In the traditional H_2 or H_∞ design, these two channels are usually combined together with different weighting functions and can be optimized only for either H_2 or H_∞ norm. In [12], a LMI based multi-objective strategy is proposed to treat each channel separately with different norm criterions. Such design

technique provides more design flexibility compared with traditional design and is adopted for the control design in this project.

The control objective is to minimize $\|T_1(s)\|_2$ subjected to $\|T_2(s)\|_\infty < \gamma$. This can be interpreted as maximizing system disturbance rejection performance with guaranteed system robustness against unstructured additive uncertainties. This sort of mixed H_2 / H_∞ synthesis problem can be solved via LMI optimization [36][37]. Based on this synthesis, the resultant controller suggested a relatively simple control structure that was used for the final field testing and tuning. The following important parameters are chosen for the controller design:

- $\gamma = 1.2$:The constraint means that the robustness margin guaranteed by the controller is 1/1.2=0.83

- $W_{y_h} = \dfrac{s + 0.1\pi}{2(s + 0.04\pi)}$: The penalty on the lateral deviation is set high on low frequency only due to high frequency measurement noise.

- $W_{\delta_f} = \dfrac{200000s^2 + 4398200s + 4934800}{s^2 + 439.823s + 98696}$: The weight on the steering control input is designed to penalize high frequency control effort to avoid high frequency chattering and actuator saturation.

- $W_d = diag[\dfrac{3\times10^{-5}s^2 + 0.0029s + 0.132}{s^2 + 8.8s + 39}, \dfrac{13s^2 + 1172s + 52637}{s^2 + 8.8s + 39}, \dfrac{20s^2 + 1759s + 78956}{s^2 + 8.8s + 39}]$
  All the disturbances are assumed dominant at low frequency.

Snowblower lateral dynamics can be regarded as a linear parameter-varying system with respect to vehicle speed v_r. Due to the large mass and slow operating speeds, the speed variations during operation are generally small. A practical approach for the synthesis of the controller is to design the controller at each speed grid point and use interpolation for implementation. The dashed lines in Figure 10.3 and 10.4 show the frequency responses of the synthesized controller at $v_r = 1m/s$. The solid lines in Fig 10.3 show two relative low-order controllers (5th for from ε_s to δ_f; and 6th for from y_h to δ_f) that match the synthesized controllers at the same speed. As shown in Figure 10.4, the steering angle input is always in the opposite direction (i.e., $\delta_f = -\varepsilon_s$) of the vehicle angle at low frequency. This negative vehicle angle feedback is the key component that provides a damping effect sufficient enough to damp out oscillations due to the vehicle flexible mode, discovered in this section. Further examinations of the synthesized controllers at different speeds suggested the following relatively simple controller structure:

$$\delta_f = G_c(s)(-G_{c\varepsilon}(s)\varepsilon_s + G_{cy}(s)y_h), \tag{10.3}$$

where $G_c(s)$ is a low-pass filter that removes unwanted high frequency control behaviors; $G_{c\varepsilon}(s)$ is a lag-lead compensator for the "negative" vehicle angle feedback; and $G_{cy}(s)$ is an "integrator" plus a lag-lead compensator for the blower head position feedback. Because of the associated "physical" meanings of the controller parameters, these low-order controllers are relatively easy to be tuned in the field. The specific matched "low-order" controllers in Figure 10.3 and 10.4 are listed below as an example:

$$G_c(s) = \frac{6.911^2(s+43.982)}{43.982(s^2+2*0.55*6.911s+6.911^2)} \tag{10.4}$$

$$G_{c\varepsilon}(s) = 0.73\frac{43.982}{(s+43.982)}\frac{2.3876^2(s^2+2*0.18*5.0265s+5.0265^2)}{5.0265^2(s^2+2*0.42*2.3876s+2.3876^2)} \tag{10.5}$$

$$G_{cy}(s) = 0.1\frac{(s+0.9425)(s+0.06283)}{s^2}\frac{2.3876^2(s^2+2*0.18*6.2832s+6.2832^2)}{6.2832^2(s^2+2*0.42*2.3876s+2.3876^2)} \tag{10.6}$$

The designed controller is implemented with 50 Hz sampling rate. A more detailed presentation of control design and implementation can be found in [38].

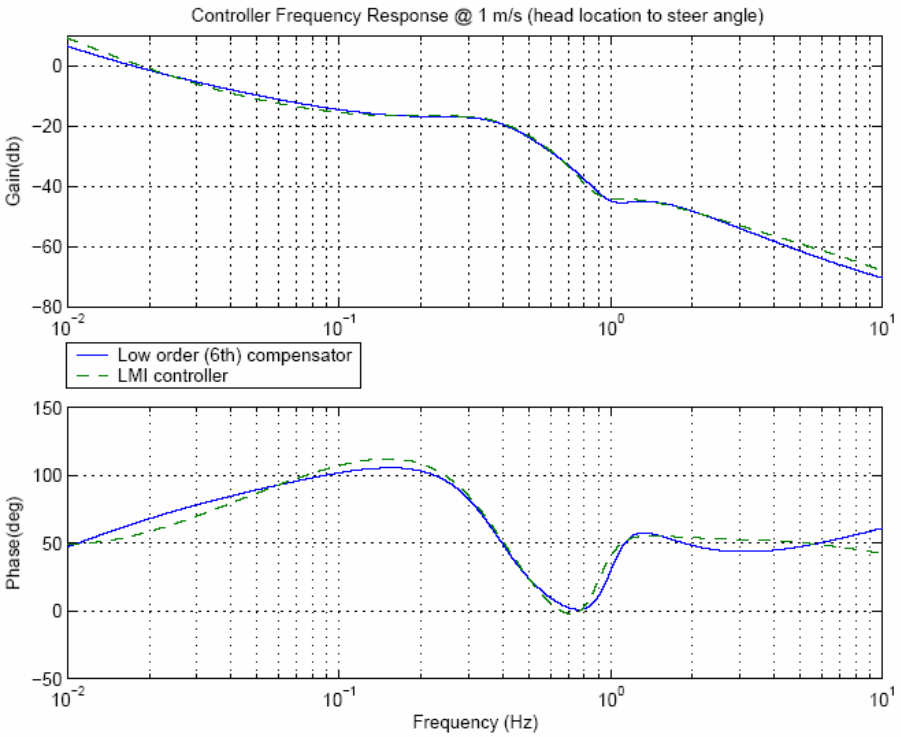

Figure 10. 3 Synthesized and matched 6th order controller frequency responses from lateral deviation at blower head to steering angle for $v_r = 1m/s$

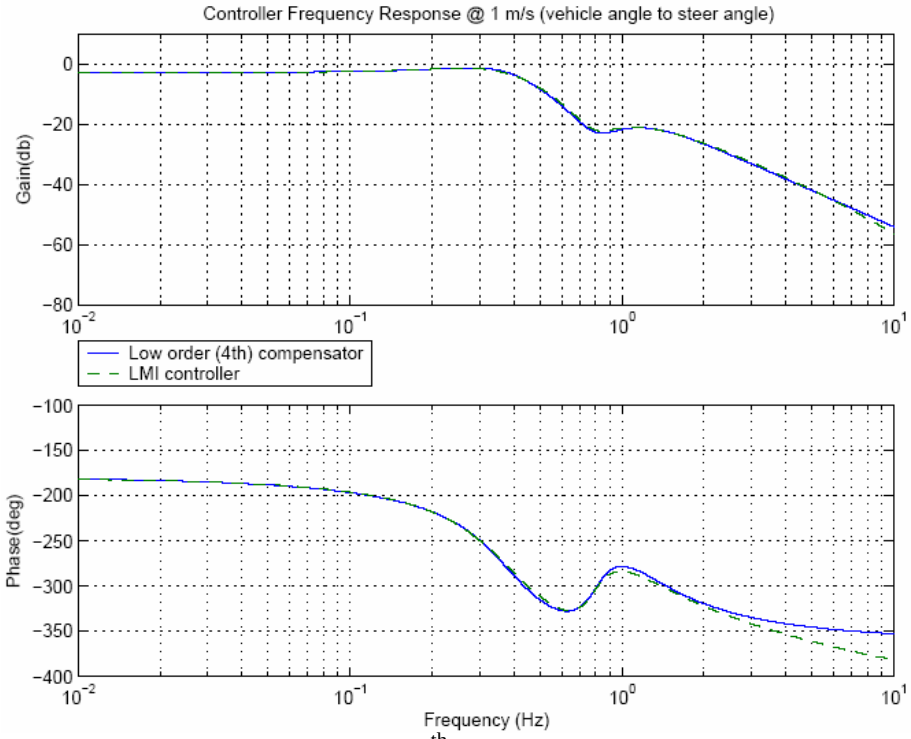

Figure 10. 4 Synthesized and matched 5th order controller frequency responses from vehicle yaw angle to steering angle for $v_r = 1m/s$

10.3 Integrated Control

In order to control the snowblower accurately along guardrail under varying and large nonlinearities, uncertainties and disturbances, the above controller needs to be integrated with other key control algorithms in the system. The key control algorithms that collectively constitute the necessary intelligence control of the automated system are:

- A robust high-gain "lane-keeping" controller that accurately follows the "magnets" under all operational conditions even without slope and curvature information
- Adaptive exception controls which is a planning algorithm that can cope with any imaginable "abnormal" scenarios, such as sudden potholes, guardrail touching, actuator saturation, unknown limit cycle oscillations, and operator mistakes or interventions
- A dependable "transition" controller that executes "on-demand" transitions between automated and manual control under all operational conditions
- A simple and transparent HMI/DVI that facilitates clear operator state awareness and prompts timely and correct responses under both normal and emergency scenarios
- A smart steering servo controller that unerringly carries out the steering command under highly nonlinear mechanical characteristics and unpredictable disturbances

- A fault detection and management control that detects system irregularities and provides a warning while, at the same time, conducts preventive actions

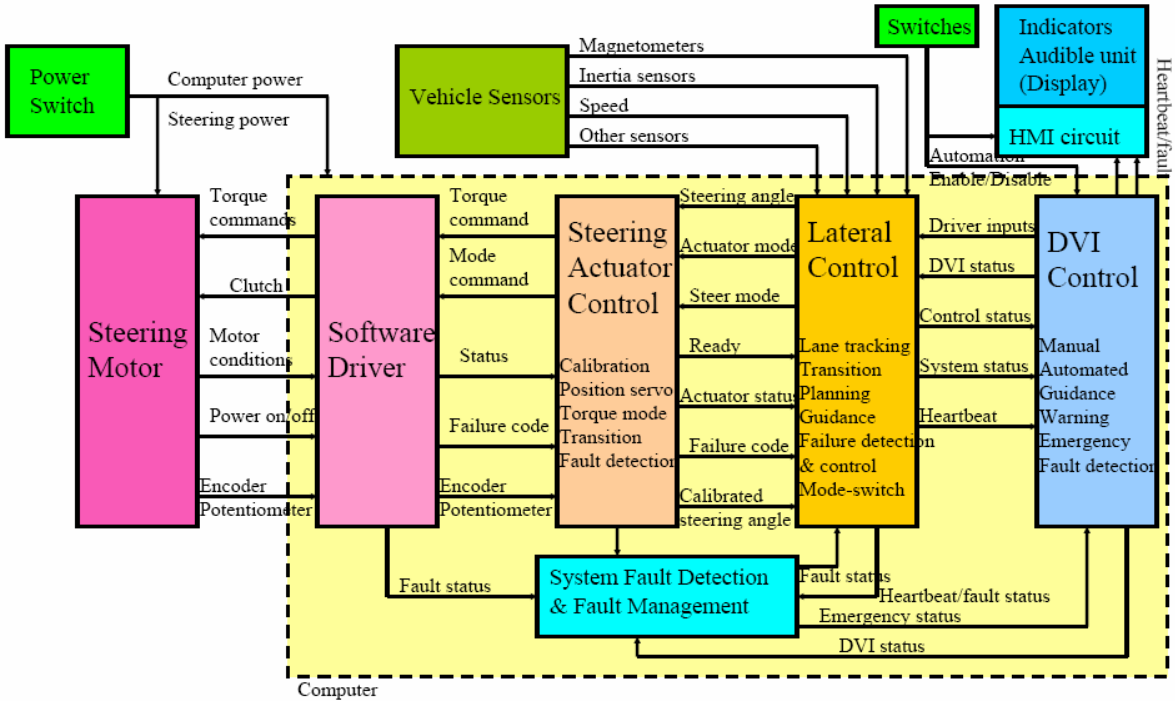

Figure 10. 5 Control algorithm structure

Figure 10.5 illustrate the control algorithm structure that includes lateral control algorithm, steering actuator control algorithm, and DVI/HMI control algorithm, as well as fault detection algorithm. The lateral control algorithm includes also the robust high-gain lane-keep algorithm with gain scheduling ability (described in Section 10.2), transition algorithm with transition state machine, planning algorithm using the outputs from transition, control, DVI and fault state machines.

11. Human Machine Interface/Driver Vehicle Interface

11.1 Design Concept

The term human machine interface (HMI) or driver-vehicle interface (DVI) refers not only the physical switches, status LEDs, or any other graphic displays that were added to the vehicles, but refers also to the more global concept of information flow between the driver and the vehicle and how transitions between vehicle states occur. Under normal driving circumstances, the driver constantly receives information about the vehicle by watching the road, proprioceptively sensing the steering wheel angle, listening to the engine and road noise, and sensing vehicle accelerations. Drivers then use that information in a feedback loop comparing it to the commands that are being given on the steering wheel, gas pedal, and brake. Once the control of the vehicle becomes automated, the driver still receives the output or visual information from the road, but loses any sense of the input side of the equation or what the vehicle was commanded to do. Thus, the display aspect of the driver-vehicle interface attempts to replace the missing input in the driver feedback loop by providing answers to the following three questions:

1. What is the current status of the vehicle or what does the vehicle think that it is doing?
2. What has the vehicle been commanded to do now or in the very near future?
3. How can the driver anticipate a change in the system?

The HMI development becomes a challenging task because of the special operational environment of the snowblower: constant loud noise, hectic work load and pressure, as well as the need for the driver to repeatedly scan outside the windshield for possible obstacles often under low visibility condition. To make a HMI feasible and effective under such constraints, the following are the four “design principles” for the snowblower HMI concept for this project (and possibly in general):

- Simple: contain only the necessary information
- Transparent: require minimum attention from the driver
- Intuitive: require minimum memorization
- Safe: safety critical information has redundancy

The goal of the HMI is to allow the operator to acquire in real-time the following automated snowblower information:

- Current “control” status: manual or automation
- System is ready to transition to automation
- Transition to automation successful
- System has a problem or fault
- System require driver intervention

And provide the driver with intuitive means to either transition to automation or transition back to manual steering easily and precisely.

11.2 HMI Components and Location

Figure 11.1 shows a diagram of the physical components that made up the HMI system, including computer, HMI circuit, and other HMI components that directly interface with the driver. These other HMI components can be categorized as either driver inputs or vehicle status displays. There were three driver inputs added to the vehicle, an emergency (kill) switch, a transition switch, and an auto-system switch. Two types vehicle status displays were also added to the vehicle, an array of four LEDs as status display (green, blue, white and red), and another array of seven LEDs as guidance display (3 green's, and 4 red's); both on the upper instrument panel. There is also a speaker to provide audio.

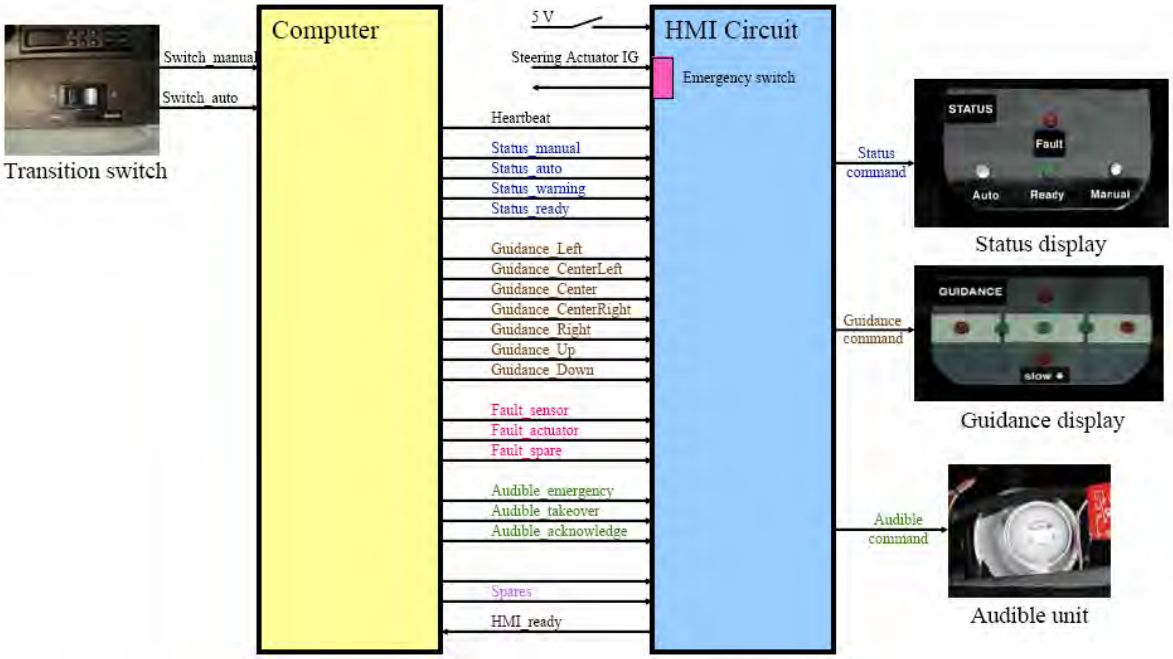

Figure 11. 1 HMI system and components

Transition Switch

The transition switch is located under the radio, and is slightly toward the right front of the driver (see Figure 11.2); it allows the operator to switch the system on and off. The switch is a typical three-position, momentary-action, rocker switch, which measured 15 mm wide by 25 mm long. The center position is neutral. Pressing the switch forward will send a request to the control computer to engage the automated system that is ready to be engaged. When the rocker switch is released, it returns to the neutral position. Pressing the switch backwards or to the rear will send a request to the control computer to disengage the automated systems that is currently engaged. See Figure 11.3 for an illustration.

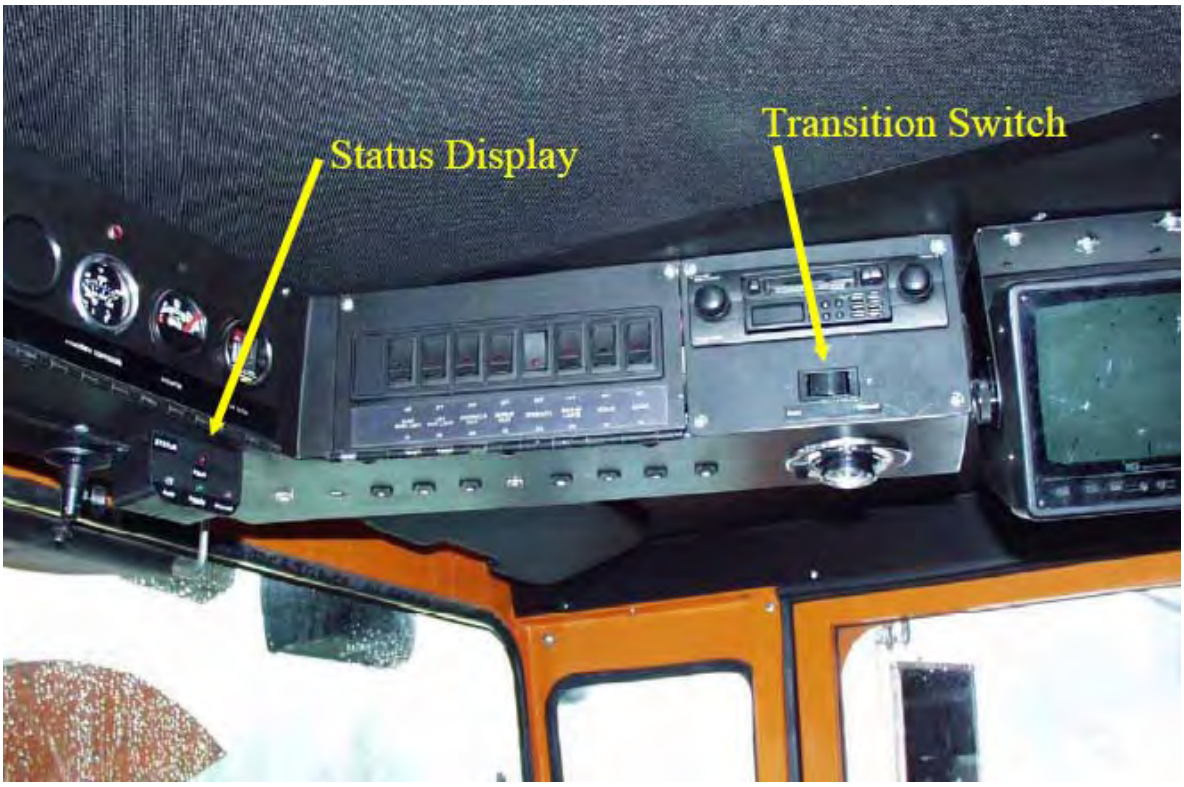

Figure 11. 2 Location of the transition switch

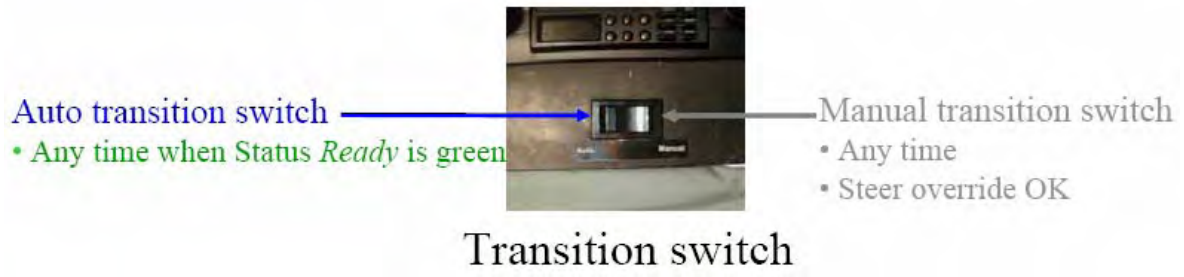

Figure 11. 3 Transition switch actions

Emergency Switch

An emergency button is located on the console just right to the operator right hand, allowing the driver to "kill" the steering actuator at any time (see Figure 11.4). Although the steering actuator is designed to be overtaken by the driver at any time, the additional "Emergency Button" increases the safety margins for the field operations. The kill switch is a standard IDEC Type AYW401-R push-pull kill switch, typically used for automotive and industrial applications. Although a commercial system would not likely provide the driver with a kill switch, safety concerns with the prototype nature of the system dictated that the driver have a quick, simple, and reliable way of disengaging any automated systems in the event of a problem. Both the kill switch and the transition switch are placed in the locations that are within easy reach by the driver's right hand.

Auto System Switch

One "System Switch" was used as a development tool is purposely left in the system during the field test for development convenience, as shown in Figure 11.4. The system will turn on automatically if this switch is remained in the "ON" position. Operator can use this switch to shut down the system when the system is not in use, or re-boot the system, by switching it on and then off, during a trouble-shooting procedure. In the final implementation, this switch may be moved to a location that is only accessible by the maintenance personnel, and it will likely to be in the ON position during the winter operational season.

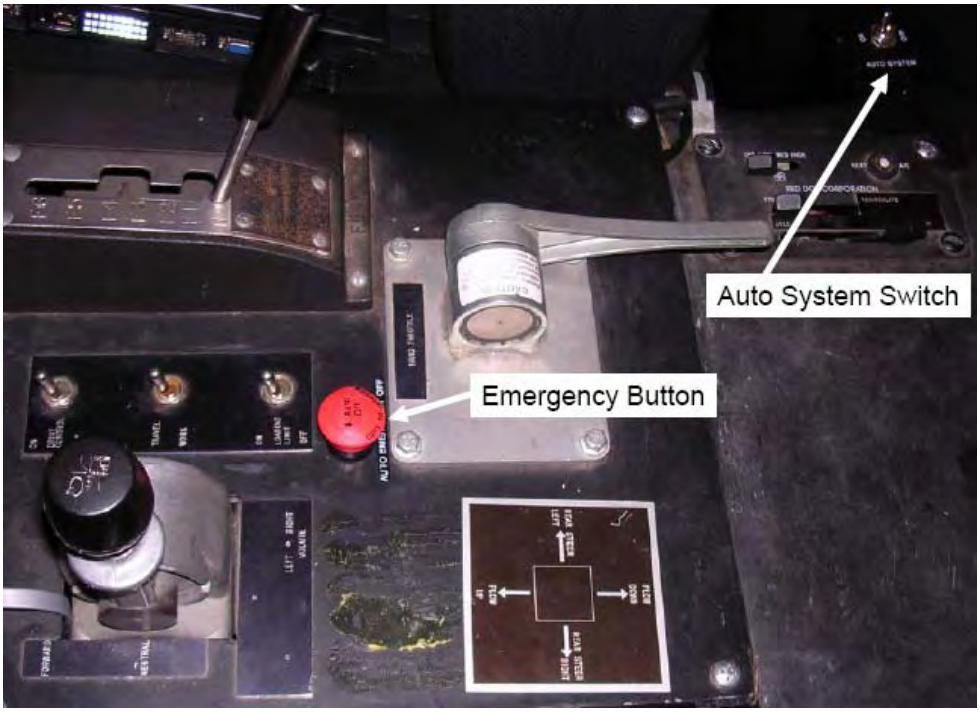

Figure 11. 4 Emergency button and Auto system switch on the center console

Status Display

The status LED's is the most important HMI display. It is located underneath the air filter indicator as shown in Figure 11.5. The status display provide the driver with the automated system's current status. This upper instrument panel LED status display, as shown in Figure 11.5 and Figure 11.6, consists of four colored LED's mounted beneath the upper instrument panel, slightly to the upper right of the driver, below the air filer, and arranged in a straight-line pattern to provide easily perceptible coding through position as well as color. The general color meaning is described in Table 11.1, and the actual LED states are described in Table 11.2. Each LED is an LEDTRONICS PF50-T, sunlight-visible, panel mount unit with a viewing angle of 12-15 degrees. The LED display is connected directly to one HMI circuit control outputs that are also connected to the digital I/O boards from the computer. This four-LED setup was chosen to provide a simplistic overview of the most important system states, with nearly instantaneous updates.

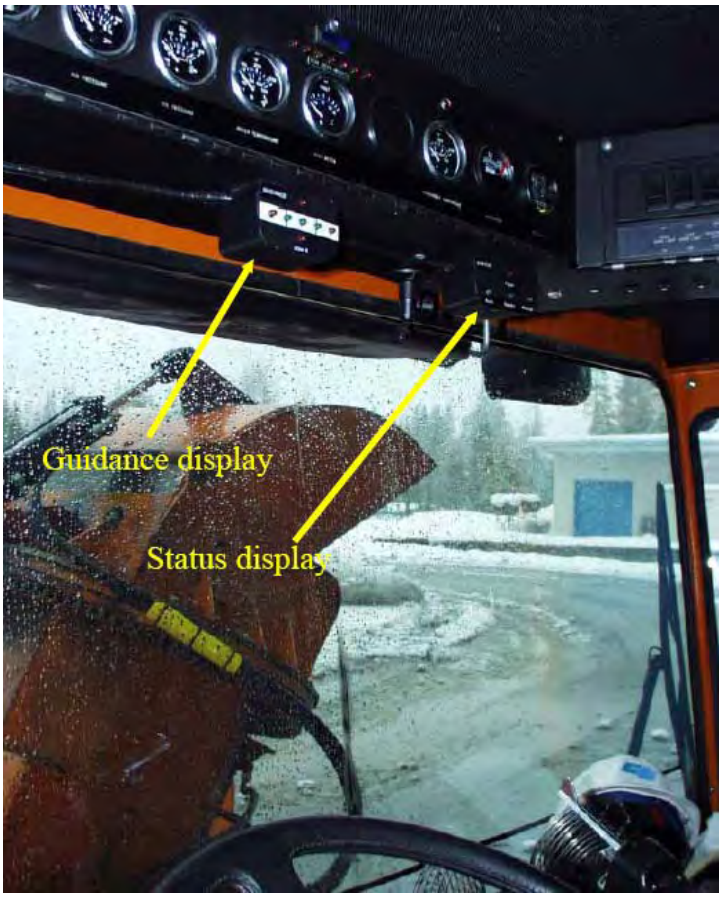

Figure 11. 5 Locations of the status display and guidance display

Ready:
ON SOLID – system on & ready to transition to auto
FLASHING – system is booting up

Auto:
ON SOLID – auto steering is on
FLASHING – system on & auto steering pending

Manual:
ON – System on & under manual steering control

Fault:
ON SOLID – system problem, no transition to Auto
FLASHING – emergency takeover (during Auto)

Figure 11. 6 General meanings of the status display

Table 11.1 Color Stereotypes, Common Automotive Uses, and HMI LED Use.

Color	Common Stereotypes	Common Automotive Uses	HMI LED Use
Green	General On/Off Go OK, Good	Turn signals, some indicator lights, and cruise control	Ready for the transition to automatic control
Blue	General On/Off	High-beam headlight and air conditioner indicators	Automation is engaging or is in control
White	General indication w/o special meaning	Common illumination	Provide redundant indication for manual state
Red	General On/Off Stop Warning or Failure	Warning lights and icons for seat belts, door ajar, oil pressure, temperature, etc.	System failure or driver has overridden the automation

Table 11.2 Status LED Display State Table.

Event	Green	Blue	White	Red
System Start-up	Blinking	Off	Off	Off
Manual Driving or Automation Not Ready	Off	Off	Solid	Off
Transition to Automation				
Automation Ready	Solid	Off	Solid	Off
System Failure	Off	Off	Off	Solid
Transfer in Progress	Solid	Blinking	Off	Off
Transfer Complete (Automation On)	Solid/Off	Solid	Off	Off
Transfer Failed - Manual Driving	Off	Off	On	Off
All Automation Modes - Overrides and Faults				
Driver Overrides Steering Initially	Solid/Off	Solid	Off	Blinking
Driver Overrides Steering for 2 seconds	Solid/Off	Off	On	Off
Kill Switch Depressed	Off	Off	On	Solid
Lateral Control System Failure-first 5 sec	Off	Off	On	Blink
Lateral Control System Failure-after 5 sec	Off	Off	On	Solid
Automated Driving				
Approaching End of Magnets	Solid/Off	Solid	Off	Blinking

Guidance Display

The guidance LED's is located underneath the voltmeter, and is slightly to the left of the status display (see Figure 11.5). The guidance display is a supportive display that provides additional information to help the driver learn to transition into automation. This display, as shown in Figure 11.7, consists of seven colored LED's and is separated into two parts: speed indicators, and blower head indicators. The top and bottom red LED's are the speed indicators. A blinking top indicator warns the driver that the speed is too low for continuous automation. On the other hand, a blinking bottom red indicator instructs the driver to slow down. The middle five LED's display the position of the tip of the blower head with respect to the guardrail. Each green LED represents additional 10

cm of distance to the guardrail; and each red LED indicates the last 5 cm with respect to the guardrail. The two green LED's with a vertical mark are used to indicate the tracking target for the blower head. The right one is for tracking the guardrail on the right shoulder; and the left one is for tracking the guardrail on the left shoulder. The blower head indicators are used to support the driver (1) to position the snowblower with appropriate crab angle prior to engage automation; (2) to provide a visual guide on how the automated system is performing. In addition, when the outside red LED (e.g. left most red LED when tracking right shoulder guardrail) blinks, it indicates to the drive that the snowblower is positioned with a "wrong" crab angle – a useful operational information to the driver.

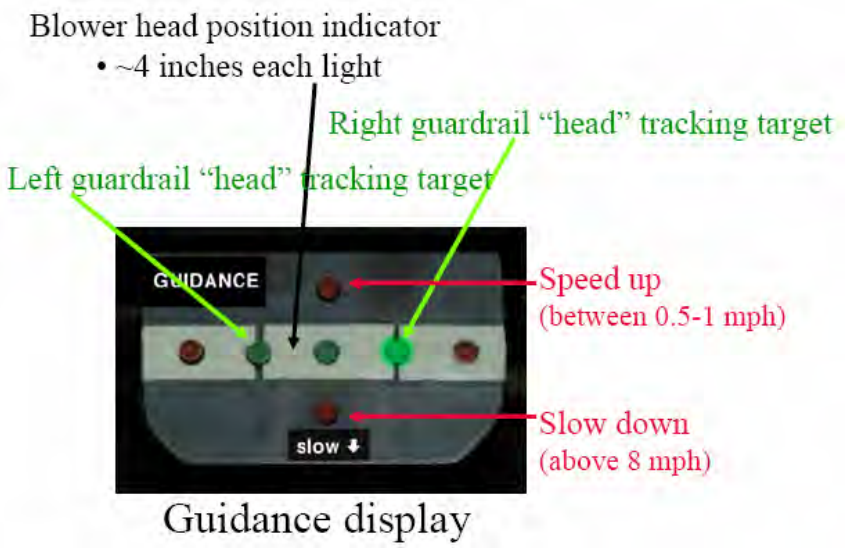

Figure 11. 7 General meaning of the guidance display

Audible Unit

An audible unit (see Figure 11.8) is located inside the center console that is right of the driver. The audible unit reduces the need for the driver to continuously monitor the display especially for emergency situations. It produces the following three different sounds:

- Acknowledgment: a short but slightly soft tune that confirms a successful transition from manual steering to automatic steering
- End of magnets: a soft but continuous intermittent sound that signals the approaching of the end of guardrail. The driver can take over steering function at any point. The sound starts at 10 meter before the end of the guardrail, and continuously until the magnets ends. The sound would turn into emergency sound if the drive does not take over control when the magnet trail ends.
- Emergency: a sharp intermittent sound with increasing volume that instructs the driver to take over control now. The typical reasons for emergency sound are: system or component failure during automatic control and running out of magnet trail.

Audible unit (3 sounds)

- Acknowledgement
  - Transition to Auto
- End of magnets
  - End of automation
- Emergency
  - Take over control now

Figure 11. 8 Audible unit

12. Procedure, Training, and Operator Survey

This section describes the project areas that are directly related to operators and operations: operation procedure, training, interview and survey. The human factor results from interview, field test feedback and survey, as well as field ride-along help create an automated system (including operation procedure) that the operators can accept and would use.

12.1 Operation Procedure

Three different operation procedures are listed and described in this section: (1) normal operation (simple and intuitive); (2) boot-up sequence (turn-key); and (3) engaging the automated steering system.

Normal Operation

1. The operator approaches the guardrail the same way as “manual” operations. The guidance indicators display the current position of the blower head to support this procedure.
2. The operator can switch to automatic steering control by pushing on the “auto” switch whenever the “green” status light is lit. The green status light lit indicates magnets were read and the blower head points toward the guardrail. The automatic system will automatically determine whether the guardrail in on the left or right side of the blower based on the magnetic coding.
3. The “blue” status light will remain lit when the snowblower is under automated control. The operator can switch to manual control any time by pushing the “manual” button or by over-powering the steering wheel.
4. The “red” status light will flash with simultaneous emergency sound to notify the operator that there is a fault developed and detected by the system and to request the operator to take over steering control
5. The driver can transition back to manual control by either pushing the “manual” switch; or by overriding the steering wheel.
6. Manual small correction of the steering wheel is allowed.

Boot-up Sequence

1. The system boots up automatically when the ignition switch is on. However, the “auto-system” switch should be left in the “on” position.
2. The “green” LED flashes during the system warm up period (computer booting up). Should the computer fail to boot up successfully, the “red” LED will lit.
3. The “green” LED will be off when the computer is successfully booted up. When the “manual” (white) LED is on and “red” LED is off, the system is on, ready, and under manual steering control.

How to engage automated steering control

1. The automated system “sees” the magnets, and thus the guardrail (4 ft away), when one of the front magnetometer reads the magnetic strength, typically starting at a distance about 2-3 feet away from the guardrail.

2. The operator should first position the snowblower with a correct “crab” angle, as he/she normally would before “engaging” the guardrail. A correct crab angle generally means that the blower head is pointed toward the guardrail. More specifically, the tail end of the blower should be 0.5-2 feet further away from the guardrail than that of the front tip of the blower head.
3. The operator should control the blower within acceptable speed range. The recommended speed range is between 0.5 mph to 8 mph.
4. “Stop and go” is an acceptable operation mode of the automated snowblower, however, the automated system may bring the snowblower away from the guardrail (up to 10 cm) if consecutive magnets are miss-read.
5. When Conditions 1-4 are satisfied, the “green” LED will be lit and the automated system is ready to engage at any time. The operation needs only to push the “auto” switch to initiate the manual-to-automated process. The transition process normally (95% of time) is “immediate” and the “blue” LED will be lit. However, there are situations that the driver pushes the “auto” switch just when the “green” LED is changing from on to off. In such situations, the “blue” LED blinks for a few seconds while the automated control system uses additional logics to attempt to engage the steering control. The “blue” LED will be off should such attempt fail; and the driver needs to wait for the “green” LED to be on again in order to re-start this process again.

12.2 Test Procedure and Training

Since the field tests were conducted during the busy winter operation period, and any available operators were used, several operators had very limited training in automated snowblower prior to the tests. A typical test procedure and training for a new operator was as follows:

1. the researcher conducted a 10-15 minute short descriptions of the system in the maintenance yard
2. the driver pushed the switches for turning the automated control off and on a couple of times in the maintenance yard
3. the operator did everything that he would normally perform for snow removal operations once he left the yard and headed to the freeway
4. the operator pushed the switch for automated control as instructed by the ride-along researcher for the first guardrail when the ‘ready” light was on
5. the operator switched off automated control when the noise that signaled “end of magnets” sounded, as instructed by the ride-along researcher for the first guardrail
6. the operator switched on and off as suggested by the automated system when he reached the second guardrail if he felt comfortable in doing so
7. the researcher conducted a short operator interview and the operator filled in a human factor questionnaire

For future operator training, the researchers suggest that it can be part of normal snow removal training with procedures similar to the one above with slightly longer description. It would be very convenient and effective if there is a short test track somewhere inside a maintenance yard. The short descriptions of the system would include the answers to the following questions:

What is the automated snowblower?
How does it work?
What do the status light means?
How to correctly position the snowblower?
How to use the guidance indicator?
How to transition between manual and automation?

A simple operation instruction is shown below in the Figure 12.1 and 12.2.

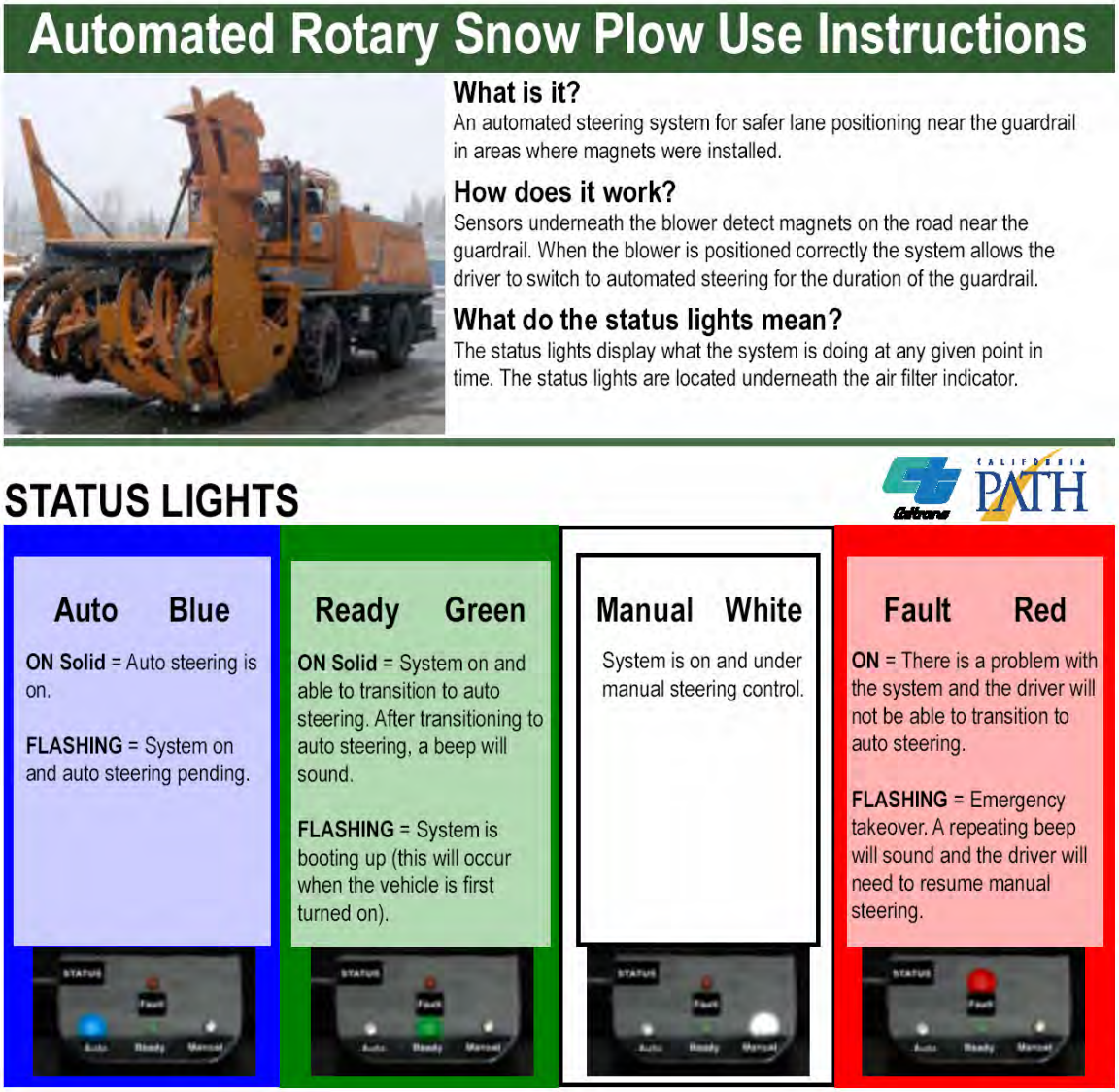

Figure 12. 1 Automated Rotary Snow Plow Use Instruction (1)

Figure 12. 2 Automated Rotary Snow Plow Use Instruction (2)

12.3 Operator Interview and Human Factor Study Preparation

This section discusses areas with respect to the human factor studies. Since the project was concluded before a full field operational tests was conducted. The results of the human factor study will be preliminary. However they are included for information of future studies. This section presents (1) the initial interview and conclusion prior to the design of the automated system; (2) the application to the Committee for Protection of Human Subject; (3) the questionnaire and results from the operators that had performed field operational tests.

Initial Interview before Design

A number of trips were made to Kingvale to gather operational information from the snow blower operator before and during the development of the automated system. Several key issues were discovered which had significant design implications. Among them, the variations of the front wheels normal load due to operator raising the blower box and the frequent rear steering adjustment increase the difficulties of automatic

steering control design. The following items are results from these operator field interviews:

1. The steering action is usually "smooth" during normal plowing operations. It is not affected much by the direction or the amount the snow that is blowing, however it is quite sensitive to how the blower box is pushed on the ground. When the front tires are raised too much, the blower will lose its ability to steer. The operator usually controls the front vehicle weight to between 500-1000lb to ensure the right amount of the snow is cut as well as the right pressure is exerted to the front wheel.
2. The operator usually adjusts the position of the "box" on a constant basis depending on whether the hydraulic of the box leaks, the slope of the road or bank, or the amount of snow to be removed.
3. The operator usually sets the rear wheel steering in a way that the rear edge of the vehicle is about 0.5-1 foot away from the edge of the road or guardrail. The operator usually set it before going into a straight section or a guard rail section. However, some correction will need to be made from time to time because the blower will start cutting into the rail should the angle is too sharp.
4. The operator is required to keep a distance as close as possible to the guard rail - so they will ride on the guard rail. The operator commented that 4-inch gap could even be too much.
5. When the blower is "riding" on the guardrail, there is generally a smooth vibration (~1 Hz according to description). However the blower can eat into the guardrail if there is a big dent on the guardrail due to vehicle collisions. This is one of the scenarios the operator might steer fast.
6. The brake is rarely used during normal operations.
7. The ability to tilt is more important than telescope for the steering wheel function because of the way the cab is designed. Some operator will need to straighten up the steering wheel before they can get in and out of the cab.

Application to the Committee for Protection of Human Subject

In order to collect subjective data from drivers, applications to the Committee for protection of human subjects would need to be approved. The following is the approved application letter which describes clearly the plan and methods for the driver data collection:

Committee for the Protection of Human Subjects

Applicant Name:	Joanne Lins (P.I. Professor Tomizuka)
Department:	Institute of Transportation Studies California PATH
Project Title:	Development of the Advanced Rotarty Plow (ARP) for Snow Removal Operations

We are developing a system for CalTrans snowblower operations to aid drivers for snow removal operations. The system will automate lateral lane keeping over areas that are close to guardrails.

This team consists of staff from both UC Berkeley and UC Davis. The project is sponsored by CalTrans and will be incorporated into maintenance operations this winter regardless of any data collection efforts.

We are planning on collecting data that has a human element in order to study the effectiveness of such a system. The human performance data will be used only for evaluating the system. It will not be used for evaluating the drivers. This is similar to a previous development project regarding a snowplow driver assist system (CPHS 99-2-7).

As a reminder, the team already has in place a secure procedure of data collection that provides a level of privacy acceptable to CPHS. This procedure is well described in the 1999-2-7 application and subsequent communications with the Chair should additional detail be desired by the committee.

All driver identification will be stripped from the data. We will utilize numbers (e.g. 1, 2, etc) in place of identifying descriptors (e.g. names or driver numbers). Any photographs or videos produced for dissemination will either conceal driver characteristics (e.g. masked faces), obtain written consent from drivers or will more likely use research staff members as models.

The CalTrans employees who will use this system will be involved in the development process from the beginning and are aware that we would like to collect objective data beyond subjective design suggestions.

Verbal informed consent to collect the data will be acquired from the driver prior to collection activities. Below is an example of verbal informed consent phrasing.

"I would like to ask you some questions regarding your opinion of the driving conditions (road surface, visibility) and the quality/acceptability of the Snowblower system. I would also like to collect vehicle dynamics data (speed, lane position). I will record your identity as part of the research notes. Your name will be coded to your responses and the list of codes will be stored separately from your responses and will not be shared with anyone outside of the research team. This information will not be associated with you or be used as a means of evaluating your performance. We are only interested in evaluating the system. By doing this, we will be able to observe the degree to which the system helps you.

The data collected will not have your identity in it. We may share this with CalTrans and UC Davis.

We will not use your name or other identifying information in any reports of the research. We will conceal your identity in any photographs or videos that we take during this process unless we obtain your written consent.

Your participation is voluntary. You are free to refuse to take part. You may refuse to answer any questions and may stop taking part in the study at any time. Whether or not you participate in this research will have no bearing on your standing in your job.

Is this ok with you?"

We plan to solicit driver responses to questions in order to collect subjective data. For example, the driver may be asked to identify roadway surface condition (snow, ice, slush/wet, or dry) and to evaluate the performance of the system.

In addition, we plan to collect measurements of vehicle dynamics (e.g. lateral position in the lane with respect to the guardrail), route efficiency (e.g. route completion time), and safety (e.g. forward and lateral distance to potential obstacles). Much of this data is already used by the system to maintain operation (e.g. computation of next position requires current position detection).

All drivers will be assigned a code number. The link between the number and the driver's name will be kept confidential. All written notes that list this linkage will be kept in a locked office. (Care will be taken to keep such notes to one or two copies.) Data will be stored by time and date in a locked location.

Data will be shared with CalTrans DOT and UC Davis only at their request. As there will be no names present in the data, the identity of the drivers will not be apparent. Our liaisons with CalTrans and UC Davis will be made aware that this data is solely for the purpose of evaluating the snowblower system and that attempts at linking drivers' identities to the data are strictly forbidden.

Our previous study on snowplows (CPHS 99-2-7) was authorized to use a verbal consent protocol.

12.4 Operator Feedback Questionnaire and Preliminary Results

Two Caltrans snowblower operators were introduced to the system on 2003-2004 seasons at the Kingvale maintenance yard. One of the operators had been driving snowblowers for 3 years and the other for 18 years. On a scale of 1 to 5 (1 being novice and 5 being expert) the operators rated themselves a 4 and a 4 plus.

Both operators were given a short powerpoint instruction presentation (with similar material described in Section 12.2) and then individually went for a drive on the snowblower with a researcher who answered any questions they had about the system. The trial drive was in the Kingvale maintenance yard. The track tested included a right curve, sloping pavements and pot holes. The drivers had experience transitioning from manual to auto steering and back to manual steering. The first driver had 3 runs and the second driver had two runs. Two runs for each driver were videoed – the video includes a

camera on the drivers face, a camera on the displays and two external cameras – one looking forward and one looking backward as shown in Figure 12.3.

Once the drivers had completed the test driver they were given a questionnaire and then asked some debrief questions following the protocol described above – the results of which are recorded below. This was the first time either operator had experienced the automated system. The responses from the operators are listed in *Italic*. As a summary, the operators learned to use the system quite easily; they generally had very favorable impressions of the system, performance and concept after the test runs.

Figure 12. 3 Camera views of snowblower operator testing

Questionnaires and Results

General Operational Questions:

1. Please describe the system and how it works the way that you would to another blower driver that has not yet seen or used the system.

   Operator 1: "*The system is designed to find and follow a specific line of magnets taking the guess work out of how far off the guard rail the machine is*"

   Operator 2: "*Embedded magnets adjacent to guard rail structure and on board sensors on rotary blower will enable rotary to remove snow next to rail without*

contacting rail with machine parts causing damage to guard rail or machine. Auto steer keeps machine at proper distance from guard rail system can be put in manual mode if necessary"

2. Please describe the type of training that you feel new drivers should have as an introduction to this system. Please comment on the information in the instruction sheet. What should be added, what should be removed?

   "(1) Give reasons for the system (2) share video static display (3) actual course with guard rail, obstructions (signs, light poles etc.)"

3. How long do you think you would need to become comfortable with this system?

   Operator 1: "*12 hour shift*"

   Operator 2: "*Would want to operate thru differing snow conditions in our territory. System is easy enough to learn, it is how different snow conditions and loads will effect system operation*"

4. Did you feel that you knew enough about what the system was doing at any given time to feel comfortable operating the system on the roadside? Please elaborate on your answer.

   Operator 1: "*Yes it was easy to engage and override*"

   Operator 2: "*Yes under these conditions, I am familiar with the purpose + reasons behind the system. Again weather conditions, snow loads actual production will bare out confidence level*"

5. Did the system ever lead you to make an inappropriate maneuver or error in judgment? (If so please describe)

   Operator 1: "*No*"
   Operator 1: "*No*"

6. For future development what additional information would you like to see displayed to the driver?

   Operator 1: "*The less the better keep it as simple as possible*"

   Operator 2: "*Changing the system audible system to a bell, chime, chirp, instead of siren meant for machine functions*"

7. Having seen the automated system did your opinion on how valuable it could be for snow blowing operations change? Please indicate what your opinion was before and after seeing the system work.

Operator 1: "*Yes – opinion before a waste of time and money, opinion after-system works, helpful to driver*"

Operator 2: "*Could be quite an asset in poor visibility, definitely cut down on guard rail damage*" In discussion with the human factor researcher before this driver experienced the system, but, after he had training the driver also said "*if weary it's a definite plus, need to know it's limit and it's a tool – have choice to use it or not*"

For the following questions, please rate how well the system performs:

How easy is the system to use overall?	(very easy) 1 2 3 4 5 (not easy)	2	1
How much do you like the system overall?	(a lot) 1 2 3 4 5 (not at all)	1	3
If you had more time to practice with the system, would you like it more?	(yes) 1 2 3 4 5 (no)	1	2
Rate the system in terms of increasing the efficiency of your snow removal tasks	(helpful) 1 2 3 4 5 (not helpful)	2	2
Do you think that they system is beneficial in terms of increasing your safety?	(yes) 1 2 3 4 5 (not at all)	3	1

Warning Sounds:

Please ask the researcher to play the system sounds to you before answering the following question.

8. Did you feel that the warning sounds were easily heard over the noise of the blower?

   Operator 1: "*Yes*"

   Operator 2: "*Yes*"

9. Do you think that they would be heard over the sound of the radio and normal snow blowing operations?

   Operator 1: "*Yes*"

   Operator 2: "*Yes but could include visual light*"

10. Were the sounds appropriate/ did they help to quickly convey the right message? Do you think that other sounds may be more appropriate, if so please describe.

Operator 1: "*The emergency take control sound needs to be changed, it resembles the sounds the machine makes when overheated, low oil; etc.*"

Operator 2: "*No*" – (is referring to the emergency take control for the same reasons as above – comment added by the human factor researcher)

11. Did the sounds cause ever lead you to make an inappropriate maneuver or error in judgment? (If so please describe)

    Operator 2: "*Could have*" (is referring to the emergency take control for the same reasons as above – comment added by the human factor researcher)

12. On a scale of 1 to 5 (with 1 being very annoying and 5 being pleasant/not annoying at all) please rate the following warning sounds:

    Emergency take control:
    Operator 1: "1", Operator 2: "1"
    Coming to the end of the magnets take control:
    Operator 1: "1", Operator 2: "5"
    Acknowledgement that system has transitioned to auto:
    Operator 1: "5", Operator 2: "5"

Method of Display & Control Questions:

For the Status Display please answer the following questions:

1. As if explaining to another driver new to the system please describe that way that these lights work?

   Operator 1: "*Auto – machine has found magnets & is steering*
   Manual – operator is steering machine
   Fault – machine is off line, cannot pick up magnets
   Ready – machine is ready to take over when you push auto switch"

   Operator 2: "*Manual – white in manual mode operator has control*
   Auto – blue – system is auto tracking steering
   Ready – green – system is in ready mode for auto mode
   Fault – red – system is in fault not over sensor etc"

2. Please describe any difficulties that you feel that you or other drivers may have in understanding the way the lights work. Please include any instances where the system did not operate in the way that you expected that it would.

   Operator 1: "*no problem*"

   Operator 2: "*lights and sequence are not a problem*"

3. Please comment on the location of this display?

   Operator 1: "*there are a lot of gauges, lights and other things going on at the same time in the cab, it would just take some time for the operator to get use to where and how system works*"

   Operator 2: "*display is ok*"

4. Please describe or draw any alternated ways to display the information that is conveyed by the status display?

   Operator 2: "*Put all of system in one grouping or module*" (the driver elaborated on this in the post questionnaire debrief. The driver would like a module that could be moved by the operator to the best location for left and right guardrails. The driver also felt that the displays need to be placed along the horizontal line in which they are currently placed and that the switch could be moved alongside. The driver felt that other drivers could easily reach the switch if placed up front and that when there arm moved to activate it - would not block the drivers forward view "*as their arm would only be up there for a second and they are going so slow anyway*"

For the Guidance Display please answer the following questions:

1. As if explaining to another driver new to the system please describe that way that these lights work?

   Operator 1: "Depending on what side of the road your cutting on you want the green light with the line through it on, the lights on either side are on/off when machine compensates pot holes, slopes, etc."

   Operator 2: "Light position lit represents distance from rail each outside left, right are extremes of machine placement in relationship of guardrail. Each light is an indicator of how many inches away ie 4 from next."

2. Please describe any difficulties that you feel that you or other drivers may have in understanding the way the lights work. Please include any instances where the system did not operate in the way that you expected that it would.

   Operator 1: "*Not a problem*"

   Operator 2: "*It is OK*"

3. Please comment on the location of this display?

   Operator 2: "*Could be grouped as complete system pod*"

4. Please describe or draw any alternated ways to display the information that is conveyed by the guidance display.

   Operator 2: "*what ever kind of grouping of indicators, switching should be readily visible, accessible to operator's front vision overhead front console*"

For the auto/manual control switch please answer the following questions:

1. Did the control work the way that you thought it would? If not, please elaborate.

   Operator 1: "*Yes*"

   Operator 2: "*Yes*"

2. Did you have any difficulties transitioning between auto and manual or manual to auto? If so please elaborate.

   Operator 1: "*No*"

   Operator 2: "*No*"

Additional comments from questionnaire debrief:

Operators suggested that the current minimum speed needed to be able to transition to auto steer (2mph) is not low enough. One operator said that as a worst case scenario they may move 30 feet or less in 10 minutes. Conditions that may cause low speed include but are not limited to:

- amount and moisture content of snow – more of each results in a slower cut, (a wet snow full box cut is the slowest – this refers to a cut that is the full width and possibly height of blower)
- operating temperature of machine
- where the material needs to be cast to – for short cast reduce speed. Cast distance depends on geographical location (road layout, slope, intersection etc), where snow needs to go and what structures (signs etc) are around

One driver was concerned about meeting the catching conditions of having the rear of the blower with 1 ½ ' of the front, saying that in "*some types of snow, the road angle etc can push the blower away from the guard rail and that this may not be obtainable*"

One driver was asked his opinion of the instruction card – his comment "*its good, all the important parts are there & its kept simple*"

13. Tests and Results

Several types of vehicle experiments and tests were conducted during the project period. These tests can be grouped into the following test categories based on the time and the purpose of the test: initial tests on the Richmond Field Station (RFS) test track (2002), initial test on the test track at the Kingvale maintenance yard (2003), simulated guardrail test with operator at Kingvale track (2003-2004), final tuning test at the Richmond Field Station test track (2004), and field operational test along I-80 guardrail (2005). This section describes the results of and the lessons learned from these tests. These results were used to support operator feedback, system validation, and performance evaluation.

13.1 Initial Algorithm Test at RFS

The first lateral control algorithm was implemented during 2002. The algorithm was intended to only test the feasibility of accurately tracking the blower along the magnetic line. The algorithm did not contain any nonlinear algorithm, nor did it have any intelligence to deal with uncertainties or operations. The result is shown in Figure 13.1 and 13.2. The result does indicate the basic feasibility of such lateral control at various speeds. However, the algorithm is at its very early stage and it needs to be redesigned to address the proper initialization, to add algorithms to deal with transition, load changes, sensor noises, rear steering effects and tire or chain effects. As seen in Figure 13.1 and 13.2, the controller keeps the head position at the center of the lane rather than the tip along guardrail (which will be offset by 22 cm away from the center). It should also be noted that the 6-ton blower head was not installed for these test. Furthermore, many additional modifications, including algorithm to perform transition, to improve accuracy, to deal with loading changes and tire stiffness changes, and rear steering variations, to desensitize against various sensor limitation and noises, are also identified during these initial tests.

The initial results also indicate that the steering actuator servo meets the basic performance requirements. The fundamental difficulty of the servo design is the extreme nonlinearities of the front steering mechanism. The torque required to steer the front tire varies significantly with respect to the front-loading conditions. For example, the steering hydraulic assist system cannot move the front tires by more than 50 degrees when the blower head is raised and the vehicle is stopped. In fact, the steering actuator motor often does not have enough torque capacity when the vehicle is at lower speeds or when the commanded rate of change is high. However, these limitations have to be considered under “normal” operating conditions and are required to be overcome by the servo controller. Figure 13.3 shows the resultant steering position servo under normal operation at RFS without snow chains. The steering angle does follow the command almost all the time, and the power saturation and rate limitation generally do not show up explicitly during normal automated operation.

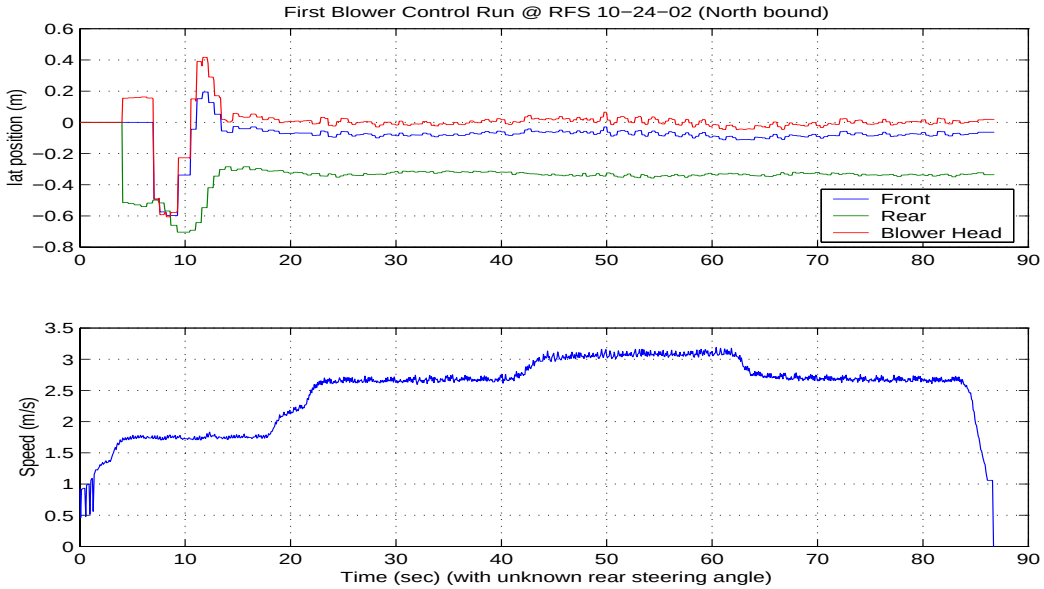

Figure 13. 1 Initial test result at RFS test track (1st north bound run)

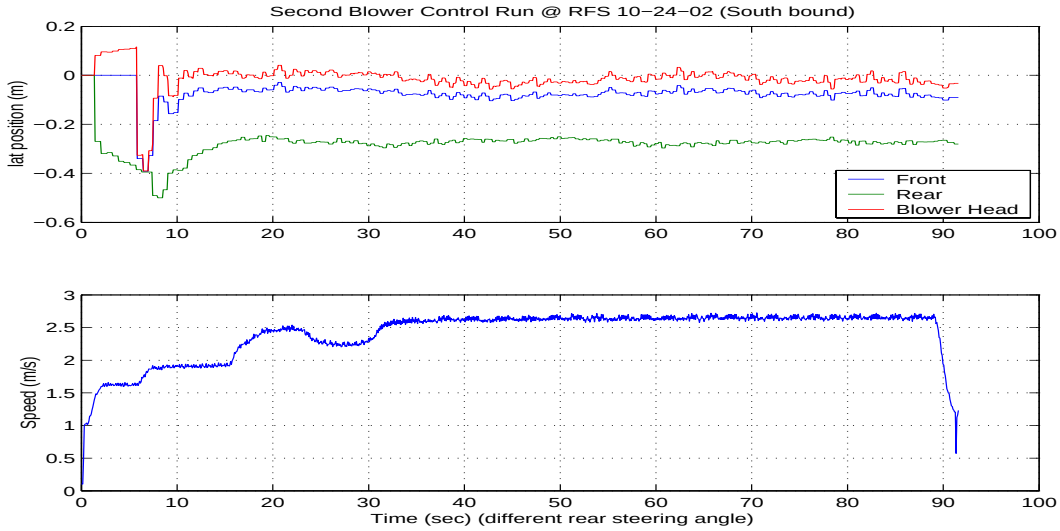

Figure 13. 2 Initial test result at RFS test track (2nd south bound run)

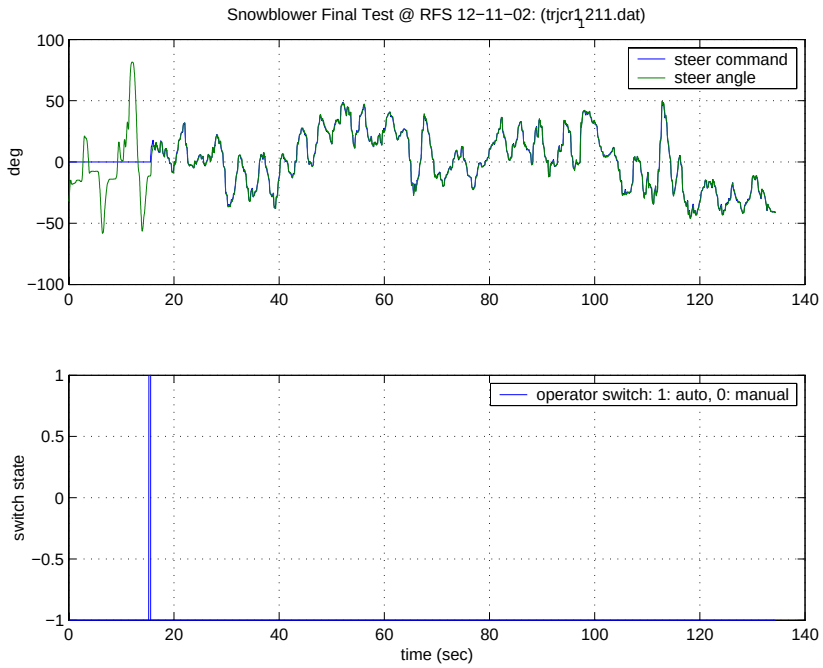

Figure 13. 3 Servo performances for the steering actuator

13.2 Initial Prototype System Test at RFS

An initial steering control algorithm including offset tracking, desensitization against rear steering, manual/automated transition, HMI coordination has been implemented with accuracy within approximately 10 cm and tested at RFS test track. The initial stability problem caused by the huge inertia of the blower head has been identified and solved. However, the likelihood of additional instability resulting from icy road surface, tire chains nonlinearities, possible impact from the guardrail, large uncertain forces from snow removal would likely need to be re-addressed when the system encounters the first winter environment.

Lateral Control

The lateral control algorithm was re-tuned when the blower head was added to the vehicle body (although the chute was not installed). Added to the control algorithm included: transition ability, and guardrail offset tracking. The result is shown in Figure 13.3. The blower head is basically bounded by 10cm peak-to-peak around the target location (~25cm). The result demonstrated the feasibility of automated lateral control for the snowblower operations. However, the algorithm needs to be redesigned to address the load changes and possible chain effects under the winter operational environment.

Transition Control

The manual/automated transition algorithm was first developed and tested at the RFS test track. The transition algorithm needs to coordinate the driver demand, vehicle condition, automated system status and steering actuator limitations, and perform transition in a timely fashion. The design difficulty results from the demanding

operational scenarios, such as transitioning at location very close to the guardrail. Figure 13.4 shows the results of blower head tracking 0.25 m (at the guardrail location) while the driver switches the automated system on and off.

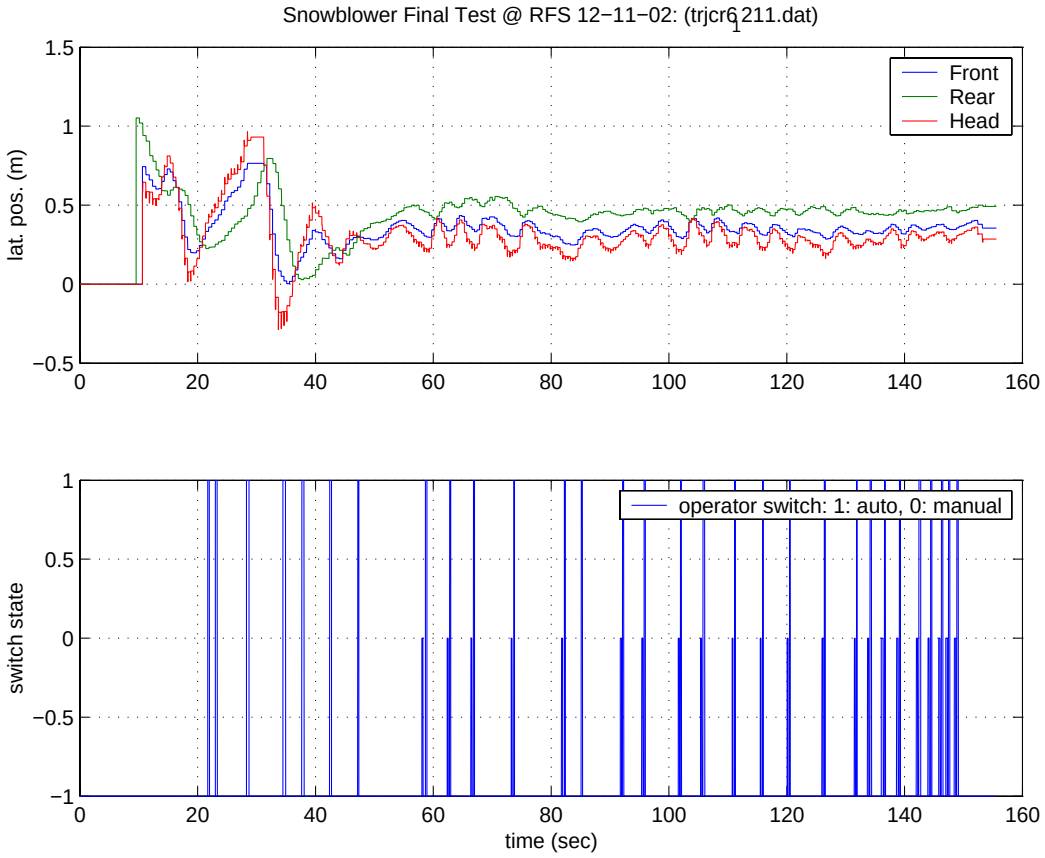

Figure 13. 4 Lateral and transition control

Human Machine Interface (HMI) control

A simple HMI design that will be used for the first winter tests was developed and implemented first at the RFS test track. The HMI design consists of one operator switch, four control indicators, seven guidance indicators; several fault indicators and three audible warnings. It reflects the control status and integrates with the control/transition algorithm in the system. Figure 13.5 shows a typical example of the HMI operation. The HMI design might need to be modified based on the operator feedback after the winter operational tests.

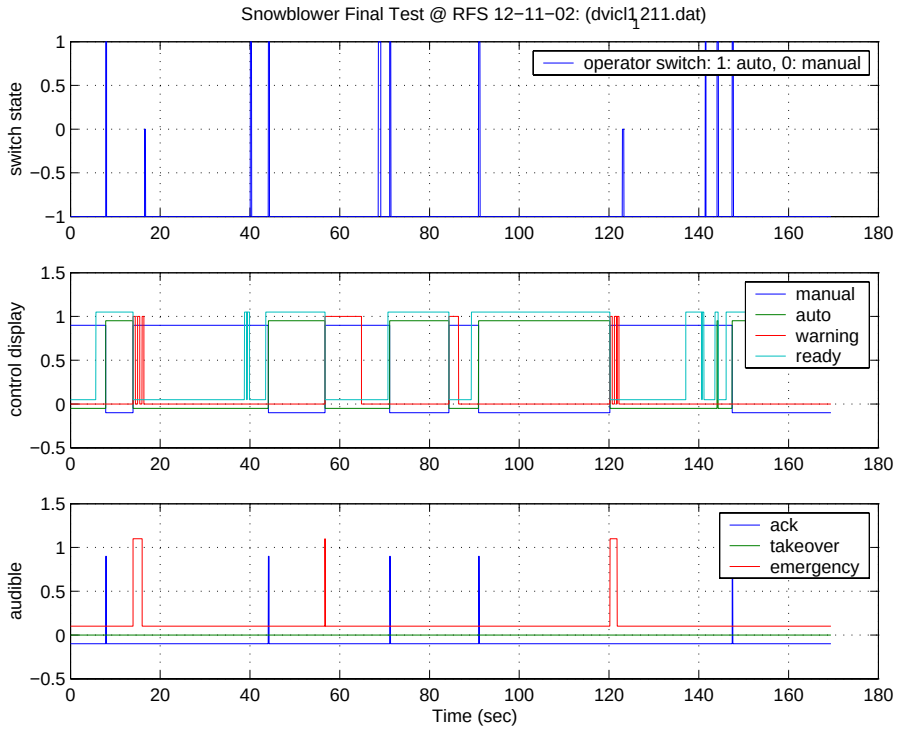

Figure 13. 5 HMI control and display results

13.3 Initial Kingvale Maintenance Yard Tests

The first tests conducted at the short (130m) test track at the Caltrans maintenance yard were made during March 2003 right after the automated snowblower, with chute installed (see Figure 13.6), arrived at Kingvale. During the initial testing on the short magnet track in the yard, several major problems that were not observed at Richmond Field Station were discovered:

1. The blower steering control was less stable with the chute installed. With the new chute, the blower exhibits more oscillatory behavior, from 10 cm peak-to-peak at RFS to almost 20 cm peak-to-peak tracking errors in the Kingvale yard. The chute, weighted at least a half-ton or more, was installed on the “head” section of the blower and was installed after the blower left RFS.

2. The very rough road surface on the test track, with many cracks, "potholes" (some as large as 2 meter in diameter – see Figure 13.6), and the unevenly slope down northward on the west end of the track, created large overshoots and controller counter-reactions. Dependent on the speed, the rear steering angle, the relative entering/exiting conditions relative to the potholes, the movement of the chute or blower head angle, and the controller gains, the 20-ton blower can exhibit additional overshoots as large as 15-20cm (when the conditions were "right"). The guardrail can be easily damaged with such overshoot if such overshoot goes toward the "guardrail" side. To make matter worse, most operators argued that the maximum tracking error

should be less than 10 cm (or even less than an inch according to some operators). And the road condition along guardrail (shoulder) is often uneven with potholes and cracks. In that sense, the rougher than normal track condition in the Kingvale yard became a “perfect” test track for the development.

3. The stability condition (or oscillation) getting worse while snow chain was put on one of the front tire (it was put on after the snowblower arrived in Kingvale).

4. The chance of occasionally hitting the guardrail exists. They occurred under big bumps, which may create additional 10-15 cm overshoots. Lower controller gains may reduce certain controller reaction toward potholes under certain initial conditions (not the initial overshoot), yet the controller need to remain in the "high gain" area to sufficiently react to plow loading, ice pack, rear steering, etc, and to keep an accurate tracking. Unfortunately, the controller does not distinguish between potholes or guardrail or road/plowing disturbances.

5. There could be a once-in-a while, rare but exist, stability problem. Once instability starts, it tends to stay for a while as a limit cycle oscillation of the whole vehicle. Such phenomenon was created by the highly blower nonlinear system that "intensified" itself while the blower got into any situations resemble larger angle oscillation. Such "vehicle" nonlinearity was a result of the combination of huge inertia and high CG location, the tire nonlinearity (with chain), the high/low road friction interchanges, the oscillatory natural of the blower head, the (unavoidable) under-power of the steering actuator, the very speed-sensitive lateral stability conditions, unknown "super-elevation" along the guardrail, and the possible/changing large rear steering angle.

Figure 13. 6 Snowblower arrived at Kingvale Maintenance yard

13.4 Problem-Solving Test at Kingvale Maintenance Yard Tests

PATH staffs tested the system in the yard for many operating scenarios and continuously re-design and re-tuned the steering controllers in order for the snowblower to re-achieve the 10 cm peak-peak error under various operational conditions. Problem 1-3 were resolved. However, Problem 4 and 5 in Section 13.3 are two fundamental and difficult control problems with respect to this natural oscillator (the snowblower) under such accuracy requirements, and under such varying and huge nonlinearities/uncertainties/disturbances; especially when we found out that it's difficult even to manually maintain a straight line on the track through these potholes. Lower controller gain may reduce certain controller reaction toward potholes under certain initial conditions (not the initial overshoot), yet the controller need to stay in "high gain" to sufficiently react to various operation loads and reject disturbances. The controller does not distinguish between potholes or guardrail or road or plowing disturbances. Once an oscillation starts, it tends to stay for a while: a limit cycle oscillation of the whole snowblower body. The "limit cycle" oscillation was created by the highly blower nonlinear system that "intensified" itself whenever the blower got into any kind of larger angle oscillation. One particular critical reason that discovered during this period is the "tire suspension mode" as described in Section 9.2 and 10.1.

To control the snowblower with high accuracy under such varying and huge nonlinearities, uncertainties and disturbances, is like controlling a large natural oscillator with small actuators. Once the researchers understood the causes of the problems and redesigned the controller (as described in Section 10.2), a workable candidate system was achieved with tracking error bounded by 10cm. The reaction to the bump were generally "well behaved" and kept away from the guardrail. However there would be chances that a few cm overshoot into the guardrail under either a very large pothole, or several continuous potholes, and when the "initial conditions" were most unfavorable (there are situations human operators can not prevent!). The data also suggested that, under some of these situation (such as sinking into a pothole when the blower is 1 inch away to the guardrail), the steering system has no ability to stop this process in a timely fashion-the steering actuator command was even saturated under such conditions. Under these worst scenarios, hopefully the controller will help the guardrail "stop and slow down" the blower head and minimize the damage to the guardrail.

13.5 Simulated Guardrail and Operator Feedback at Kingvale

Once the tasks in Section 13.4 were completed, the development process shifted to the introduction of the first prototype instrumented Advanced Rotary Plow to the Caltrans operators during winter 2003. The automated system was installed with the first version of the control and operator interface software. The first version software included the smart steering actuator servo function, automated steering control and driver transition functions, operator HMI functions, and sensor signal processing functions.

A section of simulated guardrail was set up using traffic cones and tape along a segregated test track with embedded magnets inside the Kingvale maintenance yard. The test scenarios included: left/right guardrail tracking, different crab angle tracking, different blower head (box) position and chute orientation, speeds from stop to 9 mph, various initial transitioning conditions, and various emergency shut off situations. This method provided an effective and safe environment for the system's development as well as for the initial operator training and feedback.

The purposes of using the "simulated" guardrail for initial operation system introduction were:

- effectively utilizing the limited time to obtain timely operator feedback and comments
- providing early assessment for the feasibility and acceptability of the snow blower automated control
- gaining valuable first-hand feedback for further improvements

The operator training and introduction tasks conducted included

- preparing operator questionnaire and training material
- setting up a simulated guardrail in the Kingvale yard
- setting up/practicing/confirming simulated guardrail operation before the operator training starts
- conducting operator training
- operator simulating guardrail snow removal operation on the magnet track with simulated guardrail with data recording
- conducting operator interview and human factor questionnaires
- reporting results

Section 12.4 summarized the operator feedback. However, two problems remained:

1. the tip of the blower head may hit the guardrail under big road bumps such as the 6 inch deep potholes in the yard;
2. the controlled blower experienced occasional oscillation problems.

13.6 Stakeholder Demonstration

A project status-update meeting and demonstration of the Advanced Rotary Plow (ARP) was presented in the Caltrans Maintenance Yard at Kingvale, CA (on I-80, 90 miles east of Sacramento) on October 15, 2003. The various stakeholders are members from Caltrans, Nevada DOT and Alaska DOT. The meeting included presentations of the work performed to date as well as ARP ride-along demonstration under automatic steering by following magnets embedded in the yard pavement. The demonstration was conducted using the modified ARP: magnetometer sensor bars were added to the front and rear of the ARP, a steering actuator was incorporated into the steering column, a control computer was added, control software created, and an operator interface installed in the cab. The demonstration aimed at verifying the initial performance goals of the ARP and obtained early feedback and comments from the stakeholders. The operation procedure demonstrated consisted of the following relatively easy steps:

1. The operator approaches the guardrail the same way as “manual” operations. The guidance indicators display the current position of the blower head to support this procedure.
2. The operator can switch to automatic steering control by pushing on the “auto” switch whenever the “green” status light is lit. The green status light lit indicates magnets were read and the blower head points toward the guardrail. The automatic system will automatically determine whether the guardrail in on the left or right side of the blower based on the magnetic coding.
3. The “blue” status light will remain lit when the snowblower is under automated control. The operator can switch to manual control any time by pushing the “manual” button or by over-powering the steering wheel.
4. The “red” status light will flash with simultaneous emergency sound to notify the operator that there is a fault developed and detected by the system and to request the operator to take over steering control

The following scenarios were demonstrated along the 150 m magnet track in the Kingvale yard:

1. Approaching guardrail, switching to automated steering control
2. Operating at various snowblower speeds including stop and go, very low speeds as well as speed up and slow down
3. Turing on and off plow clutch, moving blower chute toward left and right; moving blower head up or down
4. Manually changing rear steering, performing manual and automated transitions
5. Operating at different road conditions including slope, elevation changes and rough road surfaces

During the over-three-hours ride-along demonstration to more than 30 stakeholders from 3 states, all participants were impressed by the performance. The researchers were especially surprised by the positive comments from those who had previous experience working with snow removal equipment. Comments like "It works!" and "Having the system keep the front in (on the guard rail) while the operator can use the rear steer for different snow accumulations and (road) turns is just what we need." were encouragements to the team.

The data collected during the stakeholder demonstration (see Figure 13.7 for example) revealed that

- the controller generally did a good job of keeping the front of the blower head within 0.5-5.0 inches to the simulated guardrail,
- the controller generally adjusted the front steering angle correctly to compensate for the rear steering controlled by the operator (until the rear part of the snowblower got beyond the sensor range),
- the automated control effort extended to speed above 0.5 mph as designed,
- the tracking error increases when the blower head is moved to a higher position as the analysis indicated, and
- there were possibilities that the blower head might come to a brief contact with the guardrail caused by certain events such as a very large and deep potholes or

the driver mistakenly steers the blower into the guardrail with sharp rear steering angle. The data review provide an early glace of areas that need further attentions during the coming initial road tests along I-80. The following figure shows an example of the data collected during October 15th demonstration.

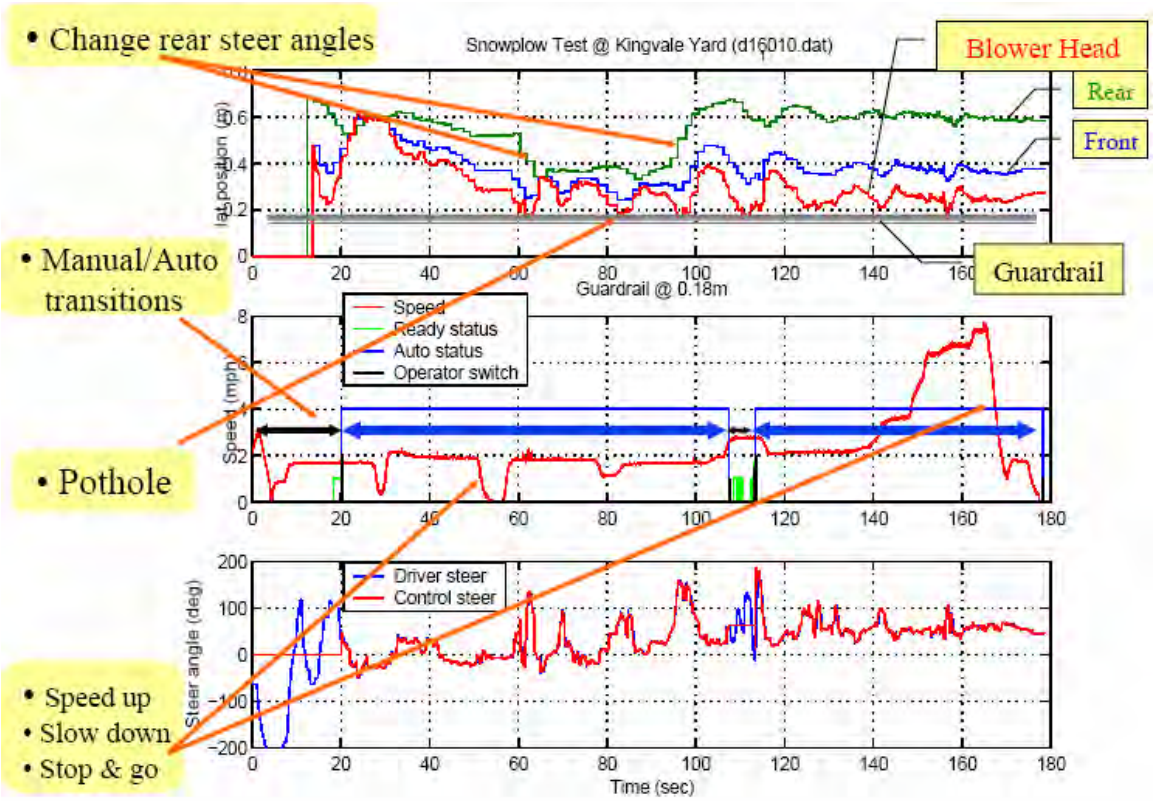

Figure 13. 7 Data collected during stakeholder demonstration

Two technical issues relating to hardware installation were raised during previous operator test drives and demonstrations are:

- "Low speed" operation did not reach speed that was low enough, and
- The survivability of the rear magnetic sensor bar during road operation was in doubt especially when cutting in and out of drainage locations

The speed sensor and its associated signal-processing algorithm were modified to extend to low speed operations from 2 mph to below 0.5 mph (refer to Section 6.1). This seemed to reach low enough speed for normal low speed operations. However, further field test may require additional modifications. Thee rear magnetometer bar was removed after the stakeholder demonstration and will be modified as described in Section 6.3.

13.7 Final RFS System Calibration

During the period before 2004 winter season, the snowblower was transported to RFS to modify the rear magnetometer bar as indicated in Section 6.3 and 13.6. The research team took advantage of this period to perform final system calibration before the 2004-

2005 winter field tests. The team has modified, implemented, and tested a new steering control algorithm that used the new rear magnetometer bar, improved the control stability margins when the blower head is at the up position, and shorten the initial manual to automatic transition trajectory catching time. The team also simplified the operating procedure to a "turn key" operation. In addition, an emergency button was installed to the system enabling the driver to turn off the system with only one push button should it become necessary (see Section 11.2).

Before the Blower can be shipped back to Kingvale for the coming winter operation, there were several tasks related to the steering controller design needed to be accomplished. Since the distance between the rear bar and the front bar was shortened from 5.08 meters to 2.59 meters, the noise to signal ratio for controlling the blower head has also doubled. The increase noise factor would require a new tuning in control parameters. Second, it was observed that the blower head had a tendency to oscillate when the head is raised high enough above the ground. Although this is not a typical operational configuration, but it indicates a potential hidden stability problem. The analysis had indicated the sources of this reduced stability margins came from the body coupling to the added dynamic lag from the tire compliance at low speeds (also described in Section 9.2). New controller would need to be re-designed, inserted, and implemented to lessen this in-stability effect. Finally, an operator suggested that the initial automatic "catching phase" of the blower approaching the guardrail seemed to be too long after the driver requested a transition and the blower had initialized automatic control. This also requires modifications to both control algorithm and its corresponding trajectory planning during the initial catching (approaching) phase of the control transition.

During this quarter, the following modifications had been added to the automatic steering controller and they resolved the issues listed above.

- New parameters tuning and some specific nonlinear adaptation with respect to noise characteristics were added to the following blower software estimators: blower vehicle angle estimator, blower travel angle estimator, as well as the road radius estimations. These changes enable transparent usages of most of the "old" control algorithms using the new rear magnetometer bar under higher noise to signal ratio.
- A new gain-scheduling was added to the steering controller that modified the phase characteristics of the controller at low speeds. This modification addresses the stability problems resulted from the increased phase lag with the semi-non-minimal phase characteristics of the yaw motion at low speed.
- A new trajectory planning was added to the original "controller trajectory planning routine" to speed up the initial catching phase as soon as the driver pushes the automatic transition switch. A new initial controller transition scheduling was also added to accommodate a faster controller response in a shorter transition distance.

Extensive testing was then conducted at the test track at Richmond Field Station to verify those changes. Those tests included:

- Left guardrail tracking and right guardrail tracking.

- Different crab angle tracking (from small to large)
- Up and down blower head, and rotate chute positions
- Different speed from stop and go to 9 mph.
- Various initial transitioning conditions
- Various emergency shut off scenarios
- Simulated guardrail tracking using traffic cones along the test track at the Richmond field station (with sharpest curvature of 110 meters, compared to 400 meters at I-80 along guardrail)

Figure 13. 8 Simulated guardrail testing at Richmond Field Station

Figure 13.8 and 13.9 shows the setup for the simulated guardrail runs at the test track at the Richmond Field Station. Figure 13.10 to Figure 13.12 illustrate the examples of those test results.

Figure 13. 9 Curve section on the simulated guardrail testing at RFS

Figure 13.10 shows a simulated guardrail run for the ARP with the new control software with the new rear magnetometer bar at Richmond Field Station test track with constant crab angle (~5 degrees) along the left guardrail with speed from 2.5 mph to 4 mph. It can be observed that the head of the snowblower tracks very well along the left guardrail and almost never touches it. The standard deviations of the tracking error under automation are 5.8 centimeters, and 3.0 centimeters for total time under automation, and for automation after initial catching phase, respectively.

Figure 13.11 shows a similar simulated guardrail run for the ARP as in Figure 1 except that the driver has changed the crab angle from 4 degree to 4.5 degree to 7.5 degree to 0 degree at time = 25 second, 52 second, 175 second and 240 second, respectively, by changing the rear steering during automatic steering control. Similarly, one can observe that the head of the snowblower tracks very well along the left guardrail and almost never touches it. The standard deviations of the tracking error under automation are 4.0 centimeters, and 3.4 centimeters for total time under automation, and for automation after initial catching phase, respectively. The speed of the automatic operation was very similar to those in the previous run from 2.5 mph to 4 mph.

Figure 13.12 shows a simulated guardrail run for the ARP along the right guardrail. The driver has changed the crab angle from 3.5 degree to 5 degree to 2 degree to -0.5 degree, and hence triggered the auto-ejection process at around time = 146 second; the driver then switched off the automatic steering at time = 152.5 second, and switched back on at time = 158.5 second. The transitions in control state were basically instantaneously. And the plot shows that the "catching phase" was within 10 magnets. Furthermore, the driver has covered a large range of traveling speed from stop up to 8.5 mph. More significantly, the driver has changed the speed drastically between time = 113 second to 132 second by consecutively provided full brake and full throttling three times from stop to 8.5 mph as shown in Figure 13.12. Even under these severe operational scenarios, the head of the snowblower tracked very well along the right guardrail almost without touching it. The standard deviation of the tracking error under automation is 7.1 cm for automation after initial catching phase.

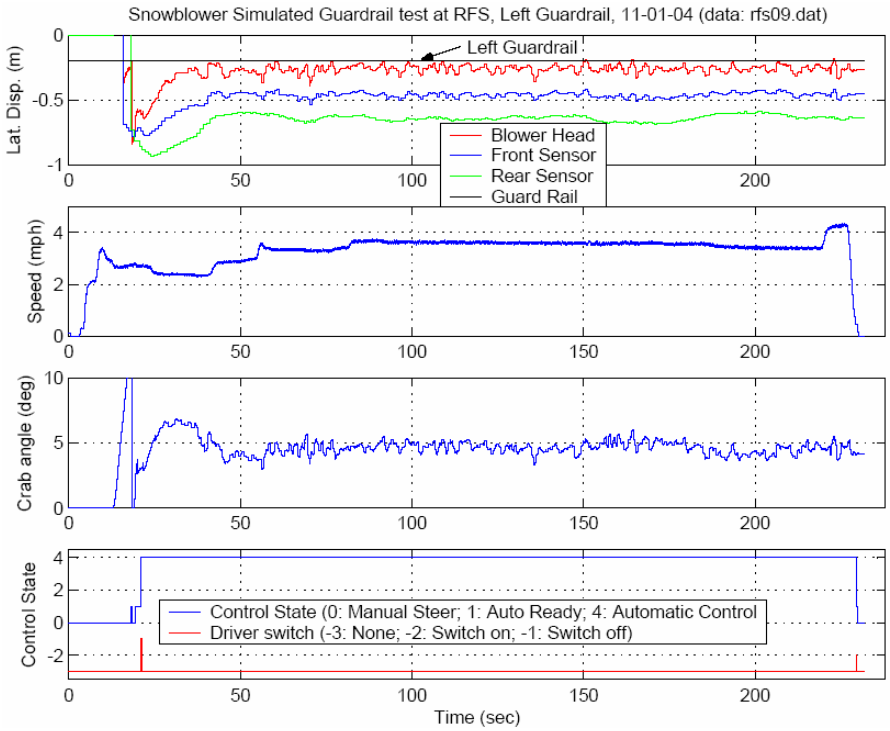

Figure 13. 10 ARP Simulated Guardrail Tests at RFS (Left Guardrail, 11-01-04): Constant Rear Steering

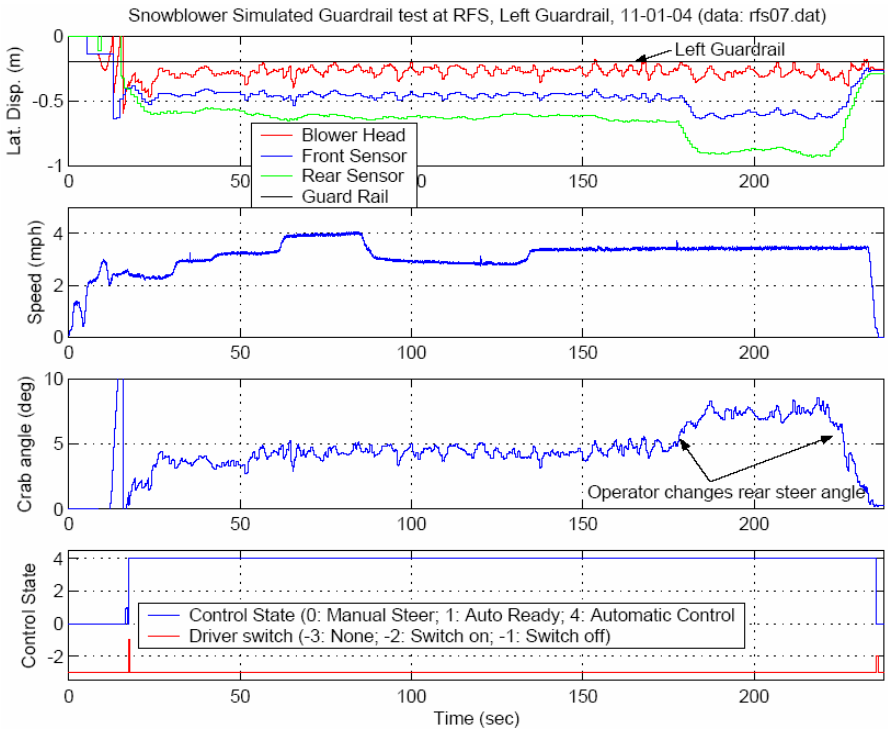

Figure 13. 11 ARP Simulated Guardrail Tests at RFS (Left Guardrail, 11-01-04): Changing Rear Steering

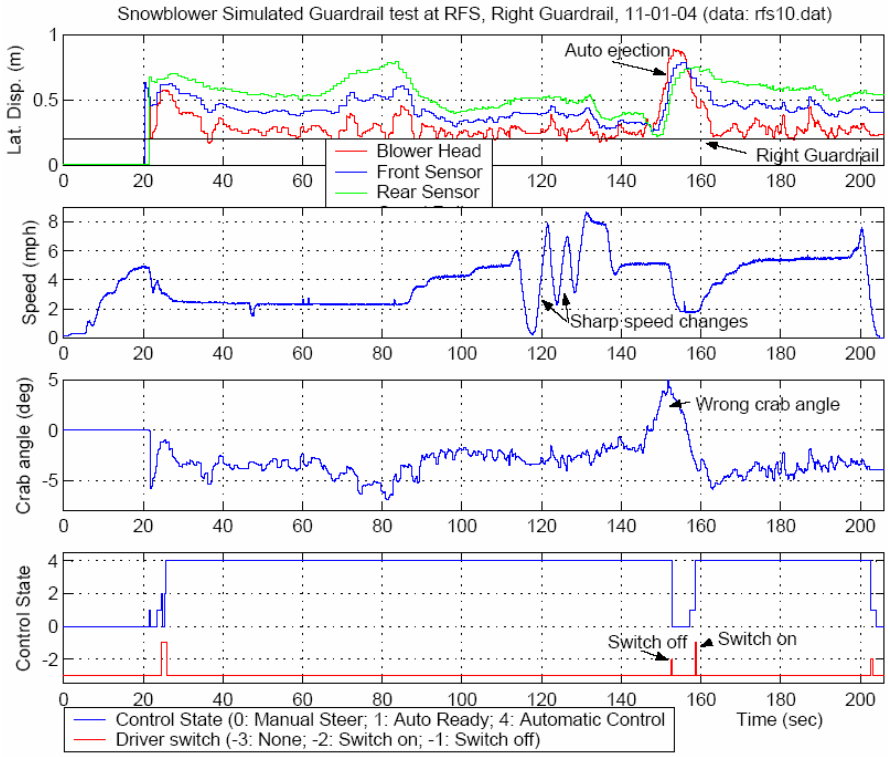

Figure 13. 12 ARP Simulated Guardrail Tests at RFS (Right Guardrail, 11-01-04): Rear Steering Change, Wrong Crab Angle, Auto-Ejection, Sharp Speed Changes, Switch on/off

13.8 Initial I-80 Guardrail Tests:

The ARP was shipped to Kingvale/Marysville during early 2004-2005 winter season. Tests were first conducted along the Interstate-80 highway under fair weather conditions on ground free of snow. Operator performed “snow removal functions” as normal operations. These tests provided an opportunity for the researcher to make final corrections according to the operator feedback and the data analysis results.

Figure 13. 13 Automatic steering along guardrail on I-80 on Dec. 2004

The following is what the PATH staff has concluded during the initial testing of the modified system along guardrail:

1. The system performs the automated steering function as designed along the guardrail (without pushing snow as seen in Figure 13.13)
2. There is a possible bug in the initialization phase of the trajectory planning software which might have been inadvertently inserted just before the blower left Berkeley last October.
3. There is likely a calibration "gap" between two outside magnetic sensors that we did not discover until we tried to control the blower with a very large crab angle.
4. The "automatic-ejection" function that automatically steers the blower away from the guardrail when the operator selects a wrong crab angle (i.e. steers the rear tire into the guardrail) need to be modified. After discussions with the operator, we have decided to modify the "ejection" to no more than one foot since many

shoulder areas in I-80 are too narrow and moving the blower into the traffic lane may create a safety problem.

5. An automatic warning sound will need to be included in lieu of the automatic ejection function so that the operator knows there is a wrong crab angle should there be one (i.e. rear of the blower is closer to the guardrail than the front); this sound will allow the operator to correct the crab angle in time.

After analyzing the causes for the above discovered software problems, and coded all the new solutions including fixes for software bugs, bounded "ejection" (by one feet), signal processing smoothing, and warning sounds for wrong crab angles. The team then conducted addition I-80 guardrail road test under no snow condition to confirm that the system is ready to perform winter operational field test. Figure 13.14 shows the weather and road condition on the final verification trial day (2/3/2005): good weather with no snow on the ground.

Figure 13. 14 Test run on a fair weather condition (2/3/2005)

Figure 13.14 shows the data of an automated test run along right guardrail #1 on I-80 for the snowblower with no snow on the ground on Feb. 3, 2005. The driver changed the crab angle from -3 degrees to -1 degrees, and changed speed from 2 mph to 4 mph. It can be observed that the head of the snowblower tracks very well along the right guardrail (located at 20 cm in this figure) and almost never touches it (such contact, should it happened, was never observed or felt). The standard deviation of the tracking error under automation is 3.3 cm for total time under automation. Moreover, the automation was transition immediately once the driver pushed the auto switch and transitioned back to driver when he pushes the manual switch. The results suggested that the system is ready for the first winter operational tests.

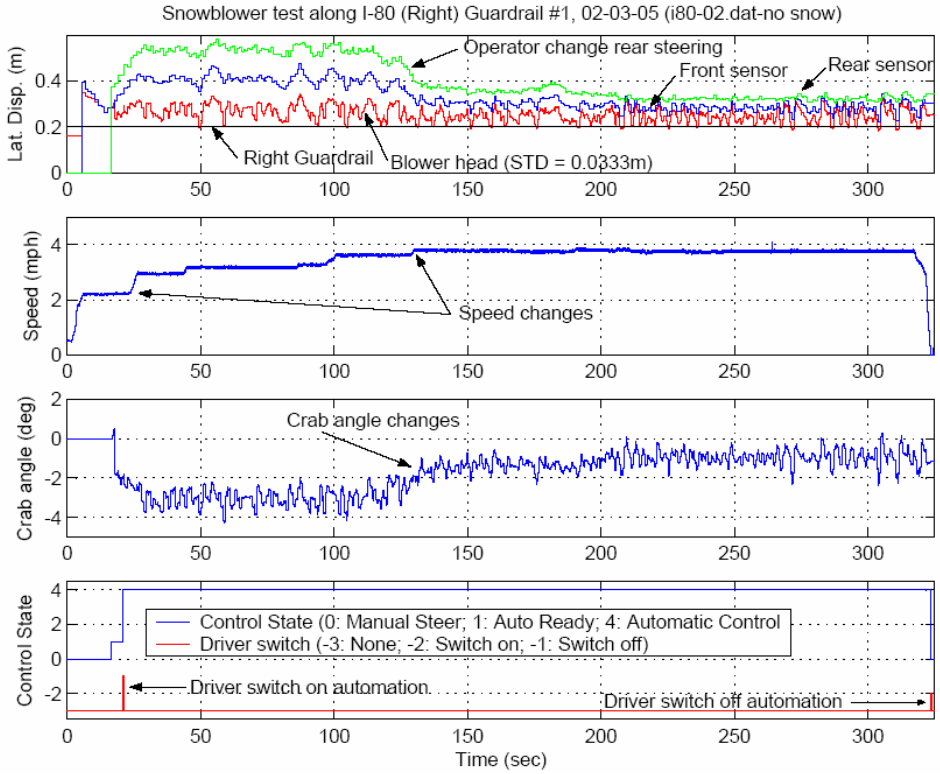

Figure 13. 15 Snowblower Tests along Guardrail on I-80 (Right Guardrail #1, 02-03-05): No Snow on the Ground

13.9 Winter Operational Field Tests

The purpose of the winter operational field tests is to allow typical snow removal operators using the automated system performing snow removal tasks under real winter operational environment. This particular type of tests is the toughest tests under the most stringent conditions. The results and feedback would provide important feedback to both the design and the performance of the prototype system. It would also test the hardware integrity with respect to the blower chassis vibration.

The research team made eight trips to the Kingvale yard to tested automatic steering operations along the guardrails that equipped with magnets on I-80. Three test runs were conducted with three different operators on three different trips. Two initial field tests were conducted along the guardrails of the Interstate-80 under real winter operational conditions: the first one with light snow conditions (March 4, 2005), and the second one under a heavy winter storm, blowing accumulated wet snow (March 22, 2005).

Five operators test operated the automated snowblower during the 2004-2005 winter season. Since the field tests were conducted during the busy winter operation period, and any available operators were used, several operators had very limited training in automated snowblower prior to the tests. Typical test runs were conducted on westbound right shoulder from Soda Spring to Kingvale where there are three sections of the

guardrail equipped with magnets. A typical test procedure for a new operator has been described in Section 12.2.

Figures 13.14, 13.16 and 13.17 show three different test conditions on three different trial days with three different operators for comparison. The test conditions on each of these trial days were:
2/3/2005: Good weather with no snow on the ground
3/4/2005: Fair weather with some leftover snow on the ground
3/22/2005: Stormy weather with heavy accumulated wet snow on the ground

It is worthwhile noticing that Figure 13.14, 13.16 and 13.17 were taken approximately at the same guardrail section. Figure 13.17 also shows a faint trace of the guardrail after the automated snowblower has passed; and indicates the closeness of the blower head to the guardrail. Figure 13.18 shows an operator "hand-free" operation during a field test run along a section of guardrail while a truck was passing by.

Figure 13. 16 Test run on a light snowy day (3/4/2005)

Figure 13. 17 Field test (blowing wet snow during a winter storm 3/22/2005)

Figure 13. 18 Operator using automated steering control along I-80 guardrail

Figures 13.19 – 13.21 presents the detailed data plots from the saved data during these test runs. It should be noted that the test runs on March 22nd, 2005 were conducted at heavy snow conditions with large amount of wet snow accumulated on the ground. The general observations and conclusions are:

1. The system performed the automated steering function as designed along the guardrail, with and without blowing snow.

2. The operators learned to use the system quite easily; and they generally had very favorable impressions on the system, performance and concept after the test runs. In particular, they liked the following:
    a. The operational procedure was simple;
    b. The LED was simple to understand;
    c. The automatic control system seemed to be working;
    d. If the system can function continuously, it would provide significant help to the blower operations. (This comments generally made after they had experienced the operations.)

3. The following are the areas need improvements:
    a. The operational speed for automatic control should be as low as 0.3 m/s (the current lowest speed for operation is 0.8 m/s)
    b. The system should improve its ability to automatically compensate for the combination of the following operational conditions: heavy wet snow, large crab angle, sharp curve, and large super-elevations
    c. The operator would like to have the option to choose the distance to the guardrail for different operations
    d. The system should allow for certain negative crab angle for certain special operations such as in the case when the operator uses it to compensate for large snow cut on a curve

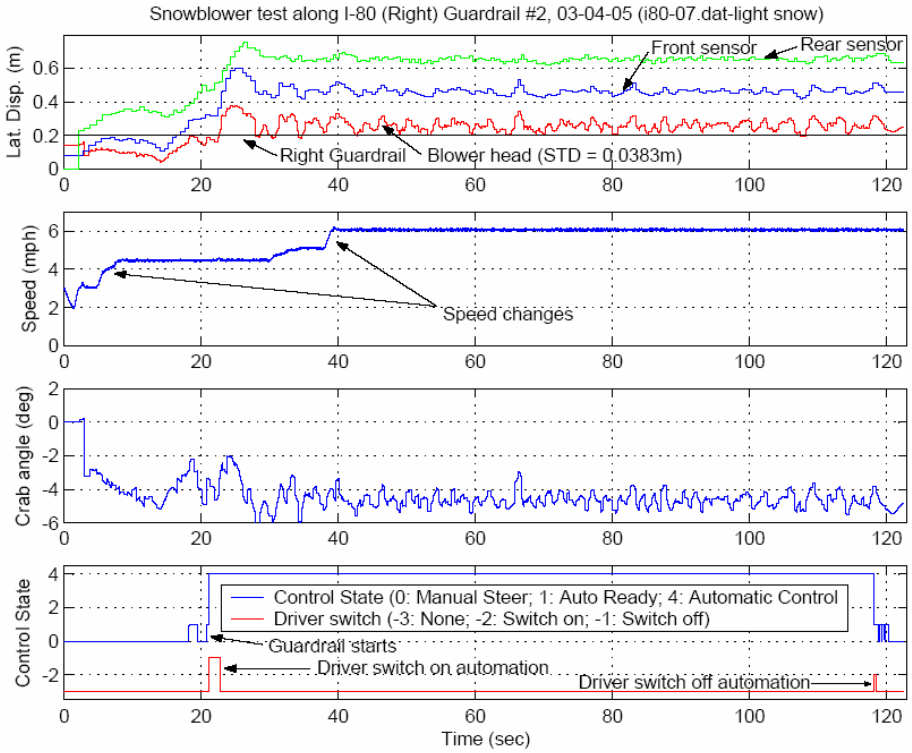

Figure 13. 19 Snowblower Tests along Guardrail on I-80 (Right Guardrail #2, 03-04-05): Light Snow on the Ground

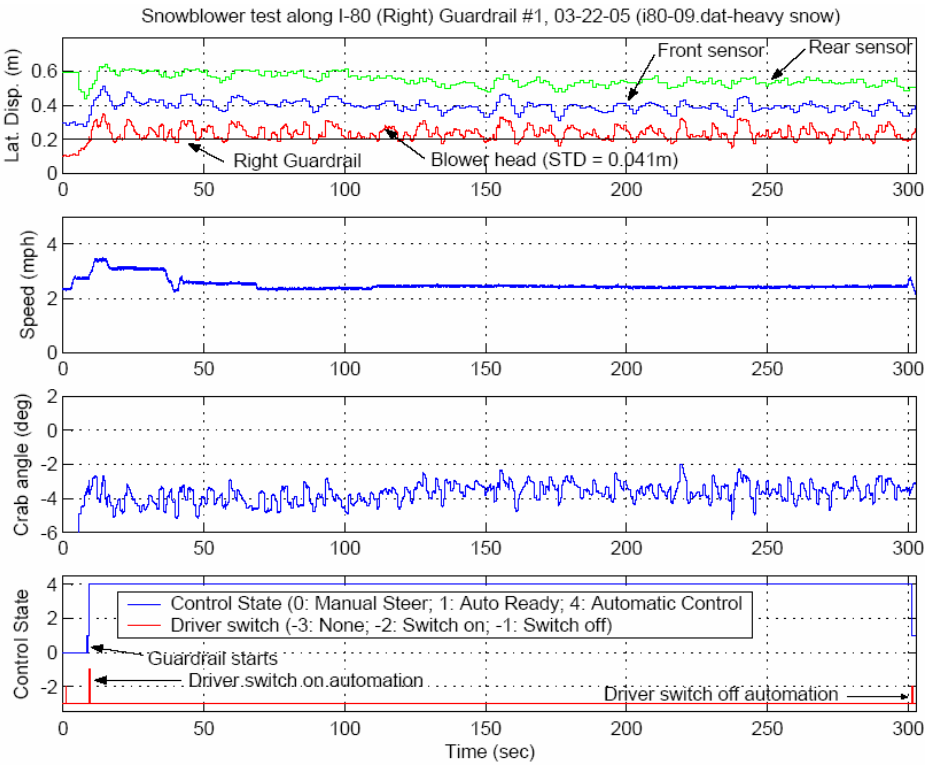

Figure 13. 20 Snowblower Tests along Guardrail on I-80 (Right Guardrail #1, 03-22-05): Heavy Wet Snow on the Ground

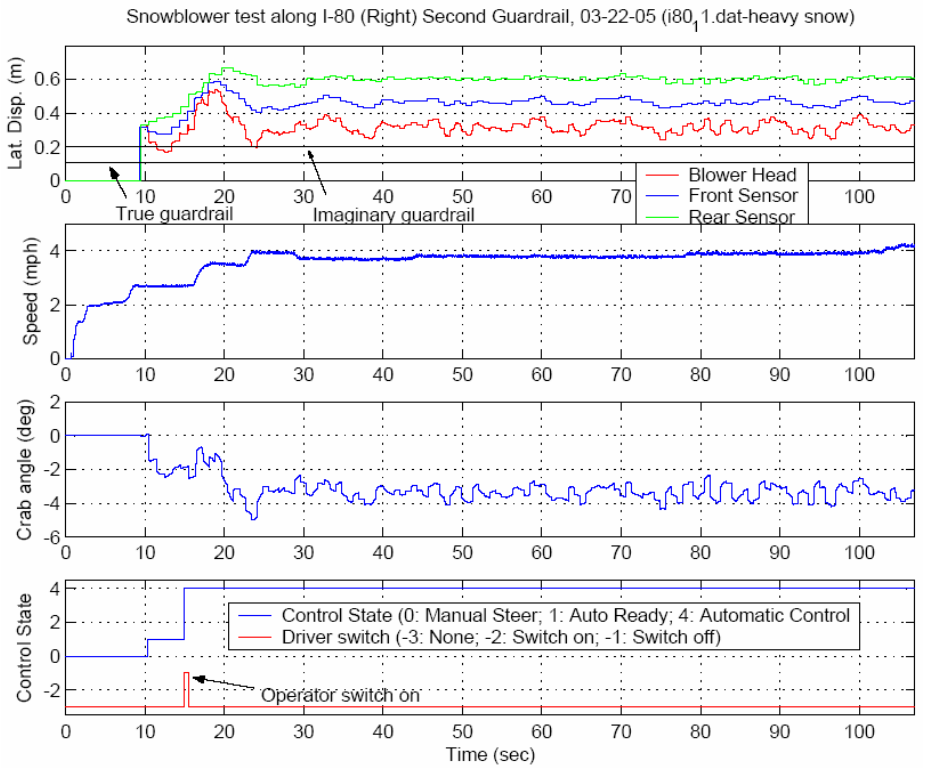

Figure 13. 21 ARP Tests along Guardrail on I-80 (Right Guardrail #2, 03-22-05): Heavy Wet Snow on the Ground

Figure 13.19, 13.20 and 13.21 present the detailed data plots from the data saved during these test runs. Figure 13.19 shows an automated test run along right guardrail #2 on I-80 for the snowblower during a winter operation with light snow on the ground on March 4, 2005. The driver kept a constant crab angle (~-4.5 degrees) with speed changing from 3 mph to 6 mph. It can be observed that the head of the snowblower tracks also very well along the right guardrail (located at 20 cm as indicated in the figure) and almost never touches it. The standard deviation of the tracking error under automation is 3.8 centimeters for total time under automation. It should also be noted that guardrail #2 has a continuous sharp left turn with a 400-meter radius of curvature, and exhibits large super-elevation sloping into the lane center. These road conditions should tend to drag the blower away from the guardrail. However, the data shows that such an effect was not significant; the controller compensated well enough for it, at least when the blower was blowing light snow off the ground.

Figure 13.20 shows an automated test run along right guardrail #1 on I-80 for the snowblower during a severe late winter storm that lasted two days. The test was conducted on March 22, 2005, after a significant amount of wet snow had already accumulated on the ground. The driver kept an almost constant crab angle (~-4 degrees); with speed ranging from 2 mph to 3 mph. According to the operator, the load of snow-cutting was heavier than in a normal operation for this particular test run because he operated at a speed slightly higher than what he normally would do under the same condition. It can be observed that the head of the snowblower still tracked very well along the right guardrail. Although a few locations in Fig. 12 have shown possible slight brushing against the guardrail, no contact was felt by the operator during operation (these positions “overshoots” may have been caused by the amplification of the measurement noise in computing the blower head location). The standard deviation of the tracking error under automation was 4.1 centimeters for the total time under automation. By comparing Figure 13.20 and Figure 12.19, it can also be observed that the standard deviation of the tracking error increased from 3.3 cm to 4.1 cm when blowing wet and heavy snow.

Figure 13.21 shows the test run along guardrail #2 on I-80 for the ARP under automated control, with constant crab angle (~-3.5 degrees), and with speed changing from 3 mph to 4 mph. Because this was the first time the automated steering control was used under any measurable amount of operational loading conditions, we artificially modified the controller to control the blower at an additional 10 cm distance to the guardrail as a pre-cautionary measure. As a result, after normalization, the true guardrail was at 10 cm for this test run, and the “imaginary” guardrail was at 20 cm. Although the head of the snowblower tracks very well along the guardrail (imaginarily located at 20 cm), an additional 7 centimeters distance to the “imaginary” guardrail can be observed. The standard deviation of the tracking error under automation is 4.8 cm for total time under automation, which is larger than the one exhibited in Figure 13.19 when there was little snow to blow. The additional tracking error (both 1-cm additional STD and the 7-cm “bias” can be explained by the large load created by the continuous sharp left turn (400 meter radius of curvature) plus the large super-elevation sloping into the lane center.

The large slope away from the guardrail drags the blower away from the guardrail especially when the blower is pushing and blowing a large load of snow with a large crab angle.

One problem in the current system observed during the tests on March 22, 2005 was the "low-speed" limitations. The lateral position was not consistently calculated when the blower speed was under 0.8 m/s. This problem was a result of the combination of the insufficient sensitivity of the speed sensor as well as the parameter setting of the magnetometer signal processing. By post-processing the available speed data, we found out that the driver can drive as low as 0.3 m/s (0.7 mph) during heavy snow removal operations by asking the operator to drive to the lowest speed that he might operate such machine continuously under such operational conditions (as shown in Figure 13.22). This low-speed limitation problem potentially reduces the operational reliability of the system since the automated system would not be able to distinguish between a stopped snowblower and the one with very-low speeds. We also observed this behavior during the road tests when the steering controller reduced the current commends to the DC motor to save power at very low speed because the controller thought the blower was not moving. This problem can be relatively easy to resolve by changing the speed sensor either electronically or mechanically and retuning the parameters for the magnetometer signal processing.

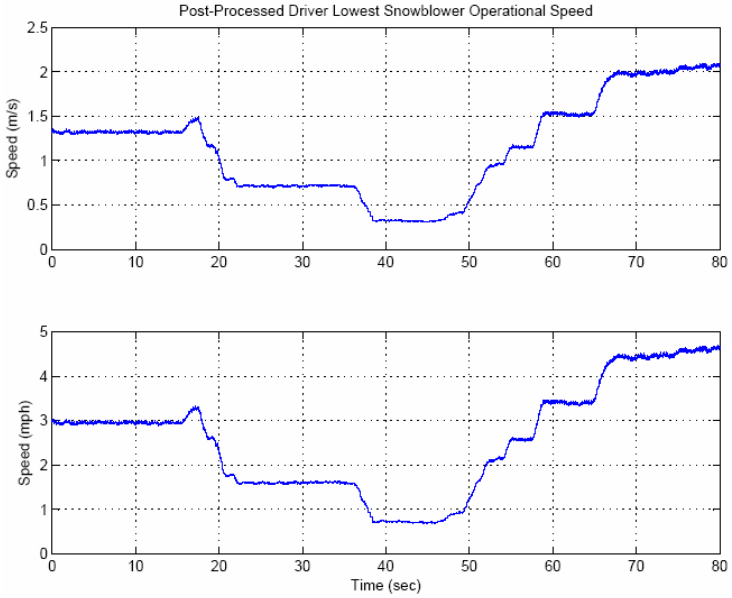

Figure 13. 22 Post-processed lowest snowblower operational speeds

14. Conclusion and Recommendation

This report describes a real-world application of the lane guidance technologies, which involved the design, implementation and field testing of an automated ARP for highway operation along guardrails. The objective is to minimize damage to and maintenance costs of the snowblower, guardrail, and other elements of the infrastructure by deploying highly accurate and robust automated steering. In addition, application of precision steering control can potentially increase operational and public safety by reducing driver fatigue. The design difficulties lay on keeping a tight tolerance under all practical operational scenarios and very stringent conditions, including uneven road surface, snow chain effects, variable front tire normal load, large and variable snow removal forces, driver rear steering inputs, and any possible operator interventions.

The report presents critical tasks involved in this project: problem formulation that explains the design difficulties and defines the system requirements; a new low-speed vehicle model that reveals the source of the low-speed oscillation problem; a basic controller synthesis design that leads to a low-order feedback implementation; a magnetic signal processing algorithm that achieves sub-centimeter lateral position accuracy; a smart steering servo controller that unerringly carries out the steering command under highly nonlinear characteristics and unpredictable disturbances; a human machine interface that results in favorable human factor results from the operator feedback; instrumentation of a prototype ARP system that includes detailed hardware, software and HMI; and data that reports test results from various stages of development including filed tests that yield successful demonstration and positive operator responses. However, deployment issues, such as maintainability, cost effectiveness, reliability, and commercialization feasibility, are not discussed in the report.

The major tasks within the Automated ARP that have been accomplished are listed as follows:

1. Completed system design (2002)
2. Installed, tested and refined sensors and signal processing algorithms (2002-2004)
3. Installed, developed and tested the steering actuator, including its hardware, software and servo algorithm (2002-2003)
4. Developed, tested and refined automated control algorithms (2002-2004)
5. Developed, installed, tested, and refined operator interface components including sounds, display and switches (2003-2004)
6. Successfully conducted operator training and interviews (2003-2004)
7. Successfully demonstrated the first prototype system to stakeholders (California, Nevada and Alaska) at Kingvale yard with simulated guardrails (10/17/2003)
8. Modified and tested the second prototype “turn-key” system along guardrails under no-snow conditions (12/2004-3/2005)
9. Successfully conducted the first operational trial along guardrails on I-80 under heavy snow condition (2005)

The general observations and conclusions from the initial operational tests are:

1. The automated steering system guides the snowblower along the guardrail as designed, with and without snow blowing.

2. The operators learned to use the system quite easily; they generally had very favorable impressions of the system, performance and concept, after the test runs. They expressed willingness to accept and use the system. In particular, they were pleased with the following factors:
   a. The operational procedure was simple;
   b. The LED was simple to understand;
   c. The automatic control system seemed to be working;
   d. If the system could function continuously, it would provide significant help to the blower operations.

   (These comments were generally made after they had experienced automated operations.)

3. The following are the areas that can be further improved:
   a. The speed for continuous automatic control should be able to maintain speeds as low as 0.3 m/s (the current lowest speed for continuous operation is 0.5 m/s).
   b. The system should further improve its ability to automatically compensate for the combination of the following extreme operational conditions: heavy wet snow, large crab angle, sharp curve, and large (opposite direction) super-elevations. Currently, a slight increase in the tracking offset (up to 4-5 cm) can be observed.
   c. The operator would like to have the option to select different distances from the guardrail for automation.
   d. The system should allow negative crab angles for certain special operations, e.g., the case when the operator uses it to compensate for a large snow cut on a sharp curve. Currently, when such a condition is detected, the system automatically extends the tracking distance to the guardrail to prevent the back end of the snowblower from hitting the guardrail.

As an anecdotal example, in the questionnaires the operators filled out after the trial, they responded to the question:

Having seen the automated system, did your opinion on how valuable it could be for snow blowing operations change? Please indicate what your opinion was before and after seeing the system work.

Driver 1: "Yes – opinion before: a waste of time and money, opinion after: system works, helpful to driver."

Driver 2: "Could be an asset in poor visibility, definitely cut down guardrail damage."

The initial operator trial and survey, operational test results, and the stakeholders' feedbacks strongly indicated the following:

- The concept of applying automated steering control to snowblower operation is feasible; the application will improve safety and efficiency of the snow removal operations.

- The implementation of the current automation technology to the snowblower is likely to succeed.
- The operators liked the system performance and would accept and use the system.

The following is a list of what the team would suggest to strengthen and improve the system as well as possible future work:

1. Modify the speed sensor and the magnetometer signal processing algorithm so that the automated system can perform at speed as low as 0.1-0.3 m/s.
2. Redesign the computer system using hardware platforms suitable for the harsh environment, such as the PC104 platform.
3. Include an adaptive tracking scheme that can automatically adjust the tracking distance so that the system can use a supervisory level of control to compensate for operational scenarios where heavy wet snow, large crab angle, sharp curve, and large super-elevations occur at the same time.
4. Address the comments from the operators, such as automatically accommodating for negative crab angle during certain operations.
5. Conduct comprehensive field operational tests in a more extensive winter operational conditions, and review the corresponding comments and results.
6. Address deployment issues such as reliability, redundancy, cost, installation, maintenance, and commercialization.
7. Explore integration with other position sensing systems such as DGPS to extend the automated operation beyond guardrail sections.

References

[1] H.-S. Tan, "An Automated Snowblower for Highway Winter Operation," *Intellimotion*, Vol. 10, no. 4, pp. 1-6, 2004

[2] A. Broggi, M. Bertozzi, A. Fascioli, C. Guarino Lo Bianco and A. Piazzi, "The ARGO Autonomous Vehicle's Vision and Control Systems," *International Journal of Intelligent Control Systems*, vol. 3, no. 4, 1999, pp. 409-441.

[3] Q. T. Luong, J. Weber, D. Koller, and J. Malik, "An Integrated Stereo-Based Approach to Automatic Vehicle Guidance," *Proceedings of the 5th ICCV*, pp. 52-57, 1995.

[4] "Validation Report, Intelligent Vehicle Initiative, Specialty Vehicle Field Operational Test", *MN/DOT – US DOT Cooperative Agreement DTFH61-99-X-00101*, July 2002

[5] J. Farrell, H.-S. Tan and Y. Yang, "Carrier Phase GPS-aided INS based Vehicle Lateral Control". *ASME Journal of Dynamics Systems, Measurement, and Control*, Vol. 125 no. 3 pp339-353 2003.

[6] Lee Alexander, Max Donath. "Differential GPS Based Control of Heavy Vehicles". *Proceedings of the IEEE/IEEJ/JSAI International Conference on Intelligent Transportation Systems*, Tokyo, Japan, pp. 662-7, October, 1999

[7] H.-S. Tan, B. Bougler and W.-B. Zhang, "Automatic Steering Based on Roadway Markers - From Highway Driving to Precision Docking," *Vehicle System Dynamics*, vol. 37, no. 5, pp. 315-339. 2002

[8] K. Aoki, T. Suyama, "A concept of intelligent multi-mode transit system based on automated bus" *IEEE Intelligent Vehicles Symposium* 2000, pp. 590 – 595

[9] H.-S. Tan, B. Bougler, and A. Steinfeld, "Snowplow Steering Guidance with Gain Stabilization," *Vehicle System Dynamics*, vol. 36, no. 4-5, November, 2001, pp. 279-305

[10] J. C. Dixon, *Tires, Suspension, and Handling*, Cambridge University Press, 1991.

[11] W. F. Milliken and D. L. Milliken, *Race Car Vehicle Dynamics*, SAE International, 1995.

[12] P. S. Hingwe and M. Tomizuka, "Robustness and Performance Issues in the Lateral Control of Vehicles in Automated Highway Systems", *Ph.D. Thesis*, 1997.

[13] L. Ljung, *System Identification:Theory for Users*, 2nd edition, Prentice Hall, 1998

[14] J. Y. Wong, *Theory of Ground Vehicles*, 2nd edition, John Wiley and Sons, Inc., 1993.

[15] H. Peng and M. Tomizuka, "Vehicle Lateral Control for Highway Automation", *Ph.D. Thesis*, 1992.

[16] S. Haykin, *Adaptive Filter Theory*, 4th edition, Prentice Hall, 2001.

[17] Shladover, S.E., 1991, "Program on Advanced Technology for the Highway (PATH)," in Road Transport Informatics (RTI)/ Intelligent Vehicle-Highway Systems (IVHS), 24th International Symposium on Automotive Technology and Automation.

[18] Furukawa, Y., Abe, M., 1997, "Advanced chassis control systems for vehicle handling and active safety", Vehicle System Dynamics, **28**(2), pp.59-86.

[19] Tan, H.-S., Bougler, B, Zhang, W.-B., 2002, “Automatic steering based on roadway markers: from highway driving to precision docking,” Vehicle System Dynamics, **37**(5), pp.315-38.
[20] “2003 Annual Report,” California Partners for Advanced Transit and Highways (PATH), pp.18-19.
[21] Obata, K. et al., 2001, “Development of Automatic Contaner Yard Crane,” Mitsubishi Heavy Industries Technical Review, **38**(2), pp. 62-66.
[22] Ridha, R.A., Satyamurthy, K., Hirscheft, L.R., 1985, “Finite element modeling of a homogeneous pneumatic tire subjected to footprint loadings,” Tire Science Technology, **13**, pp91-110.
[23] Wong, J.Y., 1993, Theory of Ground Vehicle, John Wiley & Sons Inc, pp.35-40.
[24] Pacejka, H.B., Bakker, E., 1993, “The magic formula tire model,” Tyre models for vehicle dynamics analysis, Amsterdam, Swets and Zeitlinger.
[25] Weber, R. and Persch, H.-G., 1976, “Frequency response of tires – slip angle and lateral force,” SAE paper no: 760030.
[26] Wallentowitz, H., Kohn, P., and Holdmann, P., 1999, “Dynamic Properties of Tyres – Testing and Simulation,” SAE paper no: 1999-01-0790.
[27] Maurice, J.P. and Pacejka, H.B., 1997, "Relaxation Length Behaviour of Tyres," Vehicle System Dynamics, Vol. 27 supplement.
[28] Pacejka, H.B., Besseling, I., 1997, “Magic formula tyre model with transient properties”. 2nd International tyre colloquium on tyre models for vehicle dynamic analysis, Berlin, Germany.
[29] Collins, R.L., 1971, “Theories on the Mechanics of Tires and Their Applications to Shimmy Analysis”, Journal of Aircraft, **8**(4), pp. 271-277.
[30] Fenton, R.E., Melocik, G.C., and Olson, K.W., 1976, “On the steering of automated vehicles: theory and experiment”. IEEE Transactions on Automatic Control, **21**, pp. 306-315.
[31] Feng, K.-T., Tan, H.-S., and Tomizuka, M., 1998, “Automatic steering control of vehicle lateral motions with the effect of roll dynamics”. Proc. of the American Control Conference, pp. 2248-2252.
[32] Fancher, P.S., Mallikarjunarao, C., and Nisonger, R.L., 1979, “Simulation of the Directional Response Chacteristics of Tractor-Semitrailer Vehicles,” Report UM-HSRI-79-9, PB 80-189632, U.S. Department of Commerce, National Technical Information Service.
[33] S.-L. Koo, H.-S. Tan, "Dynamic-deflection tire modeling for low-speed vehicle lateral dynamics", submitted to *ASME Journal of Dynamic Systems, Measurements, and Control*
[34] H.-S. Tan, J. Guldner, S. Patwardhan, C. Chen and B. Bougler, “Development of an Automated Steering Vehicle Based on Roadway Magnets - A Case Study of Mechatronic System Design,” *IEEE/ASME Transactions on Mechatronics*, vol. 4, no. 3, Sept., 1999, pp. 258-272
[35] C. Scherer, P. Gahinet and M. Chilali, “Multiobjective Output-Feedback Control Via LMI Optimization,” *IEEE Transactions on Automatic Control* , Vol. 42, no. 7 pp896-911, 1997

[36] S. Boyd, L. El Ghaoui, E. Feron, and V. Balakrishnan, *Linear Matrix Inequalities in Systems and Control Theory*. Philadelphia, PA: SIAM, 1994

[37] P. Gahinet, A. Nemirovski, A. J. Laub, and M. Chilali, *LMI Control Toolbox for Use with MATLAB*, The Mathworks Inc., 1995

[38] H.-S. Tan, Fanping Bu, "Snow Removal Control Based on Multi-Objective Optimization", in preparation.